

## **ALCONPAT International**

### **Founders members:**

Liana Arrieta de Bustillos – **Venezuela**  
Antonio Carmona Filho - **Brazil**  
Dante Domene – **Argentina**  
Manuel Fernández Cánovas – **Spain**  
José Calavera Ruiz – **Spain**  
Paulo Helene, **Brazil**

### **Board of Directors International:**

#### **President of Honor**

Angélica Ayala Piola, **Paraguay**

#### **President**

Carmen Andrade Perdrix, **Spain**

#### **Managing Director**

Pedro Castro Borges, **Mexico**

#### **Executive Secretary**

José Iván Escalante García, **Mexico**

#### **Technical Vice President**

Enio Pazini Figueiredo, **Brazil**

#### **Administrative Vice President**

Luis Álvarez Valencia, **Guatemala**

#### **Manager**

Paulo Helene, **Brazil**

## **Revista ALCONPAT**

### **Editor in Chief:**

Dr. Pedro Castro Borges  
Centro de Investigación y de Estudios Avanzados del  
Instituto Politécnico Nacional, Unidad Mérida  
(CINVESTAV IPN – Mérida)  
Merida, Yucatan, **Mexico**

### **Co-Editor in Chief:**

Dr. Francisco Alberto Alonso Farrera  
Universidad Autónoma de Chiapas  
Tuxtla Gutiérrez, Chiapas, México

### **Executive Editor:**

Dr. José Manuel Mendoza Rangel  
Universidad Autónoma de Nuevo León,  
Facultad de Ingeniería Civil  
Monterrey, Nuevo Leon, **Mexico**

### **Associate Editors:**

Dr. Manuel Fernandez Canovas  
Universidad Politécnica de Madrid.  
Madrid, **Spain**

Ing. Raúl Husni

Facultad de Ingeniería Universidad de Buenos Aires.  
Buenos Aires, **Argentina**

Dr. Paulo Roberto do Lago Helene  
Universidade de São Paulo.  
São Paulo, **Brazil**

Dr. José Iván Escalante García  
Centro de Investigación y de Estudios Avanzados del  
Instituto Politécnico Nacional (Unidad Saltillo)  
Saltillo, Coahuila, **Mexico**.

Dr. Mauricio López.  
Departamento de Ingeniería y Gestión de la Construcción,  
Escuela de Ingeniería, Pontificia Universidad Católica de  
Chile  
Santiago de Chile, **Chile**

Dra. Oladis Troconis de Rincón  
Centro de Estudios de Corrosión  
Universidad de Zulia  
Maracaibo, **Venezuela**

Dr. Fernando Branco Universidad  
Técnica de Lisboa  
Lisboa, **Portugal**

Dr. Pedro Garcés Terradillos  
Universidad de Alicante  
San Vicente, **Spain**

Dr. Andrés Antonio Torres Acosta  
Instituto Tecnológico y de Estudios Superiores de  
Monterrey, Querétaro  
Querétaro, **Mexico**

Dr. Luiz Fernández Luco  
Universidad de Buenos Aires –  
Facultad de Ingeniería – INTECIN  
Buenos Aires, **Argentina**

**JOURNAL OF THE LATIN-AMERICAN  
ASSOCIATION OF QUALITY CONTROL,  
PATHOLOGY AND RECOVERY OF  
CONSTRUCTION**

<http://www.revistaalconpat.org>

With great satisfaction, we present the first issue of the eleventh year of the ALCONPAT Journal.

The objective of the Journal is the publication of contributions on basic or applied research directly related to solving problems about quality control, pathology and recovery of constructions, with related case studies being welcome in these areas.

This V11N1 edition begins with a work from **Brazil**, where Hygor Thairony Parreira Vilela and colleagues evaluate the effectiveness of the use of different levels of crystallizing additive to prevent the alkali-aggregate reaction in mortars. The analysis was carried out by means of expansion tests of mortar bars by the accelerated method, in parallel with tests of mechanical resistance, capillarity, porosity and percentage of voids. It was observed that the presence of alkaline products in the additive composition significantly increased the initial expansions within the first week. Regarding the results of mechanical resistance, water absorption and voids, the product was satisfactory, improving the properties of the mortars. In general, the results attest to the effectiveness of the additive in sealing voids and pores, but not in inhibiting the alkali-aggregate reaction.

In the second work, Alejandro Flores-Nicolás and colleagues from **Mexico** evaluate the effect of corrosion of reinforced concrete without and with the addition of low carbon graphite powder. The phase identification processes and the physical-electrochemical properties of the concrete were analyzed by using X-ray diffraction techniques (XRD), scanning electron microscopy (SEM), half-cell potential, electrochemical noise (EN) and resistance to polarization. linear (RPL). The samples were studied for 168 days in saline solution. The results show that when adding graphite powder in an amount of 2.5% by weight of the cement, the resistance to compression was increased compared to the control sample. Electrochemical tests show that the corrosion of reinforcing steel in concrete increased as the level of graphite replacement increased.

The third article comes from **Brazil**, where Renata dos Santos Kimick and colleagues comparatively analyze the waterproofing systems used in the Brazilian market. The products evaluated were asphalt emulsion, acrylic resin and thermoplastic resin. To evaluate the effectiveness of the systems, tightness, absorption by immersion and capillarity tests were carried out, the latter being also analyzed by thermographic images. For the efficiency analysis of the systems, an accelerated aging pattern was adopted, which consisted of alternating the samples in wet and dry cycles. The results indicate a good performance for the studied systems, which in comparison with the non-impermeable series presented lower absorbances (approximately 300%). The accelerated aging test indicated, after 140 days of age, a reduction in the performance of the waterproofed series.

In the fourth article from **Spain**, Pedro Garcés Terradillos and colleagues have studied the feasibility of a combined treatment of electrochemical chloride extraction (ECE) and cathodic protection (CP) in reinforced concrete structures using a conductive cement-graphite paste as anode. It has been proven that the prior application of an electrochemical chloride extraction treatment leads to a greater durability of the anode. It has been shown that, for reinforced concrete structures located in aggressive marine environments, the combination of electrochemical treatments, first ECE to reduce the content of chlorides and then CP to maintain passivation conditions, is capable of providing adequate protection conditions to the reinforcement, provided that the appropriate current density value is applied, in accordance with the average content of chlorides present in reinforced concrete structures.

The fifth article, by Rogerio Taygra Vasconcelos Fernandes and colleagues, comes from **Brazil**; they studied the feasibility of using drones to map and inspect pathological manifestations in asphalt pavements in comparison with the traditional method. Sample plots were established every 20 m, 6 m long, totaling 20 stations, which had their pathological manifestations noted and the Global Severity Index calculated for the study area. The results obtained with the reference and alternative methodologies were compared based on the pathologies identified and the time spent in the surveys. The results demonstrated viability for the use of Drones in the inspection of asphalt pavement pathologies, based on the DNIT 006/2003 - PRO Standard, obtaining results like the traditional methodology with a significant reduction in operating time (33.3%).

The sixth work of this issue is written by Carlos Aire and L. Aguilar from **Mexico**, they evaluate three tests to characterize the behavior of concrete shot with metallic fibers in the primary lining of the tunnel of CDMX metro line 12. Three square panels (UNE 14488-5), three round panels (ASTM C1550) and four cylinders for Barcelona test (UNE 83515) were made. All can be used as quality control methods for fiber-reinforced concretes (FRC) in underground constructions, however, greater variability was found in the results of circular panels, in addition to being the specimens with greater complexity for their elaboration and test. Therefore, the application of the Barcelona test is recommended for quality control on site because it is easier to prepare, handle and execute the sampling and test.

In the seventh work, from **Brazil**, Ramiro Daniel Ballesteros Ruiz and colleagues evaluate the use of unmanned aerial vehicles (UAVs) as a visual tool for the inspection of pathological manifestations on facades through an exploratory study. At present, UAVs are becoming increasingly important in civil construction as a new mechanism for obtaining data and visual inspection, optimizing time. The research strategy considers three different stages: bibliographic review, the experimental procedure and, finally, data processing, with the aim of verifying the feasibility of the inspection procedure. The convenience of using UAV is evident, particularly where access is difficult, which can reduce time, costs and generate greater security, in addition to the 3D reconstruction of the building to be inspected and generate more accurate diagnoses.

In the eighth paper, from **Spain**, Vicente Alegre and S. Villalba discuss the example of a real case in which, on an existing tunnel, a building with fiber optic instrumentation is

built that allows the monitoring of the load history of a structure from its installation. To verify that the tunnel is not structurally affected during the construction period, sections of it are instrumented and the microdeformations that occur are measured, which are compared with those of the model. The ovalizations and tensions in the vault have been appreciated during the different phases of the construction process, all of them being below the limit values established in the contingency plan. This technique has made possible to validate the works carried out throughout the process.

The last article that closes this issue is written is by Willians Perley Alexandre da Silva and colleagues from **Brazil**, who present the use of the thermographic camera integrated in UAV in building inspection processes. The development of this work was based on a systematic review of articles and works related to the subject, investigating the characteristics and operation of thermographic cameras, the use of UAVs and the factors that influence the detection of pathological manifestations. The results allowed to identify the advantages and limitations of the integration of cameras and UAV, demonstrating the viability and effectiveness of the joint use. As a contribution, this work provided the development of a flight protocol that orders the steps and procedures necessary to perform an inspection using the thermal camera integrated in UAV.

We are confident that the articles in this issue will constitute an important reference for those readers involved with questions about evaluations and characterizations of materials, elements, and structures. We thank the authors participating in this issue for their willingness and effort to present quality articles and meet the established deadlines.

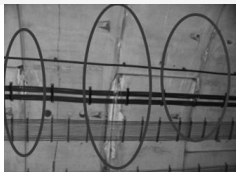
Exactly 10 years ago, in January 2011, we were launching the first issue of the Alconpat Journal (RAVIN1). 10 years away, I must give wide recognition to the original editorial staff and to those who have joined to this initiative that has led us to where we are now. But undoubtedly, the greatest recognition is deserved by our articles' authors, who have trusted in our journal and invested time, money and effort to publish their research work with us, despite the fact that many of them have had better options in their moment. Finally, our readers, without them we are nobody, a special thanks for reading, downloading, and citing us. Your preference will undoubtedly give us, in a short period of time, opportunities to continue improving through better tools for consultation and indexing. Many, many thanks to all. During 2021 we will celebrate these 10 years with some academic celebratory activities that we will make known in each edition.

On behalf of the Editorial Board

A handwritten signature in black ink, appearing to read 'Pedro Castro Borges', written over a circular stamp or mark.

Pedro Castro Borges

Editor in Chief



## CONTENT

Page

### BASIC RESEARCH

**Vilela, H. T. P., Teixeira Filho, M. G., Campos Neto, T. F.:** Effects of the use of crystallizing admixtures on mortar alkali-aggregate reactions and absorption. 1 - 17

**Flores-Nicolás, A., Flores-Nicolás, M., Uruchurtu-Chavarín, J.:** Corrosion effect on reinforced concrete with the addition of graphite powder and its evaluation on physical-electrochemical properties. 18 – 33

### APPLIED RESEARCH

**Kmick, R. S., Gazolla, M. G., da Silva Junior, R. M., Capraro, A. P. B., Moreira, K. A. W.:** Comparative analysis of the effectiveness and efficiency of three waterproofing systems. 34 – 47

**Garcés Terradillos, P., Climent, M. A., Carmona, J., Sánchez de Rojas, M. J.:** Service life increase of reinforced concrete structures exposed to marine environments through the application of electrochemical techniques. 48 – 60

**Vasconcelos Fernandes, R. T., Fonseca Cabral, A., Batista Dantas, G. C., Varela Tinoco, V. N., Azevedo da Silveira, B. D., Sousa Junior, A. M.:** Mapping of pathological manifestations in asphalt pavement through the use of drones. 61 – 72

**Aire, C., Aguilar, L.:** Fiber reinforced shotcrete control tests in the Mexico City metro line 12 tunnel. 73 – 87

**Silva, Ruiz, R. D. B., Lordsleem Júnior, A. C., Rocha, J. H. A.:** Inspection of facades with Unmanned Aerial Vehicles (UAV): an exploratory study. 88 – 104

### STUDY CASE

**Alegre, V., Villalba, S.:** Advances in the implementation of optical fiber on structures. The present of an implementation with a future. 105 – 122

### DOCUMENTARY RESEARCH

**Silva, W. P. A., Lordsleem Júnior, A. C., Ruiz, R. D. B., Rocha, J. H. A.:** Inspection of pathological manifestations in buildings by using a thermal imaging camera integrated with an Unmanned Aerial Vehicle (UAV): a documental research. 123 – 139

## Effects of the use of crystallizing admixtures on mortar alkali-aggregate reactions and absorption

H. T. P. Vilela<sup>1\*</sup> , M. G. Teixeira Filho<sup>1</sup> , T. F. Campos Neto<sup>2</sup> 

\*Contact author: [hygorencivil@outlook.com](mailto:hygorencivil@outlook.com)

DOI: <https://doi.org/10.21041/ra.v11i1.461>

Reception: 18/03/2020 | Acceptance: 23/10/2020 | Publication: 01/01/2021

### ABSTRACT

This article aims to evaluate the effectiveness of using different levels of crystallizing admixture in preventing the alkali-aggregate reaction in mortars. The analysis was carried out by means of expansion tests of mortar bars by the accelerated method in parallel with mechanical performance, capillarity, porosity and void index tests. The presence of alkaline products in the admixture composition significantly increased initial expansions within the first week. Regarding the mechanical performance, water absorption and void results, the product was satisfactory, improving mortar properties. In general, the results attest to the effectiveness of the admixture in sealing voids and pores, but not in inhibiting the alkali-aggregate reaction.

**Keywords:** alkali-aggregate reaction; crystallizing admixture; mortars.

**Cite as:** Vilela, H. T. P., Teixeira Filho, M. G., Campos Neto, T. F. (2021), "*Effects of the use of crystallizing admixtures on mortar alkali-aggregate reactions and absorption*", Revista ALCONPAT, 11 (1), pp. 1 – 17, DOI: <https://doi.org/10.21041/ra.v11i1.461>

<sup>1</sup> Faculdade de Engenharia Civil, Universidade de Rio Verde (UniRV), Rio Verde – GO, Brasil.

<sup>2</sup> Professor Mestre, Faculdade de Engenharia Civil, Universidade de Rio Verde (UniRV), Rio Verde – GO, Brasil.

#### Contribution of each author

In this work, the author H. T. P. Vilela contributed with the activities of conceptualization, development, results and discussion, writing and preparation of the original text; M. G. Teixeira Filho contributed to the activities of conceptualization, development, results and discussion; T. F. Campos Neto contributed with conceptualization, supervision, discussion of results, writing and review.

#### Creative Commons License

Copyright 2021 by the authors. This work is an Open-Access article published under the terms and conditions of an International Creative Commons Attribution 4.0 International License ([CC BY 4.0](https://creativecommons.org/licenses/by/4.0/)).

#### Discussions and subsequent corrections to the publication

Any dispute, including the replies of the authors, will be published in the third issue of 2021 provided that the information is received before the closing of the second issue of 2021.

## **Efeitos do uso de aditivos cristalizantes na reação álcali-agregado e absorção das argamassas**

### **RESUMO**

Este artigo tem como objetivo avaliar a eficácia do uso de diferentes teores de aditivo cristalizante na prevenção da reação álcali-agregado em argamassas. A análise foi realizada por meio de ensaios de expansão de barras de argamassa pelo método acelerado em paralelo com ensaios de desempenho mecânico, capilaridade, porosidade e índice de vazios. Observou-se que a presença de produtos alcalinos na composição do aditivo aumentou significativamente as expansões iniciais dentro da primeira semana. No que se refere aos resultados de desempenho mecânico, absorção de água e vazios, o produto se mostrou satisfatório, melhorando as propriedades das argamassas. De modo geral, os resultados atestam a eficácia do aditivo na selagem de vazios e poros, mas não na inibição da reação álcali-agregado.

**Palabras clave:** reação álcali-agregado; aditivo cristalizante; argamassas.

## **Efectos del uso de aditivos cristalizantes en la reacción de álcali-agregado y la absorción de morteros**

### **RESUMEN**

El artículo tiene como objetivo evaluar la efectividad del uso de diferentes niveles de aditivo cristalizante para prevenir la reacción álcali-agregado en morteros. El análisis se realizó mediante ensayos de expansión de barras de mortero por el método acelerado en paralelo con ensayos de resistencia mecánica, capilaridad, porosidad y porcentaje de vacíos. Se observó que la presencia de productos alcalinos en la composición del aditivo aumentó significativamente las expansiones iniciales dentro de la primera semana. En lo que se refiere a los resultados de resistencia mecánica, absorción de agua y vacíos, el producto fue satisfactorio, mejorando las propiedades de los morteros. En general, los resultados dan fe de la eficacia del aditivo para sellar vacíos y poros, pero no para inhibir la reacción álcali-agregado.

**Palabras clave:** reacción álcali-agregado; aditivo cristalizante; morteros.

### **Legal Information**

Revista ALCONPAT is a quarterly publication by the Asociación Latinoamericana de Control de Calidad, Patología y Recuperación de la Construcción, Internacional, A.C., Km. 6 antigua carretera a Progreso, Mérida, Yucatán, 97310, Tel.5219997385893, [alconpat.int@gmail.com](mailto:alconpat.int@gmail.com), Website: [www.alconpat.org](http://www.alconpat.org)

Reservation of journal title rights to exclusive use No.04-2013-011717330300-203, and ISSN 2007-6835, both granted by the Instituto Nacional de Derecho de Autor. Responsible editor: Pedro Castro Borges, Ph.D. Responsible for the last update of this issue, Informatics Unit ALCONPAT, Elizabeth Sabido Maldonado.

The views of the authors do not necessarily reflect the position of the editor.

The total or partial reproduction of the contents and images of the publication is carried out in accordance with the COPE code and the CC BY 4.0 license of the Revista ALCONPAT.

## 1. INTRODUCTION

Important advances regarding construction material durability studies have been noted in recent years. These assessments allow for the identification of material behavior patterns in view of their interaction with the environment, in addition to the determination of other fundamental aspects, such as the fulfillment of the useful life of projects and buildings.

Concrete and mortar are the most applied construction industry materials and the alkali-aggregate reaction (AAR) is noted as one of their various types of degradation. In general, this is a pathological manifestation related to mineralogical and chemical-physical properties, and the result of the combination of these three categories is a damaging expansive effect. This phenomenon exhibits a high degree of complexity, and must be avoided (Junior and Ferro, 2016).

The AAR is one of the most frequent pathological cement structure phenomena and one of the most relevant concerning durability. Briefly, it can be defined as chemical reactions between certain aggregate components and alkaline hydroxides present within the pores of the cementitious matrix. These reactions do not exhibit a pre-established time for their appearance, since they are associated to several factors, such as the amount of alkalis in the matrix susceptible to the reaction, ambient temperature and humidity, aggregate reactivity and, finally, the nature of the material (Figure 1) (Silva, 2007).

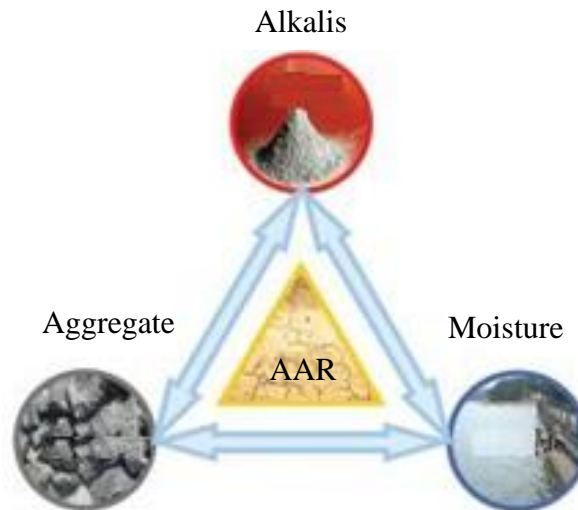


Figure 1. Determining factors for AAR occurrence and evolution (Couto, 2008).

More precise definitions can be made by distinguishing among different types of AAR. The alkali-carbonate reaction (ACR) originates from the reaction of the alkaline hydroxides of Portland cement or other sources and aggregates consisting of clayey dolomitic limestone, whereas the alkali-silica reaction (ASR) is based on the reaction of the hydration products of Portland cement and aggregates containing siliceous material (ABNT NBR 15577-1, 2018). For this research, ASR was approached as a general AAR in general.

Cement has a good influence on the occurrence of this manifestation since, when hydrated, it releases alkalis in the matrix, which are accessible through the matrix pores. AAR can also occur due to alkaline minerals from the aggregates, from pozzolans present in the cement composition and even products present in the mixing water used (Rolim, 2010).

Another factor which greatly influences ARR is moisture, which, in turn, may be associated to two functions in deleterious reactions, namely ionizing and transporting alkaline and hydroxyl ions throughout the pores of the cementitious matrix, which can be absorbed by ARR products. In this way, the alkaline silicon gel expands in the presence of water, which can lead to the appearance of cracks. Therefore, greater AAR prevention is required for building components in frequent contact with moisture (Couto, 2008).

It is known that concrete and mortar porosity is a determining factor concerning the chemical resistance of the material. Crystallizing admixtures, also called healing agents, are widely applied in components that maintain frequent contact with water, such as reservoirs, sewage systems and water treatment plants. These products are hydrophilic materials that react easily in the presence of water, generating a crystalline structure through calcium carbonate crystallization. Therefore, it is expected that their application will result in increased material density and reduced water absorption, since the precipitated crystals of this reaction are insoluble. In addition, crystallizing admixtures result in increased hydrated calcium silicate content in the matrix, ensuring better mechanical performance of cementitious materials (Roig-Flores et al., 2015).

Given the above, this article aims to assess the effectiveness of applying different levels of crystallizing admixtures in preventing the alkali-aggregate reaction in mortars. This analysis was performed by means of capillarity and porosity absorption tests, the determination of mortar bar expansion by the accelerated method and mechanical sample performance.

## 2. MATERIAL

### 2.1. Cement

CPV-ARI cement was used, due to its purity, avoiding any type of change in the aggregate reactivity results. This is one of the cements most prone to the occurrence of AAR, due to its lower slag content and compound fineness. The physical properties of this cement are presented in Table 1, meeting NBR 16697 specifications (ABNT, 2018).

Table 1. Results of Portland cement physical characterization tests.

Assay characteristics	Reference standard	Standard specifications	Result	Unit
Residue in a #200 sieve	ABNT NBR 11579:2012	$\leq 6.0$	5.4	%
Specific mass	ABNT NBR 16605:2017	Non-applicable	3.0	g/cm <sup>3</sup>

### 2.2. Fine aggregate

The fine aggregates were used according to Table 2, considering the ideal amounts of each fraction. To be able to meet this relationship, two different fine aggregates were required, obtained within a radius of approximately 170 km from Rio Verde, GO, Brazil.

Table 2. Required particle size of the material for AAR testing.

Sieve with mesh opening (ABNT NBR NM ISO 3310-1)		Material amount in mass	
Sieved	Retained	%	G
4.75 mm	2.36 mm	10	99.0
2.36 mm	1.18 mm	25	247.5
1.18 mm	600 µm	25	247.5
600 µm	300 µm	25	247.5
300 µm	150 µm	15	148.5

(ABNT NBR 15577-4, 2018)

To ensure compliance with the data presented in Table 2, specific mass, unit mass and particle size tests were performed according to ABNT NBR NM 52: 2003, ABNT NBR NM 45: 2006 and ABNT NBR NM 248: 2009 standards, respectively. The results are presented in Table 3.

Table 3. Results of fine aggregate characterization tests

Aggregate	Specific mass	Unit mass	Fineness module
Fine sand	2,630 kg/m <sup>3</sup>	1.513 kg/m <sup>3</sup>	1,42
Coarse sand	2,621 kg/m <sup>3</sup>	1.579 kg/m <sup>3</sup>	2,54

### 2.3. Admixture

The crystallizing admixture content was defined according to the cement mass of the mortars, and the manufacturer indicates levels ranging from 0.8% to 1.2%. Cardesa and Zephir (2014) used 0.8%, 2.0% and 3.0% and Takagi, Lima and Helene (2012), 2.5%. Both groups of researchers obtained satisfactory results in terms of mixture crystallization and waterproofing. Therefore, 1% and 2% were adopted in the present study. Tables 4 and 5 display the additive data provided by the manufacturer.

Table 4. Characteristics of the crystallizing admixture presented in the technical sheet available on the manufacturer's website.

Characteristic	Corresponding value	Unit
PH	10 – 13	%
Fusion point	1000	°C
Aspect Specific mass	Solid gray powder 1.1	- g/cm <sup>3</sup>
Odor and odor limit	Cement characteristic	-

Penetron Admix (2018)

Table 5. Chemical composition of the admixture provided by the manufacturer.

Chemical name	CAS N°	%
Portland cement	65997-15-1	65 to 80
CTS-15-1*	Industrial secret	10 to 30
CTS-15-2*	Industrial secret	5 to 10
Calcium and magnesium hydroxide (CaMg(OH) <sub>4</sub> )	39445-23-3	1.5 to 6
Magnesium and calcium hydroxide oxide (Ca(Mg(OH) <sub>2</sub> O)	58398-71-3	1.5 to 6
Calcium hydroxide	1305-62-0	1 to 2

\* Industrial secret - The exact percentage (concentration) of the composition was retained as an industrial secret.

Penetron Admix (2018)

### 3. METHODS

The investigation method followed the step flow chart presented in Figure 2. All the steps described below are intended to meet the requirements of the NBR 15577-4 standard (ABNT, 2018).

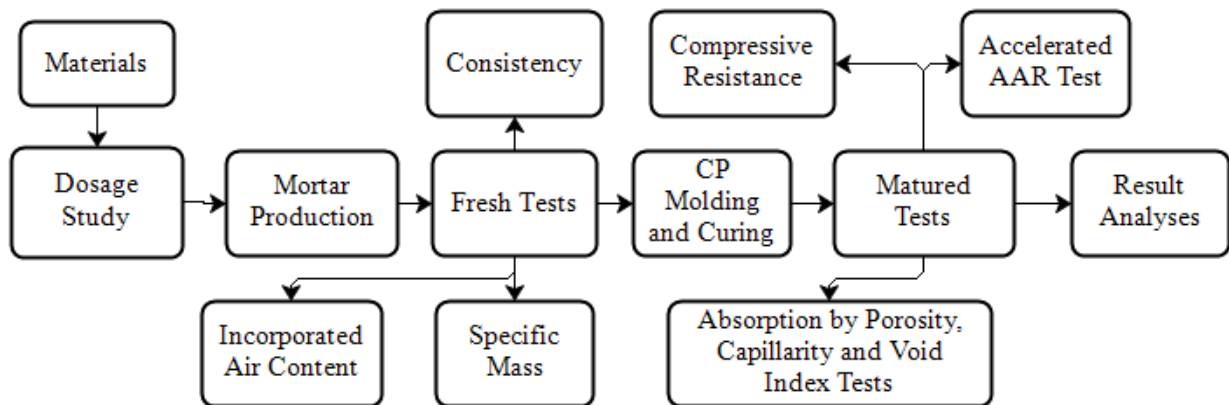


Figure 2. Methodological structure of the research.

#### 3.1. Trace determination

To determine mortar expansion by the accelerated method, the trace is composed of 1 part of cement, 2.25 parts of aggregate and a water/cement ratio (w/c) of 0.47. To mold three mortar bars, whose specific aggregate (d) mass is greater than or equal to 2.45 g/cm<sup>3</sup>, 440 grams of cement and 990 grams of aggregate must be adopted.

The tests were carried out according to Figure 2, and the traces were defined according to Table 6, with a reference mixture (AR) without additive and two mixtures (AA1 and AA2) containing 1% and 2% crystallizing admixture contents. During the mixture production mixtures, the admixture was previously diluted in the mixing water, as specified by the manufacturer.

Table 6. Unit traces of the studied mortars.

Trace	Cement	Sand	Water	Crystallizing admixture
AR	1	2.25	0.47	-
AA1	1	2.25	0.47	0.01
AA2	1	2.25	0.47	0.02

### 3.2. Fresh tests

The tests regarding mortar specific mass and incorporated air content were carried out according to the NBR 13278 standard (ABNT, 2005). Incorporated air was determined by using the results of the specific mass obtained through the relation between the theoretical and estimated masses. Mixture consistencies were evaluated applying NBR 13276 standard recommendations (ABNT, 2016).

### 3.3. Specimen molding and curing

Cylindrical and prismatic specimens were molded in accordance with NBR 7215 (ABNT, 2019) and NBR 13729 (ABNT, 2005) standards, respectively. The prismatic specimens (30x25x285mm) for expansion assessments were molded according to the NBR 15577-4 standard (ABNT, 2018), in two densified layers with 20 strokes each. For the accelerated AAR testing, at least three mortar bars are required for each aggregate. The bars were cured in a humid chamber at 23 °C for 24 hours, with their faces protected from splashes. After this period, the mortars were removed from the molds and placed in a thermoregulatory bath containing a sodium hydroxide solution. This last step is an integral part of the test procedure in the hardened state.

### 3.4. Hardened state tests

As established by NBR 15577-4 (ABNT, 2018), the mortar molds were immersed for 30 days in a NaOH solution (sodium hydroxide - 1.0 N), as displayed in Figure 3. During this period, eight specimen dimension readings were obtained, with one mandatory at 16 days and the other at 30 days after molding.

The compressive strength test was performed with cylindrical specimens according to the NBR 7215 standard (ABNT, 2019), while the flexural tensile strength test was performed according to the NBR 13279 standard (ABNT, 2005), using prismatic test pieces, both under a hydraulic press, as shown in Figure 4.

The capillarity absorption (in grams per square centimeter), void indices and porosity absorption (both in percentage) tests were performed according to NBR 15259 (ABNT, 2005) and NBR 9778 (ABNT, 2005) standards, respectively. These tests were carried out to evaluate the crystallizing effect of the admixture and associate it to a possible delay in mortar AAR.



Figure 3. Mortar specimens immersed in a NaOH solution for expansion tests.

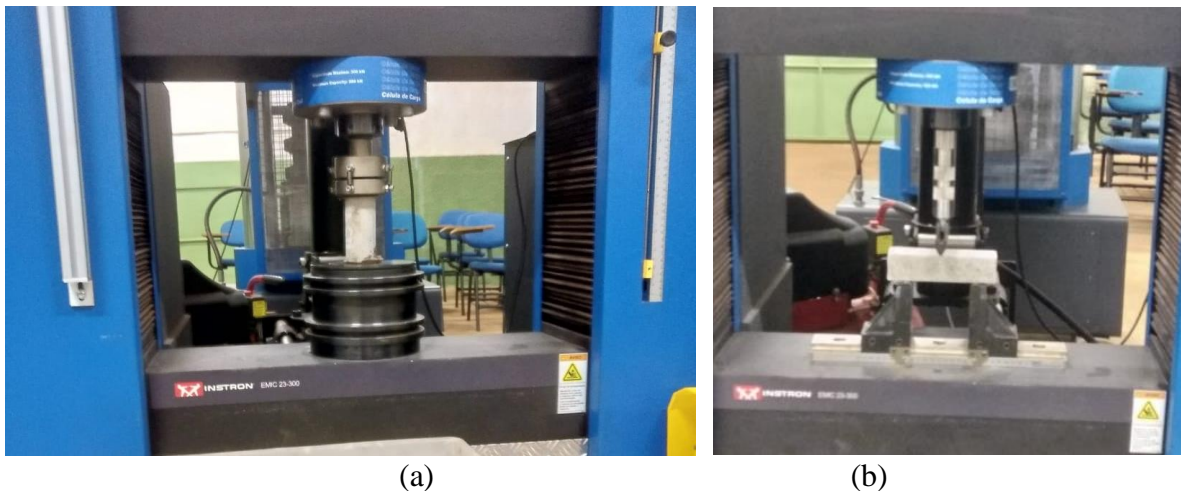


Figure 4. Photographic records of mortar specimen compressive strength (a) and flexural tensile strength (b) tests at 28 days.

### 3.5. Result analysis

All data concerning the accelerated AAR test were analyzed and compared following the tables provided by the NBR 15577-1 standard (ABNT, 2018), which determined potential aggregate reactivity, degree of occurrence risk, consequences, and reactivity classification (Figure 5). The other tests were carried out to expand and complement the approach of admixture effect assessments concerning mortar performance and behavior.

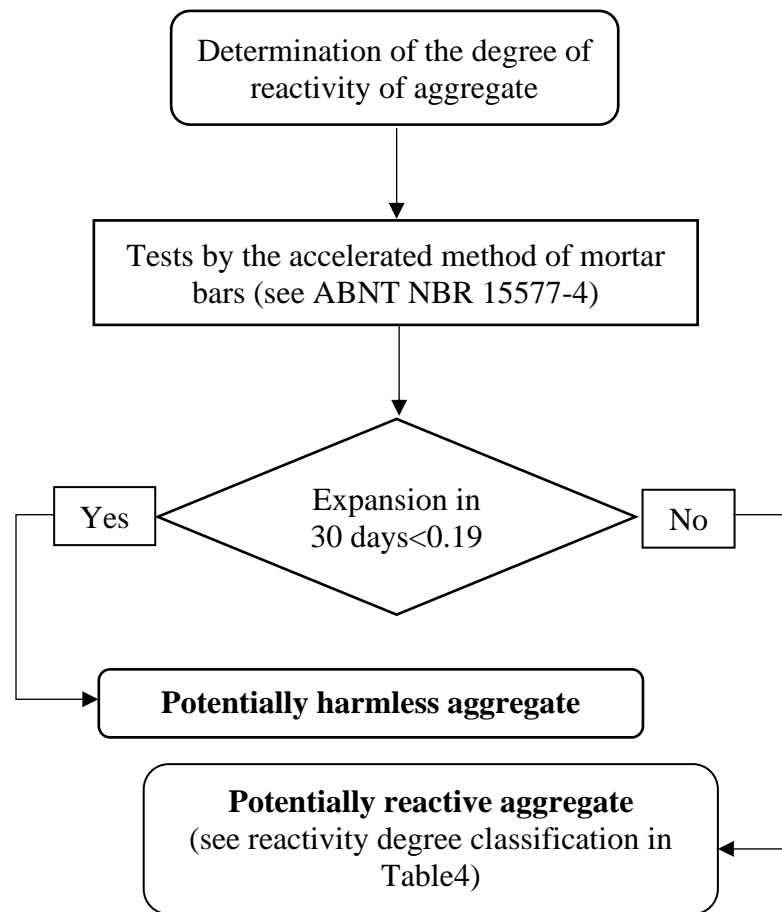


Figure 5. Procedure for determining the aggregate reactivity degree as established by the NBR 15577-1 standard (ABNT, 2018).

## 4. RESULTS AND DISCUSSION

### 4.1. Fresh assays

Table 7 presents the results of the tests carried out with the fresh mixtures. The healing additive leads to fresh mortar effects, where increasing admixture content increases the specific mass and spreading, while decreasing incorporated air content.

Table 7. Specific mass, spreading and incorporated air content results for fresh.

Trace	Specific mass	Spreading	Incorporated air content
AR	2216.87 kg/m <sup>3</sup>	267 mm	1.05 %
AA1	2226.51 kg/m <sup>3</sup>	278 mm	0.34 %
AA2	2228.92 kg/m <sup>3</sup>	283 mm	0.09 %

The mixtures registered non-expressive specific mass increases which, in turn, can be explained by the fineness of the admixture. The finer grains of the admixture fill interstitial voids and increase mixture cohesion by up to 0.5%.

Although the admixture is very similar to cement, spreading did not decrease, and, instead, increased fluidity was observed. This is due to the different chemicals present in the mixture, which can act as a water-reducing plasticizer. The spreading increase indicates that the admixture can reduce the water/cement ratio to a certain consistency, as reported by Cardesa and Zephir (2014). Some researchers, such as Moreira (2016) and Takagi, Lima and Helene (2012), identified loss of consistency with the use of similar admixtures, although not the same product in utilized herein. Manufacturers can use different chemicals in the production of crystallizing admixtures and, in the case of the product assessed in the present study, consistency was improved.

Regarding both, incorporated air content and specific mass, the fineness of the material is responsible for reducing the air content with increasing amounts of admixture. This reduction in the fresh state can contribute to reductions in the void index, capillarity, and porosity of the hardened mixtures.

#### 4.2. Hardened assays

The hardened assay results are presented in Figures 6 to 13. Figure 6 presents the results regarding the compressive strength of the tested mortars. Increasing additive resulted in increased compressive strength, as the AA2 mixture obtained the best performance, followed by AA1 and AR, respectively.

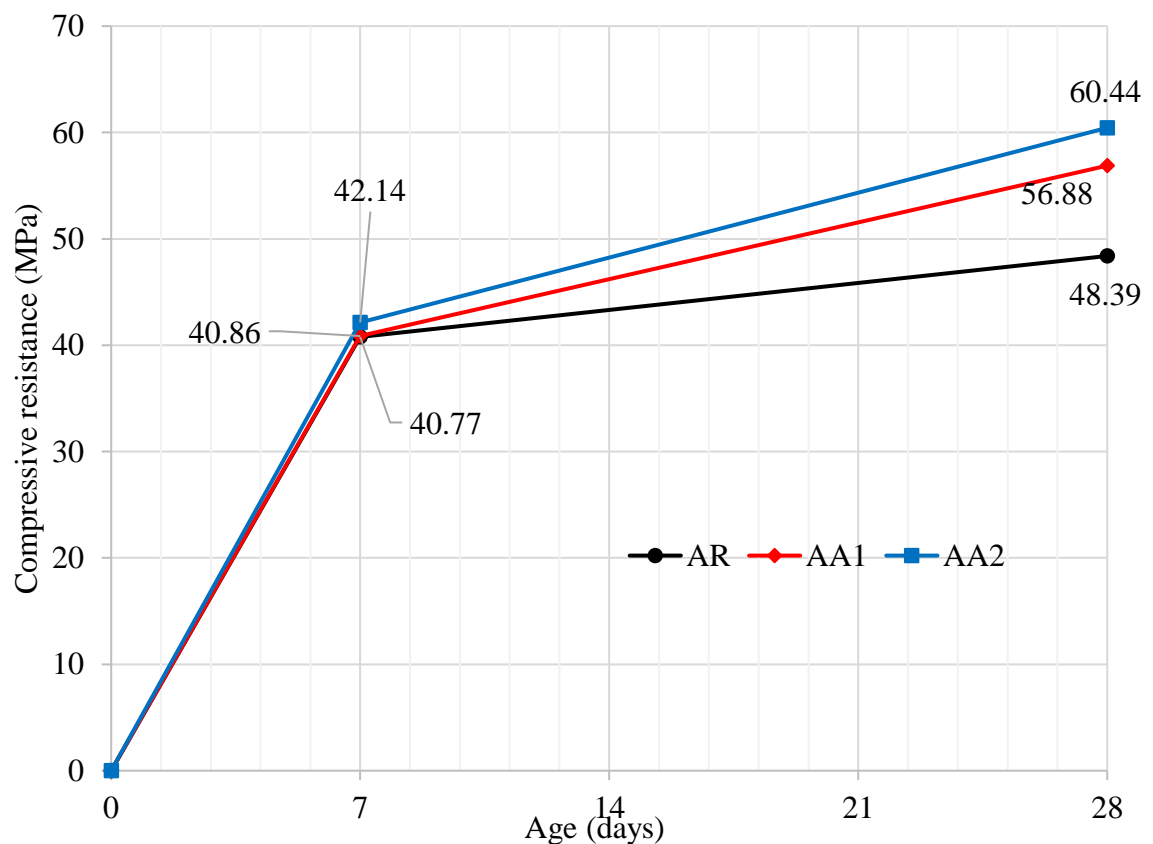


Figure 6. Results of the mortar compressive strength tests (MPa) at 7 and 28 days.

This behavior is similar to that observed by Takagi, Lima and Helene (2012), Cardesa and Zephir (2014) and García-Vera, Tenza-Abril, Saval and Lanzón (2019), who reported that concretes mortars containins 1% or more crystallizing admixtures under the cement mass displayed increased compressive strength when compared to mixtures containing no admixtures.

At seven days, an approximation of the resistance results of the three mixtures is observed, due to

the short period of time elapsed since the mortar production for the admixture reaction, since their reactivity is dependent on cement hydration reactions. However, at 28 days, a noticeable resistance gain of the admixture containing samples compared to the reference mixture is observed. Mortar AA2 reached a resistance 24.9% higher than AR, while AA1 reached a value around 17.5% higher than AR. As no information between the mixtures was altered other than the use of the admixture, resistance gain is solely due to the admixture use.

Figure 7 presents the results related to the flexural tensile strength tests, where a performance gain is verified with the use of the crystallizing product, similarly to what was noted in the compressive strengths assays. The AA2 mixture once again achieved the best result, reaching a value approximately 12.8% higher than AR, while AA1 presented a resistance 11.3% higher than the reference.

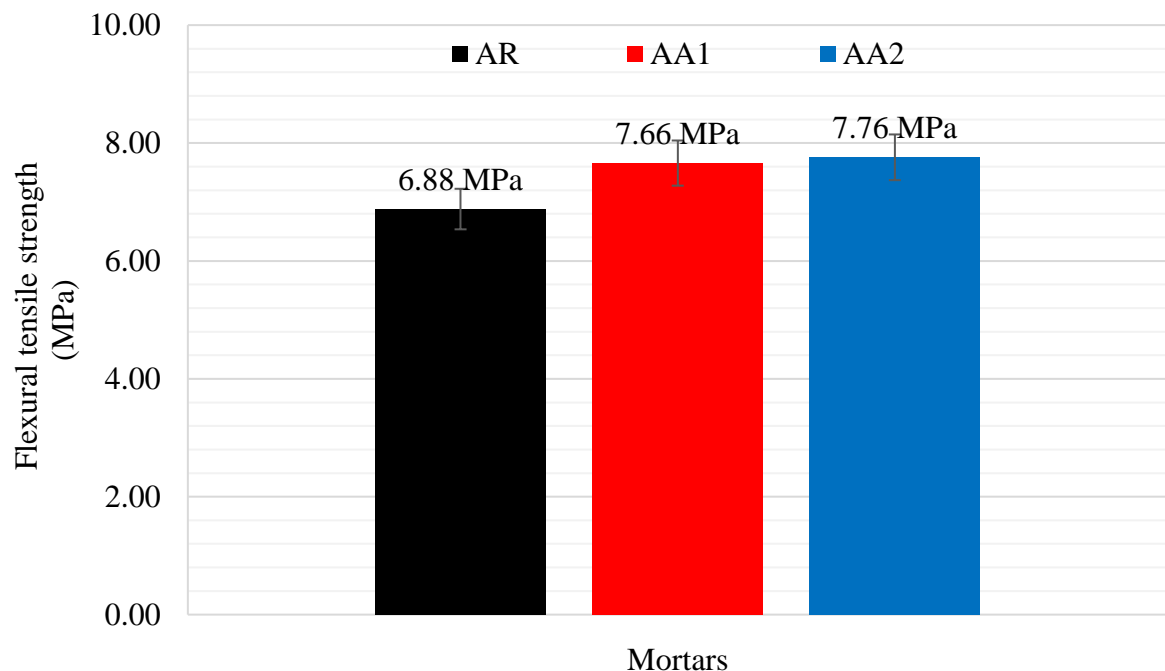


Figure 7. Flexural tensile strength tests (MPa) results of the evaluated mortars.

The gain in tensile strength when flexing mortars containing admixtures is explained by the crystallizing action of this product, which results in larger massive cross section areas, thus increasing the material's carrying capacity. This gain in tensile strength, even if not expressive, was also reported by Moreira (2016) when evaluating mixtures containing 0.8% of crystallizing admixtures.

According to the admixture manufacturer, this material is capable of filling cracks and voids of up to 0.5 mm. Figure 8 presents microscopic images under a 35x magnification of the cross sections of the specimens containing (Figure 8a) and not containing (Figure 8b) the admixture. Figure 8b also displays a portion of the material of a different color from the standard without the admixture, indicative of the healing power of this chemical.

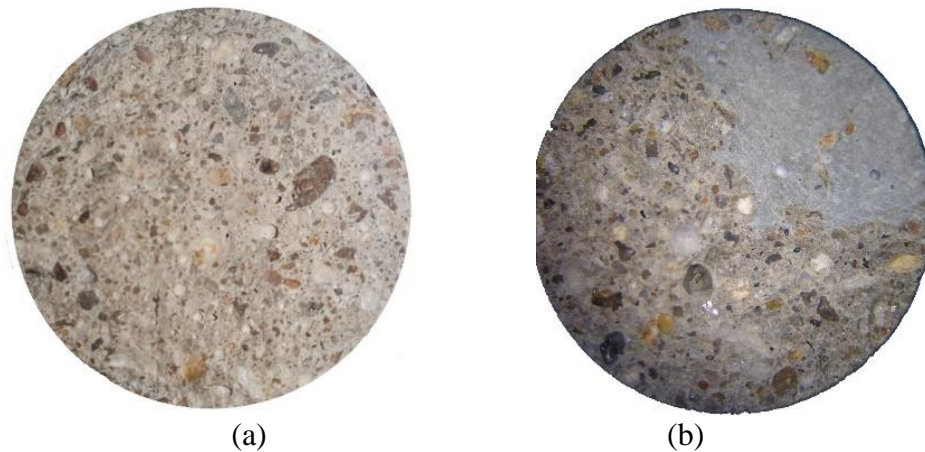


Figure 8. Microscopic image of the cross section of the specimen without the admixture (a) and containing 2% of the admixture (b), both after rupture at 28 days. Images under 35x magnification.

Bearing in mind that the specimen contained some internal irregularities, possibly caused during its production, the admixture reacted and filled the small internal voids located inside the specimens. Its distribution was homogeneous, although crystallization occurs exclusively in the mass voids and, for this reason, a region was formed resulting from the admixture action, displayed in Figure 8. No fine aggregate concentrations are found in the “healed” area, which, in accordance to data presented by the Japan Concrete Institute at JCI-TC075B (2009), corroborate the idea of the crystallizing effect.

Figures 9 and 10 display the results obtained through the porosity water absorption test and void indices performed according to the requirements of the NBR 9778 standard (ABNT, 2005). The presence of the healing admixture reduces both mixture porosity water absorption and void indices.

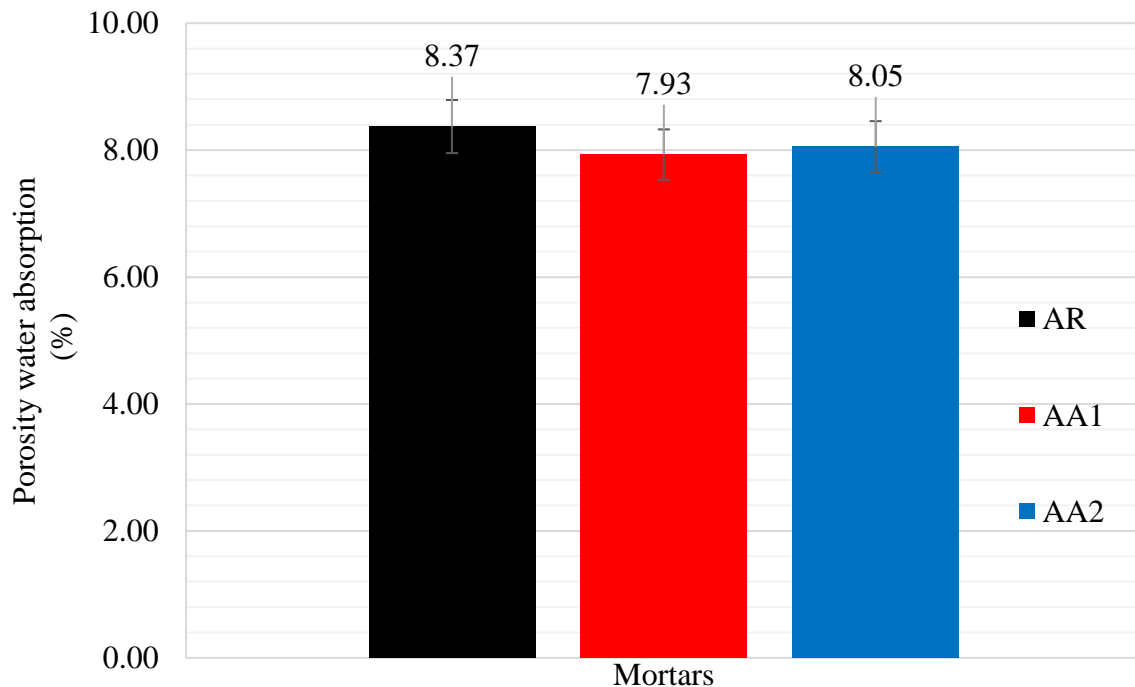


Figure 9. Porosity water absorption test or pressure water absorption (%) results in mortar specimens immersed in water at 28 days.

This test, because it is carried out with specimens under pressure, identifies the open and closed porosity and the total void indices of the mortars. The specimen containing 1% of the admixture attained the best results, attesting that the range of contents indicated by the manufacturer is adequate. By increasing the admixture content to a value higher than the indicated range, a new increase is observed both in porosity and in the void index. However, even though the results of mortars containing the admixture are better than the reference mixture, the difference between them is not significant, with the largest reduction in porosity and void rate of around 5.3%.

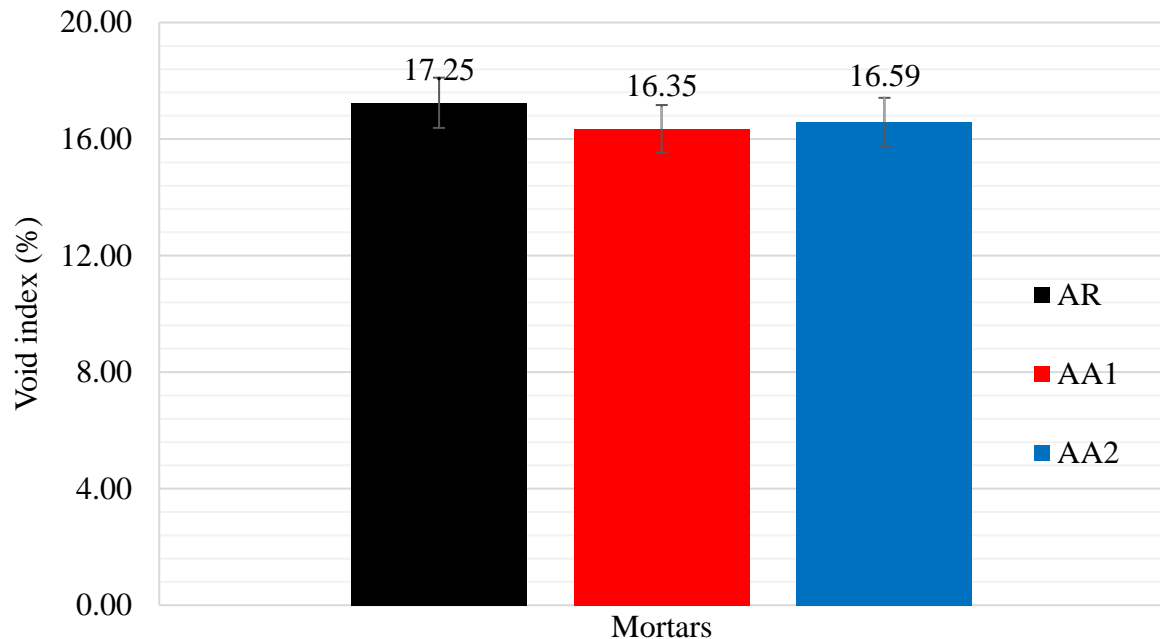


Figure 10. Void index (%) test results of mortar specimens immersed in water at 28 days.

Figures 11 and 12 display the results obtained in the absorption and capillarity coefficient tests, performed according to the NBR 15259 standard (ABNT, 2005). Capillarity absorption is defined by the cross-sectional area being measured in constant contact with water, in grams per square centimeter. The addition of the healing admixture above 1% considerably reduces mortar capillarity absorption.

The capillarity values, given the result shown in Figure 11, can reduce by approximately 20%, again attesting the sealing power of the admixture. Similar results were reported by Takagi, Lima and Helene (2012) and Pazderka and Hájková (2016), both using 2% admixture.

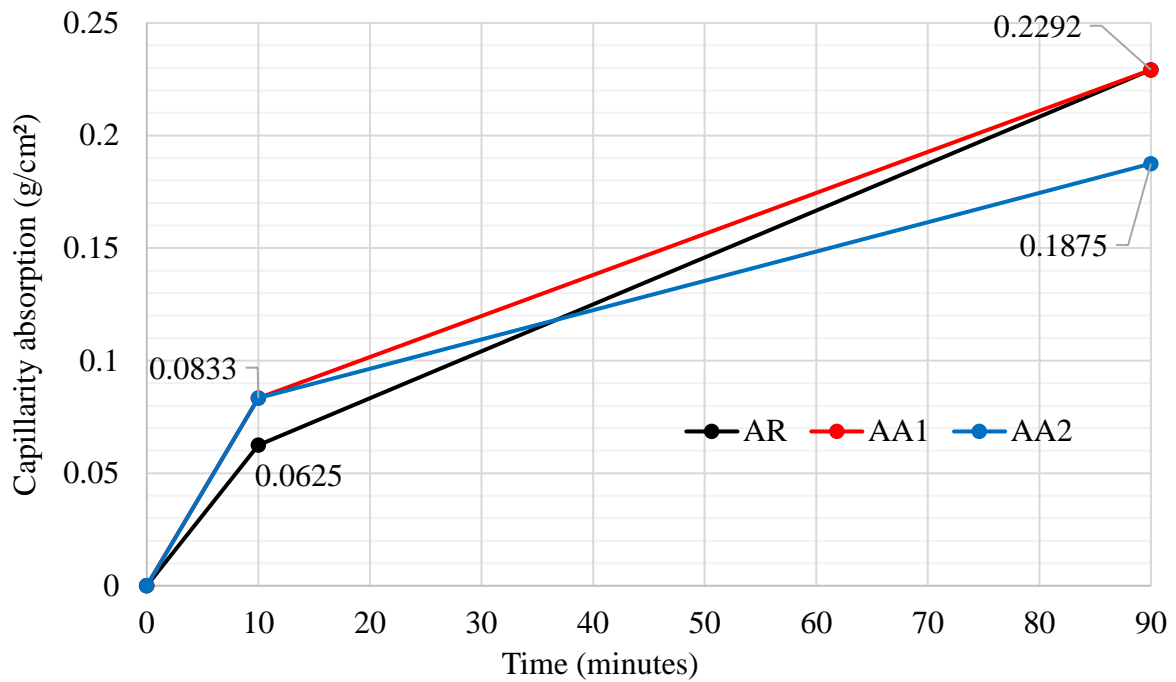


Figure 11. Water absorption capillarity (%) test results in a mortar specimen in contact with a water layer at a constant level of 5mm.

The capillarity coefficient refers to the slope of the line that passes through the representative points of readings taken at 10 and 90 minutes, calculated by subtracting the masses recorded in these determinations.

The higher the admixture content, the lower the capillarity coefficient and, consequently, the lower the capillarity absorption for a fraction of time. As in the previous data, the AA2 mixture presented the best results, reaching a coefficient about 37.5% lower than the RA, while AA1 reached a reduction of 12.7% compared to the RA.

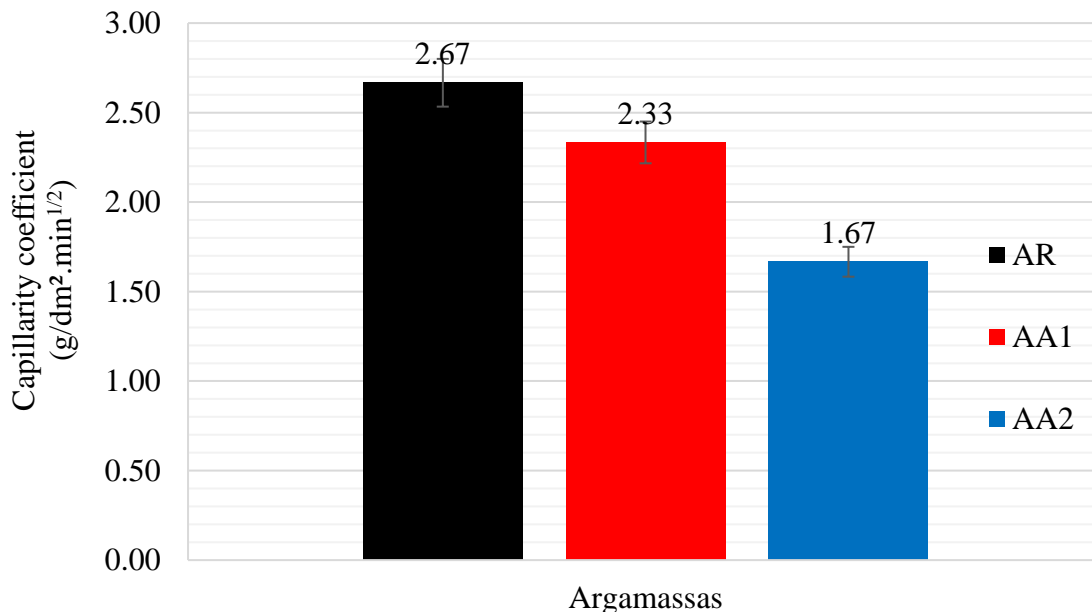


Figure 12. Capillarity coefficients (g/dm<sup>2</sup>.min<sup>1/2</sup>) of the mortars, determined with readings taken at 10 and 90 minutes.

Figure 13 presents the results regarding the expansion determinations during the accelerated ARR mortars tests according to the NBR 15577-4 standard (ABNT, 2018). A high initial expansion, at 6 days, was observed in mortars containing the crystallizing admixture.

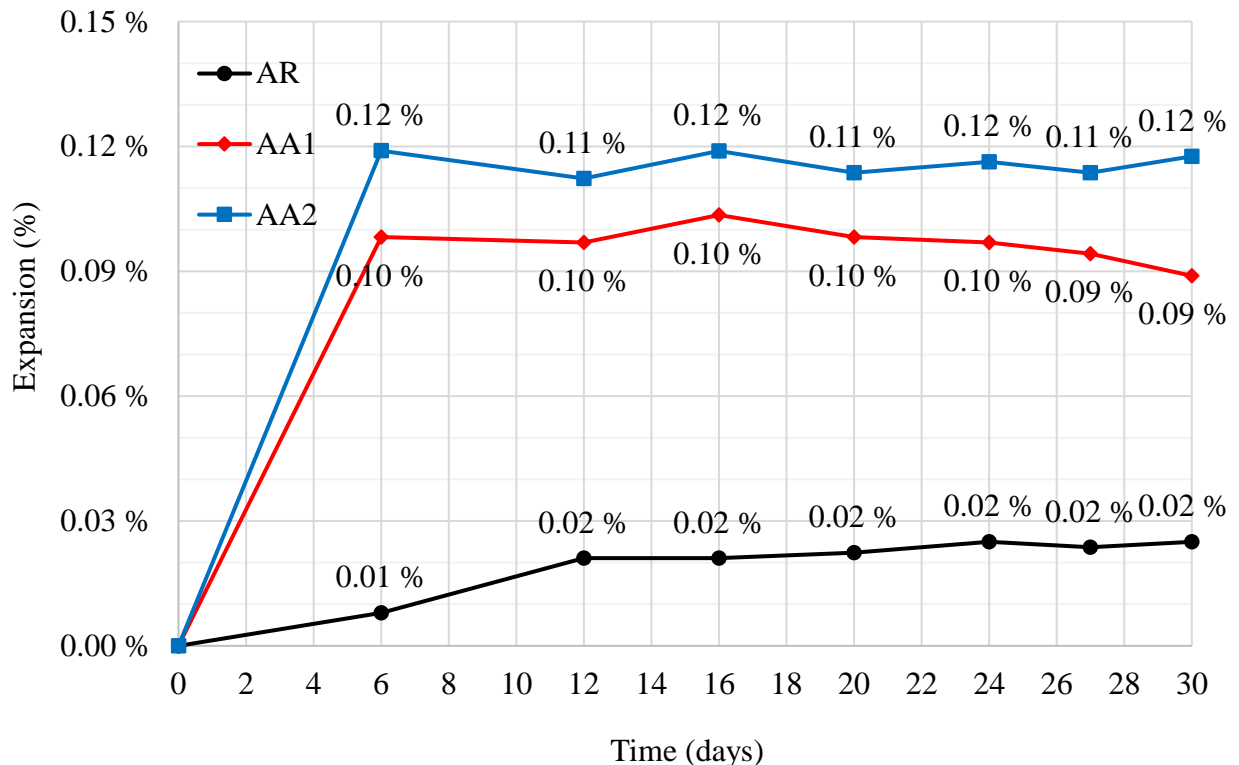


Figure 13. Expansion (%) of mortar specimens during accelerated AAR tests recorded for 30 days after molding.

This result indicates that the alkaline products present in the admixture composition, described in Table 5, may have led to the evolution of the expansions in the first week, considering that an evident initial volumetric evolution increase is noted with increasing admixture contents.

The differences between mortar variations are significant, where AA2 underwent an initial expansion at 6 days about 1100% higher than RA, while AA1 exhibited a 900% increase in expansion compared to RA. However, after this 6-day period, expansion ceased, specimen dimensions stabilized and, consequently, percentage expansions decreased as a function of time, to 500% and 350%, respectively.

The expansions were clearly caused by the admixture, as the AR mortar exhibited much lower values. The chemical admixture composition indicates that the reactions may have been caused by magnesium, although further research focusing on microstructural assessments is required.

Regardless, the admixture seems to display an activation time of approximately one week, starting void and pore sealing and controlling volumetric mortar variations beginning at the moment of expansion stabilization.

It is important to note that these readings were recorded on small-sized mortar prismatic specimens. If applied on a large scale, the use of the admixture may require some attention to the limits set by the manufacturer, in order to avoid further inconveniences.

The use of products that inhibit alkali-aggregate reactions, such as pozzolanic materials, is indicated, as they will inhibit initial expansions and prevent damage to concrete or mortar

components in the early stages, allowing admixture constituents to seal pores and voids. However, admixture behavior analyses in conjunction with pozzolanic materials, such as active silica, should be evaluated and remains as a suggestion for future research.

Finally, regarding the potential reactivity classification of the aggregate, considering the limits established in the NBR 15577-1 standard (ABNT, 2018), the material proved to be potentially harmless grade R0, i.e. the mortar bar expansion at 30 days was less than 0.19%. Although the differences between the mortar expansions are high, the degree of risk related to this classification is negligible, and no mitigation action due to ARR is necessary, depending on the aggregate.

## 5. CONCLUSIONS

The crystallizing admixture used herein, did not cooperate in the first days regarding the inhibition of the alkali-aggregate reaction. On the contrary, the presence of alkaline products in the admixture composition increased initial expansion until the admixture reacted with cement hydration products. Therefore, the use of ARR-inhibiting materials, such as pozzolans, is indicated in parallel with healing admixtures of similar chemical composition.

Nevertheless, the admixture use was quite satisfactory concerning mechanical performance, water absorption and void indices when present at 1% and 2%. Admixture use resulted in compression and flexion traction resistance gains, in addition to decreased void indices and porosity absorption. However, its greatest asset lies in the significant reduction of capillarity coefficients and absorption, indicated for elements in constant contact with water, such as reservoirs and basic sanitation systems.

## 6. REFERENCES

- Associação Brasileira De Normas Técnicas. (2019). *NBR 7215: Cimento Portland - Determinação da resistência à compressão de corpos de prova cilíndricos*. Rio de Janeiro.
- Associação Brasileira De Normas Técnicas. (2009). *NBR 9778: Argamassa e concreto endurecidos - Determinação da absorção de água por imersão - Índice de vazios e massa específica*. Rio de Janeiro.
- Associação Brasileira De Normas Técnicas. (2016). *NBR 13276: Argamassa para assentamento e revestimento de paredes e tetos - Determinação do índice de consistência*. Rio de Janeiro.
- Associação Brasileira De Normas Técnicas. (2005). *NBR 13278: Argamassa para assentamento de paredes e revestimento de paredes e tetos - Determinação da densidade de massa e do teor de ar incorporado*. Rio de Janeiro.
- Associação Brasileira De Normas Técnicas. (2005). *NBR 13279: Argamassa para assentamento e revestimento de paredes e tetos - Determinação da resistência à tração na flexão e à compressão*. Rio de Janeiro.
- Associação Brasileira De Normas Técnicas. (2005). *NBR 15259: Argamassas para assentamento e revestimento de paredes e tetos – Determinação da absorção de água por capilaridade e do coeficiente de capilaridade*. Rio de Janeiro.
- Associação Brasileira De Normas Técnicas. (2018). *NBR 15577-1: Agregados - Reatividade álcali-agregado Parte 1: Guia para avaliação de reatividade potencial e medidas preventivas para uso de agregados com concreto*. Rio de Janeiro.
- Associação Brasileira De Normas Técnicas. (2018). *NBR 15577-4: Agregados - Reatividade álcali-agregado Parte 4: Determinação da expansão em barras de argamassa pelo método acelerado*. Rio de Janeiro.
- Associação Brasileira De Normas Técnicas. (2018). *NBR 16697: Cimento Portland - Requisitos*. Rio de Janeiro.

- Cadersa, A. S., Zephir, D. (2014), Effect of Penetron Admix on the Properties of concrete. *University Of Mauritius Research Journal*, v. 20, Réduit.
- Couto, T. A. (2008). *Reação Álcali-Agregado: estudo do fenômeno em rochas silicosas*. 2008. 191 p. Dissertação de Mestrado em Engenharia Civil, Escola de Engenharia Civil, Universidade Federal de Goiás, Goiânia.
- García-Vera, V. E., Tenza-Abril, A. J., Saval, J. M., Lanzón, M. (2019). *Influence of Crystalline Admixtures on the Short-Term Behaviour of Mortars Exposed to Sulphuric Acid*. *Materials*, v. 12, n. 82, p. 16. <https://doi.org/10.3390/ma12010082>
- Japan Concrete Institute, JCI - TC075B. (2009). *State-of-the-art report of the JCI Technical committee TC-075B: Autogenous healing in cementitious materials*. In: 4<sup>o</sup> International Conference on Construction Materials: Performance, Innovations and Structural Implications, ConMat'09. Nagoya, Japan.
- Junior, A. B., Ferro, I. P. (2016). *Reação álcali-agregado: um breve estudo da ocorrência nos blocos da ponte Paulo Guerra – Recife/PE*. In: Congresso Brasileiro de Patologia das Construções (CBPAT). *Anais...* Belém: ALCONPAT.
- Moreira, M. M. (2016). *Efeito do aditivo redutor de permeabilidade em concretos com diferentes tipos de cimento Portland – Contribuição aos processos de autocatização*. 162 f. Dissertação de Mestrado em Estruturas e Construção Civil, Departamento de Engenharia Civil e Ambiental, Universidade de Brasília, DF.
- Pazderka, J., Hájková, E. (2016). *Crystalline admixtures and their effect on selected properties of concrete*. *Acta Plytechnica*, n. 56, p. 306-311. <https://doi.org/10.14311/AP.2016.56.0306>
- Penetron (2018). *Penetron Admix*. Lorena, Penetron.
- Roig-Flores, M., Moscato, S., Serna, P., Ferrara, L. (2015). *Self-healing capability of concrete with crystalline admixtures in different environments*. *Construction And Building Materials*, v. 86, p. 1-11. <http://dx.doi.org/10.1016/j.conbuildmat.2015.03.091>.
- Rolim, P. H. B. (2010). *Reação álcali-agregado: avaliação do método químico de ensaio*. 109 f. Dissertação de Mestrado, Faculdade de Engenharia Civil, Universidade Federal de Santa Catarina, Florianópolis.
- Silva, P. N. (2007). *Reação álcali-agregado nas usinas hidrelétricas do complexo Paulo Afonso/CHESF.: Influência da Reação nas Propriedades do Concreto*. 2007. 241 f. Dissertação de Mestrado, Faculdade de Engenharia Civil, Universidade de São Paulo, São Paulo.
- Takagi, E. M., Lima, M. G., Helene, P. R. L. (2012). *Contribuição para estudo do efeito da autocatização em concretos ativado por catalisadores cristalinos em estruturas de túneis submetidas à exposição contínua de água*. In: Congresso Brasileiro de Túneis e Estruturas Subterrâneas, 3, *Anais...* São Paulo: Seminário Internacional “South American Tunnelling”.

## Corrosion effect on reinforced concrete with the addition of graphite powder and its evaluation on physical-electrochemical properties

A. Flores-Nicolás<sup>1</sup> , M. Flores-Nicolás<sup>1</sup> , J. Uruchurtu-Chavarín<sup>1\*</sup> 

\*Contact author: [juch25@uaem.mx](mailto:juch25@uaem.mx)

DOI: <https://doi.org/10.21041/ra.v11i1.501>

Reception: 28/07/2020 | Acceptance: 06/11/2020 | Publication: 01/01/2021

### ABSTRACT

The corrosion of reinforced concrete without and with the addition of graphite powder with low carbon content was evaluated. Phase identification processes and physical-electrochemical properties of the concrete were analyzed using X-ray diffraction techniques (XRD), scanning electron microscopy (SEM), half-cell potential, electrochemical noise (EN) and linear polarization resistance (LPR). Samples were studied for 168 days in saline solution. The results show that, when adding graphite powder in an amount of 2.5% by weight of cement, the compressive strength increased if compared with the control sample. The electrochemical tests show that the higher the level of graphite replacement, the higher the level of corrosion in concrete.

**Keywords:** reinforced concrete; graphite; corrosion; chlorides.

**Cite as:** Flores-Nicolás, A., Flores-Nicolás, M., Uruchurtu-Chavarín, J. (2021), " *Corrosion effect on reinforced concrete with the addition of graphite powder and its evaluation on physical-electrochemical properties*", Revista ALCONPAT, 11 (1), pp. 18 – 33, DOI: <https://doi.org/10.21041/ra.v11i1.501>

<sup>1</sup> Centro de Investigación en Ingeniería y Ciencias Aplicadas (CIICAp), Instituto de Investigación en Ciencias Básicas y Aplicadas (IICBA), Universidad Autónoma del Estado de Morelos, Cuernavaca, México.

#### Contribution of each author

In this work, the author A. Flores-Nicolás contributed with the original idea, data collection, experimental methodology, discussion of results and the writing of the work. The author M. Flores-Nicolás contributed with the coordination of the experiments, writing and review of the work. The author J. Uruchurtu-Chavarín contributed with the overall coordination of the work, review, author orientation and supervision of the activities.

#### Creative Commons License

Copyright 2021 by the authors. This work is an Open-Access article published under the terms and conditions of an International Creative Commons Attribution 4.0 International License ([CC BY 4.0](https://creativecommons.org/licenses/by/4.0/)).

#### Discussions and subsequent corrections to the publication

Any dispute, including the replies of the authors, will be published in the third issue of 2021 provided that the information is received before the closing of the second issue of 2021.

## **Efecto de la corrosión del concreto reforzado con adición de polvo de grafito y su evaluación en sus propiedades físico-electroquímicas**

### **RESUMEN**

En este trabajo se evaluó el efecto de la corrosión del concreto reforzado sin y con adición de polvo de grafito con bajo contenido de carbono. Los procesos de identificación de fases y las propiedades físico-electroquímicas del concreto se analizaron mediante técnicas de difracción de rayos X (DRX), microscopía electrónica de barrido (MEB), potencial de media celda, ruido electroquímico (EN) y resistencia a la polarización lineal (RPL). Las muestras se estudiaron durante 168 días en solución salina. Los resultados muestran que al adicionar polvo de grafito en cantidad de 2.5% en peso del cemento, se incrementó la resistencia a la compresión en comparación con la muestra control. En las pruebas electroquímicas se demuestra que la corrosión del acero de refuerzo en el concreto se incrementó al aumentar el nivel de reemplazo de grafito.

**Palabras clave:** concreto reforzado; grafito; corrosión; cloruros.

## **Efeito na corrosão do concreto reforçado com adição de pó de grafite e sua avaliação nas propriedades físico-electroquímicas**

### **RESUMO**

Neste trabalho avaliou-se o efeito da corrosão do concreto armado sem e com adição de pó de grafite com baixo teor de carbono. Os processos de identificação de fases e as propriedades físico-electroquímicas do concreto foram analisados por técnicas de difração de raios X (DRX), microscopia eletrônica de varrimento (MEV), potencial de meia célula, ruído eletroquímico (EN) e resistência à polarização linear (RPL). As amostras foram testadas em solução salina durante 168 dias. Os resultados mostram que ao adicionar pó de grafite em uma quantidade de 2,5% em peso do cimento, a resistência à compressão foi aumentada em comparação com a amostra de controle. Em testes eletroquímicos, mostra que a corrosão das armaduras de aço no concreto, aumentou conforme o nível de substituição de grafite aumentou.

**Palavras-chave:** concreto reforçado; grafite; corrosão; cloretos.

### **Legal Information**

Revista ALCONPAT is a quarterly publication by the Asociación Latinoamericana de Control de Calidad, Patología y Recuperación de la Construcción, Internacional, A.C., Km. 6 antigua carretera a Progreso, Mérida, Yucatán, 97310, Tel.5219997385893, [alconpat.int@gmail.com](mailto:alconpat.int@gmail.com), Website: [www.alconpat.org](http://www.alconpat.org)

Reservation of journal title rights to exclusive use No.04-2013-011717330300-203, and ISSN 2007-6835, both granted by the Instituto Nacional de Derecho de Autor. Responsible editor: Pedro Castro Borges, Ph.D. Responsible for the last update of this issue, Informatics Unit ALCONPAT, Elizabeth Sabido Maldonado.

The views of the authors do not necessarily reflect the position of the editor.

The total or partial reproduction of the contents and images of the publication is carried out in accordance with the COPE code and the CC BY 4.0 license of the Revista ALCONPAT.

## 1. INTRODUCTION

Reinforced concrete is one of the most used materials in the construction industry in the vast majority of civil works and has been transformed into one of the most resistant structures due to its mechanical properties. Numerous investigations have studied the durability of reinforced concrete structures because it requires high technology for its conservation and maintenance needs (Vidaud and Vidaud, 2012). Corrosion of reinforcing steel is one of the main causes of durability of concrete. This phenomenon is affected by the type of environment to which it is exposed to and then damaging the structure over time. Necessarily, the concrete paste gives steel a dual nature protection to embedded steel; first it acts as a physical barrier that isolates it from the environment, and second the liquid enclosed in the pores of the concrete is an electrolyte that passivates it permanently (González and Jimmy, 2003). These properties are affected, so using new materials in concrete paste is important to improve its physical properties and extend the durability of concrete structures.

Currently, the use of cement-based compounds with carbon particles and other additions, are new composite materials with some excellent physical and chemical properties that make them suitable for use in technologically advanced products (Chung, 2000). The main carbon materials added to concrete include carbon fibers, graphite flakes, graphite powder or carbon nanotubes, this research being directed to the use of graphite powder. Graphite is an allotropic form of the carbon element, consisting of sheets of carbon atoms (graphenes) that form a flat condensed ring system. There are two possible ways of stacking them: the hexagonal Bernal (ABAB) and the rhombohedral (ABCABC) types; the structure called “simple hexagonal” (Tascón, 2007).

(Heymsfield et. al., 2013) have incorporated this element into the concrete paste and reported that the absorption of graphite powder decreased as the size of the graphite powder aggregate increased, in consequence, the mechanical resistance of the mix design increased as the size of the graphite powder aggregate increased. Also, indicates that the graphite content could improve mostly thermal conductivity properties and reduce the specific heat capacity (Wu et. al., 2014).

(Yuan et. al., 2012) studied ground expanded graphite (G) with high temperature and reported that compressive strength decreases with the addition of graphite and increasing w/c ratio, while, thermal conductivity and the volume of heat capacity increases with the addition of graphite. On the electrochemical properties tests it shows that a decrease in the level of corrosion occurs when the carbon material addition ratio is increased (Garcés et. al, 2007).

(Ha et. al., 2005) investigated the corrosion of reinforcing steel embedded in ordinary Portland cement and reported severe corrosion when the level of carbon and fly ash increased. The condition of wetting and drying with sodium chloride NaCl 3% was found between 6% and 8% of carbon mixed with fly ash.

This research topic presents a study on the corrosion behavior of reinforced concrete, with addition of graphite powder (GP) as a partial substitute for the weight of cement and analysis on its physicochemical properties.

## 2. EXPERIMENTAL PROCEDURE

### 2.1 Preparation of test pieces

The concrete mixes were prepared using the ACI design method (ACI. 211.1-91, 2002), a theoretical design resistance of  $250 \text{ kg/cm}^2$  after 28 days of curing period and a concrete slump of  $12 \pm 2 \text{ cm}$ ; using Portland cement CPC 30 R (ASTM C-150, 2020); as fine aggregate river sand was used with a maximum nominal size of 4.75 mm and coarse aggregate of crushed stone maximum size of 19 mm. Conventional corrugated 1018 reinforcing steel was used and abraded paper was used for pre-cleaning. Graphite powder (GP) was added in the following percentages: 0% (sample control), 2.5%, 7.5% and 15% regarding the weight of the cement. Table 1 shows the main characteristics of the GP.

Table 1. Characteristics of the GP used.

Material	Diameter ( $\mu\text{m}$ )	Density ( $\text{g/cm}^3$ )	Humidity (%)	Hardness (Mohs)
GP	63	2.22	2.5	1-2

The dosage of the materials used in this work is mentioned in Table 2. The weight of the fine and coarse aggregates was not modified, also no additive was used in the concrete mix. More water was added to samples M3 and M4 with a graphite quantity of 7.5% and 15% by weight of cement, because the paste was not very workable, and this maintained the concrete slump range of  $12 \pm 2 \text{ cm}$  for the 4 mix designs.

Table 2. Mix design ratio for  $1 \text{ m}^3$ .

Material	M1-0%	M2-2.5%	M3-7.5%	M4-15%
Cement (Kg)	366	357	339	311
Water(l)	218	218	235	251
w/c	0.59	0.61	0.69	0.81
Sand (Kg)	817	817	817	817
Gravel (Kg)	903	903	903	903
GP (Kg)	000	009	027	055

The preparation of concrete samples was done according to (ASTM C-31, 2019). For electrochemical tests 3 cubic specimens 10 cm per side were made from the same mix design, as shown in Figure 1. Three corrugated rods were embedded in each cubic specimen, of dimensions 0.95 mm in diameter. The length of the embedded rod was 5.5 cm. At the interface between the paste and the atmospheric environment, the rod was covered with approximately 5 cm long with teflon tape around the rod.

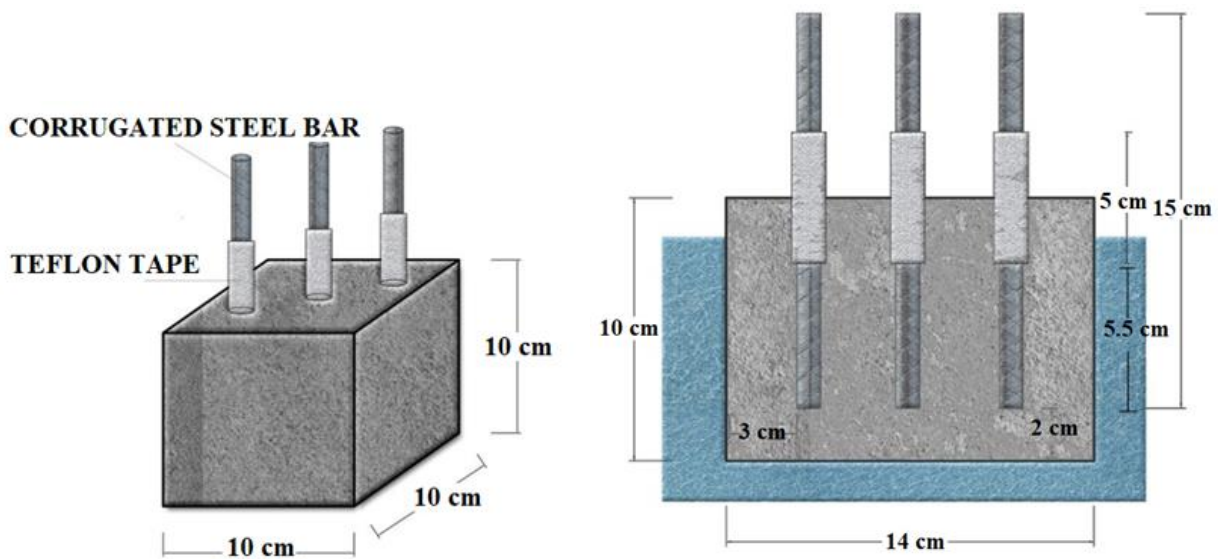


Figure 1. Cubic dimensions of concrete specimen.

Specimens were cured for 28 days, in adequate humidity conditions. Electrochemical measurements started 24 hours after the cubic specimens were immersed in a 3% saline solution of sodium chloride, for 168 days of exposure.

### 2.1.1 Determination of the porosity of concrete

Measurement of air content was performed by the pressure method and type B pressure meter container according to (ASTM C-231, 2017). The porosity of concrete ( $P$ ) or total voids in the composite material was modeled (1) as a function of: the water/cement ratio, the degree of hydration of the cement ( $h$ ), the volume of trapped air ( $A$ ), the amounts of fine aggregates (sand,  $A_f$ ) and coarse aggregate (gravel,  $A_g$ ), and cement ( $c$ ) and the specific gravities of the aggregates ( $\rho_f$  y  $\rho_g$ ). The value of 0.7 for cement hydration was applied in this study (Solís-Carcaño y Moreno, 2006).

$$P = \frac{\left[\left(\frac{a}{c}\right) - 0.36h + \left(\frac{A}{c}\right)\right]}{0.317 + \left(\frac{1}{\rho_f}\right)\left(\frac{A_f}{c}\right) + \left(\frac{1}{\rho_g}\right)\left(\frac{A_g}{c}\right) + \left(\frac{A}{c}\right)} \quad (1)$$

## 2.2 Compressive strenght technique

The compressive strength test, was performed according to the parameters of (ASTM C-39, 2020) standard. Cylindrical samples with standard dimensions were built with 15 cm in diameter and 30 cm high. The compression test was carried out at 7, 14 and 28 days of curing, to observe the increase in resistance upon reaching maximum value for the curing time. Cylinder uniformity was performed with neoprene plates and a constant load was applied until the sample failed.

## 2.3 Electrochemical techniques

### 2.3.1 Half cell potential measurement

Standard (ASTM C-876-09, 2009), sets intervals on corrosion potential ( $E_{\text{corr}}$ ) that indicate the probability in corrosion of the surface and the possible risk for the rebar. With the obtained values it is feasible to make a diagnosis of the degree of corrosion of the rebar embedded in concrete. Half cell potential measurement analysis was performed based on the use of saturated silver/ silver

chloride reference electrode (Ag/AgCl). The potential measurement of each steel bar embedded in the concrete was determined, the recorded value is the average of these three measurements. Measurements were made over 168 days of salt solution exposure. A multimeter and a switch that connected the two electrodes were used, between the silver/silver chloride and steel bar. Table 3 presents the conversion of the corrosion half-cell potentials used to the saturated copper / copper sulfate reference electrode by adding +50 mV (Berkeley et. al., 1990; Chess et. al., 1998).

Table 3. Criteria for measuring the risk of damage to concrete reinforcing steel, measuring the half-cell potential.

$E_{corr}$ vs Cu/CuSO <sub>4</sub> (mV)	$E_{corr}$ vs Ag/AgCl (mV)	Risk of harm (%)
> -200	>-150	10% probability of corrosion
Between -200 A -350	Between -150 A -300	Uncertainty Zone
< -350	< -300	90% probability of corrosion

### 2.3.2 Electrochemical noise technique

Corrosion is considered as a process in equilibrium and with constant kinetics, while, in the case of electrochemical noise, imbalances in electrochemical reactions are recorded in very short time intervals (Goellner et. al., 2004). For the electrochemical noise measurements, it was used a Gill AC-ACM Instruments, 1024 reading samples were taken with a constant interval of 1 point/second. The configuration for measurement was three nominal identical steel rods, whereas the third electrode nominally identical to the two working electrodes acts as a reference electrode (Sánchez-Amaya et. al., 2009; Blanco et. al., 2019).

Electrochemical noise can be characterized by common statistical parameters such as the mean, the variance and the standard deviation; in particular the use of the potential/current standard deviations can be done separately, either by its quotient. Called noise resistance ( $R_n$ ), in the expression (2) it is calculated as the quotient between the standard deviations of the potential over current records (Sánchez et. al., 2005; Bertocci et. al., 1997).

$$R_n = \frac{\sigma V}{\sigma I} \quad (2)$$

In addition to what was mentioned above, another statistical value is used for the analysis of current noise, according to the equation (3) being the ratio of the standard deviation to the root mean square, called “localization index or pitting” (L.I ó I.P), (Sánchez et. al., 2005).

$$L.I = \frac{\sigma I}{rms} \quad (3)$$

Table 4 shows the range of localization index values representing the type of corrosion in the reinforcing steel.

Table 4. Locazation index values.

Location index	Corrosion type
0.001 - 0.01	Generalized
0.01 –0.1	Mixed
0.1 – 1	Localised
> 1	Start of pitting

According to the ranges of values (Rincón and DURAR et. al., 1997), the service life of reinforced concrete can be determined from the current density ( $i_{corr}$ ), with the data established in Table 5.

Table 5. Service life level in the steel / concrete system.

$i_{corr}$ ( $\mu\text{A}/\text{cm}^2$ )	Corrosion level
< 0.1	Negligible
0.1 –0.5	Moderate
0.5 – 1	High
> 1	Very high

### 2.3.3 Linear polarization resistance technique

For the measurement of resistance of linear polarization using the same Gill AC-ACM Instruments, a small voltage signal was applied between -50 mV and +50 mV around the corrosion potential (ASTM G-59-97, 2014). The linear polarization method,  $R_p$ , can be obtained graphically by the expression (4) as the tangent to the polarization curve in  $E_{corr}$  (Román et. al., 2016).

$$R_p = \frac{dE}{di} \quad (4)$$

From the Stern-Geary equation (5), corrosion current density was related  $i_{corr}$ , with the  $R_p$ , through a constant of proportionality B (Román et. al., 2016). Constant B can acquire the values of 0.026 V to 0.052 V, depending on the type of system analyzed (Sagües, 1991).

$$I_{corr} = \frac{B}{R_p} \quad (5)$$

## 3. RESULTS AND DISCUSSION

### 3.1 X-ray diffraction characterization

Figure 2 details the GP diffractograms obtained from the XRD techniques, orderly fit polycrystalline solid shown and with a peak intensity with values of  $2\theta$  approximately  $26^\circ$  and  $27^\circ$ . These values are similar to some reported by authors who describe the characteristic peak of graphite (Yuan et. al., 2012). Two different crystalline forms of carbon are presented: hexagonal (2H) and rhombohedral (3R).

The 2H structure, is the most common form in the phases identified with 39.9% values and the 3R with 27.4% values, with a total addition of 67.3% in carbon content. The sample contains 32.6% of clay components as: quartz, smectic phyllosilicates, kaolinite, mica.

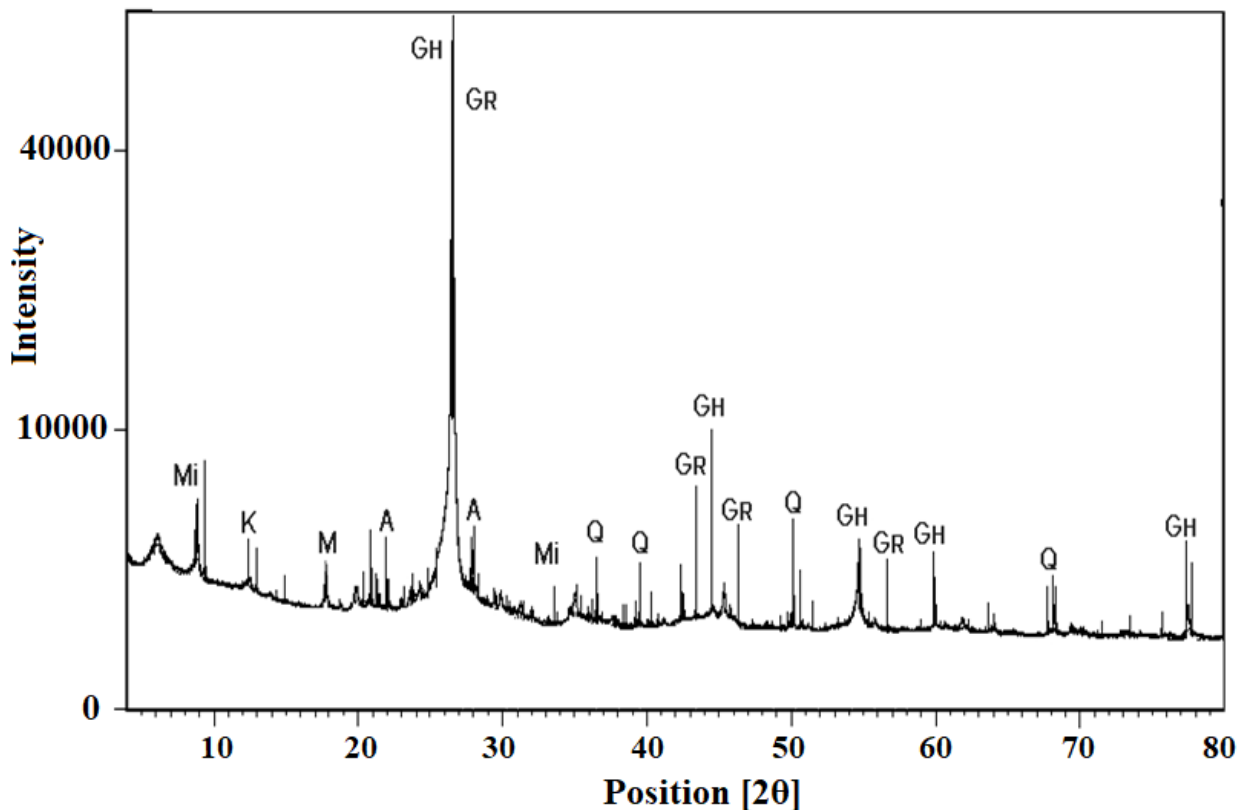


Figure 2. X-ray diffractograms of the GP. Mi: mica; K: kaolinite; M: montmorillonite; G<sub>H</sub>: graphite (2H); G<sub>R</sub>: graphite (3R); A: anortite; Q: Quartz.

Figure 3 corresponds to the diffractograms of the control sample and with the addition of GP, after 28 days curing period. The 28 day hydrated cement produces the following phases: calcium hydrated silicate (CSH) which is responsible for the adherence and resistance with binders, ettringite (E) that gives greater cohesion to cement and portlandite (CH) that maintains alkalinity, that is, the paste pH at high values between 12-13 (Helena and Lucia, 2011; Giraldo and Tobón, 2006).

Figure 3a shows the crystalline phases of hydration of concrete: high peaks of quartz (Q) and calcite (Ca) were observed; in addition to dolomite (D) and plagioclase or Andesine (A). The main abundant elements that appear in the control sample are Q y Ca, due to the main presence of limestone in the cement.

Figure 3 b), c) and d) show the samples with different percentage of graphite, as it can be seen a peak intensity that does not increase with increasing GP, which shows that there is an absence of direct participation in the hydration of the concrete paste. It is observed that the XRD analysis does not show a strong intensity in the CH and CSH peaks; various authors indicate that peaks with values of  $2\theta$  approximately  $29^\circ$  can be assigned to the CSH phase, and peaks with  $2\theta$  values approximately  $18^\circ$  and  $34^\circ$  can be assigned to CH (Giraldo and Tobón, 2006; Becerra, 2014). The absence of portlandite in the diffractogram may be due to the fact that the sample comes from the cylinder surface, where carbonation effects can obscure identification (Vetter et. al., 2019).

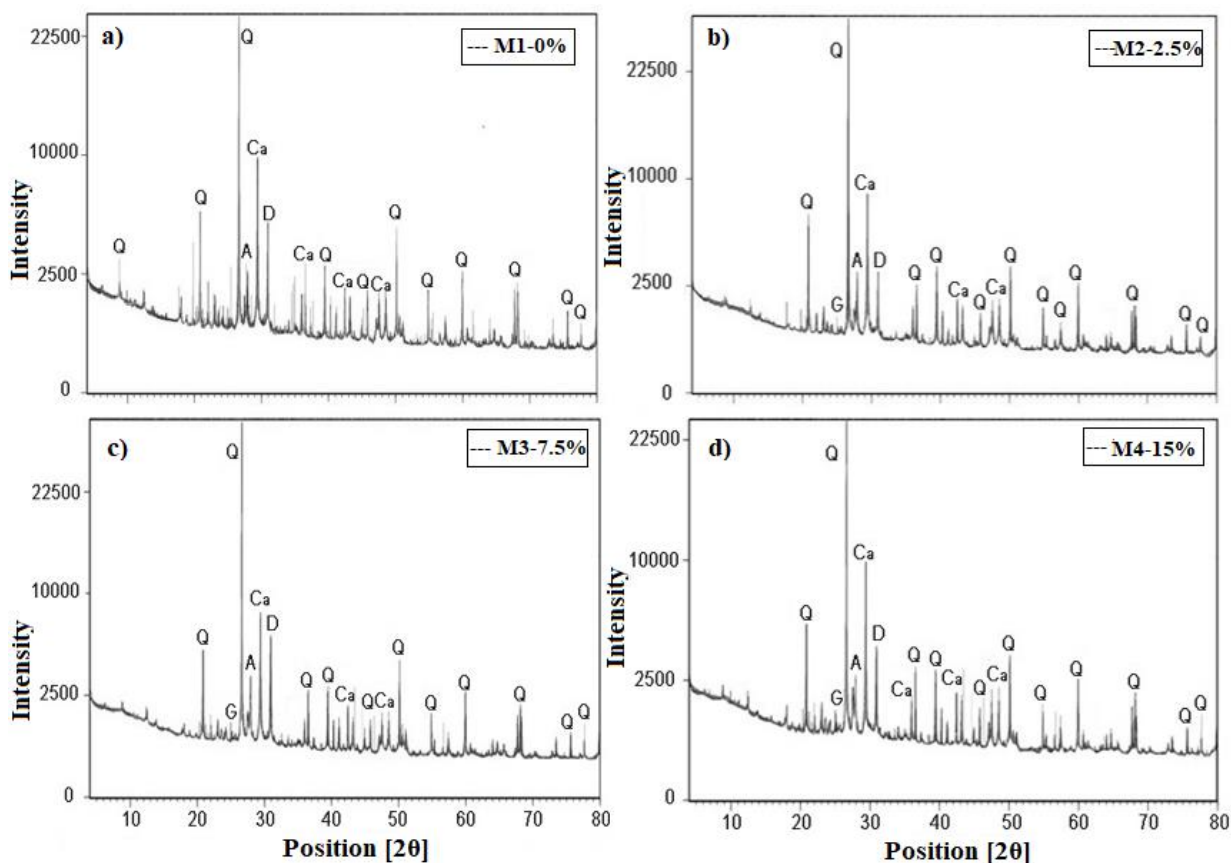


Figure 3. X-ray diffractograms of concrete paste. a) M1-0%, b) M2-2.5% c) M3-7.5% y d) M4-15%. Q: quartz; Ca: calcite; D: dolomite; G: graphite; A: andesine, cured at 28 days.

### 3.2 Scanning electron microscope characterization

The SEM micrographs of the concrete are presented in Figure 4, the visual analysis of Figure 4a belongs to the control sample M1, microcracks (m) can be seen in the paste matrix, as a result of the compressive resistance and sample extraction technique. Together calcium silicates hydrated were observed (CSH), and greater presence of portlandite (CH) and ettringite (S). For the visual analysis of the S crystals they are elongated shapes, generally in fibrous habitats or in the form of long rods. CH normally occurs as thin hexagonal platelets, often tenths of a micrometer wide (Vetter et. al., 2019).

Figure 4b corresponds to the micrograph of sample M3 with 7.5% GP, a compact structure with greater CSH formation is visualized, filling the empty areas of the cement matrix, reducing the porosity of the concrete and improving the adhesion on the carbon particle (GP).

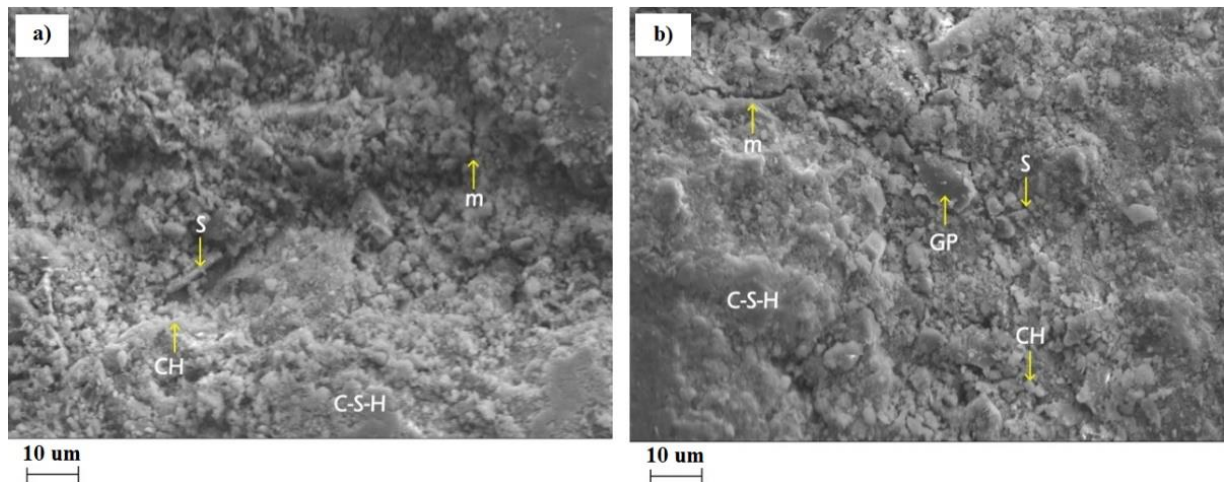


Figure 4. SEM micrograph, a) M1-0% and b) M37.5% of GP, cured for 28 days.

### 3.3 Concrete porosity

Table 6 shows the percentage values of concrete porosity. As it can be seen, by adding graphite content in 2.5% by weight of cement, the mixture acquires a higher water absorption and affects the water/cement ratio compared to the control sample. Sample M1 has a porosity percentage of 22% with w/c ratio of 0.59, the results show that in the M2 design with 2.5% GP the porosity of the concrete decreases with respect to the sample M1; the samples M3 and M4 register a greater increase in the w/c ratio due to the increase in the amount of water added with values of 0.61 and 0.81.

In terms of concrete durability, an increase in the porosity of the paste, causes environmental agents to require the material to be permeable in order to penetrate through the mass of the material; these agents are also added for their internal transport by diffusion (Solís-Carcaño and Moreno, 2006).

Table 6. Porosity of concrete.

Samples	w/c	Porosity (%)
M1-0	0.59	22.00
M2-2.5	0.61	19.30
M3-7.5	0.69	20.80
M4-15	0.81	24.80

### 3.4 Compressive resistance

Table 7 shows the average values of compressive resistance ( $f'c$ ) after 7, 14 and 28 days of curing. The control sample M1-0, was designed for a theoretical resistance of 250 kg/cm<sup>2</sup>, during the 28 days of curing. It acquired an average maximum experimental resistance of 258 kg/cm<sup>2</sup>, exceeding the theoretical design value. Sample M2 with 2.5% GP, an increase in compressive resistance is observed at early ages of 7 days with a value of 242 kg/cm<sup>2</sup>. During the 28 days of curing the compressive resistance increased by 4.6% compared to the strength of the control sample. Sample M3 with 7.5% GP, during the days of curing a constant increase of  $f'c$  is observed reaching a final resistance to compression of 267 kg/cm<sup>2</sup>; sample M4 with 15% GP shows a low  $f'c$  with a value of 244 kg/cm<sup>2</sup>, due to the increased amount of water added.

Table 7. Compressive resistance values ( $f'c$ ).

Samples	Compressive resistance (Kg/cm <sup>2</sup> )		
	7 days	14 days	28 days
M1-0	181.5	235.9	257.7
M2-2.5	242.0	267.3	271.5
M3-7.5	199.9	241.8	266.8
M4-15	188.9	222.1	244.2

### 3.5 Half-cell potential

After 168 days immersed in 3% sodium chloride (NaCl) saline solution, the results of the corrosion potential ( $E_{corr}$ ) are detailed in Figure 5. A decrease in potential was observed in the first days for all samples, acquiring more negative values between -100 mV and -250 mV, estimating a 10 percent probability to uncertainty zone. The concrete resistivity and the oxygen in the pores of the concrete matrix are factors that influence the potential values (Castellote et. al., 2002). GP is a conductive material added to concrete; should involve reducing electrical resistivity and increased transport of the chloride ions, causing non-protective oxide formation in the metal. As there are two conductive materials such as reinforcing steel and GP, indicating that the less noble material will develop a higher level of corrosion. This fact shows why the negative values of the corrosion potential in the GP samples.

Over time, all samples with addition of GP had a more negative decrease in potential values, entering a 90% corrosion probability zone. Between days 84 and 148, constant corrosion potential values can be seen, between -280 mV to -400 mV, indicating the possible formation of dense layers of non-protective oxide on the steel.

All samples at the end of the experiment on day 168 of immersion, are located in the 90% corrosion probability zone, the sample M4 with 15% GP is the one with the most negative potential value of -460 mV due to the factors described above and also an amount of water added.

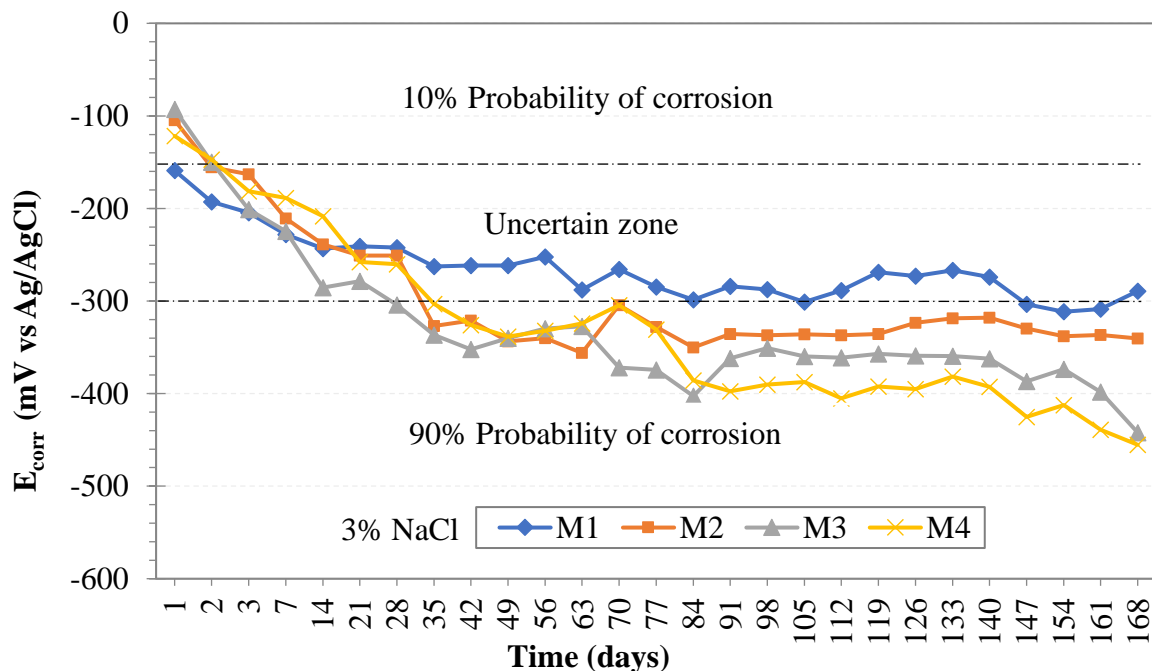


Figure 5. Corrosion potential values ( $E_{corr}$ ).

### 3.6 Electrochemical noise

The average of the resistance oscillations of the electrochemical noise is presented in Figure 6. At the start of the measurement all samples presented low  $R_n$  values between  $1 \times 10^4 \Omega \cdot \text{cm}^2$  and  $1 \times 10^5 \Omega \cdot \text{cm}^2$ ; during days 28 and 70. Sample M1 and M3 presented high and low fluctuations of  $R_n$ , possibly due to the formation of protective oxide films, holding the metal passive. At the end of day 168 of exposure to the saline medium, all samples maintained low noise resistance values around  $1 \times 10^4 \Omega \cdot \text{cm}^2$ .

The GP addition in concrete paste in different percentage, affects the electrochemical properties of the metal, acquiring very low  $R_n$  values, This event can be explained due to the change of oxygen at the steel/concrete interface, as a consequence of the change of the porosity percentage of the paste. Also, the content of GP decreases the resistivity of the concrete; with lower  $R_n$  values indicating high corrosion process of the metal over time (Zhao et. al., 2007).

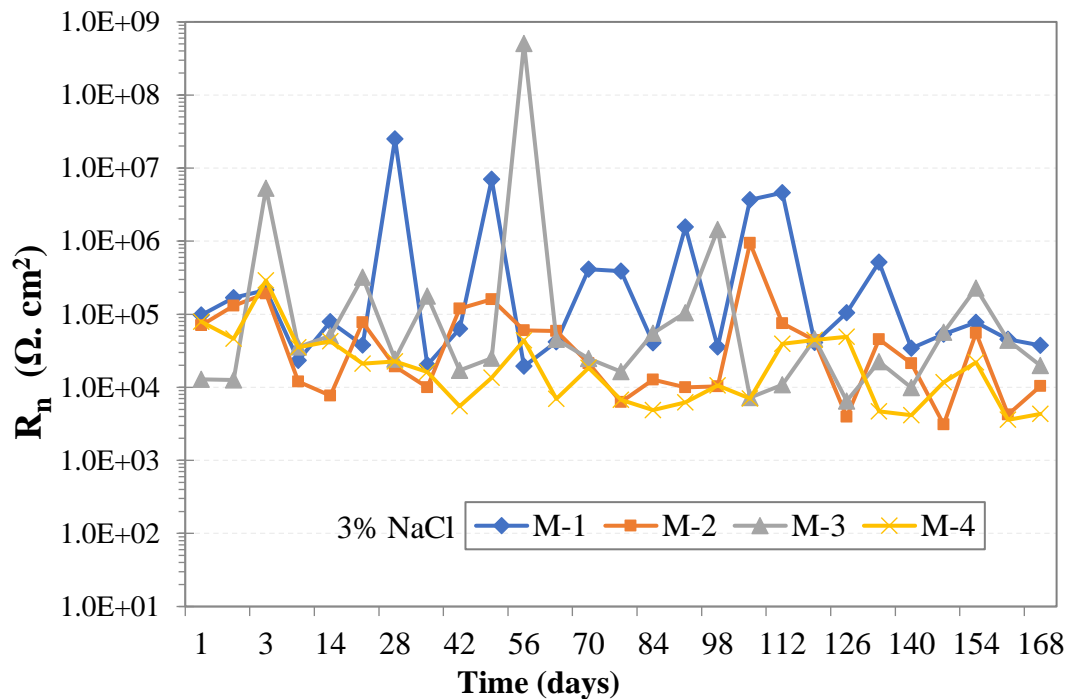


Figure 6. Electrochemical noise values ( $R_n$ ).

The values of the localization index are shown in Figure 7, at the beginning of the test until the end of the exposure. Localized type events or corrosion may be observed, because there is a high dissolution rate of the metal at discrete places on its surface (Sanz et. al., 1999). This represents a higher potential risk, due to its difficult detectability as it manifests itself in specific areas (Salazar-Jiménez, 2015). If the exposure time is prolonged, the start of pitting can occur in the metal.

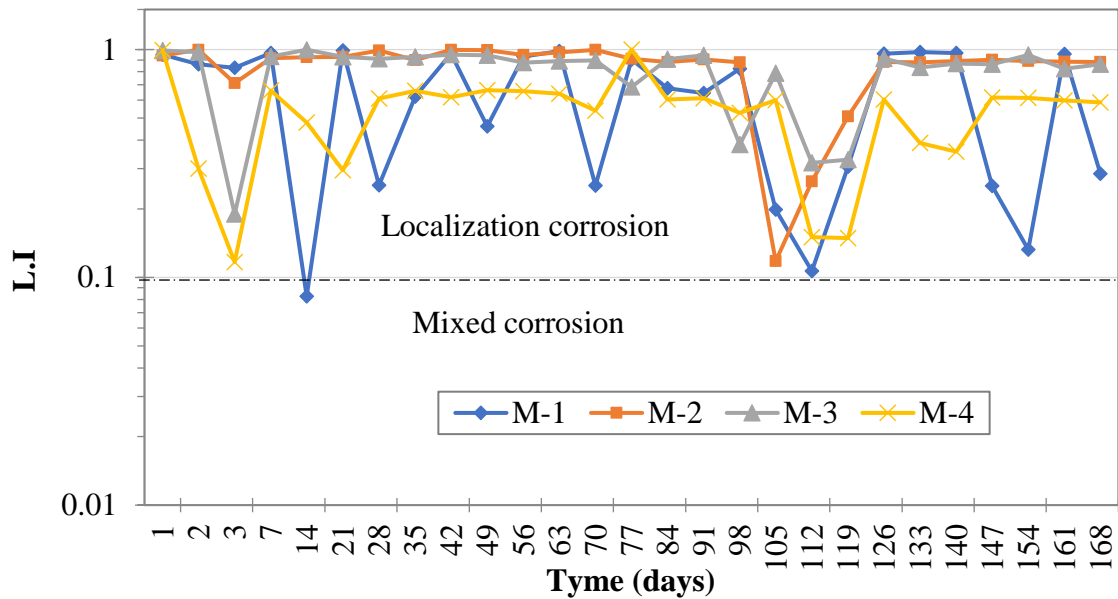


Figure 7. Localization index (L. I.) values of the reinforcing steel.

The values of the useful life level of reinforced concrete are detailed in Figure 8, where all samples at the time of being immersed in an environment after 24 hours were registered. Very high  $i_{corr}$  values can be observed, between 0.1 and 0.5  $\mu\text{A}/\text{cm}^2$ , presenting a range of corrosion between moderate and very high. This behavior coincides with the negative values of the corrosion potential test. Samples with replacement level of GP respectively present very high  $i_{corr}$  values as can be seen and it increases over time, demonstrating very high corrosion on reinforcing steel and in the useful life of concrete.

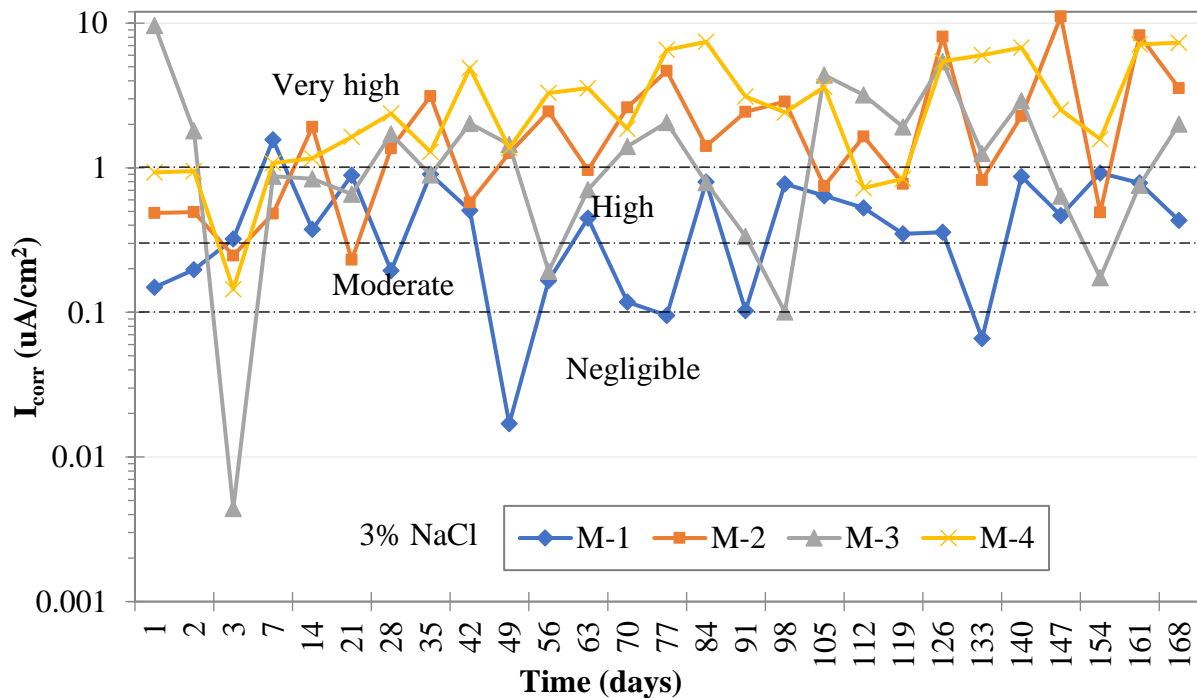


Figure 8. Level of useful life of reinforced concrete.

### 3.7 Linear polarization resistance

Figure 9 shows the polarization resistance values over time, and very low  $R_p$  values can be observed in the 24 hours of immersion and until the end of the measurements in the LPR experiment. During days 42 and 70 there is an increase in the  $R_p$  of samples M1 and M2, maybe indicating a decrease in the rate of metal corrosion. Such high  $R_p$  values are an indication that the steel is passive (Blanco et. al., 2019). Samples with GP content, acquired constant values between  $1 \times 10^1 \Omega \cdot \text{cm}^2$  and  $1 \times 10^3 \Omega \cdot \text{cm}^2$ . High interaction with chloride ions can occur at the steel/ concrete interface registering very low  $R_p$  values. Chloride ions are shown to have depassivated the metal and the material has high corrosion at certain times as immersion times progress.

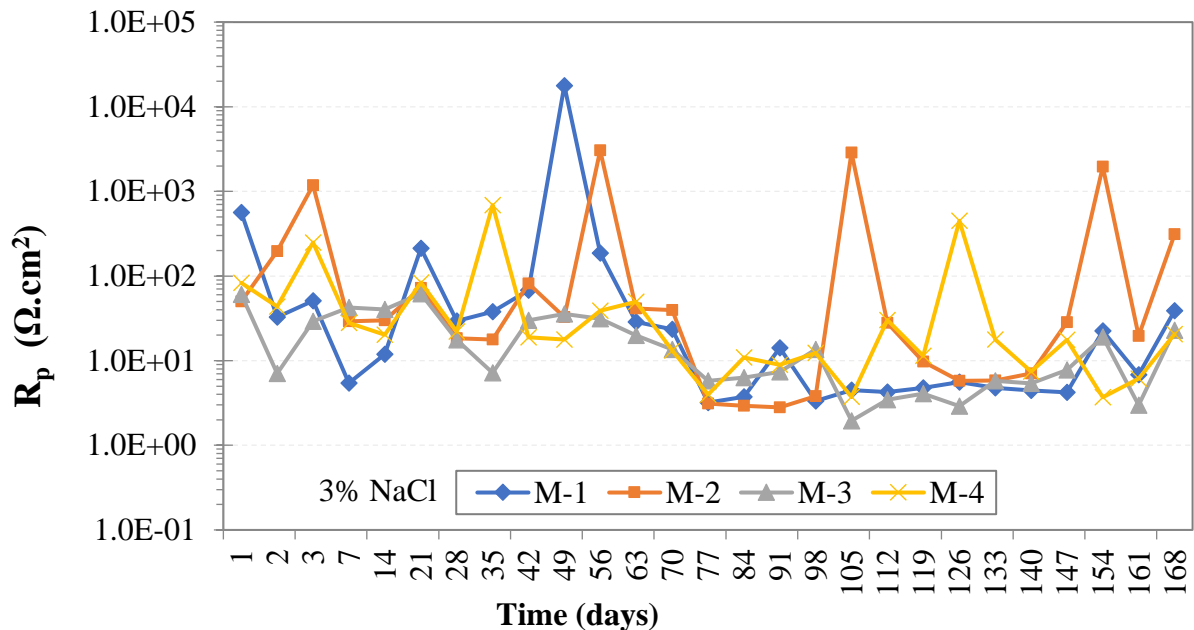


Figure 9. Polarization resistance values ( $R_p$ ) in the course of time.

## 4. CONCLUSIONS

In the present work and within the scope of this research the following conclusions can be drawn: In compressive resistance test, the sample M2 with 2.5% GP content, presented a high value in the mechanical properties of concrete with respect to the control sample but the percentage of porosity in the concrete paste decreased; this fact may be due to the absorption of water by the GP particles in the concrete matrix.

In the samples' addition of 7.5% and 15% GP, higher water content was required increasing the w/c ratio.

In XRD techniques, the GP added to the concrete had no interaction in the process of the crystalline phases of hydration of the concrete.

All the samples immersed in saline medium presented negative corrosion potential with values between -290 mV and -450 mV, entering into a 90% corrosion probability zone.

In the electrochemical measurements of the samples, they presented low  $R_n$  and  $R_p$  values, between  $1 \times 10^1 \Omega \cdot \text{cm}^2$  and  $1 \times 10^4 \Omega \cdot \text{cm}^2$ , indicating a high corrosion process on the reinforcing steel.

The level of useful life of reinforced concrete with GP additions, showed a high to very high level of corrosion with current density values ( $I_{\text{corr}}$ ) greater than  $1 \mu\text{A}/\text{cm}^2$ .

Corrosion type for reinforcing steel bars was in the localized corrosion range, from the first days of immersion and constantly with the advancement of the exposure time to the saline medium, with localization index values between 0.1 and 1.

## 5. ACKNOWLEDGEMENTS

CONACyT (Consejo Nacional de Ciencia y Tecnología de México).

## 6. REFERENCES

- American Concrete Institute (2002) “ACI. 211.1-91: *Standard Practice for Selecting Proportions for Normal, Heavyweight, and Mass Concrete*” (Reapproved 2009),1-38.
- ASTM International. (2019). “ASTM C31 / C31M-19a, *Standard Practice for Making and Curing Concrete Test Specimens in the Field*” [https://doi.org/10.1520/C0031\\_C0031M-19A](https://doi.org/10.1520/C0031_C0031M-19A)
- ASTM International. (2020). “ASTM C39 / C39M-20, *Standard Test Method for Compressive Strength of Cylindrical Concrete Specimens*”. [https://doi.org/10.1520/C0039\\_C0039M-20](https://doi.org/10.1520/C0039_C0039M-20)
- ASTM International. (2020). “ASTM C150 / C150M-20, *Standard Specification for Portland Cement*”. [https://doi.org/10.1520/C0150\\_C0150M-20](https://doi.org/10.1520/C0150_C0150M-20)
- ASTM International. (2017). “ASTM C231 / C231M-17a, *Standard Test Method for Air Content of Freshly Mixed Concrete by the Pressure Method*”. [https://doi.org/10.1520/C0231\\_C0231M-17a](https://doi.org/10.1520/C0231_C0231M-17a)
- ASTM International. (2009). “ASTM C876-09, *Standard Test Method for Corrosion Potentials of Uncoated Reinforcing Steel in Concrete*”. <https://doi.org/10.1520/C0876-09>
- ASTM International. (2014). “ASTM G59-97, *Standard Test Method for Conducting Potentiodynamic Polarization Resistance Measurements*”. <https://doi.org/10.1520/G0059-97R14>
- Becerra, J. (2014). “*Efectos de la sílice amorfa en las propiedades cristalquímicas y mecánicas del hormigón en un medio salino*”. Thesis, Universidad Austral de Chile, p. 76.
- Berkeley, K. G., Pathmanaban, S. (1990), “*Cathodic protección of reinforcement steel in concrete*”, Ed. Butterworths, United Kingdom, ISBN 0-408-03270-1.
- Bertocci, U., Gabrielli, C., Huet, F., & Keddah, M. (1997). “*Noise resistance applied to corrosion measurements: I. Theoretical analysis*”. Journal of the Electrochemical Society, 144(1), 31.
- Blanco, Y. D., Campos, E. C. M., Valdés, C. I. R., Uruchurtu, C. J. (2019). “*Natural additive (nopal mucilage) on the electrochemical properties of concrete reinforcing steel*”. Revista ALCONPAT, 9(3), 260-276. doi: <https://doi.org/10.21041/ra.v9i3.429>
- Castellote, M., Andrade, C., Alonso, C. (2002) “*Accelerated simultaneous determination of the chloride depassivation threshold and of the nonstationary diffusion coefficient values*”, Corrosion Science, 44, 2409-2424, 2002. doi: [https://doi.org/10.1016/S0010-938X\(02\)00060-4](https://doi.org/10.1016/S0010-938X(02)00060-4)
- Chess, P., Gronvold and Karnov, (1998), “*Cathodic protección of steel in concrete*”, E&FN Spon, United Kingdom, ISBN 0-419-23010-6.
- Chung, D. D. L. (2000). “*Cement reinforced with short carbon fibers: a multifunctional material*”. Composites Part B: Engineering, 31(6-7), 511-526. doi: [https://doi.org/10.1016/S1359-8368\(99\)00071-2](https://doi.org/10.1016/S1359-8368(99)00071-2)
- Garcés, P., Andi6n, L. G., De la Varga, I., Catalá, G., Zornoza, E. (2007). “*Corrosion of steel reinforcement in structural concrete with carbon material addition*”. Corrosion science, 49(6), 2557-2566. doi: <https://doi.org/10.1016/j.corsci.2006.12.009>
- Giraldo, M. A., Tob6n, J. I. (2006). “*Evoluci6n mineral6gica del cemento portland durante el proceso de hidrataci6n*”. Dyna, 73(148), 69-81.
- Goellner, J. (2004). “*Elektrochemisches Rauschen bei der Korrosion*”, Werkstoffe und Korrosion, Vol. 55, pp. 727-734, doi: <https://doi.org/10.1002/maco.200403810>
- González, J., & Jimmy, R. (2003). “*Inspecci6n y Diagn6stico de Corrosi6n en Estructuras de Hormig6n Armado para Aplicaciones Portuarias*” (Doctoral dissertation, Tesis, Facultad de Ingeniería en Mecánica y Ciencias de la Producci6n, Escuela Superior Politécnica del Litoral).

- Ha, T. H., Muralidharan, S., Bae, J. H., Ha, Y. C., Lee, H. G., Park, K. W., Kim, D. K. (2005). "Effect of unburnt carbon on the corrosion performance of fly ash cement mortar". *Construction and Building Materials*, 19(7), 509-515. doi: <https://doi.org/10.1016/j.conbuildmat.2005.01.005>
- Helena, J., Lucia, M. D. (2011). "X-ray diffraction study of hydration processes in the Portland cement". *Journal of Applied Engineering Science*, 1(1), 79-86.
- Heysfield, E., Osweiler, A. B., Selvam, R. P., Kuss, M. (2013). "Feasibility of anti-icing airfield pavements using conductive concrete and renewable solar energy". (No.DOT/FAA/TC-13/8).
- O.T. de Rincón y Miembros de la red DURAR, "Manual de Inspección, Evaluación y Diagnóstico de Corrosión en Estructuras de Hormigón Armado", CYTED. Maracaibo, Venezuela, 1997 (1era.Ed).
- Román, A. S., Barrientos, M. S., Harms, F., Mendez, C. M., Ares, A. E. (2016, April). "Resistencia corrosión de acero inoxidable AISI 304L en biodiesel de soja". In ANALES AFA (Vol. 27, No. 1). doi: <https://doi.org/10.31527/analesafa.2016.27.1.14>
- Sagües, A. A. (1991). "Critical Issues in Electrochemical Corrosion Measurement. Techniques for Steel in Concrete". CORROSION/91, NACE. Paper 141.
- Salazar-Jiménez, J. A. (2015). "Introducción al fenómeno de corrosión: tipos, factores que influyen y control para la protección de materiales". *Revista Tecnología en Marcha*, 28(3), 127-136.
- Sánchez, A., Sanjurjo, M., Bouzada, F., Urrejola, S. (2005). "Análisis estadístico de los registros de ruido electroquímico obtenidos en la corrosión del aluminio". *Revista de metalurgia*, 41(5), 330-339. doi: <https://doi.org/10.3989/revmetalm.2005.v41.i5.222>
- Sánchez-Amaya, J. M., Bethencourt, M., Gonzalez-Rovira, L., Botana, F. J. (2009). "Medida de ruido electroquímico para el estudio de procesos de corrosión de aleaciones metálicas". *Revista de metalurgia*, 45(2), 142-156. doi: <https://doi.org/10.3989/revmetalm.0807>
- Sanz, J. L. P., Torres, C. L., Cano, E., Bastidas, J. M. (1999). "Estudio de impedancia de la corrosión del acero inoxidable AISI 316L en las regiones pasiva y de picadura". *Revista de metalurgia*, 35(6), 368-378. doi: <https://doi.org/10.3989/revmetalm.1999.v35.i6.645>
- Solís-Carcaño, R, Moreno, E. I. (2006). "Análisis de la porosidad del concreto con agregado calizo". *Revista de la Facultad de Ingeniería de la UCV*, 21(3), 57-68.
- Tascón, J. M. (2007). "Materiales de carbono: estructuras y formas. Óptica pura y aplicada". 40(2),149-159.
- Vetter, M., Gonzalez-Rodriguez, J., Nauha, E., Kerr, T. (2019). "The use of Raman spectroscopy to monitor phase changes in concrete following high temperature exposure". *Construction and Building Materials*, 204, 450-457. doi: <https://doi.org/10.1016/j.conbuildmat.2019.01.165>
- Vidaud, E., & Vidaud, I. (2012). "La carbonatación en el concreto reforzado", *Construcción y tecnología en concreto*. Pág, 21-23.
- Wu, S. P., Wang, P., Li, B., Pang, L., Guo, F. (2014). "Study on mechanical and thermal properties of graphite modified cement concrete". In *Key Engineering Materials* (Vol. 599, pp. 84-88). Trans Tech Publications Ltd. doi: <https://doi.org/10.4028/www.scientific.net/KEM.599.84>
- Yuan, H. W., Lu, C. H., Xu, Z. Z., Ni, Y. R., Lan, X. H. (2012). "Mechanical and thermal properties of cement composite graphite for solar thermal storage materials". *Solar energy*, 86(11), 3227-3233. doi: <https://doi.org/10.1016/j.solener.2012.08.011>
- Zhao, B., Li, J. H., Hu, R. G., Du, R. G., Lin, C. J. (2007). "Study on the corrosion behavior of reinforcing steel in cement mortar by electrochemical noise measurements". *Electrochimica Acta*, 52(12), 3976-3984. doi: <https://doi.org/10.1016/j.electacta.2006.11.015>

## Comparative analysis of the effectiveness and efficiency of three waterproofing systems

R. S. Kmick<sup>1</sup>, M. G. Gazolla<sup>1</sup>, R. M. da Silva Junior<sup>1</sup>,  
A. P. B. Capraro<sup>\*2</sup>, K. A. W. Moreira<sup>1</sup>  
\*Contact author: [anapcapraro@gmail.com](mailto:anapcapraro@gmail.com)  
DOI: <https://doi.org/10.21041/ra.v11i1.509>

Reception: 11/09/2020 | Acceptance: 30/10/2020 | Publication: 01/01/2021

### ABSTRACT

The objective of this study was to comparatively analyze waterproofing systems used in Brazil. The evaluated products were: asphalt emulsion, acrylic resin and thermoplastic resin. In order to evaluate the effectiveness of the systems the tests measured the tightness and the absorption by immersion and capillarity, the last one was also analyzed by thermographic images. For the systems efficiency analysis an accelerated aging pattern was adopted, which consisted of alternating the samples in wet and dry cycles. The results indicate a good performance for the studied systems, in comparison to the non-impermeable series, it presented lower absorbance (approximately 300%). The accelerated aging test indicated, after 140 days of age, a reduction in the performance of the waterproofed series.

**Keywords:** waterproofing systems; effectiveness; efficiency; accelerated aging; yield reduction.

**Cite as:** Kmick, R. S., Gazolla, M. G., da Silva Junior, R. M., Capraro, A. P. B., Moreira, K. A. W. (2021), "*Comparative analysis of the effectiveness and efficiency of three waterproofing systems*", Revista ALCONPAT, 11 (1), pp. 34 – 47, DOI: <https://doi.org/10.21041/ra.v11i1.509>

<sup>1</sup> Engenharia Civil, Centro Universitário Araucária, Araucária, Brasil.

<sup>2</sup> Departamento de Construção Civil, Universidade Federal do Paraná, Curitiba, Brasil.

### Contribution of each author

In this work, the authors Renata dos Santos Kmick, Micheli Gazolla and Renato Moura da Silva Junior contributed to the discussion of the original idea and experimentation and data collection. The author Ana Paula Brandão Capraro contributed to the discussion of the original idea, writing of the work and discussion of results. The author Kirke Moreira contributed to the data collection and writing of the work.

### Creative Commons License

Copyright 2021 by the authors. This work is an Open-Access article published under the terms and conditions of an International Creative Commons Attribution 4.0 International License ([CC BY 4.0](https://creativecommons.org/licenses/by/4.0/)).

### Discussions and subsequent corrections to the publication

Any dispute, including the replies of the authors, will be published in the third issue of 2021 provided that the information is received before the closing of the second issue of 2021.

## Análise comparativa da eficácia e eficiência de três sistemas impermeabilizantes

### RESUMO

O objetivo desse estudo foi analisar comparativamente sistemas de impermeabilização empregados no mercado brasileiro. Os produtos avaliados foram: emulsão asfáltica, resina acrílica e resina termoplástica. Para avaliação da eficácia dos sistemas foram realizados os ensaios de estanqueidade, absorção por imersão e capilaridade, sendo esse último também analisado por imagens termográficas. Para a análise da eficiência dos sistemas foi adotado um padrão de envelhecimento acelerado, o qual consistiu na alternância das amostras em ciclos de molhagem e secagem. Os resultados indicam um bom desempenho para os sistemas estudados, que quando comparados a série não impermeabilizada apresentaram absorções inferiores (aproximadamente 300%). Já o ensaio de envelhecimento acelerado indicou, posteriormente aos 140 dias de idade, redução do desempenho das séries impermeabilizadas.

**Palabras clave:** sistemas de impermeabilização; eficácia; eficiência; envelhecimento acelerado; redução de desempenho.

## Análisis comparativo de la efectividad y eficiencia de tres sistemas de impermeabilización

### RESUMEN

El objetivo de este estudio fue analizar comparativamente los sistemas de impermeabilización empleados en el mercado brasileño. Los productos evaluados fueron: emulsión de asfalto, resina acrílica y resina termoplástica. Para evaluar la efectividad de los sistemas, se realizaron pruebas de estanqueidad, absorción por inmersión y capilaridad, siendo este último también analizado por imágenes termográficas. Para el análisis de eficiencia de los sistemas, se adoptó un patrón de envejecimiento acelerado, que consistía en alternar las muestras en ciclos húmedos y secos. Los resultados indican un buen desempeño para los sistemas estudiados, que en comparación con las series no impermeables presentaron absorbancias más bajas (aproximadamente 300%). La prueba de envejecimiento acelerado indicó, después de 140 días de edad, una reducción en el rendimiento de la serie impermeabilizada.

**Palabras clave:** sistemas de impermeabilización; efectividad; eficiencia; envejecimiento acelerado; reducción de rendimiento.

### Legal Information

Revista ALCONPAT is a quarterly publication by the Asociación Latinoamericana de Control de Calidad, Patología y Recuperación de la Construcción, Internacional, A.C., Km. 6 antigua carretera a Progreso, Mérida, Yucatán, 97310, Tel.5219997385893, [alconpat.int@gmail.com](mailto:alconpat.int@gmail.com), Website: [www.alconpat.org](http://www.alconpat.org)

Reservation of journal title rights to exclusive use No.04-2013-011717330300-203, and ISSN 2007-6835, both granted by the Instituto Nacional de Derecho de Autor. Responsible editor: Pedro Castro Borges, Ph.D. Responsible for the last update of this issue, Informatics Unit ALCONPAT, Elizabeth Sabido Maldonado.

The views of the authors do not necessarily reflect the position of the editor.

The total or partial reproduction of the contents and images of the publication is carried out in accordance with the COPE code and the CC BY 4.0 license of the Revista ALCONPAT.

## 1. INTRODUCTION

Waterproofing systems are essential to ensure the durability of any construction, and neglecting them can result in infiltration, which provides pathological mechanisms such as leaching, concrete degradation, corrosion of reinforcement and deficiency in renderings (Aldea and Shah, 1999).

A material considered waterproof is one that prevents water from passing from one plane to the other. It is also understood as a substrate that does not absorb more than 2.5% moisture when compared to a reference sample (Basheer et al., 2001).

The lack of information about the techniques and the use of inappropriate materials, among other factors, for a long time were responsible for the failures in waterproofing (PICCHI, 1986). The cost of a good design and a good execution waterproofing can represent 1% to 3% of the value of a work. Furthermore, damage and maintenance of waterproofing systems cost between 5% to 10% of the value of the project (Bauer et al., 2010).

New standards, such as the case of NBR 15575 (ABNT, 2013), and updates of existing standards recommend meeting the needs and performance of buildings, requiring that all housing systems meet a minimum level of performance throughout of the useful life determined in the project.

Currently, the most used waterproofing system is the one that uses asphalt emulsion (Menezes, 2018), however, suppliers have invested a lot in new products development researches, expanding the options and bringing benefits such as durability of the buildings and costs reduction.

According to Andrello and Takagi (2017), applying a product with higher performance saves costs on the application and maintenance of the building. In addition, as claimed by Andrello and Takagi (2017), companies have products with the same purpose, however, the characteristics from each product change. If the consumer or the applicator do not pay attention to this, they can apply a product in the same way in different cases not reaching the expected performance.

Taking into consideration the facts above, the present study aimed to compare the effectiveness and efficiency of three waterproofing systems, provided and recommended by national suppliers for use in non-transitable roof slab. For the analysis of the effectiveness of the waterproofing systems, which implies the success of the system as a waterproof layer, the waterproofing test (NBR 15575-3, 2013), immersion absorption (NBR 9778, 2005) and capillary absorption were performed (NBR 9779, 2012) at an early age, shortly after the curing of the applied systems. For the analysis of the system efficiency, expressing the performance over time, the same immersion absorption tests (NBR 9778, 2005) and capillarity absorption (NBR 9779, 2012) were performed, however, after the exposure of the samples in wetting and drying cycles, aiming to represent an accelerated aging cycle of the systems.

## 2. EXPERIMENTAL PROCEDURE

This study included the development of an experimental program, with the production of concrete samples and protection thereof with the waterproofing material to be evaluated.

### 2.1 Waterproofing materials

To choose the three waterproofing products it was taken into account: (i) the application site, which is recommended for the same purpose among the three products, a recommendation made by the suppliers; (ii) the products are standardized; (iii) and the classification, regarding the useful life, by the Brazilian Institute of Waterproofing (BIW), with three intervals of expected useful life being chosen.

Three membranes were then chosen, which met the criteria for manufacturing and applying the standards NBR 9685 (ABNT, 2005), NBR 13321 (ABNT, 2008), NBR 15885 (ABNT, 2010) and the BIW service life criteria, cited by Morgado et al. (2018). The products, their respective standards and useful lives are shown in Table 1.

Table 1. Waterproofing products used in research.

Product group	Membranes		
Standard (ABNT, NBR)	9685:2005	13321:2008	15885:2010
Product	Asphalt emulsion	Acrylic resin	Polymeric resin
Useful life	8	16	26

The asphalt emulsion membrane is based on asphalt modified with polymers and is emulsified in water, ready for use and non-aggressive to the environment. According to the supplier, kept confidential for ethical reasons, its characteristics are: good performance in elasticity and flexibility, adherence, easy handling and application. The product can be applied indoors, forming a continuous and seamless membrane, with resistance and durability. Its uses can be in terraces, flower boxes, retaining walls, cold rooms, gutters, small slabs, walls and cold floors.

The acrylic resin membrane is a one-component material ready for use. Due to its characteristics, mentioned by the supplier, also kept confidential, it is considered an excellent waterproofing and has good durability, easy application, good elasticity, is resistant to UV rays, with good adhesion on cementitious substrates and fiber cement and reflects sun rays, reducing part of the heat absorbed by the structure. Its application can be in arched and inclined roofs, concrete slabs, concrete gutters, balconies and terraces, reservoir roofs and fiber cement tiles.

Thermoplastic resin is a flexible, two-component waterproofing agent based on acrylic polymers with cement and reinforced with fibers, especially suitable for structures subject to movement. It is recommended to use it in hydraulic structures that have contact with drinking water, wet areas such as bathrooms, balconies and facades, roof slabs with occasional passage and with their appropriate expansion joints, pools and reservoirs, flower boxes, among others. It presents high flexibility and elongation, being able to be exposed to the weather (resistant to U.V) and resistant to high positive hydrostatic pressures. Additionally, conforming to the supplier, it is easy and quick to apply and can be applied manually or designed, without the need for curing.

The description of the waterproofing products that were used in this research is shown in Table 2.

Table 2. Characteristics of waterproofing products used.

Product	Component	Characteristics
Asphalt emulsion	Asphalt (40-70% concentration)	Density: 0.95 to 1.05 g/cm <sup>3</sup> Viscosity: 9000 to 12000 Cps Black color
Acrylic resin	Water, mineral fillers, acrylic emulsion, pigment, stabilizers, defoamer, biocide.	Density: 1.2 g/cm <sup>3</sup> Viscosity: 1000 to 2500 Cps White color
Thermoplastic resin	Acrylic Polymers (Thermoplastic Resin), Portland Cement (25 -50% concentration)	Density: 1.60 g/cm <sup>3</sup> Gray color

## 2.2 Study samples

The samples used in the study were made with Portland cement concrete CPV-ARI, 35 MPa of strength, mixture proportion of 1: 1: 6 with a water/cement ratio of 0.495. The cement used has a specific mass of 3.13 g/cm<sup>3</sup>, the fine aggregate has a maximum dimension of 2.4 mm and a specific mass of 2.62 g/cm<sup>3</sup> and the coarse aggregate used was a gravel 1, with a specific mass equal to 2.65 g/cm<sup>3</sup>.

For the analysis of product performance, 32 cylindrical specimens 0.10x0.20m and 4 slabs, with dimensions of 0.6 x 0.6 x 0.07 m, were molded. After the concrete was cured for 28 days of the samples, the products were applied, according to the guidelines of the technical sheets (Table 3).

Table 3. Application of waterproofing products used.

Product	Specification	Intervals between layers	Drying time
Asphalt emulsion	2 to 3 layers	12 hours	5 days
Acrylic resin	3 to 4 layers	6 hours	1 days
Thermoplastic resin	Thickness between 2 to 4 mm	6 hours	7 days

## 2.3 Experimental analysis

The concrete samples were subjected to experimental tests, which aimed to evaluate the effectiveness and efficiency of the product used as waterproofing.

For the analysis of the systems effectiveness, which is the initial performance of the products when compared to the reference series, the tests of waterproofing, absorption by immersion and absorption by capillarity were performed without any protection.

The results of the tests of absorption by immersion and absorption by capillarity, which are qualitative because they present percentage differences in absorption, were analyzed statistically, using the Tukey test, with 95% confidence. The purpose of the test was to indicate the smallest statistically significant difference between the analyzed results. Therefore, with the 95% confidence interval, the series (reference and the three waterproofed) were compared, in order to evaluate the statistical difference between them in the quantitative tests performed.

For the waterproofing test, four slabs were used, three of them with the products selected for the research and one for the comparison of unprotected behavior, the reference sample. The slabs were subjected to the waterproofing test, which consists of exposing the samples to a 0.03 m water slide for 72 hours, through a transparent and sealed container, as recommended by Annex C NBR 15575-3 (ABNT, 2013), Figure 1.



Figure 1. Waterproofing test performed in the laboratory.

In addition, 12 10 x 20 cm specimens were used to perform the immersion absorption test, according to NBR 9778 (ABNT, 2005), 3 for each product applied and 3 for the reference series, without application. After the application and drying of the products, the specimens remain in an oven for 72 hours, at 40°C. This drying temperature was adopted to prevent the deterioration of the material. After drying, the masses of the dried samples were obtained and, after the immersion periods (24, 48 and 72 hours), the masses of the immersed samples were also obtained.

In addition, the capillarity water absorption test was performed, according to NBR 9779 (ABNT, 2012). Twenty specimens were used, 5 of which were waterproofed in half, with each product and 5 as a reference, without product application. Only the lower part was waterproofed, because it was the only sample part in contact with the water during the test. After the drying time of the products, the specimens remained in an oven at a temperature of 40°C for 72 hours and cooled to room temperature for 24 hours. After the determination of the dry mass, the specimens were exposed to a 10 mm constant water layer. During the test, the saturated mass of the specimens was determined at intervals of 3 h, 6 h, 24 h, 48 h and 72 h. After determining the masses, the specimens were broken by diametrical compression, to allow measurement of the water distribution inside using infrared thermography.

To evaluate the efficiency of the products, that is their performance over time, an accelerated aging condition was adopted, which consisted of the weekly cycling of the cylindrical specimens used in the immersion absorption test. The adopted cycle alternated the samples between a condition of wetting (immersion) and drying (exposure to the sun and the outdoor weather). The aging pattern was adopted because it has already been used in other studies that sought to accelerate aging (Gao et al., 2013; Gong et al., 2016; Jiang and Niu, 2016).

The samples used in the analysis of accelerated aging were subjected to three sets of cycles, each consisting of 8 cycles (8 weeks), with the ages of analysis being 84, 140 and 196 days. At the ages mentioned, the specimens were subjected to the procedures mentioned in the immersion absorption test.

### 3. RESULTS

#### 3.1 Waterproofing test

After submitting the slabs to the waterproofing test, they were observed for 72 hours. However, in the evaluated period, recommended by NBR 15575 (ABNT, 2013), the appearance of bubbles, infiltration in the lower part of the slabs and the lowering of the water level in the reference of 0.03 m was not observed. Figure 2 shows part of the four slabs studied, indicating the tightness of all systems.

As all the slabs were considered watertight, no behavioral difference that could be identified by this test was verified between the reference sample (without protection) and the waterproofed samples.

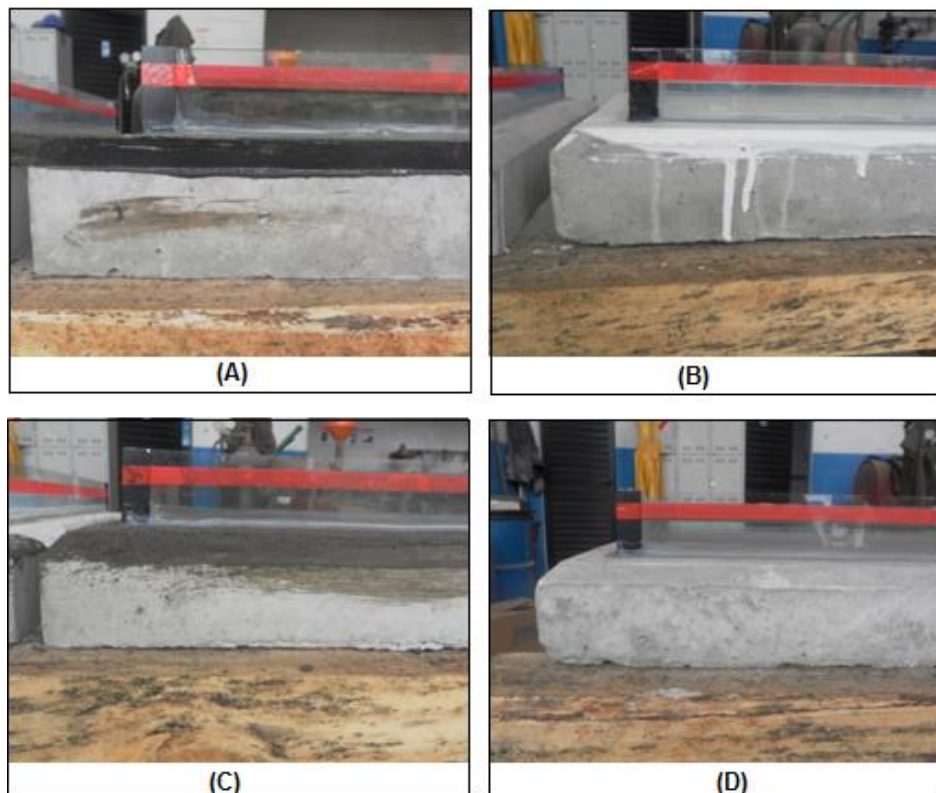


Figure 2. Waterproofing test result after 72 hours. A - Slab with asphalt emulsion; B - Slab with acrylic membrane; C - Slab with thermoplastic resin; D - Reference slab.

#### 3.2 Immersion absorption test

Figure 3 presents the results obtained for the immersion absorption rate. The initial average rate, in 24 hours, of waterproofed specimens was 0.3%, against 5.17% of reference specimens. After the 72-hour period, a small increase in rates was observed, with the average absorption rate of waterproofed specimens being 0.4%, and 5.23% for the reference series. Considering the 2.5% reference absorption mentioned by Basheer et al. (2001), it is noted that only waterproofed samples can be considered as watertight substrates.

By comparatively analyzing the results obtained for the waterproofed series, a very similar behavior was noted between them, and a satisfactory one if compared to the reference series. By the standard deviation obtained, the asphalt emulsion and thermoplastic resin series could be considered statistically equivalent, by the Tukey test, in all readings performed. At the final age evaluated, 72 hours of testing, the acrylic membrane revealed the lowest value statistically validated, among all series evaluated, indicating the best performance during this test.

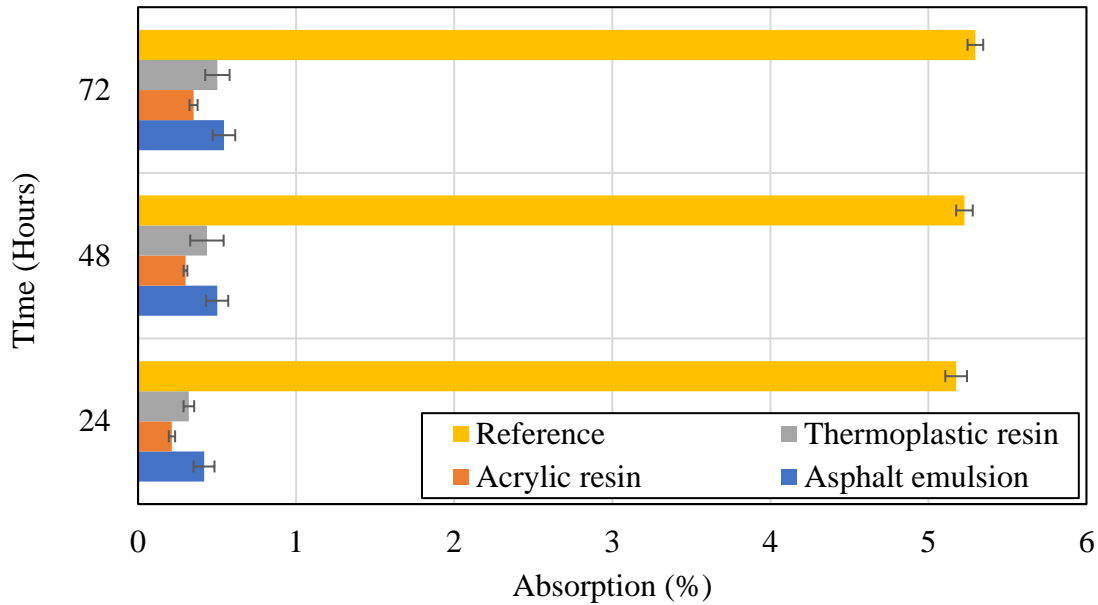


Figure 3. Result of the immersion absorption test.

### 3.3 Capillary absorption test

In the first periods of the test, 3 and 6 hours, the behavior of the specimens with the waterproofing products can be considered similar, since the average absorption rate in these periods was approximately 0.659%, all of which are considered statistically equivalent by the statistical test applied. However, in the last reading interval of the test, 72 hours, the specimens of the thermoplastic resin series had the lowest absorption rate of 1.05%, against an average of 2.34% of the other products. At the end of the test, the reference series had an absorption 7.9 times greater than the series of thermoplastic resin, indicating the best behavior. The asphalt emulsion and acrylic membrane remained statistically equivalent, considering the greater variability of standard deviation between them, as shown in Figure 4.

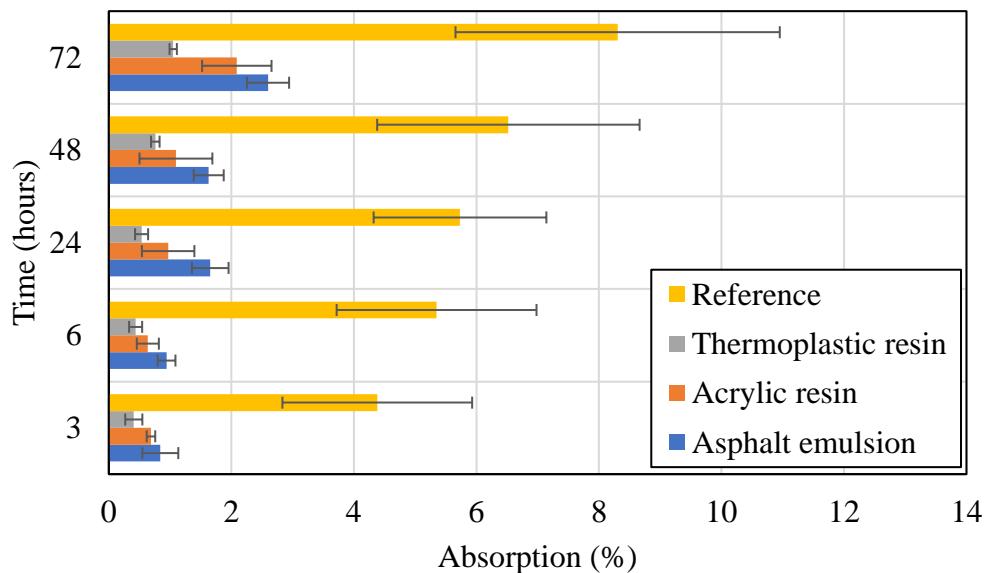


Figure 4. Result of the capillarity absorption test.

The better performance of the thermoplastic resin in the capillary absorption test confirms the indication of Pezzolo (2013) for the use of the material for waterproofing in baseboards of drywall walls.

The visual analysis of the specimens that was submitted to the diametrical compression test and later to the analysis by infrared thermography, allowed the confirmation of the inferior performance of the reference series and the similar performance between the waterproofed series.

Figure 5 shows the specimens of the reference series that were submitted to the diametrical compression test. For the case of this series an average capillary rise height of 4.3 cm was noted.

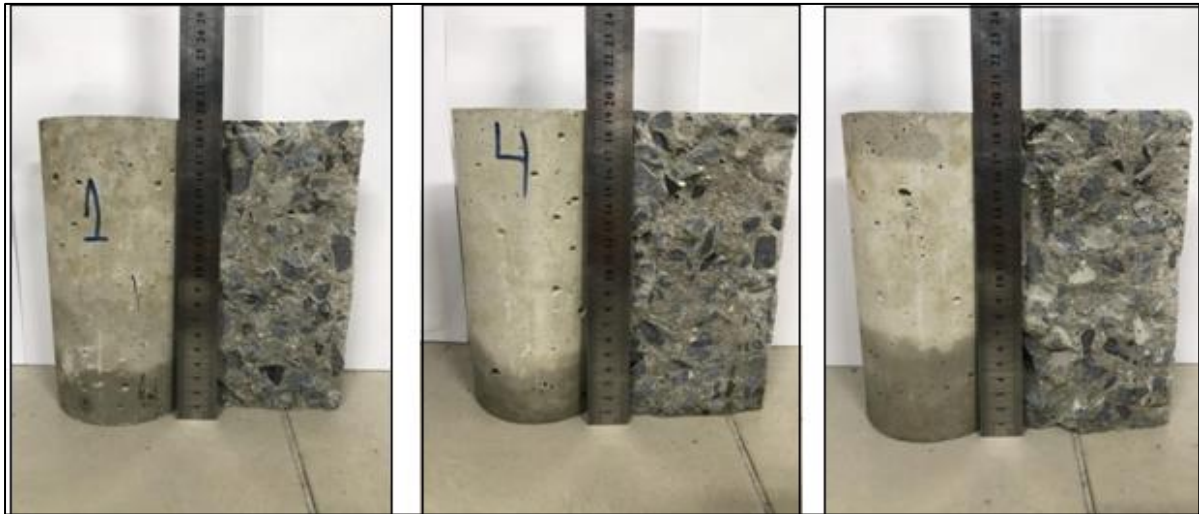


Figure 5. Specimens of the reference series after the diametrical compression test.

The thermographic images for the reference series, Figure 6, confirm the percolation of water into the specimen, since the temperature obtained in the test was the lowest among the series studied (23.1 °C).

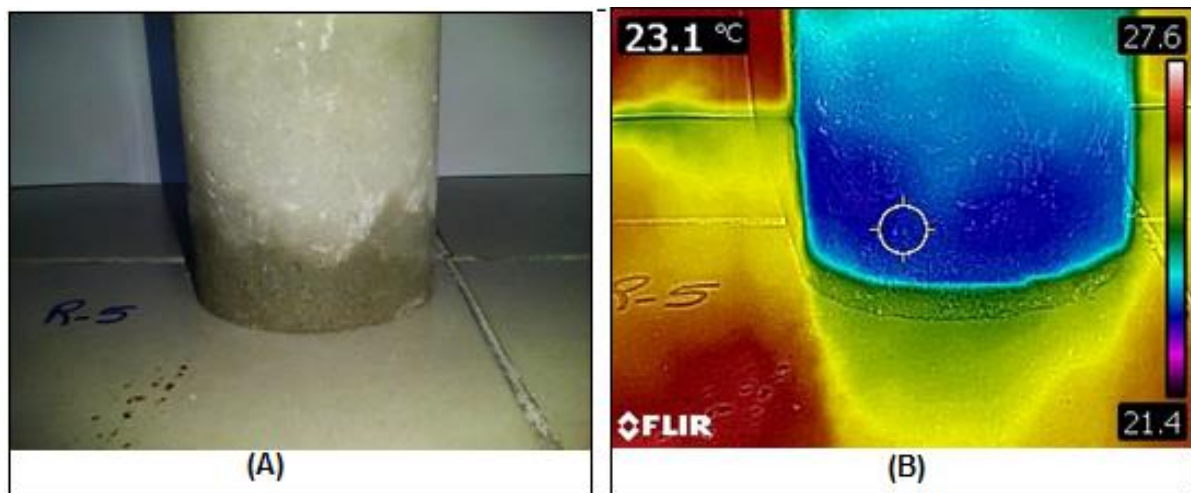


Figure 6. Thermographic image for the reference series. A - Specimen after the diametrical compression test; B - Specimen during the thermography test.

Figure 7 presents the specimens of the waterproofed series after the diametrical compression test. For these series, the difficulty of obtaining readings of capillary rise was greater and the analysis was performed using thermographic images, presented in Figures 8, 9 and 10. The temperatures recorded in the thermographic images are close to the minimum indicated in the reference scale, on the right side of each image, indicating the water absorption region.

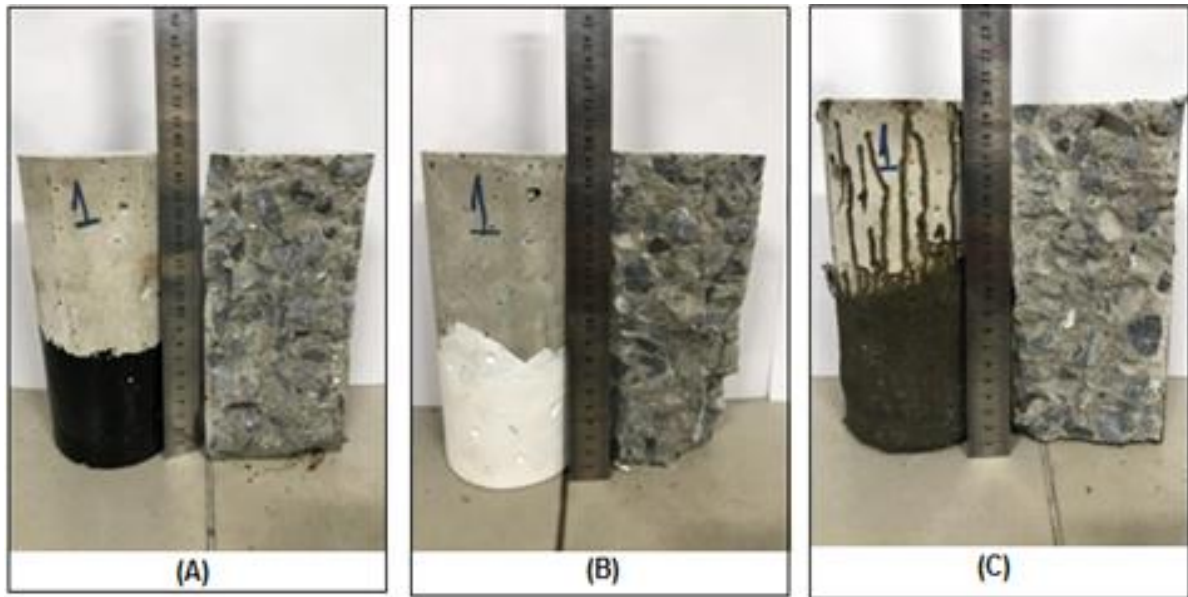


Figure 7. Specimens of the waterproofed series after the diametrical compression test. A - Sample with asphalt emulsion; B - Sample with acrylic resin; C - Sample with thermoplastic resin.

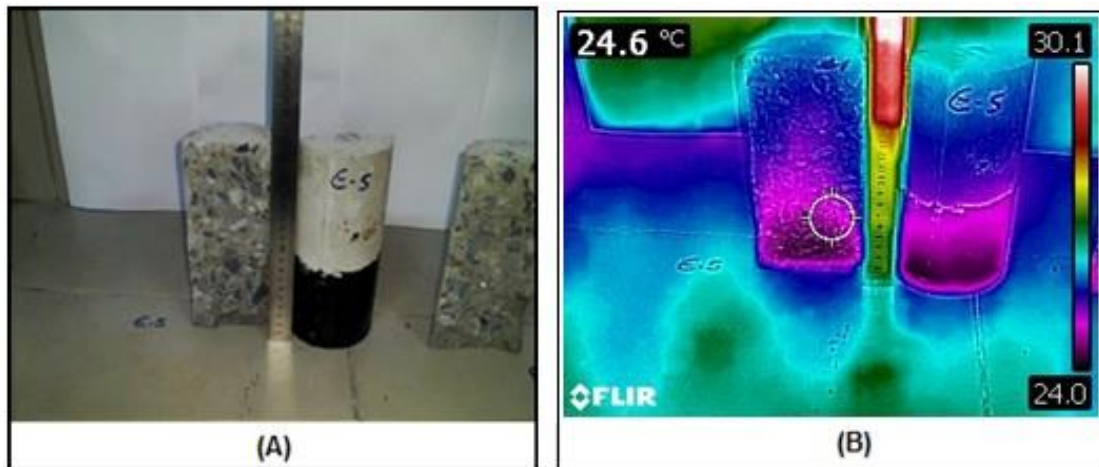


Figure 8. Thermographic image for the series with asphalt emulsion. A - Specimen after the diametrical compression test; B - Specimen during the thermography test.

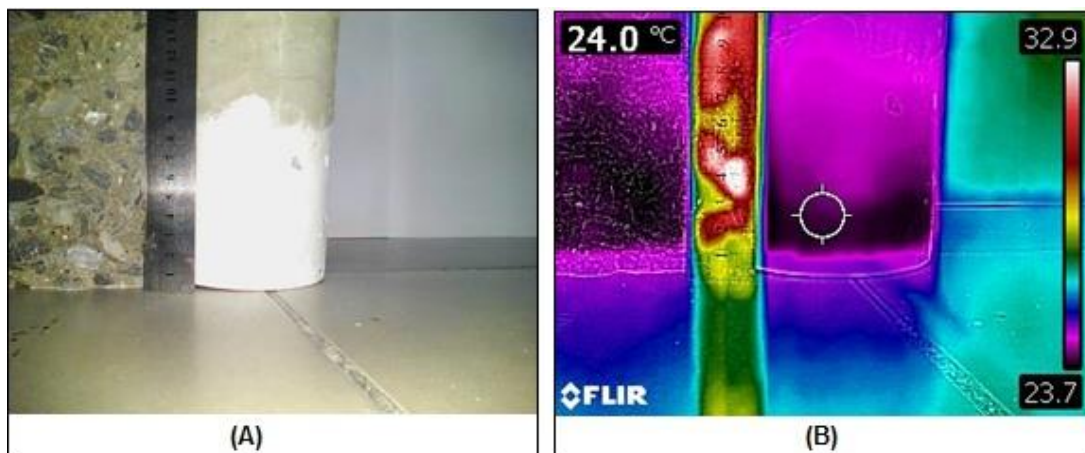


Figure 9. Thermographic image for the series with acrylic resin. A - Specimen after the diametrical compression test; B - Specimen during the thermography test.

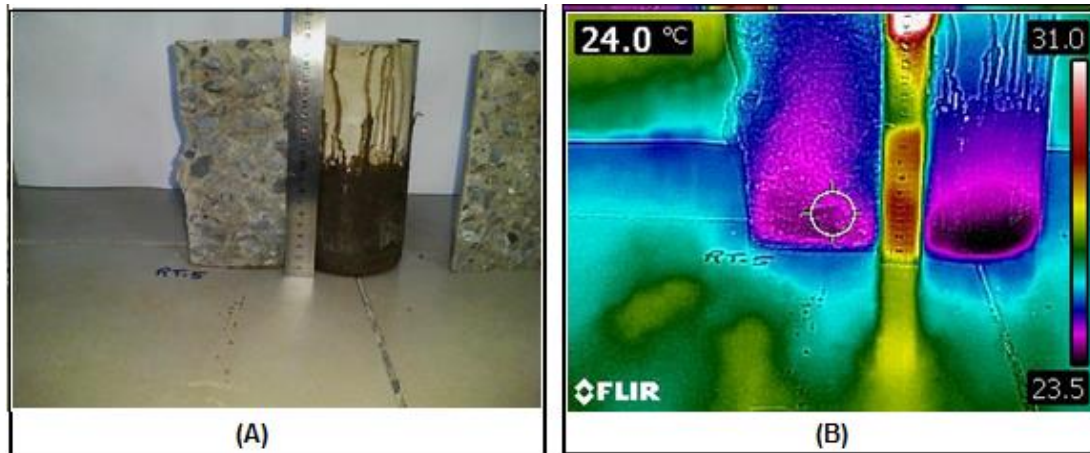


Figure 10. Thermographic image for the series with thermoplastic resin. A - Specimen after the diametrical compression test; B - Specimen during the thermography test.

The thermography test indicated among the waterproofed series the best performance for the asphalt emulsion series, which had the highest temperature of 24.6 °C. The series of acrylic membrane and thermoplastic resin showed the same temperature indicating a similar behavior of 24 °C.

According to the literature, the variation from 1 °C to 2 °C is considered an indication of problems (Cortizo, 2007; Freitas *et al.*, 2014). Therefore, the temperature difference observed between the reference series and the waterproofed series is sufficient to indicate better performance of these series.

Despite the small temperature variation observed, the studied thermographic images proved to be adequate for the detection of absorption, since the visual analysis in the broken specimens confirmed the capillary rise. In addition, regarding the small variation, the literature still reports that variations in the order of 1°C are already susceptible to identification of infiltration in concrete elements (Maldague, 2001; Merlino, Matias e Farias, 2015; Lourenço, Matias e Faria, 2017; Rocha, Santos, Oliveira, Albuquerque e Póvoas, 2018).

### 3.4 Immersion absorption after accelerated aging

The absorption test after the accelerated aging process, shown in Figure 11, indicates reduced absorption for the reference series over time. The result was expected whereas the continuous hydration of Portland cement causes pores filling, consequently decreasing the permeability of the material (Rossignolo, 2005). Moreover, once the specimens were subjected to time, the influence of the carbonation phenomenon is possible, which may have contributed to the filling of the pores with calcium carbonate (CaCO<sub>3</sub>), and reduction of the materials absorbent capacity, as reported by Ngala and Page (1997). The absorption results of the reference series were from 5% at the initial age to 3% at the final age studied, confirming the pore filling.

All waterproofed series showed lower absorption at 84 days than that presented at 28 days, also explained by the drying and fixing of the products in the period. However, after 140 days it was possible to notice a behavioral inversion, the series started to show greater absorptions when compared to the age of 28 days.

It should be noticed that the three waterproofing products tested, according to their suppliers, could be applied outdoors, such as roof slabs. Therefore, no matter how much they were subjected to wetting and drying cycles, the performance should not have been impacted. According to Silveira and Granato (2013), the waterproofing system must be able to withstand all types of request during its useful life, whether mechanical or chemical. Therefore, the choice of the system must always take into account the active requests, so that the applied material meets the proposed demand.

The values obtained in this test still confirm the greatest performance of the waterproofed series, with the average absorption between them, at 196 days, 0.52%, against 3.0% of the reference series. However, the necessity to observe the performance of these materials over time is highlighted, once their inefficiency would lead to a direct loss in the useful life of concrete structures. Since the proposal of the work is the evaluation of application of the systems in roof slabs, it is expected that the systems resist the action of UV rays, as well as the hygroscopic request for constant wetting and drying.

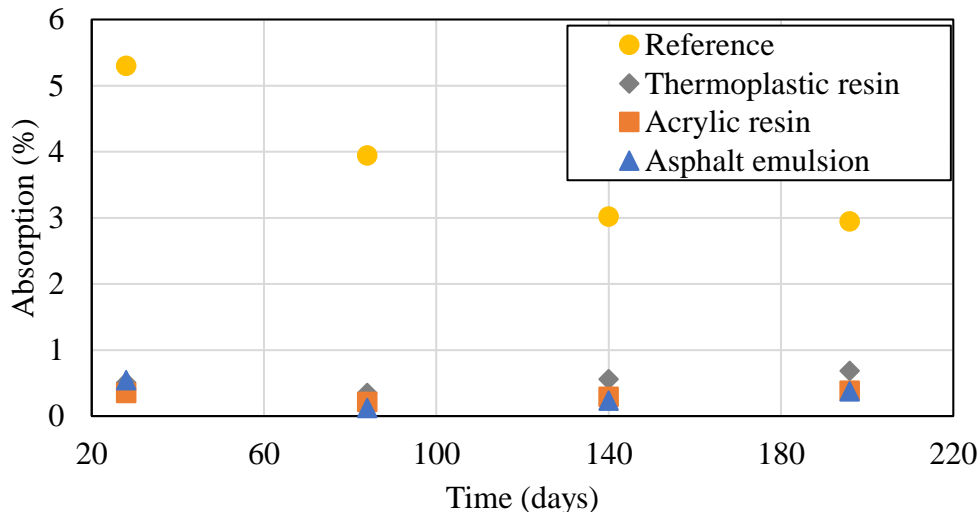


Figure 11. Result of the immersion absorption test after accelerated aging.

#### 4. CONCLUSIONS

The results obtained in this study allowed to present the conclusions listed below:

- The waterproofing test indicated similar behavior among all the series studied, and infiltration, percolation or any other indication of failure in the three series observed cannot be observed in the period indicated by NBR 15575 (ABNT, 2013);
- The immersion absorption test once again indicated similar behavior among the products studied. However, in this case, to indicate at the end of the test the best performance of the acrylic membrane, with the absorption of the material equal to 0.35% was possible;
- The capillary absorption test indicated a better performance for the thermoplastic resin, confirming its indication for use in baseboards;
- Thermographic images helped to visualize the percolation of water into the specimens, confirming the better performance (higher temperatures) for the waterproofed series;
- Finally, accelerated aging was sensitive to indicate a behavioral change between the waterproofed series. However, at the end of the test their performance was still much higher (about 6 times) than the reference series. It is recommended to monitor these materials for a longer period of study, in order to verify their efficiency and confirm their useful life time in service.

## 5. ACKNOWLEDGMENTS

The authors thank the support of the Brazilian agencies CNPq, Capes and Fundação Araucária for their financial support, the Federal University of Paraná (UFPR), the Graduate Program in Civil Construction Engineering (PPGECC), the UNIFACEAR University Center and the concrete company NOVAMIX for the aid given to the study.

## 6. REFERENCES

- Aldea, C., Shah, S. P., Karr, A. (1999) “Permeability of cracked concrete” *Materials and Structures*, 32, pp. 370–376. <https://doi.org/10.1007/BF02479629>
- Andrello, J. M., Takagi, E. (2017) “*Debate técnico: impermeabilização in loco*” *Construção Mercado - Técnica*, PINI.
- Associação Brasileira de normas Técnicas. (2005). *NBR 9685: Emulsão Asfáltica para Impermeabilização*. Rio de Janeiro.
- Associação Brasileira de normas Técnicas. (2005). *NBR 9778: Argamassa e concreto endurecidos - Determinação da absorção de água, índice de vazios e massa específica*. Rio de Janeiro.
- Associação Brasileira de normas Técnicas. (2008). *NBR 13321: Membrana acrílica para impermeabilização*. Rio de Janeiro.
- Associação Brasileira de normas Técnicas. (2010). *NBR 15885: Membrana de Polímero Acrílico com ou sem Cimento para Impermeabilização*. Rio de Janeiro.
- Associação Brasileira de normas Técnicas. (2012). *NBR 9779: Argamassa e concreto endurecidos – Determinação da absorção de água por capilaridade*. Rio de Janeiro.
- Associação Brasileira de normas Técnicas. (2013). *NBR 15575: Edificações habitacionais - Desempenho*. Rio de Janeiro.
- Basheer, I., Kropp, J., Cleland, D. J. (2001) “Assessment of the durability of concrete from its permeation properties: a review” *Construction and Building Materials*, 15 (2-3), pp. 93– 103. [https://doi.org/10.1016/S0950-0618\(00\)00058-1](https://doi.org/10.1016/S0950-0618(00)00058-1)
- Bauer, E., Vasconcelos, P. H. C., Granato, J. E. (2010) “Sistemas de impermeabilização e isolamento térmico” In: ISAIA, G. C. *Materiais de construção civil e princípios de ciência e engenharia dos materiais*. São Paulo: Ed. IBRACON.
- Cortizo, E. C. (2007) “Avaliação da técnica de termografia infravermelha para identificação de estruturas ocultas e diagnóstico de anomalias em edificações: Ênfase em edificações de Patrimônio Histórico” 178f. Tese (Doutorado) - Universidade Federal de Minas Gerais, Escola de Engenharia, Departamento de Engenharia Mecânica. Belo Horizonte.
- Freitas, J. G., Carasek, H., Cascudo, O. (2014) “Utilização de termografia infravermelha para avaliação de fissuras em fachadas com revestimento de argamassa e pintura”. *Ambiente Construído*, Porto Alegre, v. 14, n. 1, p. 57-73. <http://dx.doi.org/10.1590/S1678-86212014000100006>
- Gao, J., Yu, Z., Song, L., Wang, T., Wei, S. (2013) “Durability of concrete exposed to sulfate attack under flexural loading and drying–wetting cycles” *Construction and Building Materials*. v. 39, pp. 33-38. <https://doi.org/10.1016/j.conbuildmat.2012.05.033>
- Gong, J., Cao, J., Wang, Y. (2016) “Effects of sulfate attack and dry-wet circulation on creep of fly-ash slag concrete” *Construction and Building Materials*. v.125, pp.12-20. <https://doi.org/10.1016/j.conbuildmat.2016.08.023>
- Jiang, L., Niu, D. (2016) “Study of deterioration of concrete exposed to different types of sulfate solutions under drying-wetting cycles” *Construction and Building Materials*. v. 117, pp. 88-98. <https://doi.org/10.1016/j.conbuildmat.2016.04.094>

- Lourenço, T., Matias, L., Faria, P. (2017) “*Anomalies Detection in Adhesive Wall Tiling Systems by Infrared Thermography.*” *Construction and Building Materials*, v. 148, p. 419-428. <https://doi.org/10.1016/j.conbuildmat.2017.05.052>
- Maldague, X. (2001) “*Infrared and Thermal Testing: nondestructive testing handbook.*” 3. ed. Columbus, OH: Patrick O. Moore.
- Melrinho, A., Matias, L., Faria, P. (2015). *Detecção de anomalias em impermeabilizações de coberturas em terraço através da termografia de infravermelhos.* *Tech ITT by Construlink*, 13(37), 29-38. [https://run.unl.pt/bitstream/10362/16576/1/RI%20-%20Melrinho%20et%20al\\_RIT%2037\\_2015.pdf](https://run.unl.pt/bitstream/10362/16576/1/RI%20-%20Melrinho%20et%20al_RIT%2037_2015.pdf)
- Menezes, M. (2018) “*Influência da umidade do substrato na aderência de sistema de impermeabilização com manta asfáltica aderida à maçarico*” IBI - Instituto Brasileiro de Impermeabilização, 16 p, São Paulo.
- Morgado, J. M., et al. (2018) “*Guia de aplicação da norma de desempenho para impermeabilização. Especificação, aplicação e contratação com foco no atendimento à ABNT 15575/2013*” IBI – Instituto Brasileiro de Impermeabilização, Rio de Janeiro.
- Ngala, V. T., Page, C. L. (1997) “*Effects of carbonation on pore structure and diffusional properties of hydrated cement pastes*”. *Cement and Concrete Research*, V. 27, n.7, pp. 995-1007. [https://doi.org/10.1016/S0008-8846\(97\)00102-6](https://doi.org/10.1016/S0008-8846(97)00102-6)
- Pezzolo, V. (2013) “*Conheça os tipos de impermeabilizante*” Equipe Obra Prima, PINI.
- Picchi, F. A. (1986) “*Impermeabilização de coberturas*” Editora Pini, São Paulo.
- Rocha, J. H. A., Santos, C. F. dos, Oliveira, J. B. de, Albuquerque, L. K dos S., Póvoas, Y. V. (2018) “*Detecção de infiltração em áreas inerenas de edificações com termografia infravermelha: estudo de caso*” *Ambiente Construído*, Porto Alegre, V. 18, n.4, pp. 329-340. <https://doi.org/10.1590/s1678-86212018000400308>
- Rossignolo, J. A. (2005) “*Avaliação da porosidade e do teor de CH de pastas de cimento Portland com Sílica Ativa e Látex SRB*” *Revista Matéria*, V.10, n.3, pp. 437-442. <http://www.materia.coppe.ufrj.br/sarra/artigos/artigo10654>
- Silveira, M. A., Granato, J. E. (2013) “*Diretrizes de desempenho para produtos de impermeabilização*”. 13º Simpósio Brasileiro de Impermeabilização.

## Service life increase of reinforced concrete structures exposed to marine environments through the application of electrochemical techniques

P. Garcés<sup>1\*</sup> , M. A. Climent , J. Carmona , M. J. Sánchez de Rojas 

\*Contact author: [pedro.garces@ua.es](mailto:pedro.garces@ua.es)

DOI: <https://doi.org/10.21041/ra.v11i1.518>

Reception: 21/10/2020 | Acceptance: 03/12/2020 | Publication: 01/01/2021

### ABSTRACT

In this work, the feasibility of a combined treatment of electrochemical chloride extraction (ECE) and cathodic protection (CP) in reinforced concrete structures using a conductive cement-graphite paste as anode has been studied. It has been proven that the prior application of an electrochemical chloride extraction treatment leads to greater durability of the anode. It has been shown that for reinforced concrete structures located in aggressive marine environments, the combination of electrochemical treatments, first ECE to reduce the chloride content and then CP to maintain passivation conditions, is capable of providing adequate protection conditions for the reinforcement, provided that the appropriate current density value is applied, according to the average content of chlorides present in the reinforced concrete structures.

**Keywords:** reinforced concrete, electrochemical chlorides extraction, cathodic protection.

**Cite as:** Garcés, P. Climent, M. A., Carmona, J., Sánchez de Rojas, M. J. (2021), “Service life increase of reinforced concrete structures exposed to marine environments through the application of electrochemical techniques”, Revista ALCONPAT, 11 (1), pp. 48 – 60, DOI: <https://doi.org/10.21041/ra.v11i1.518>

<sup>1</sup> Departamento de Ingeniería Civil, Escuela Politécnica Superior, Universidad de Alicante, Alacant/Alicante, España.

#### Contribution of each author

In this work the authors P.G. and M.A.C. contributed with the original idea of the research, the joint direction of the project, the joint direction of the doctoral theses of J.C. and M.J.S.d.R., discussion of results and writing of the work. The authors J.C. and M.J.S.d.R. contributed with the experimentation, data collection and participation in the discussion of results.

#### Creative Commons License

Copyright 2021 by the authors. This work is an Open-Access article published under the terms and conditions of an International Creative Commons Attribution 4.0 International License ([CC BY 4.0](https://creativecommons.org/licenses/by/4.0/)).

#### Discussions and subsequent corrections to the publication

Any dispute, including the replies of the authors, will be published in the third issue of 2021 provided that the information is received before the closing of the second issue of 2021.

## **Alargamiento de la vida útil de estructuras de hormigón armado expuestas a ambientes marinos mediante la aplicación de técnicas electroquímicas**

### **RESUMEN**

En este trabajo se ha estudiado la viabilidad de un tratamiento combinado de extracción electroquímica de cloruros (EEC) y protección catódica (PC) en estructuras de hormigón armado utilizando como ánodo una pasta conductora de cemento-grafito. Se ha comprobado que la aplicación previa de un tratamiento de extracción electroquímica de cloruros conlleva una mayor durabilidad del ánodo. Se ha demostrado que, para estructuras de hormigón armado situadas en ambientes marinos agresivos, la combinación de tratamientos electroquímicos, primero EEC para reducir el contenido de cloruros y a continuación PC para mantener las condiciones de pasivación, es capaz de proveer condiciones adecuadas de protección a la armadura, siempre que se aplique el valor de densidad de corriente adecuado, de acuerdo con el contenido medio de cloruros presente en las estructuras de hormigón armado.

**Palabras clave:** hormigón armado, extracción electroquímica de cloruros, protección catódica.

## **Extensão da vida útil de estruturas de concreto armado expostas a ambientes marinhos através da aplicação de técnicas eletroquímicas**

### **RESUMO**

Neste trabalho foi estudada a viabilidade de um tratamento combinado de extração eletroquímica de cloreto (EEC) e proteção catódica (PC) em estruturas de concreto armado usando uma pasta condutora de cimento-grafite como ânodo. Verificou-se que a aplicação prévia de um tratamento de extração eletroquímica de cloretos, acarreta uma maior durabilidade do ânodo. Foi demonstrado que, para estruturas de concreto armado localizadas em ambientes marinhos agressivos, a combinação de tratamentos eletroquímicos, primeiro EEC para reduzir o teor de cloreto e depois PC para manter as condições de passivação, é capaz de fornecer condições de proteção adequadas aos armadura, desde que seja aplicado o valor de densidade de corrente adequado, de acordo com o teor médio de cloretos presente nas estruturas de betão armado.

**Palavras-chave:** concreto armado, extração eletroquímica de cloreto, proteção catódica

### **Legal Information**

Revista ALCONPAT is a quarterly publication by the Asociación Latinoamericana de Control de Calidad, Patología y Recuperación de la Construcción, Internacional, A.C., Km. 6 antigua carretera a Progreso, Mérida, Yucatán, 97310, Tel.5219997385893, [alconpat.int@gmail.com](mailto:alconpat.int@gmail.com), Website: [www.alconpat.org](http://www.alconpat.org)

Reservation of journal title rights to exclusive use No.04-2013-011717330300-203, and ISSN 2007-6835, both granted by the Instituto Nacional de Derecho de Autor. Responsible editor: Pedro Castro Borges, Ph.D. Responsible for the last update of this issue, Informatics Unit ALCONPAT, Elizabeth Sabido Maldonado.

The views of the authors do not necessarily reflect the position of the editor.

The total or partial reproduction of the contents and images of the publication is carried out in accordance with the COPE code and the CC BY 4.0 license of the Revista ALCONPAT.

## 1. INTRODUCTION

The main enemy of the durability of concrete structures is the corrosion of steel reinforcement, and this effect is chiefly caused by penetration of chlorides ( $\text{Cl}^-$ ) in the concrete mass. When corrosion occurs, it is necessary to repair the structure if we want to use it for more time, otherwise there is a high risk of collapse. The traditional method for structures contaminated by chlorides is the replacement of the structural elements affected by the corrosion process.

Several electrochemical techniques have been successfully used to the protection and remediation of steel corrosion in reinforced concrete structures. All these techniques are based on the lowering of the electric potential of steel (Page, 1992; Mietz, 1998; Andrade, et al, 1998; Tritthart, 1998; Pedeferri and Bertolini, 2000; Bertolini, 2004; Polder, 2005). This effect can be obtained both by connection to a less noble metal, as in cathodic protection (CP) by sacrificial anodes, or by connection to the negative pole of an electric direct current source, as in CP by impressed current (Page, 1997; Pedeferri, 1996; Polder, 1998; Bertolini, et al, 1998; Glass and Chadwick, 1994). The objective of CP is to prevent the initiation of steel corrosion in new structures. On the other hand, temporary techniques are those intended to change the prevailing corrosion conditions of the structures by lowering its chloride content, such as in electrochemical chloride extraction (ECE) (Slater, et al, 1976; Vennesland, et al, 1986; Hansson and Hansson, 1993; Elsener, et al, 1993). Thus, it is not necessary to replace the contaminated concrete and, once a sufficient quantity of chlorides has been extracted, the durability of the structure is increased (Slater, et al, 1976; Vennesland, et al, 1986; Hansson y Hansson, 1993; Elsener, et al, 1993). An important aspect regarding the application of this technique is the effect that different bar arrangements may have on the efficiency of ECE when applied to a reinforced concrete structural element. Sánchez de Rojas et al, conclude that the extraction efficiency depends on the reinforcing bar arrangement. A uniform layer set-up favours chloride extraction. It is possible to reduce the chloride content in between two reinforcement layers (Garcés, et al, 2006; Sánchez de Rojas, et al, 2006). On the other hand, different solutions for the external anode have been tested, a Ti-RuO<sub>2</sub> wire mesh and a graphite felt fabric, both wrapping the concrete structure with a sandwich-like anodic system consisting of two layers of polypropylene sponge embedding the anodic material. Concluding that if sufficient care is taken with the experimental setup, the efficiency of the extraction with the sandwich-like anodic system may be similar to that obtained with a classical anode immersed in a liquid electrolyte, (Climent, et al, 2006). Finally, also concerning to the external anode, the most important advance in recent years has focused on the study of the viability of using a conductive cement paste (CCP), based on mixes of cement with different carbonaceous materials, as anodic coatings for applications of electrochemical techniques on reinforced concrete, (Pérez, et al, 2010; Carmona, et al, 2015a; Cañón, et al, 2013; Del Moral, et al, 2013; Carmona, et al, 2015b; Climent, et al, 2016; Carmona, et al, 2017; Climent, et al, 2019). For ECE treatments on structural concrete elements, even vertical or of complex shape, the use of a CCP sprayed coating as anode is feasible, because the same efficiency as conventional reference anode (Ti-RuO<sub>2</sub> mesh) is obtained (Pérez, et al, 2010). Conductive cement paste is more versatile as anode because the adaptation to various types of surfaces (vertical or more complex shapes) and the possibility of reutilization. One of the most attractive possibilities offered by these anodic conductive layers is the possibility of using a graphite–cement paste anode for combined treatments of EEC plus CP on reinforced concrete elements (Carmona, et al, 2015; Climent, et al, 2019). These treatments would be interesting in cases of structures heavily contaminated with chlorides and continuously exposed to a harsh chloride environment. It has been shown that, in the experimental conditions of this work, the anode is not damaged during the electrochemical chloride extraction step. The application of a previous chloride extraction step allows working with a lower current density at the cathodic protection step, which reduces the risk of damages of the anodic system. The operation conditions of the above

mentioned electro-chemical techniques differ in each case (Carmona, et al, 2015a; Cañón, et al, 2013; Del Moral, et al, 2013; Carmona, et al, 2015b; Climent, et al, 2016; Carmona, et al, 2017; Climent, et al, 2019). The typical current density for ECE applications on reinforced concrete elements is in the range 1–5 A/m<sup>2</sup>, while the total electric charge passed is usually between  $1 \times 10^6$  and  $5 \times 10^6$  C/m<sup>2</sup>. From an electrochemical point of view the current density should be defined as referred to electrode surface, i.e. the surface of the steel cathode. However, in engineering field applications it is sometimes difficult to know the steel reinforcement area. So, many times the current density is referred to exposed concrete surface, which, in the case of anodic overlay systems is equal to the anode area. CP typically applies current density values between 5 and 20 mA/m<sup>2</sup>, while CPre needs only 1–3 mA/m<sup>2</sup>. Nevertheless, in the case of CP the actual current density needed to effectively protect the steel is higher the higher is the Cl<sup>-</sup> content of concrete.

Next, the experimental program and main results obtained in the combined and successive application of ECE and CP, without changing the anode, using a conductive cement paste, are exposed. These treatments would be interesting in cases of structures heavily contaminated with chlorides and continuously exposed to a harsh chloride environment.

## 2. EXPERIMENTAL PROCEDURE

### 2.1 Methodology

The specimens dedicated to testing the CP or, ECE + CP were prepared with concrete admixed with Cl<sup>-</sup> ions. Table 1 indicates the nomenclature of the specimens and the electrochemical treatments applied to each one. It must be stressed that all specimens included in Table 1, even those that were not given any of the electrochemical treatments (R and P), were subjected to the same salting regime during the 24 weeks period that lasted the CP treatment: 65 ml NaCl 0.5 M weekly sprayed onto the concrete or anodic overlay surface, in order to simulate the continued chloride contamination due to exposure to a very aggressive environment as mentioned above.

Table 1 Nomenclature of specimens for application of the electrochemical techniques

Reference sample	No. specimens	Initial % Cl in concrete (% referred to cement mass)	Studied technique
P	1	0%	-
R	1	2%	-
ER	1	2%	ECE
A	1	2%	CP
EA	1	2%	ECE + CP

### 2.2. Reinforced concrete specimens

The specimens were prism-shaped reinforced concrete elements, with a dimension of  $18 \times 18 \times 8$  cm<sup>3</sup>, which were reinforced by a grid  $16 \times 16$  cm<sup>2</sup> composed of six steel bars (5 mm diameter) welded symmetrically forming squares of 5 cm side, and placed 2 cm under the anode, Fig. 1.

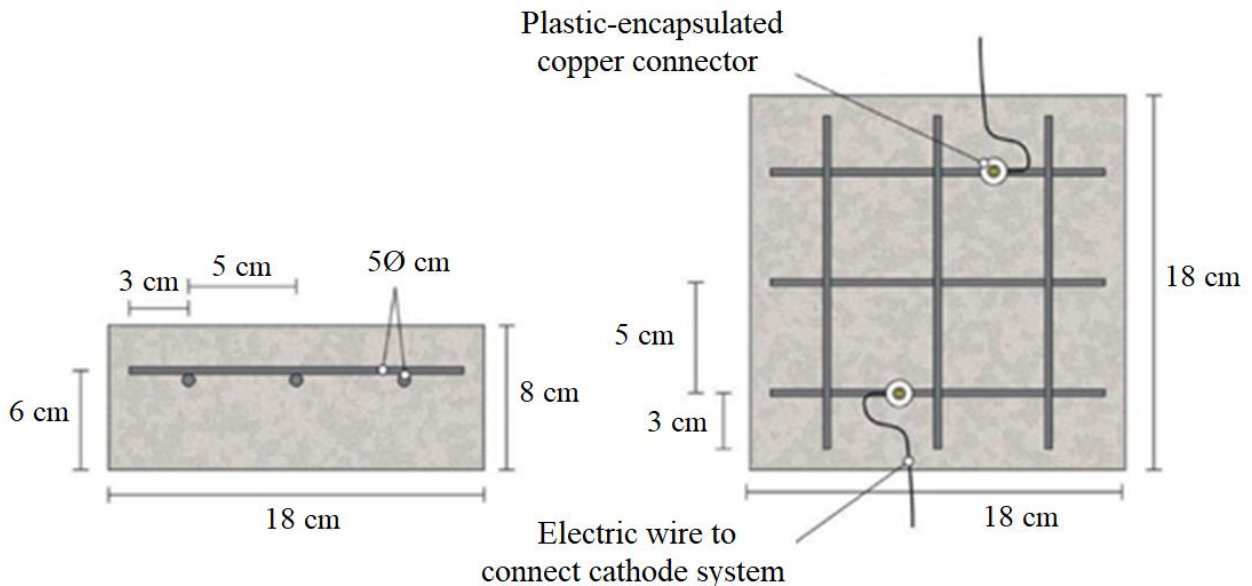


Figure 1. Sketch of reinforcement of samples and connection of the cathodic system (steel reinforcement). Adapted from (Carmona, et al, 2015).

The concrete dosage was as shown in Table 2. One mix was prepared: containing 2%  $\text{Cl}^-$  relative to cement mass for the specimens used in cathodic protection (CP) applications or combined treatment (ECE + CP), see Table 1. Once the formwork was removed, the specimens were moist-cured at 95–98% relative humidity (RH) for 28 days. The characteristics of the hardened concrete were as follows: compressive strength  $37.8 \text{ N/mm}^2$  (AENOR, 2009), porosity 11.1% (UNE, 2014), and bulk density  $2.38 \text{ T/m}^3$  (UNE EN, 2009).

Table 2. Concrete dosage for preparation of the test specimens

Material	Dosage
Portland cement CEM I 42,5 R	$250 \text{ kg/m}^3$
Water/cement ratio (w/c)	0,65
Limestone aggregate	$1890 \text{ kg/m}^3$
Superplasticizer	$2,50 \text{ kg/m}^3$
NaCl	3,3% (2% $\text{Cl}^-$ relative to cement mass)

Fig. 1 also shows the system used for connecting the reinforcement (cathode system) to the negative pole of the electric power source, through plastic isolated copper connectors screwed to the rebar.

### 2.3 Common experimental details of the electrochemical tests

All the electrochemical tests were performed using a CCP anode. The anodic overlay system was prepared by hardening a graphite–cement paste (GCP) obtained by mixing graphite powder and Portland cement at 50%–50% in mass. Water to solid mix ratio was 0.8. The resistivity of the graphite–cement paste was measured through the four-probe method (Galao, et al, 2014). Secondly, a 2 mm thick layer of this paste was applied on the surface of each specimen, and then all of them were moist cured for 10 days. After that, two grooves were performed lengthwise onto the anodic

overlay, without reaching the concrete surface, in order to receive both graphite rods to connect to the positive pole of the electric source. To finish up, these rods were overlaid with graphite–cement paste in order to join with the anode system perfectly but avoiding any contact between graphite rods and concrete.

The measurements of steel corrosion potential ( $E_{corr}$ ) and all the single electrode potentials, were performed using Ag–AgCl reference electrodes. These electrodes were housed in respective holes drilled from the exposed surface of the concrete specimen (that bearing the graphite–cement anode) to the vicinity of the rebar, Fig. 2. For this purpose, the holes were sheathed with a plastic tube, and filled with a KOH 0.2 M aqueous solution, trying to approach the physical-chemical conditions of the concrete’s inner pore solution

Two of the salted specimens were used only for determining the efficiency of the ECE process. Concrete cores were extracted from them, and their chloride content profiles were determined, in one case before and in the other case after ECE. The ECE efficiencies were calculated as the percentages of reduction of the initial chloride content. Obtaining the chloride content profiles before and after the ECE trials allowed calculating the local and overall efficiencies. The  $Cl^-$  profiles were measured following essentially RILEM recommended procedures (Vennesland, et al, 2013). Cylindrical concrete cores, 95 mm diameter and 20 mm height (up to the rebar depth), were extracted. From these cores, concrete dust samples were obtained by grinding thin (2 mm thick) successive parallel layers to the exposed surface. In this way 10 concrete dust samples were gained from each core, thus allowing the obtention of sufficiently detailed chloride content profiles. The determination of the samples’ acid soluble chloride contents was carried out by potentiometric titration, (Climent, et al, 1999; Climent, et al, 2004). All the chloride content values are expressed in this work as %  $Cl^-$  relative to cement mass.

The ECE treatments were applied galvanostatically with  $2 \text{ A/m}^2$  of current density (relative to concrete or anode surface) and  $1.5 \text{ MC/m}^2$  of charge density relative to concrete surface ( $2.6 \text{ MC/m}^2$  relative to steel surface). The external electrolyte in contact with the anode was tap water. The CP treatments were applied galvanostatically with  $15 \text{ mA/m}^2$  of current density (relative to concrete or anode surface) ( $25.5 \text{ MC/m}^2$  relative to steel surface). Both techniques, ECE and CP, were applied under laboratory conditions ( $20^\circ\text{C}$  and RH 60%). The potential data were recorded using a data acquisition system.

The application of CP consisted of two phases:

- Phase 1. First 24 weeks. The aforementioned treatment CP was continuously applied during the first 13 weeks. Then, the current was switched off for 4 weeks and after that, treatments were resumed to the end. Chloride contamination was continuously applied, even during the switch off periods.

While applying the CP treatments some electrochemical parameters were measured. During the current passing periods the feeding voltage of each specimen,  $E_{feed}$ , was obtained as the potential difference between cathode and anode; and the individual anodic and cathodic potentials,  $E_a$  and  $E_c$ , respectively, were measured against the reference electrode Ag/AgCl. Finally, in order to check the efficiency of CP as maintainer of protection conditions of steel, the “100 mV decay” criterion was used, as is specified in ISO 12696:2012. This criterion has been also extensively employed for this purpose by several researchers (Glass, et al, 2001; Liu and Shi, 2012; Dugarte, et al, 2015; Christodoulou, 2010). The method consists in obtaining the 4 h potential decay ( $E_{decay}$ ), that is the difference between  $E_c^{4h}$  (the value of  $E_c^{4h}$  after the current switch off), and the instant-off cathodic potential  $E_c^{io}$ , which in this case was measured 1 s after the current switch off. The minimum value of the 4 h depolarization must be 100 mV for an adequate corrosion protection of steel. The values of  $E_c^{io}$  were monitored with an automatic data logger able to obtain and record 500 measurements in 6 s, after the current switch off.

Once the 24 weeks processes were fulfilled, cores were extracted from all specimens of Table 1, and their respective  $\text{Cl}^-$  content profiles were obtained. This was done with the purpose of evaluating the net effect of the electrochemical treatments on the  $\text{Cl}^-$  ion uptake by the reinforced concrete specimens during the continued exposure to a very aggressive environment.

- Phase 2. At the end of Phase 1 it was observed that all the specimens had lost the steel protection condition, evidenced by Edecay values lower than 100 mV. Then, it was decided to start this second phase with the objective of recovering the protection conditions of steel by adjusting the current density of the CP treatments. The procedure was to increase progressively the current density during 4 weeks, starting with a value of 20 mA/m<sup>2</sup>, until obtaining the protection conditions ( $\Delta E_{\text{decay}} \geq 100$  mV).

### 3. RESULTS AND DISCUSSION

#### 3.1. Application of ECE

Two of the reinforced concrete specimens were subjected to an ECE treatment before starting the first phase of the CP treatments. Once finished the ECE process with the settled parameters,  $\text{Cl}^-$  content profiles were obtained, corresponding to the states before and after the ECE treatment. The local ECE efficiencies, understood as percentage of  $\text{Cl}^-$  content removed, are plotted in Fig. 2. The average of removed  $\text{Cl}^-$  was 51% of the initial content, i.e. the residual  $\text{Cl}^-$  content of concrete after ECE was approximately 1% referred to cement mass. This indicates a good performance of the ECE process applied on a conventional ordinary Portland cement concrete with the GCP anodic overlay system, for a relatively low charge density of  $1.5 \times 10^6 \text{C/m}^2$  relative to concrete surface. This result can be compared to the 41% efficiency obtained for a very similar reinforced concrete element, with the same initial amount of  $\text{Cl}^-$ , subject to an ECE treatment, using a Ti–RuO<sub>2</sub> mesh anode, and passing a total charge density of 1 MC/m<sup>2</sup> relative to concrete surface (Pérez, et al, 2010).

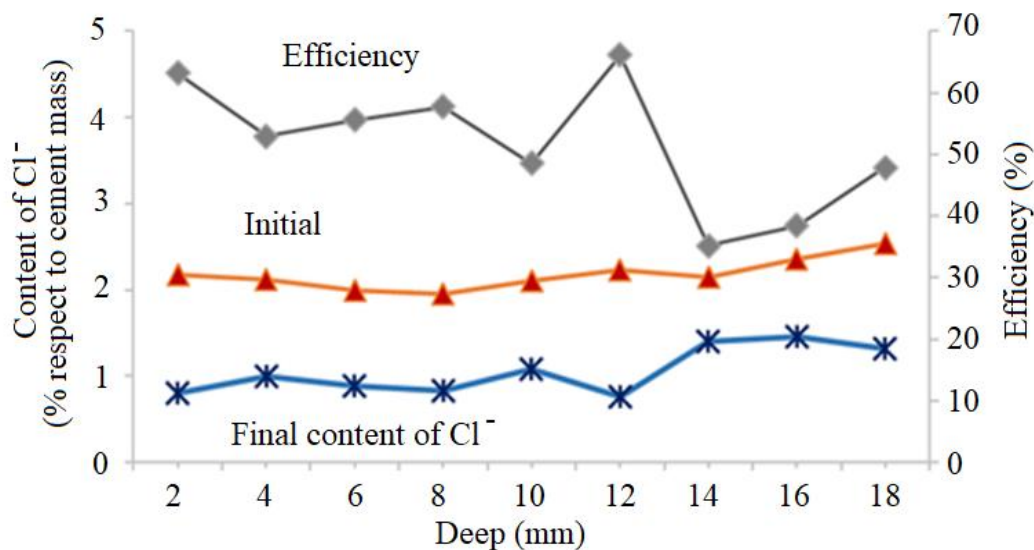


Figura 2. Chloride concentration profiles before ECE (initial) and after ECE (final) and local efficiencies of the extraction process. Adapted from (Carmona, et al., 2015)

### 3.2. First phase of electrochemical treatments

In this section we describe the results of tests carried out to investigate the performance of the CCP anodes during protective electrochemical treatments to reinforced concrete elements affected by steel corrosion due to chloride contamination, such are CP, and combined treatments of ECE + CP.

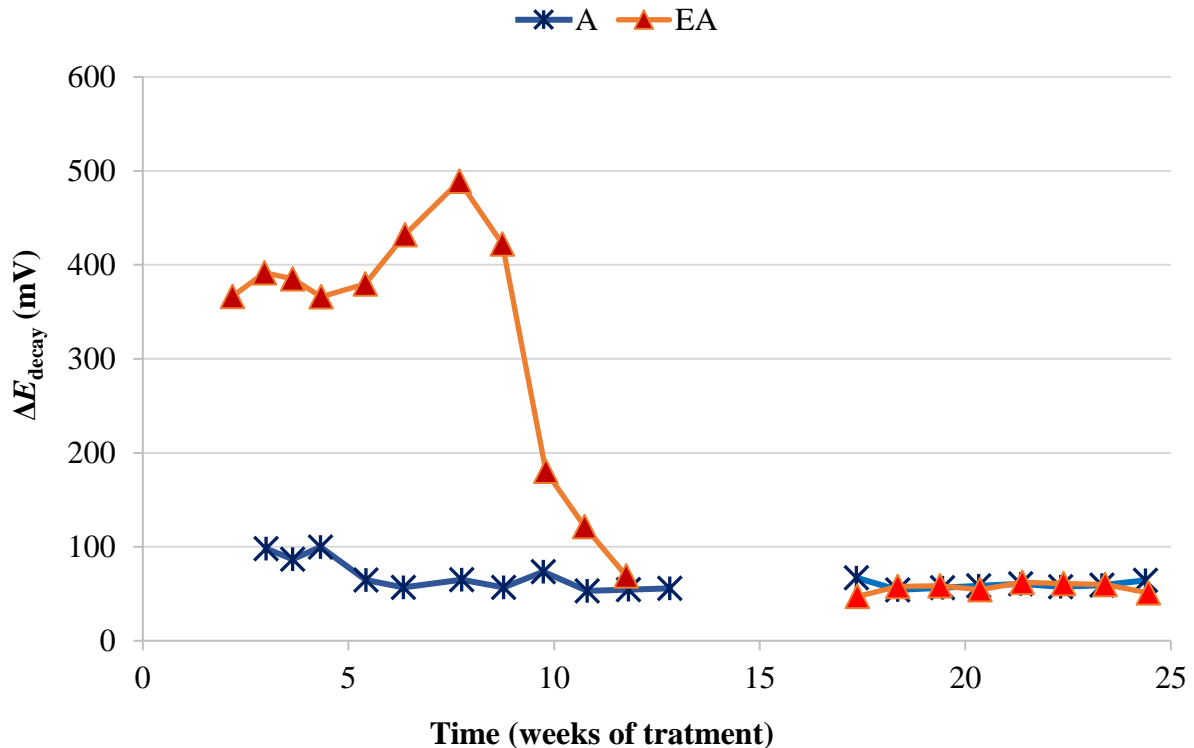


Figure 3. Evolution of  $\Delta E_{decay}$  during the CP treatments. A: CP; EA: ECE + CP. All of them subjected to  $\text{Cl}^-$  contamination during the 24 weeks. The electrochemical treatments were interrupted between week 13 and week 17. Adapted from (Carmona, et al, 2015).

To verify the effectiveness of CP treatments for protecting steel from corrosion, the “100 mV decay” criterion (ISO, 2012) was used, as stated in Section 2.3. Fig. 4 shows the evolution of the  $\Delta E_{decay}$  values for the specimens in Table 1, during the 24 weeks experiments. The  $\Delta E_{decay}$  values of the A specimen, treated only with CP, practically never reached the threshold value of 100 mV. It seems that a  $15 \text{ mA/m}^2$  current density was not sufficient to provide protection to steel in such harsh conditions: initial  $\text{Cl}^-$  content of 2% plus the continued salting regime (65 ml NaCl 0.5 M weekly sprayed onto the anodic overlay surface). Regarding the EA specimen (ECE + CP), the protection conditions of steel were kept during 11 weeks because of the current circulation, despite external  $\text{Cl}^-$  loading. Cathodic protection of  $15 \text{ mA/m}^2$  current density, relative to concrete surface, was able to keep protective conditions for the steel reinforcement if the initial  $\text{Cl}^-$  content of the specimen was about 1%.

So, in the case of the specimen with initial  $\text{Cl}^-$  content of about 2%, a higher current density would be needed for reaching the protection conditions (Pedferri, 1996). These observations corroborate the main hypothesis of the present research, i.e. in cases of reinforced concrete structures with a high  $\text{Cl}^-$  contamination subject to very harsh chloride environments, it would be advantageous to apply successively an initial ECE treatment to reduce the  $\text{Cl}^-$  content, and then maintain protective conditions to steel through a continuous CP treatment without the need of using a too high CP

current density, which could eventually impair the performance of the anodic system (Carmona, et al, 2015). These combined treatments, ECE + CP, would be more conveniently implemented with the CCP coatings since the same anode can serve both for the ECE and for the CP treatments.

Table 3. Final averaged chloride contents (expressed in %  $\text{Cl}^-$  relative to cement mass) at the end of the 24 weeks of exposure to a severe  $\text{Cl}^-$  load.

Specimen	Initial $\text{Cl}^-$ content (% ref. cem. mass)	Electrochemical treatment previous to the 24 weeks first phase	Electrochemical treatment previous to the 24 weeks first phase	Final averaged (*) $\text{Cl}^-$ content (% ref. cem. mass)
P	0%	-	-	4,93%
R	2%	-	-	6,08%
ER	2%	ECE	-	4,26%
A	2%	-	PC	5,39%
EA	2%	ECE	PC	3,41%

(\*) The final  $\text{Cl}^-$  content was calculated as the mean value of those found in the  $\text{Cl}^-$  content profile determined through the concrete cover zone (20 mm width)

At the end of Phase 1 all the reinforced concrete specimens had reached a very high degree of  $\text{Cl}^-$  contamination, as can be appreciated in Table 3. Nevertheless, some comparisons can be done on the behavior of the different cases. For instance, specimens treated with ECE + CP (EA) during Phase 1, have experienced less  $\text{Cl}^-$  ingress than the reference specimen ER, which after the ECE trial was left untreated during the phase 1. This represents a further evidence of the “chloride barrier effect”, mentioned by Pedferri (Pedferri, 1996), as one of the beneficial secondary effects of CP, as the polarity of the electric field induces a repellent effect of the negative ions, thus reducing the chloride uptake by concrete in a harsh chloride environment.

### 3.3. Second phase of electrochemical treatments

Given that after the 24 weeks of treatments of phase 1, including rest periods between the 13<sup>th</sup> and 17<sup>th</sup> weeks, the steel reinforcements in all concrete specimens had completely lost their protection conditions, and having been demonstrated that a CP of 15 mA/m<sup>2</sup> was unable to restore the protective conditions (Fig. 4), the Phase 2 was started. The external  $\text{Cl}^-$  load was discontinued since all the specimens had reached very high  $\text{Cl}^-$  contents, see Table 4. In these conditions, CP was applied with higher current densities. The question was if it would be possible to recover the protection conditions of steel by increasing the current density to the appropriate value. In the beginning of this last phase, the current density was set at 20 mA/m<sup>2</sup>. After 4 weeks in operation the threshold value of 100 mV was not reached, i.e. the protection conditions were not obtained, Fig. 6. Neither success was obtained in a second attempt at 25 mA/m<sup>2</sup> (data not shown in Fig. 6). Finally, a third step of 40 mA/m<sup>2</sup> was set. In this case, after 4 weeks, the rule of 100 mV of  $\Delta E_{decay}$  was achieved for EA and A specimens.

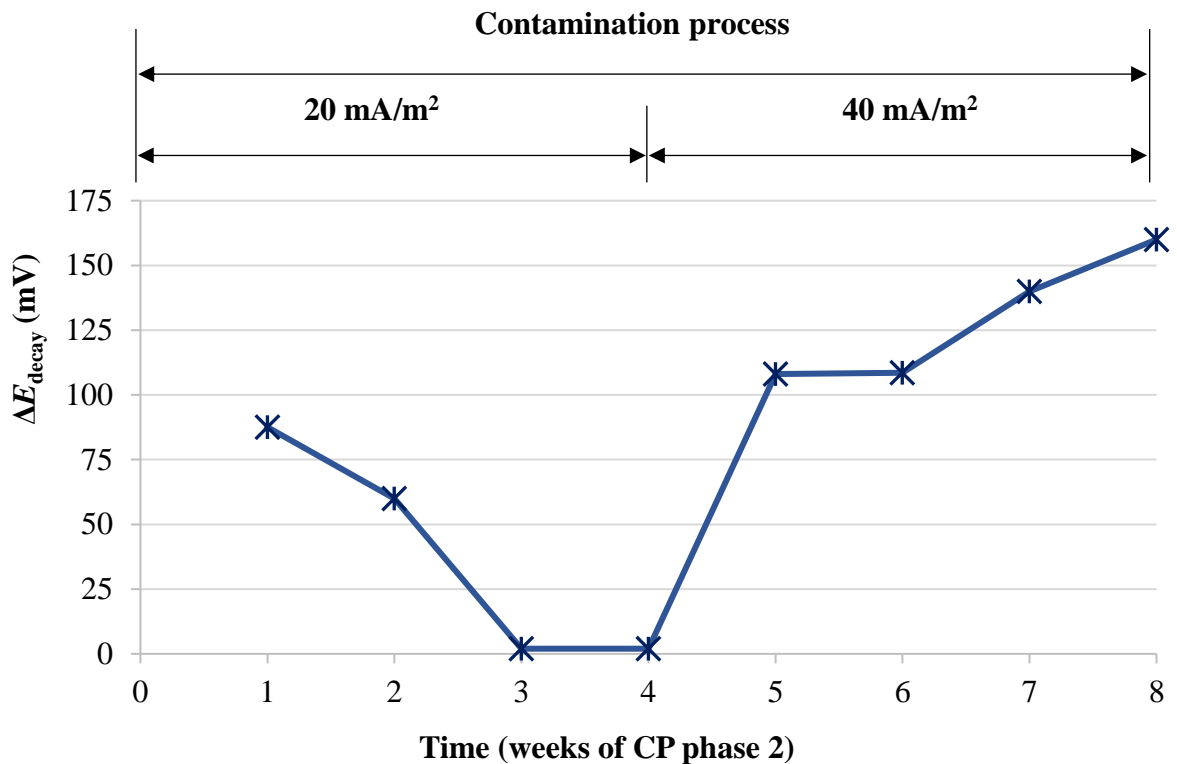


Figure 4. Evolution of  $\Delta E_{\text{decay}}$  during phase 2 of CP. First step of 4 weeks with  $20 \text{ mA/m}^2$  of current density, and third step with  $40 \text{ mA/m}^2$ . Adapted from (Carmona, et al, 2015).

Moreover, protection conditions were verified with the measurement of depolarization potential difference values 7 days after switch off [39]. In fact, more than 150 mV of  $\Delta E_{\text{decay}}$  was reached after 7 days (209 mV for EA).

#### 4. CONCLUSIONS

The results of this work point out that it is possible to use a graphite–cement paste, overlaid on the surface of a reinforced concrete element, as the anode for successive treatments of electrochemical chloride extraction, to reduce the chloride content and then cathodic protection to maintain protective conditions for the steel reinforcement.

It is possible to recover protective conditions against corrosion of steel reinforcement in concrete by applying a combined treatment of ECE followed by a continuous CP treatment. The current density value of the CP step must be set at the proper value, according to the residual chloride content in concrete.

#### 5. ACKNOWLEDGEMENTS

This research was funded by the Spanish Agencia Estatal de Investigación (AEI), and Fondo Europeo de Desarrollo Regional (FEDER) through project BIA2016-80982-R. We acknowledge also funding from the Spanish Ministerio de Ciencia e Innovación (MAT2009-10866), and Generalitat Valenciana (PROMETEO/2013/035).

## 6. REFERENCES

- Andrade, C., Castellote, M., Alonso, C. (1998), *An overview of electrochemical realkalisation and chloride extraction*, in: D.W.S. Ho, I. Godson, F. Collins (Eds.), *Rehabilitation of Structures*, Proceedings of 2nd International RILEM/CSIRO/ACRA Conference, Melbourne, Australia, 21–23, September 1998, RILEM, Melbourne, Australia, pp. 1–12
- Asociación Española de Normalización y Certificación (AENOR) (2009), *(Ensayos de Hormigón Endurecido. Parte 3: Determinación de la Resistencia a Compresión de Probetas (Testing Hardened Concrete – Part 3: Compressive Strength of Test Specimens)*, Madrid, Spain.
- Asociación Española de Normalización y Certificación (AENOR) (2014), *UNE 83980:2014 Durabilidad del Hormigón. Métodos de Ensayo. Determinación de la Absorción de Agua, la Densidad y la Porosidad Accesible al Agua del Hormigón (Concrete Durability. Test Methods. Determination of the Water Absorption, Density and Accessible Porosity for Water in Concrete)*, Madrid, Spain, (in Spanish).
- Asociación Española de Normalización y Certificación (AENOR) (2009), *UNE EN 12390-7:2009 Ensayos de Hormigón Endurecido. Parte 7: Densidad del Hormigón Endurecido (Testing Hardened Concrete – Part 7: Density of Hardened Concrete)*, Madrid, Spain.
- Bertolini, L., Elsener, B., Pedferri, P., Polder, R. B. (2004), *Electrochemical techniques*, in: *Corrosion of Steel in Concrete*, Wiley-VCH, Weinheim, Germany, pp. 345–374.
- Bertolini, L., Bolzoni, F., Pedferri, P., Lazzari, L., Pastore, T. (1998), *Cathodic protection and cathodic prevention in concrete principles and applications*, *Journal of Applied Electrochemistry*. 28, 1321–1331. <https://doi.org/10.1023/A:1003404428827>
- Carmona, J., Garcés, P., Climent, M. A. (2015a), *Efficiency of a conductive cement-based anodic system for the application of cathodic protection, cathodic prevention and electrochemical chloride extraction to control corrosion in reinforced concrete structures*, *Corrosion Science*, 96, 102–111. <https://doi.org/10.1016/j.corsci.2015.04.012>
- Carmona, J., Climent, M. A., Antón, C., De Vera, G., Garcés, P. (2015b), *Shape effect of electrochemical chloride extraction in structural reinforced concrete elements using a new cement-based anodic system*, *Materials*, 8 (6), 2901–2917. <https://doi.org/10.3390/ma8062901>
- Carmona, J., Climent, M. A., Garcés, P. (2017), *Influence of different ways of chloride contamination on the efficiency of cathodic protection applied on structural reinforced concrete elements*, *Journal of Electroanalytical Chemistry*. 793, 8–17. <https://doi.org/10.1016/j.jelechem.2016.08.029>
- Cañón, A., Garcés, P., Climent, M. A., Carmona, J., Zornoza, E. (2013), *Feasibility of electrochemical chloride extraction from structural reinforced concrete using a sprayed conductive graphite powder–cement as anode*, *Corrosion Science*. 77, 128–134. <https://doi.org/10.1016/j.corsci.2013.07.035>
- Christodoulou, C., Glass, G. K., Webb, J., Austin, S., Goodier, C. (2010), *Assessing the long term benefits of impressed current cathodic protection*, *Corrosion Science*. 52, 2671–2679. <https://doi.org/10.1016/j.corsci.2010.04.018>
- Climent, M. A., Viqueira, E., De Vera, G., López, M. M. (1999), *Analysis of acid-soluble chloride in cement, mortar and concrete by potentiometric titration without filtration steps*, *Cement and Concrete Research*. 29 (6), 893–898. [https://doi.org/10.1016/S0008-8846\(99\)00063-0](https://doi.org/10.1016/S0008-8846(99)00063-0)
- Climent, M. A., De Vera, G., Viqueira, E., López, M. M. (2004), *Generalization of the possibility of eliminating the filtration step in the determination of acid-soluble chloride content in cement and concrete by potentiometric titration*, *Cement and Concrete Research*. 34 (12), 2291–2300. <https://doi.org/10.1016/j.cemconres.2004.04.012>

- Climent, M. A., Sánchez de Rojas, M<sup>a</sup>. J., De Vera, G., Garcés, P. (2006), *Effect of type of anodic arrangements on the efficiency of electrochemical chloride removal from concrete*. ACI Materials Journal 103, 243-250.
- Climent, M. A., Carmona, J., Garcés, P. (2016), *Graphite–cement paste: a new coating of reinforced concrete structural elements for the application of electrochemical anti-corrosion treatments*, Coatings, 6 (3), 32. <https://doi.org/10.3390/coatings6030032>
- Climent, M. A., Carmona, J., Garcés, P. (2019), *Application of combined electrochemical treatments to reinforced concrete: Electrochemical chloride extraction plus cathodic protection*, Hormigón y Acero, 69 (1), 43–51. <https://doi.org/10.1016/j.hya.2018.05.003>
- Del Moral, B., Galao, O., Antón, C., Climent, M. A., Garcés, P. (2013), *Usability of cement paste containing carbon nanofibres as an anode in electrochemical chloride extraction from concrete*, Materiales de Construcción, 63(309), 39–48. <https://doi.org/10.3989/mc.2012.031>
- Dugarte, M., Sagüés, A. A., Williams, K. (2015), *Cathodic prevention for reinforcing steel in cracked concrete of chloride contaminated structures*, in: Proceedings of CORROSION 2015 Conference, NACE-2015-6102, Houston, TX, USA, 15–19 March 2015, NACE International, Houston, TX, USA, p. 11.
- Elsener, B., Molina, M., Böhni, H. (1993), *The electrochemical removal of chlorides from reinforced concrete*, Corrosion Science. 35 (5-8), 1563–1570. [https://doi.org/10.1016/0010-938X\(93\)90385-T](https://doi.org/10.1016/0010-938X(93)90385-T)
- Garcés, P., Sánchez de Rojas, M. J., Climent, M. A. (2006), *Effect of the reinforcement bar arrangement on the efficiency of electrochemical chloride removal technique applied to the reinforced concrete structures*, Corrosion Science. 48, 531–545. <https://doi.org/10.1016/j.corsci.2005.02.010>
- Galao, O., Baeza, F. J., Zornoza, E., Garcés, P. (2014), *Strain and damage sensing properties on multifunctional cement composites with CNF*, Cement and Concrete Composites. 46, 90–98. <https://doi.org/10.1016/j.cemconcomp.2013.11.009>
- Glass, G. K., Chadwick, J. R. (1994), *An investigation into the mechanisms of protection afforded by a cathodic current and the implications for advances in the field of cathodic protection*, Corrosion Science, 36 (12), 2193–2209. [https://doi.org/10.1016/0010-938X\(94\)90017-5](https://doi.org/10.1016/0010-938X(94)90017-5)
- Glass, G. K., Hassanein, A. M., Buenfeld, N. R. (2001), *Cathodic protection afforded by an intermittent current applied to reinforced concrete*, Corrosion Science. 43 (6), 1111–1131. [https://doi.org/10.1016/S0010-938X\(00\)00133-5](https://doi.org/10.1016/S0010-938X(00)00133-5)
- Hansson, I. L. H., Hansson, C. M. (1993), *Electrochemical extraction of chlorides from concrete. Part I – A qualitative model of the process*, Cement and Concrete Research. 23 (5), 1141–1152. [https://doi.org/10.1016/0008-8846\(93\)90174-8](https://doi.org/10.1016/0008-8846(93)90174-8)
- ISO (2012), *ISO 12696: 2012. Cathodic Protection of Steel in Concrete*, Geneva, Switzerland.
- Liu, Y., Shi, X. (2012), *Modeling cathodic prevention for unconventional concrete in salt-laden environment*, Anti-Corrosion Methods and Materials, 59 (3), pp. 121-131. <https://doi.org/10.1108/00035591211224663>
- Mietz, J. (1998), *Electrochemical rehabilitation methods for reinforced concretes structures: a state of the art report*, in: Publication Number 24 of the European Federation of Corrosion, IOM Communications Ltd, London, UK, pp. 57
- Page, C. L. (1992), *Interfacial effects of electrochemical protection method applied to steel in chloride containing concrete*, in: D.W.S. Ho, F. Collins (Eds.), Proceedings of the International RILEM/CSIRO/ACRA Conference on Rehabilitation of Concrete Structures, Melbourne, Australia 1992, RILEM, Melbourne, Australia, pp. 179–187.
- Page, C. L. (1997), *Cathodic protection of reinforced concrete. Principles and applications*, in: Proceedings of the International Conference on Repair of Concrete Structures, Svolve, Norway, 1997, pp. 123–132

- Pedefferri, P. (1996), *Cathodic protection and cathodic prevention*, Construction and Building Materials. 10 (5), 391–402. [https://doi.org/10.1016/0950-0618\(95\)00017-8](https://doi.org/10.1016/0950-0618(95)00017-8)
- Pedefferri, P., Bertolini, L. (2000), *Tecniche elettrochimiche (Electrochemical techniques)*, in: La Durabilità del Calcestruzzo Armato (The Durability of Reinforced Concrete), McGraw-Hill, Milano, Italy, pp. 253–273. (In Italian).
- Pérez, A., Climent, M. A., Garcés, P. (2010), *Electrochemical extraction of chlorides from reinforced concrete using a conductive cement paste as the anode*, Corrosion Science. 52 (5), 1576–1581. <https://doi.org/10.1016/j.corsci.2010.01.016>
- Polder, R. B. (1998), *Cathodic protection of reinforced-concrete structures in The Netherlands – experience and developments*, Heron 43 (1), 3–14
- Polder, R. B. (2005), *Electrochemical techniques for corrosion protection and maintenance*, in: H. Böhni (Ed.), Corrosion in Reinforced Concrete Structures, Woodhead Publishing, Cambridge, UK, pp. 215–241
- Sánchez de Rojas, M. J., Garcés, P., Climent, M.A. (2006), *Electrochemical extraction of chlorides from reinforced concrete: variables affecting treatment efficiency*, Materiales de Construcción, 56 (284), 17–26. <https://doi.org/10.3989/mc.2006.v56.i284.15>
- Slater, J. E., Lankard, D. R., Moreland, P. J. (1976), *Electrochemical removal of chlorides from concrete bridge decks*, Materials Performance, 56, 21–26.
- Tritthart, J. (1998), *Electrochemical Chloride Removal: An Overview and Scientific Aspects*, The American Ceramic Society, Westerville, OH, USA, pp. 401–441
- Vennesland, Ø., Climent, M. A., Andrade, C. (2013), *Recommendation of RILEM TC 178-TMC: testing and modelling chloride penetration in concrete, Methods for obtaining dust samples by means of grinding concrete in order to determine the chloride concentration profile*, Materials and Structures. 46, 337–344. <https://doi.org/10.1617/s11527-012-9968-1>
- Vennesland, Ø., Opsahl, O. A., Russell-Rayner, A. P. (1986), *Removal of chlorides from concrete*. European Patent Application number 86302888.2. Publication number 0 200 428.

## Mapping of pathological manifestations in asphalt pavement through the use of drones

R. T. Vasconcelos Fernandes<sup>1</sup>, A. Fonseca Cabral<sup>1</sup>, G. C. Batista Dantas<sup>1\*</sup>,  
V. N. Varela Tinoco<sup>1</sup>, B. D. Azevedo da Silveira<sup>1</sup>, A. M. Sousa Junior<sup>1</sup>

\*Contact author: [gerbeson\\_dantas@hotmail.com](mailto:gerbeson_dantas@hotmail.com)

DOI: <https://doi.org/10.21041/ra.v11i1.521>

Reception: 30/10/2020 | Acceptance: 16/12/2020 | Publication: 01/01/2021

### ABSTRACT

This work objective is to study the feasibility of the Drones' use for mapping and inspecting pathological manifestations in asphalt pavements compared to the traditional method. Sampling plots were established every 20 m, with 6 m extension, making a total of 20 stations, which had their pathological manifestations recorded and calculated with the Global Severity Index for the study area. The results obtained by the reference and alternative methodologies were confronted according to the pathologies identified and the time spent in the surveys. The results showed feasibility in the use of drones for inspection of pathologies in asphalt pavements, based on DNIT 006/2003 - PRO, obtaining results similar to those of the traditional methodology with a significant reduction of the time of operation (33.3%).

**Keywords:** road inspection; defects in flexible pavements; DNIT 006/2003; alternative methodology; drones.

**Cite as:** Vasconcelos Fernandes, R. T., Fonseca Cabral, A., Batista Dantas, G. C., Varela Tinoco, V. N., Azevedo da Silveira, B. D., Sousa Junior, A. M. (2021), "*Mapping of pathological manifestations in asphalt pavement through the use of drones*", Revista ALCONPAT, 11 (1), pp. 61 – 72, DOI: <https://doi.org/10.21041/ra.v11i1.521>

<sup>1</sup> Universidade Federal Rural do Semi-Árido, Rua Francisco Mota Bairro, 572 - Pres. Costa e Silva, Mossoró - RN, 59625-900, Brasil.

#### Contribution of each author

This work consisted of the following steps: research design, bibliographic survey, data collection, analysis of results obtained in the field, writing of the manuscript, translation, text review and evaluation of the evaluation of the research.

The author Rogerio Taygra Vasconcelos Fernandes participated in the article in the stages of research design (50%), bibliographic survey (50%), analysis of results obtained in the field (50%), writing of the manuscript (33.33%) and evaluation of the research (25%). The author Adriene Fonseca Cabral was responsible for the stages of bibliographic survey (25%), data collection (90%), analysis of results obtained in the field (50%) and writing of the manuscript (33.33%). The author Gerbeson Carlos Batista Dantas participated in the bibliographic survey (25%), manuscript writing (33.33%), translation (20%) and text review (50%). The author Vinicius Navarro Varela Tinoco participated in the stage of data collection (10%), translation (80%) and text review (25%). The author Brenno Dayano Azevedo Da Silveira participated in the research design (25%) and evaluation of the research (50%). The author Almir Mariano Sousa Junior participated in the research design stage (25%), text review (25%) and evaluation of the research (25%).

#### Creative Commons License

Copyright 2021 by the authors. This work is an Open-Access article published under the terms and conditions of an International Creative Commons Attribution 4.0 International License ([CC BY 4.0](https://creativecommons.org/licenses/by/4.0/)).

#### Discussions and subsequent corrections to the publication

Any dispute, including the replies of the authors, will be published in the third issue of 2021 provided that the information is received before the closing of the second issue of 2021.

## Mapeamento de manifestações patológicas em pavimento asfáltico por meio de uso de drones

### RESUMO

Este trabalho objetiva estudar a viabilidade do emprego de Drones para mapeamento e inspeção de manifestações patológicas em pavimentos asfálticos comparando ao método tradicional. Foram estabelecidas parcelas amostrais a cada 20 m, com 6 m de extensão, totalizando 20 estações, as quais tiveram suas manifestações patológicas anotadas e calculado o Índice Global de Gravidade para a área de estudo. Os resultados obtidos pelas metodologias de referência e alternativa foram confrontados em função das patologias identificadas e do tempo gasto nos levantamentos. Os resultados demonstraram viabilidade para emprego de Drones para inspeção de patologias em pavimentos asfálticos, tomando como base a Norma DNIT 006/2003 – PRO, obtendo resultados similares à metodologia tradicional com redução significativa do tempo de operação (33,3%).

**Palabras clave:** inspeção rodoviária; defeitos em pavimentos flexíveis; DNIT 006/2003; metodologia alternativa; drones.

## Mapeo de manifestaciones patológicas en pavimento asfáltico por medio del uso de drones

### RESUMEN

El objetivo de este trabajo es estudiar la viabilidad del empleo de Drones para mapear e inspeccionar manifestaciones patológicas en pavimentos asfálticos en comparación con el método tradicional. Se establecieron parcelas muestrales cada 20 m, con 6 m de extensión, totalizando 20 estaciones, las cuales tuvieron sus manifestaciones patológicas anotadas y calculado el Índice Global de Gravedad para el área de estudio. Los resultados obtenidos con las metodologías de referencia y alternativa se confrontaron en función de las patologías identificadas y el tiempo empleado en los levantamientos. Los resultados demostraron viabilidad para el empleo de Drones en la inspección de patologías de pavimentos asfálticos, tomando como base la Norma DNIT 006/2003 - PRO, obteniendo resultados similares a la metodología tradicional con reducción significativa del tiempo de operación (33,3%).

**Palabras clave:** inspección de carreteras; defectos en pavimentos flexibles; DNIT 006/2003; metodología alternativa; aviones no tripulados.

### Legal Information

Revista ALCONPAT is a quarterly publication by the Asociación Latinoamericana de Control de Calidad, Patología y Recuperación de la Construcción, Internacional, A.C., Km. 6 antigua carretera a Progreso, Mérida, Yucatán, 97310, Tel.5219997385893, [alconpat.int@gmail.com](mailto:alconpat.int@gmail.com), Website: [www.alconpat.org](http://www.alconpat.org)

Reservation of journal title rights to exclusive use No.04-2013-011717330300-203, and ISSN 2007-6835, both granted by the Instituto Nacional de Derecho de Autor. Responsible editor: Pedro Castro Borges, Ph.D. Responsible for the last update of this issue, Informatics Unit ALCONPAT, Elizabeth Sabido Maldonado.

The views of the authors do not necessarily reflect the position of the editor.

The total or partial reproduction of the contents and images of the publication is carried out in accordance with the COPE code and the CC BY 4.0 license of the Revista ALCONPAT.

## 1. INTRODUCTION

Road transportation is a fundamental service for the economic development in Brazil, directly influencing aspects of production and consumption, since the country has its infrastructure oriented to the road mode (Andrade; Maia; Lima Neto, 2015). Nevertheless, this model accounts for 61% of cargo transportation in Brazil and is the main system for passengers' traffic. As for social and economic aspects, this sector is responsible for generating more than 1.5 million direct jobs and contributes for 12.7% of the Gross Domestic Product of non-financial services nationally (CNT, 2017).

Despite its importance, historically little attention has been given to maintaining the infrastructure of Brazilian highways, which reflects in the depreciation of the road network, a situation that has intensified with the economic crisis that the country has been going through since 2013 (CNT, 2017). As a result of the lack of investments, it is estimated that more than 50% of the highways have some type of pathology, and of these, 19% are in a general state of poor or very bad conservation. According to the World Economic Forum (FEM), Brazil ranks 111th out of 138 countries in terms of road infrastructure quality (CNT, 2017; FEM, 2016).

Among the main reasons for the deteriorated state of the Brazilian road network, the National Department of Transport Infrastructure (DNIT, 2011) attributes the absence of a Pavement Management System (SGP), which would make possible to achieve the best possible application for public resources available and offer safe, compatible and economical road transport with the growing Brazilian demand. Without it, there is the adoption of inadequate projects for the roads, developed without detailed survey of the pavement or the situation in which the land is found (Viera, et al 2016). The base for an efficient SGP is the adoption of suitable methods for pavement evaluation, through which it's possible to verify the need for maintenance or reconstruction of the road, as well as to determine if it was built according to the project specifications (Haas; Hudson, 1978; Viera, et al 2016)

The superficial evaluation of pavements is usually executed following the DNIT 006/2003 - PRO standard, which uses the Global Gravity Index (GGI) method. This method makes possible to objectively analyze the level of deterioration of a pavement according to the incidence of surface defects, indicating its conservation conditions and assisting in making decisions regarding the necessary interventions. Although the GGI is considered an efficient method and is widespread in the technical environment, it presents as a disadvantage the need for surveys by walking, which makes its application time-consuming and costly for application in large areas.

An alternative to avoid this problem is the use of the so-called unmanned aerial vehicles (UAVs), which can fly automatically or be piloted by electronic and computational means. This equipment was designed for military purposes, initially used in missions that are too dangerous to be performed by human beings (Resende, 2015). However, in recent years, it has been gaining prominence among civil interventions, configuring an emerging technology in civil engineering with applications ranging from the inspection of works, to the inspection of structures in high-risk environments (Melo, 2016).

With regard to the application of UAVs in transport infrastructure, its embedded sensors constitute a new and economical source of information and can even assist efforts to road's maintenance (Branco, 2016; Nishar et al., 2016). Despite this, there have been few studies with this technology, especially as a tool for assessing road damage.

Thus, considering the need to optimize the road evaluation process in support of SGP and the potential offered by UAVs, it is essential to develop methodologies that enable its use in an efficient and technically appropriate way (Breen et al., 2015; Nishar et al., 2016). To this end, this work aims to study the feasibility of using Drones for mapping and inspecting pathologies on asphalt pavements, comparing and confronting their results to the traditional method of analysis.

## 2. MATERIAL AND METHODS

### 2.1 Research Area

It was used as a sample unit of the present research, a stretch of single way asphalt track with approximately 0.5 km in length that gives access to the campus of the Federal Rural University of the Semi-Arid / UFERSA, in the municipality of Angicos, state of Rio Grande do Norte - Brazil (Figure 1). This stretch, although small in length, proved to be ideal for carrying out the study due to the large number of pathological manifestations on the pavement.

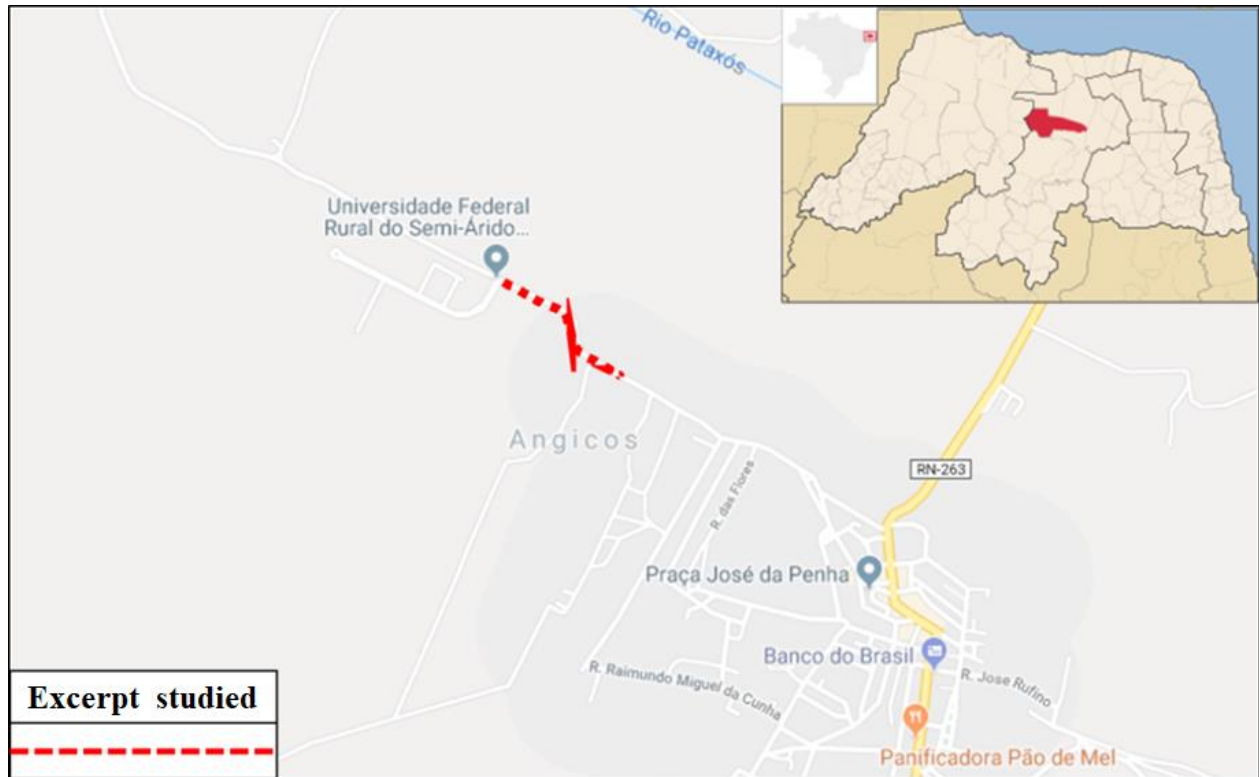


Figure 1. Research Area (Lat. 5°39'17.32"S; Lon. 36°36'37.48"O).

### 2.2 Survey of pathologies by the traditional method (reference)

To survey existing pathologies in the study area, sample plots were established every 20 m (in alternating flow-hands), each 6 m long, as established by DNIT Standard 006/2003 - PRO (Figure 2). Altogether 20 stations were considered, which had their defects noted, taking into account the section of the terrain and the types of pathological manifestation, distinguishing between cracks, plastic or consolidated corrugation, shoving, potholes, exudation, wear, patches and wheel tracks streaking. Photographic records of all types of defects found in the section under study were also made.

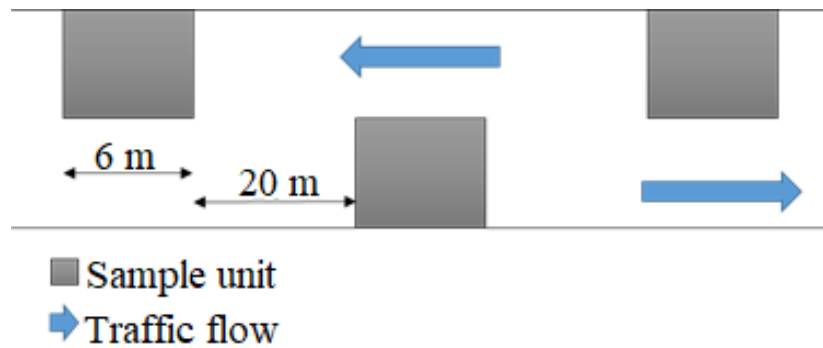


Figure 2. Distribution scheme of established sample units in the research.

### 2.3 Survey of pathologies with Drone (alternative)

To acquire the images of the research area, an Unmanned Aerial Vehicle - UAV, from the manufacturer DJI model Phantom 4 PRO (Figure 3) was used. The referred UAV is a multirotor type weighing approximately 1.5 kg and is equipped with a 20 megapixel camera (capable of shooting at 4 k / 60 fps), with a video transmission range of 7 km. The choice of equipment was based on its ease of use, flight stability, quality of the images generated and affordable price.



Figure 3. DJI model Phantom 4 PRO - UAV used in the study.

For the flight planning stages and subsequent composition of the orthoimage, the Drone Deploy application was used. It allows the flight plan to be parameterized according to the desired resolution for the original images, image overlay rate, flight lines and resulting resolution. The flight parameters used in the present study can be seen in Table 1. The orthoimage was automatically generated by the application and exported for later analysis (Figure 4).

Table 1. Flight parameters used in the survey

PARAMETER	VALUE
Altitude	70 m
Resolution	2,4 cm/pixel
Horizontal overlay rate	65%
Vertical overlay rate	75%
Flight speed	15 m/s
Flight duration	6 minutes
Number of captures	109

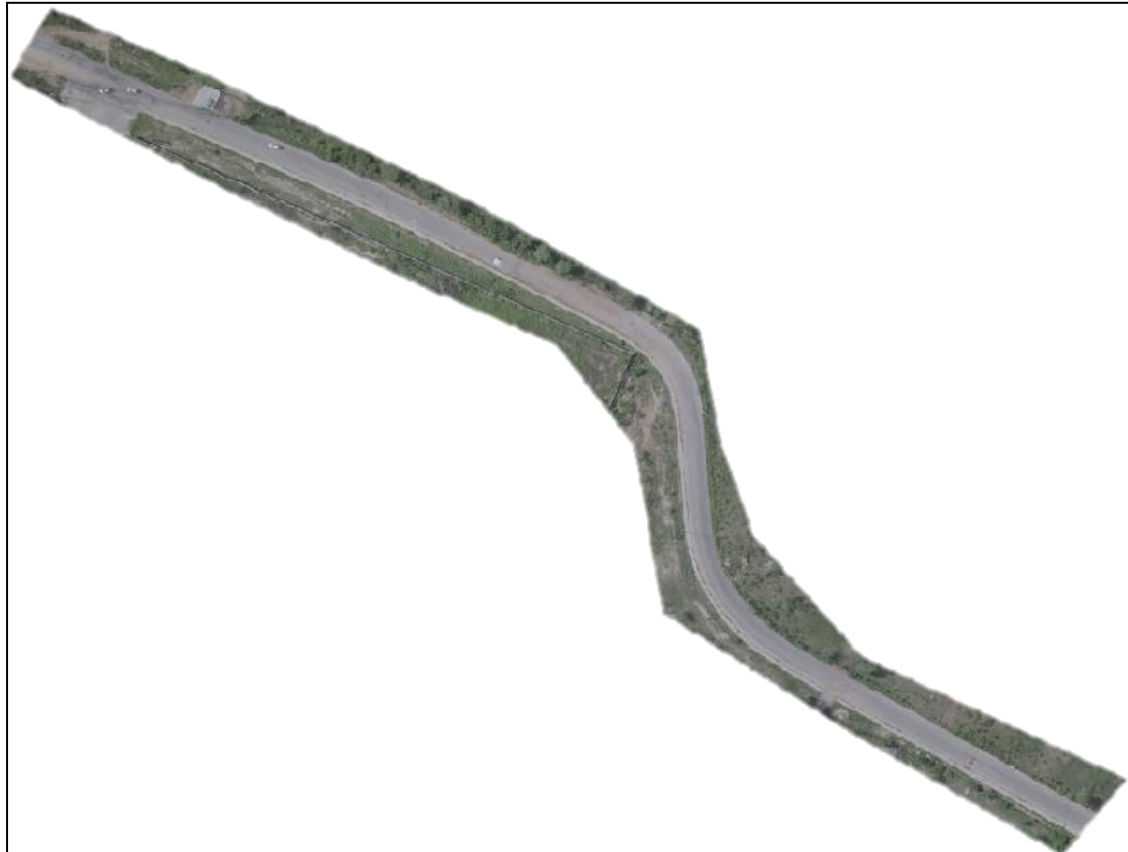


Figure 4. Research area ortoimage generated by Drone Deploy application.

#### 2.4 Global Gravity Index (GGI) calculation

After the pathologies were mapped, the Global Gravity Index (GGI) for the research area was calculated, following the recommendations of the normatization DNIT 006/2003 - PRO. Initially, the absolute frequency ( $f_a$ ) of occurrence of each type of pathological manifestation was estimated, corresponding to the number of times the occurrence was verified. Then, the relative frequency ( $f_r$ ) for each pathology was obtained, through Equation 1. For each type of pathology, the Individual Gravity Index - IGI (Equation 2) was calculated, which were later added together, resulting in the IGG (Equation 3).

$$f_r = \frac{(f_a \times 100)}{n} \quad (1)$$

Wich,

$f_a$  – absolute frequency

$n$  – number of inspections (number of samples).

$$IGI = fr \times fp \quad (2)$$

Wich,

$f_r$  – relative frequency

$f_p$  – ponderation factor (according to DNIT's table)

$$IGG = \sum IGI \quad (3)$$

The results obtained by the reference and alternative methodologies were compared according to the number and type of pathologies identified, as well as the time spent to carry out the surveys. Finally, the obtained GGI's were compared with the DNIT 006/2003 - PRO Standard, in order to determinate the concept of degradation of the analyzed section (Table 2).

Table 2. Pavement concept of degradation based on the GGI.

Concepts	Limits
Excellent	$0 < GGI \leq 20$
Good	$20 < GGI \leq 40$
Fair	$40 < GGI \leq 80$
Poor	$80 < GGI \leq 160$
Terrible	$GGI > 160$

Source: Regulation of DNIT 006/2003 – PRO

### 3. RESULTS AND DISCUSSION

#### 3.1 Comparative analysis: Drone inspection vs. Traditional inspection

The analyzed section presented a large number of pathologies in both methods employed. The total quantification of pathologies, within the 20 plots evaluated, showed very close values for both methods, being 54 for traditional inspection and 53 for inspection with the Drone, which demonstrates the viability of using the Drone to quantify pathologies on pavements (Figure 5).

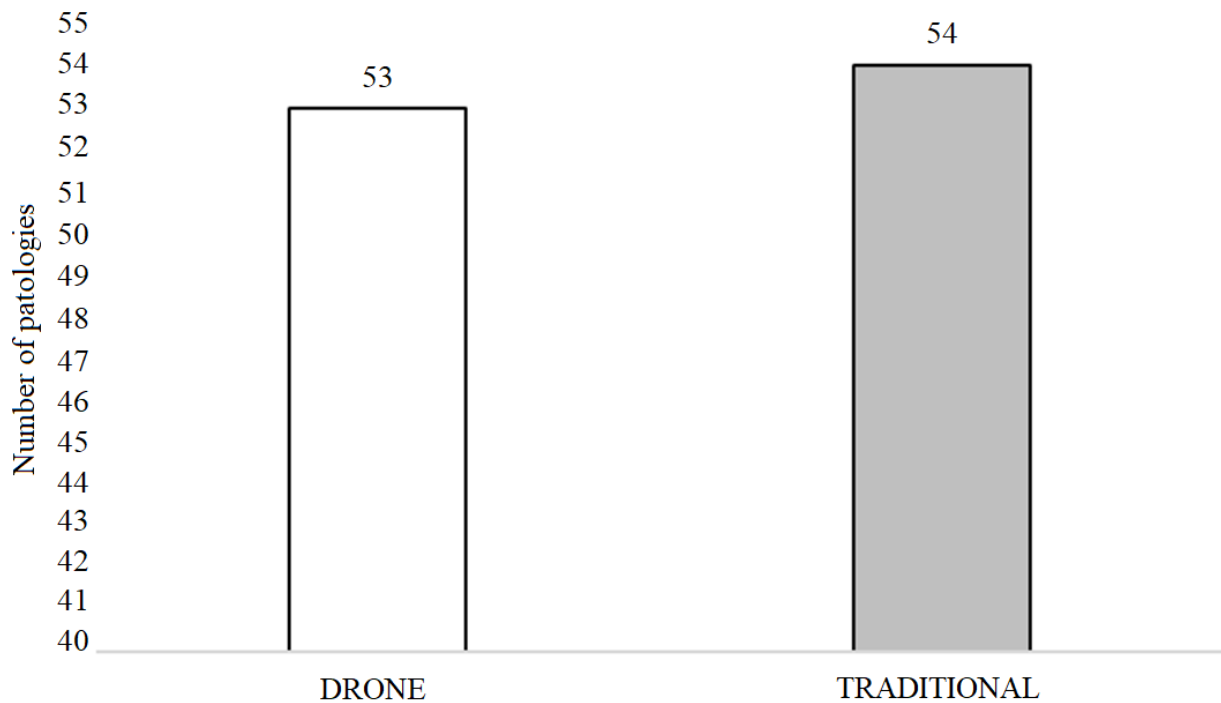


Figure 5. Identified pathologies according to inspection method.

As for the qualitative aspect, the inspection carried out with the Drone enabled the identification of 04 types of pathologies, which are: potholes (P) - concavity or hole that forms in the coating and can reach the base; cracks (F) - characterized as openings in the asphalt surface that are visible to the naked eye; patches (R) - defect characterized by the filling of pots or any other orifice, hole or depression with asphalt mix; and slip (E) - displacement in relation to the pavement layer. Regarding the types of pathologies, there was no difference between the traditional inspection method and the Drone inspection method. Regarding the number of defects by type of pathologies, there were small differences between the methods used, as shown in figure 6.

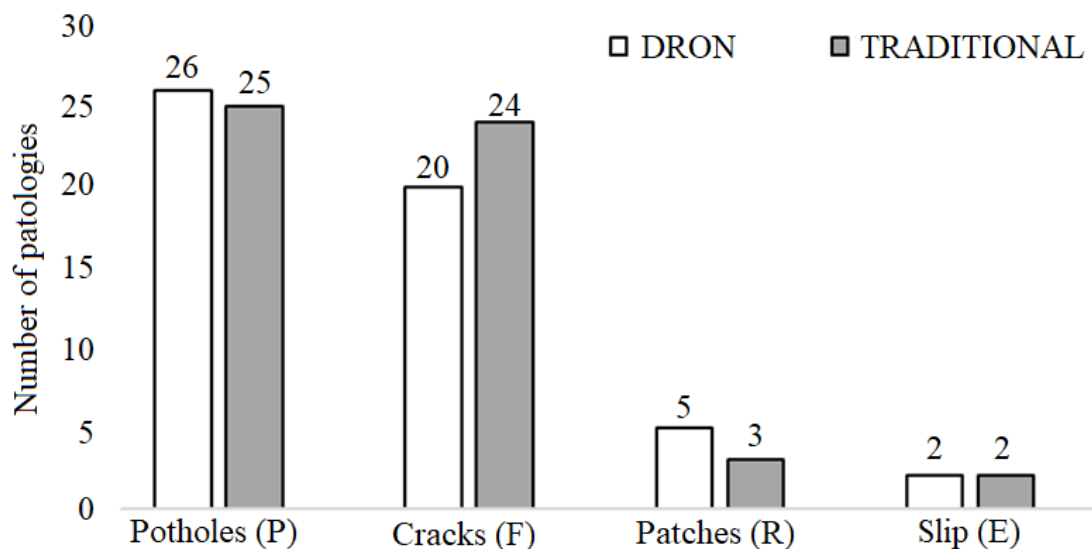


Figure 6. Identified pathologies according to its types and inspection methods.

It should be noted that the most probable cause for these differences is due to the fact that some types of pathologies can be difficult to identify by the use of images obtained by UAVs due to their quality, while traditional inspection can resolve any doubts regarding the occurrence of a pathology because it is an on-site analysis. As an example, one can compare pots and cracks. In the first case, it is easier to identify by the very nature of the pathology, which in general stands out from the rest of the pavement. In the second, it is much more difficult to identify, sometimes needing confirmation through on-site inspection. In Figure 7, it is possible to compare the images obtained with the Drone and using the traditional method, for each of the types of pathologies identified.



Figure 7. Identified pathologies according to type and inspection method.

Regarding the time spent for inspection, it was found that the analysis performed with the Drone (6 minutes of flight and 12 minutes for image evaluation) took less than 1/3 of the time spent to perform the traditional inspection (Figure 8 ). Considering that in the present study a small stretch of 0.5 km was evaluated, it is assumed that on longer stretches of large highways this difference is even greater, making the use of the Drone increasingly attractive

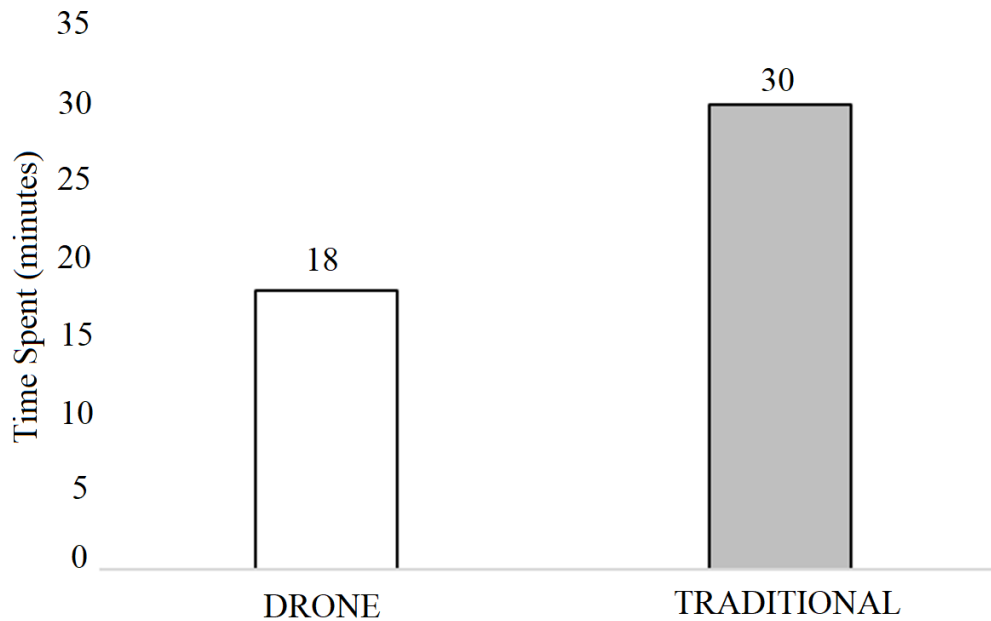


Figure 8. Time spent for inspection realization according to used methods.

### 3.2 Comparative Analysis of the results: Drone x Traditional inspection

The value obtained for the Global Gravity Index - GGI, was 302 for the realization performed with the Drone and 320 for the traditional method (Figure 9), and in both cases, according to DNIT Standard 006/2003 - PRO, the evaluated stretch was considered to be terrible ( $GGI > 160$ ). One of the points that influences this result is the presence of a large number of Potholes (P), which was found in all the studied plots, which is the pathology that most impacts traffic and contributes to accelerating the degradation of the pavement. Although there are different values, it is observed that the existing difference is not as long as, demonstrating that navigation with the aid of Drones is technically feasible.

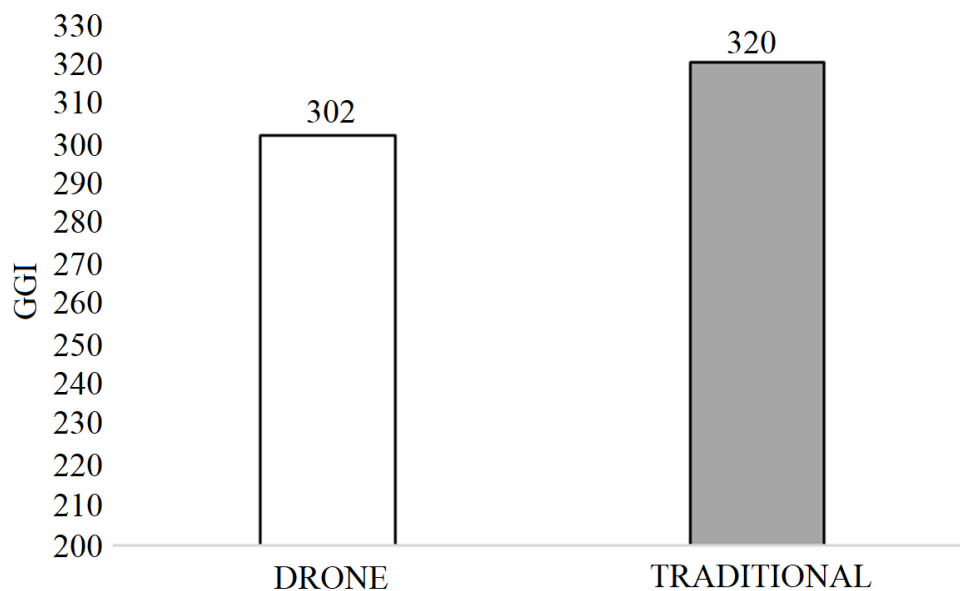


Figure 9. Global Gravity Index - GGI according to used method.

### 3.3 General Analysis of the proposed Methodology

The methodology of UAV using for pavement inspection can already be observed in works such as Parente, Felix and Picanço (2017), where, as in the present work, this tool was used in comparison with the current standard methodology. The addition of a comparative evaluation between the proposed method and the traditional one is essential for the statistical quantification of the effectiveness of any proposed alternative methodology. Therefore, another result pointed out by this work is a comparison methodology for the use of UAVs in inspections of structures of any type, when compared to traditional methods.

## 4. CONCLUSION

The use of Drones has become increasingly common in several areas of engineering, stimulated mainly by the popularization of this technology and the various possibilities offered. However, its use must be previously evaluated and traditional methodologies must be adequate so that the results provided by this equipment are reliable. The present study demonstrated the use of Drones to inspect pathologies on asphalt pavements, based on DNIT 006/2003 - PRO, obtaining approximately 94.4% of correctness, taking into account the results with the traditional methodology, with significant reduction in operating time with less than 1/3 of the time spent. It should also be noted that the present work provides subsidies for the improvement of the road evaluation process, making it possible to achieve the best possible application for the public resources and offering safe, compatible and economical road service. The proposed method can also be refined by the use of Drones with multispectral sensors, generating other results that, through infrared or three-dimensional images, can add value and different information to the service related to pavement inspections, also increasing the effectiveness of the alternative methodology.

## 5. REFERENCES

- Andrade, M. O., Maia, M. L. A., Lima Neto, O. C. C. (2015), “*Impactos de investimentos em infraestruturas rodoviárias sobre o desenvolvimento regional no Brasil - possibilidades e limitações*”. Transportes v. 23, n. 3. <https://doi.org/10.14295/transportes.v23i3.797>
- Branco, L. H. C. (2016), “*MANIAC: uma metodologia para o monitoramento automatizado das condições dos pavimentos utilizando VANTS*”. 2016. Tese (Doutorado em Infra-Estrutura de Transportes) - Escola de Engenharia de São Carlos, Universidade de São Paulo, São Carlos.
- Breen, B., Brooks, J. D., Jones, M. L. R., Robertsons, J., Betschart, S., Kung, O., Cary, S. C., Lee, C. K., Pointing, S. B. (2015), “*Application of an unmanned aerial vehicle in spatial mapping of terrestrial biology and human disturbance in the McMurdo Dry Valleys, East Antarctica*”, Polar Biology, v.38, n.4, p.573–578. <https://doi.org/10.1007/s00300-014-1586-7>
- Confederação Nacional dos Transportes (2017). *Pesquisa de Rodovias: Principais Dados*”. CNT. Disponível em: <http://pesquisarodovias.cnt.org.br/Paginas/resumo-para-imprensa>
- Departamento Nacional de Infraestrutura de Transporte (2003). DNIT 006/2003 - PRO: “*Avaliação objetiva da superfície de pavimentos flexíveis e semi-rígidos - Procedimento*”. Rio de Janeiro: 2003. 10p. Disponível em: [http://ipr.dnit.gov.br/normas-e-manuais/normas/procedimento-pro/dnit006\\_2003\\_pro.pdf](http://ipr.dnit.gov.br/normas-e-manuais/normas/procedimento-pro/dnit006_2003_pro.pdf). Acesso em: 09 abr. 2018.
- Melo, R.R.S. 2016. “*Diretrizes para inspeção de segurança em canteiros de obra por meio de imageamento com Veículo Aéreo Não Tripulado (VANT)*”. 160 f. Dissertação (Mestrado) - Curso de Engenharia Civil, Universidade Federal da Bahia, Salvador, 2016.

- Nishar, A., Richards, S., Breen, D., Robertson, J., Breen, B. (2016), “*Thermal infrared imaging of geothermal environments and by an unmanned aerial vehicle (UAV): A case study of the Wairakei - Tauhara geothermal field, Taupo, New Zealand*”, *Renewable Energy*, 86, 1256 - 1264. <https://doi.org/10.1016/j.renene.2015.09.042>
- Parente, D. C., Felix, N. C., Picanço, A. P. (2017). *Uso de veículo aéreo no tripulado (VANT) en la identificación de patología superficial en pavimento asfáltico*. *Revista ALCONPAT*, 7(2), 160 - 171. <https://doi.org/10.21041/ra.v7i2.161>
- Vieira, S., Pinho Júnior, A., Oliveira, F., Aguiar, M. (2016). *Análise comparativa de metodologias de avaliação de pavimentos através do IGG e PCI*. *Conexões - Ciência e Tecnologia*, 10(3), 20-30. <https://doi.org/10.21439/conexoes.v10i3.799>

## Fiber reinforced shotcrete control tests in the Mexico City metro line 12 tunnel

C. Aire<sup>1</sup>\*, L. Aguilar<sup>1</sup>

\*Contact author: [aire@pumas.iingen.unam.mx](mailto:aire@pumas.iingen.unam.mx)

DOI: <https://doi.org/10.21041/ra.v11i1.493>

Reception: 18/06/2020 | Acceptance: 30/10/2020 | Publication: 01/01/2021

### ABSTRACT

In this paper three tests are evaluated to characterize the behavior of shotcrete with steel fibers in the primary lining of Mexico City metro line 12 tunnel. Three square panels (UNE 14488-5), three round panels (ASTM C1550) and four cylinders for the Barcelona test (UNE 83515) were made. All of them can be used as quality control methods for Fiber Reinforced Concrete (FRC) in underground constructions, however, greater variability was found in the results of round panels, in addition to being the highest complexity samples regarding their development and test, therefore, the application of the Barcelona test is recommended for quality control on site due to the fact that the samples and test are easier to prepare, handle and execute.

**Keywords:** fiber reinforced shotcrete; energy absorption; round panels test, square panel test; Barcelona test.

**Cite as:** Aire, C., Aguilar, L. (2021), "*Fiber reinforced shotcrete control tests in the Mexico City metro line 12 tunnel*", Revista ALCONPAT, 11 (1), pp. 73 – 87, DOI: <https://doi.org/10.21041/ra.v11i1.493>

<sup>1</sup>Ingeniería Estructural, Instituto de Ingeniería, Universidad Nacional Autónoma de México. México.

#### Contribution of each author

In this work, the first author contributed with the experimental campaign (50%), the analysis of the results and the writing of the article, the second author with the experimental campaign (50%) and review of the article.

#### Creative Commons License

Copyright 2021 by the authors. This work is an Open-Access article published under the terms and conditions of an International Creative Commons Attribution 4.0 International License ([CC BY 4.0](https://creativecommons.org/licenses/by/4.0/)).

#### Discussions and subsequent corrections to the publication

Any dispute, including the replies of the authors, will be published in the third issue of 2021 provided that the information is received before the closing of the second issue of 2021.

## Ensayos de control del concreto lanzado con fibras en el túnel de la línea 12 del metro de la CDMX

### RESUMEN

En este artículo se evalúan tres ensayos para caracterizar el comportamiento del concreto lanzado con fibras metálicas en el revestimiento primario del túnel de la línea 12 del metro de la CDMX. Se elaboraron tres paneles cuadrados (UNE 14488-5), tres paneles redondos (ASTM C1550) y cuatro cilindros para ensayo Barcelona (UNE 83515). Todos se pueden utilizar como métodos de control de calidad para Concretos Reforzados con Fibras (CRF) en construcciones subterráneas, sin embargo, se encontró mayor variabilidad en los resultados de los paneles circulares, además de ser estos los especímenes con mayor complejidad para su elaboración y ensayo, por lo tanto, se recomienda la aplicación del ensayo Barcelona para el control de calidad en obra debido a que resulta más sencilla la preparación, manipulación y ejecución del muestreo y ensayo.

**Palabras clave:** concreto lanzado reforzado con fibras; absorción de energía; ensayo de paneles circulares, ensayo de paneles cuadrados; ensayo Barcelona.

## Ensaio de controle de concreto projetado com fibra no túnel da linha 12 do metrô CDMX

### RESUMO

Neste artigo três ensaios são avaliados para caracterizar o comportamento do concreto projetado com fibras metálicas no revestimento primário do túnel da linha 12 do metrô CDMX. Três painéis quadrados (UNE 14488-5), três painéis redondos (ASTM C1550) e quatro cilindros para ensaio de Barcelona (UNE 83515) foram feitos. Todos podem ser utilizados como métodos de controle de qualidade para Concreto Reforçado com Fibras (CRF) em construções subterráneas, porém, constatou-se maior variabilidade nos resultados dos painéis circulares, além de serem os corpos de prova com maior complexidade para sua elaboração e ensaio, portanto, a aplicação do ensaio de Barcelona é recomendada para controle de qualidade no local porque é mais fácil de preparar, manusear e realizar amostragem e ensaio.

**Palavras-chave** concreto projetado reforçado com fibra; absorção de energia; ensaio de painel circular, ensaio de painel quadrado; ensaio de Barcelona

### Legal Information

Revista ALCONPAT is a quarterly publication by the Asociación Latinoamericana de Control de Calidad, Patología y Recuperación de la Construcción, Internacional, A.C., Km. 6 antigua carretera a Progreso, Mérida, Yucatán, 97310, Tel.5219997385893, [alconpat.int@gmail.com](mailto:alconpat.int@gmail.com), Website: [www.alconpat.org](http://www.alconpat.org)

Reservation of journal title rights to exclusive use No.04-2013-011717330300-203, and ISSN 2007-6835, both granted by the Instituto Nacional de Derecho de Autor. Responsible editor: Pedro Castro Borges, Ph.D. Responsible for the last update of this issue, Informatics Unit ALCONPAT, Elizabeth Sabido Maldonado.

The views of the authors do not necessarily reflect the position of the editor.

The total or partial reproduction of the contents and images of the publication is carried out in accordance with the COPE code and the CC BY 4.0 license of the Revista ALCONPAT.

## 1. INTRODUCTION

Nowadays, the use of fibers in concrete has become a frequent trend in the construction industry. In our country, they initially replaced steel wire meshes in shotcrete, industrial floors, and precast elements. Worldwide, the application of this technology varies from pavements, industrial floors, slope support and architectural elements to tunnel construction (Gettu et al., 2004; Kasper et al., 2008; De la Fuente et al., 2012). Currently, steel fibers are also used in precast segments for tunnels lining (Blom, 2002), (Burgers et al., 2007), (De la Fuente et al., 2013). In Mexico, the first work sites, both in civil works and mining.

One of the main benefits provided by fiber reinforced concrete is the energy absorption capacity after cracking, meaning that regardless how much the element cracks, it may keep on withstanding the load and strain without collapsing, allowing tensile strength redistribution (De Waal, 2000), improving fracture behavior, fatigue performance and impact strength (Gopalaratnam y Gettu, 1995). Efficiency of fibers included in the concrete mix depends on (1) the fiber properties, strength, stiffness and bonding, (2) fiber distribution, volume fraction, content and orientation (Zollo, 1997). Several standardized test methods have been developed to measure energy absorption which allows to assess the fiber reinforced concrete performance. For its application, it is important to keep the following into consideration: 1) Test complexity; 2) Difficulty to prepare the samples; 3) Execution complexity; 4) Test replication; 5) Cost and applicability in real life, as well as acceptance of the test method by researchers (Kooiman, 2000). Methods proposed to evaluate FRC should be assessed according to the above-mentioned conditions to determine its practical application as Protocols in the Work Control for FRC.

Having in mind the above premises and the vast experience of Instituto de Ingeniería de la UNAM [UNAM Institute of Engineering] in research on FRC, this paper submits the results of an experimental program to evaluate SFRS in a practical case, extension of Mexico city metro line 12 (L-12). Energy absorption (toughness) of primary lining fiber reinforced shotcrete of L-12 tunnel and the complexity to prepare samples for square panel test EN 14488-5 ( $l\ 600 \times l\ 600 \times h\ 100$  mm), round panel test ASTM C1550 ( $\phi\ 800 \times e\ 75$  mm) and Barcelona test UNE 83515 ( $h\ 150 \times \phi\ 150$  mm) are evaluated. It was decided to use the international standards because during this experimental campaign, we did not have standards allowing to evaluate this type of tests in Mexico.

## 2. THE LINE 12 EXTENSION SUBWAY TUNNEL

### 2.1 Overview

Mexico City Projects and Services Secretary builds the extension of Mexico City metro line 12. It is an infrastructure project consisting of a 4.6-kilometer-long tunnel where three metro stations will be located, connecting Mixcoac and Observatorio stations, and connecting the East and West areas of Mexico City. With this Mexico City metro line 12 extension, it is estimated that the commute between Mixcoac to Observatorio Stations will be up to 60 per cent faster.

The executive project which is currently in its first stage consists of building 13 shafts between 15 and 46.5 m deep. Along the project the stratigraphic profile of the soil consists mainly of tough sandy clay, however, in some sections of the tunnel, there are soft soils with poor stability. There is no groundwater level. Where unstable soils were found, it is solved it with supporting elements, such as metal frames with 0.50 m to 1.00 m separation between them, depending on the type of soft soil. In other cases, with overexcavation, it was solved with injection products, such as cement slurry and fluid concrete, chosen according to the overexcavation size.

To build the 4.6 km long and 11 m average diameter tunnel, a conventional mechanic excavation method using roadheader tunneling equipment. To excavate the tunnel face, the roadheader is moved towards the face and the cutting head is set in motion. The face of the tunnel is then milled

off in sections with the cutting head. The average digging progress is of 1.5 m, with an average of two to three per day. After digging the top middle section, primary lining is placed to stabilize the land. This consists of applying steel fiber reinforced shotcrete (SFRS). The primary lining width is of 20 cm, placed in approximately two 10 cm layers each one. Between the primary and secondary lining, a PVC geomembrane is placed to prevent water leaks towards the final lining. The secondary lining is made of 40 cm width concrete in the vault. In this second lining layer, conventional shotcrete with no fibers is used, reinforced with rebars.

## 2.2 Control tests

The most representative property of SFRS is energy absorption. After concrete cracks, fibers start working during the cracking process, redistributing and controlling cracks spread as the SFRS lining system strains. SFRS load capacity determines the lining system performance.

SFRS energy absorption is determined by means of flexure tests. There are two traditionally used procedures: a) the panel test, round or square section, and b) the beam test. New globally used, standardized test methods have been developed to determine this. The beam test is mainly used in pavement applications.

The post-elastic performance of round/square panels subject to a point load in the center, is represented by the energy absorbed up to a specified central deflection. The typical flexure strength test methods include ASTM C1550, round panel and in EN 14488-5 square panel. The energy absorption capacity determination is the most important factor to evaluate the SFRS performance, calculated for a specified deflection, 25 mm in square panel and 40 mm in round panel. Other methods to evaluate flexure strength are the beam tests. To perform this test, SFRS panels cut in beams are required, and they are tested according to the ASTM C1609 and UNE EN-14651 standards, to determine the flexure toughness.

A recent development is the double punching test (DPT) proposed by Chen (1970) standardized by UNE 83515, known as the Barcelona test. With this test, the cylinders' toughness is determined, calculated for a 6 mm specified circumferential opening. Carmona et al., (2009), deems this test is characterized by its low complexity in test specimens' preparation, it provides a suitable FRC systematic control in the work site and poses a great specific crack surface along its height.

To evaluate the primary lining concrete performance of L-12 tunnel, II-UNAM carried out control tests, manufacturing different types of SFRS specimens obtained in the tunnel, and it launched an experimental campaign following up all concrete placement operations, emphasizing in the specimens sampling and tests.

Figure 1 shows a typical procedure of SFRS primary lining placement in L-12 tunnel. Upon arrival to the work site the concrete truck obtains a concrete sample, it measures temperature and slump for purposes of either rejecting or accepting it. In case it is accepted, the design fiber quantity is immediately included, allowing it to integrate and mix during the stated time. Once the mixing time is over, the concrete is supplied inside the tunnel by means of a pipe, received by a mixer truck that takes concrete from the shaft to the front part of the work site, adding it to the shotcrete equipment. Materials used for concrete production were: cement CPC 40RS (NMX-C-414-ONNCCE), stone aggregates: andesitic sand, 10 mm maximum limestone gravel (NMX-C-111-ONNCCE), type B and F admixture (ASTM C 494), accelerating admixture TamShot 70 AF (ASTM C 1141) and 35 mm long steel fiber, slenderness ratio ( $l/\varnothing$ ) 65, tensile strength of 1.345 (N/mm<sup>2</sup>), in a dose of 30 kg/m<sup>3</sup> of concrete. 0.50 water/cement ratio. Design compressive strength specified at 28 days is of  $f'c = 250 \text{ kg/cm}^2$ .

Three types of sampling were carried out, round panel, square panel, and blocks, with which the following tests were performed: ASTM C1550 (round panel), EN 14488-5 (square panel) and UNE 83515 (Barcelona test). All test specimens obtained for this experimental campaign belong to the same mix design and each type of sampling belongs to the same batch supplied in field.

Notwithstanding, the mix design information is not available because it is owned by the concrete supplier.



Figure 1. Primary lining placement procedure in L-12 tunnel

### 3. SQUARE PANEL TEST – EN 14488-5

Square panels, of  $600 \times 600 \times 100$  mm, were subject to a central load applied through a  $100 \times 100$  mm and 20 mm thickness square plate, according to EN 14488-5. The load and the axial displacement of the jack are registered during the test. The behavior is evaluated through the maximum load and the energy absorption for a displacement of 25 mm. The energy absorption is calculated as the area enclosed by the load-displacement curve up to the specified displacement. The test was carried out in a rigid load frame with a capacity of 500 kN and with a closed-loop control system. The displacement rate was 1 mm/min and a LVDT transducer was located at the center of the panel to measure the displacement.

Figure 2 shows the setup of the square panel test according to EN 14488-5. The rough side shall be on the top during the test, i.e. the load is applied on the spraying direction.

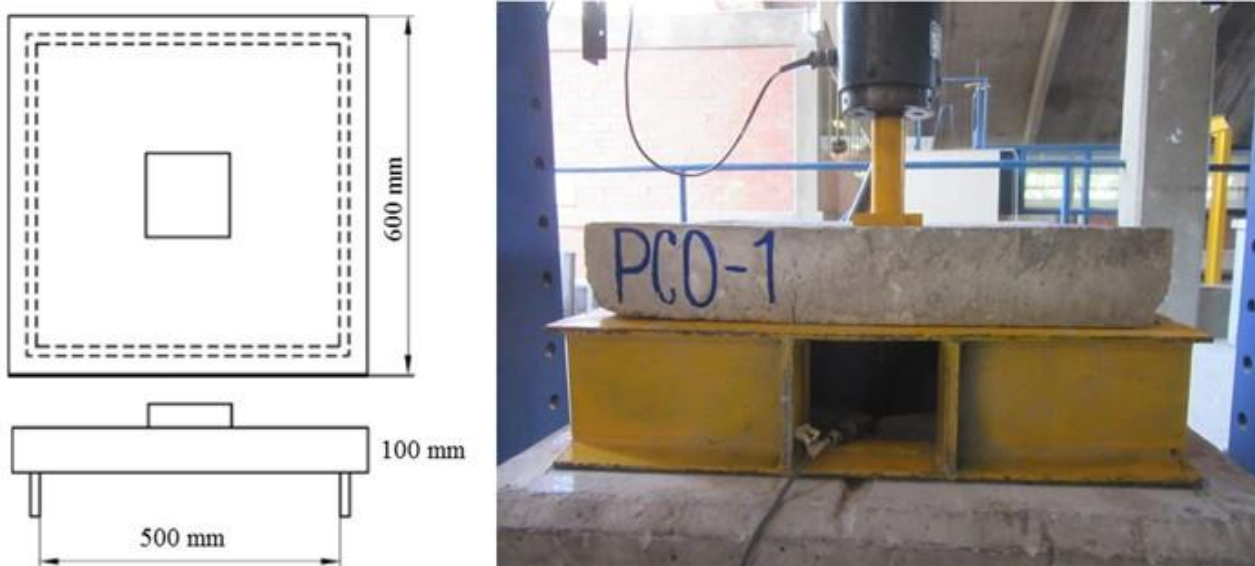


Figure 2. Panel test configuration diagram, according to EN 14488-5

The experiment test series was performed on 3 square panels, identified as PCO-1, PCO-2 and PCO-3. The specimens were obtained from the same concrete batching supplied in the primary tunnel lining. Cracks were generated in a classic pattern from the panel centers, producing multiple fragments as shown in Figure 3. In all cases, two main cracks and others secondary are observed

in each panel, going from the center to the sides of the panels. The failure was gradual due to the fibers action in the concrete matrix.



Panel 1 – PCO-1                      Panel 2 – PCO-2  
 Figure 3. Typical failure mode of the tested square panels

Figure 4 shows the load-displacement curves of the tested panels. The curves show a similar behavior, regardless the tested panel. Two stages can be identified: the ascendant initial and the descendant post-crack. In the former stage, the load gradually increases at a low displacement rate, and various peaks are reported. At this stage, the fiber contribution is very low. Once the crack appears, the fibers start working together with the concrete. The peaks reflect the descending load descends mainly due to the concrete cracking and the respective recovery due to the initial fiber contribution, until a maximum load value is reached. Then the second stage starts as a progressive descendent post-crack curve, reproducing the fiber main contribution. The test ends at a 25 mm deflection. Figure 4 shows that post-cracking behavior is very similar for the tested panels, likewise, maximum load values are very much alike; therefore, it is estimated that energy absorption will show similar values.

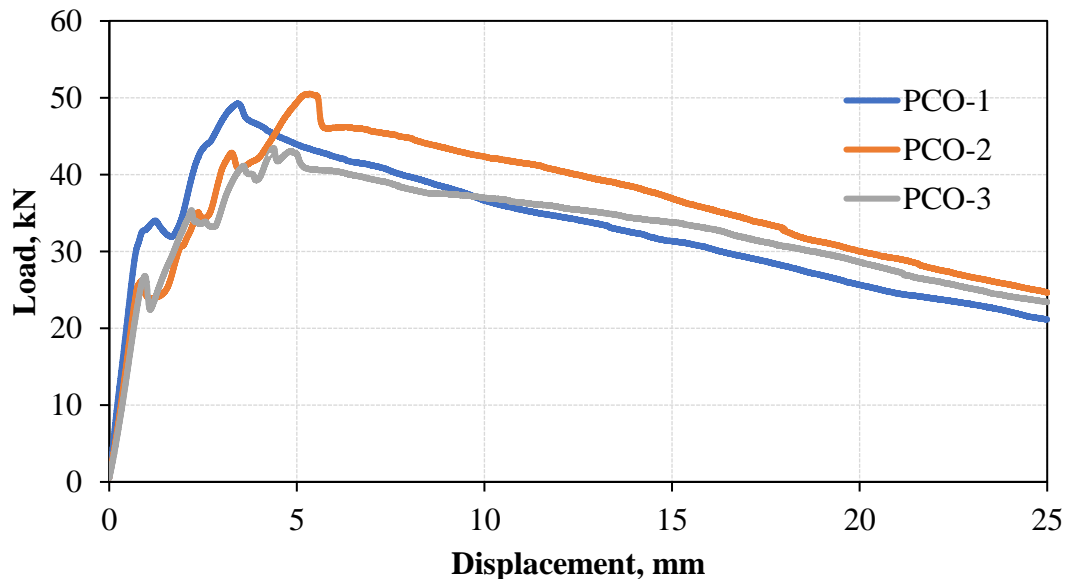


Figure 4. Load-displacement curves of the tested square panels

Toughness was determined as the area under the load-displacement curve between the origin and the 25 mm central displacement, as specified in EN 14488-5. Results are shown in Table 1. The results show that average toughness (energy absorption) of the tested panels is of 843.14, with a 5.27% variation coefficient. The repetitiveness of the results is quite acceptable.

Table 1. Toughness results,  $T_{\delta_{25\text{mm}}}$ 

ID	Panel	U	Toughness	Average
$T_{\delta_{25\text{ mm}}}$	PCO-1	Joules	820.83	$T_{\text{prom}} = 843.14 \text{ J}$
$T_{\delta_{25\text{ mm}}}$	PCO-2	Joules	894.29	C.V. = 5.27%
$T_{\delta_{25\text{ mm}}}$	PCO-3	Joules	814.31	

These test panels have a high level of complexity in their sampling, transport and testing because the specimens weigh in average 80 kg each one, in addition to requiring at least, two trained people to prepare and handle the samples during the sampling and testing. For its preparation, additional amount of concrete mix for sampling should be taken into consideration, approximately  $0.1 \text{ m}^3$  for the three test specimens, which represents an additional cost in concrete. This one will be affected by the test frequency, however, it will be applied if the project specifies its use in the Control Protocol as the evaluation method, or alternatively, use another test in case its correlation with this one is known.

#### 4. ROUND PANEL TEST – ASTM C1550

The test was performed on the specified round panels,  $75 \times \phi 800 \text{ mm}$ , in accordance with the standard ASTM C1550. In Mexico, the standard test method equivalent to ASTM C 1550 is NMX C539 (NMX 539, 2017). This test method covers the determination of flexural toughness of fiber-reinforced concrete expressed as energy absorption in the post-crack range using a round panel supported on three symmetrically arranged pivots and subject to a central point load. The fixture supporting the panel during testing shall consist of any configuration that includes three symmetrically arranged pivot points on a 750 mm diameter pitch circle. The supports shall be capable of supporting a load of up to 100 kN vertically applied on the center of the specimen. The supports shall be sufficiently rigid so that they do not displace in the radial direction. The pivots shall not restrict rotation of the panel fragments after cracking. Figure 5 shows the round panel test configuration.

The test specimen is mounted in the test apparatus by placing the molded face in the three transfer plates resting on the pivots.

During the test, the load and displacement are continuous, and the load-displacement curve is obtained which will allow to get energy absorption.

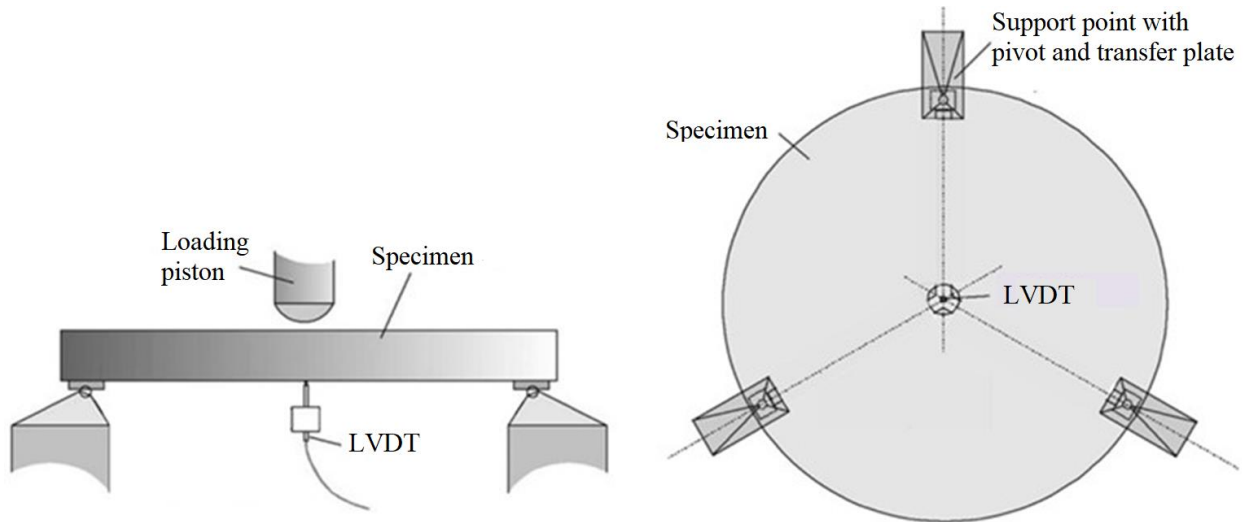


Figure 5. Panel test configuration diagram, according to ASTM C1550

The test was carried out with the same equipment used in the square panel test. The displacement rate was 4 mm/min and the test stopped at a displacement of 40 mm. A LVDT transducer with a range of 100 mm was placed at the center to measure displacement. The energy absorption is calculated for displacements of 5, 10, 20 and 40 mm.

A typical failure mechanism of round panel consisted of three radial fracture planes, as shown in Figure 6. The failure mode was progressive because of fibers in the concrete matrix, unlike the panel tests with no fibers where the failure happens suddenly according to previous experience (Aire and Rodríguez, 2011).

According to ASTM C1550, a sample shall consist of at least two successful tests. A successful test involves a failure that includes at least three radial cracks. Specimens occasionally fail in a beam-like mode involving a single crack across the specimen that is characterized by low energy absorption. The result of such a test shall be discarded. Only two specimens need be tested if both specimens fail by the required mode. In this paper, the three panels had three radial cracks.

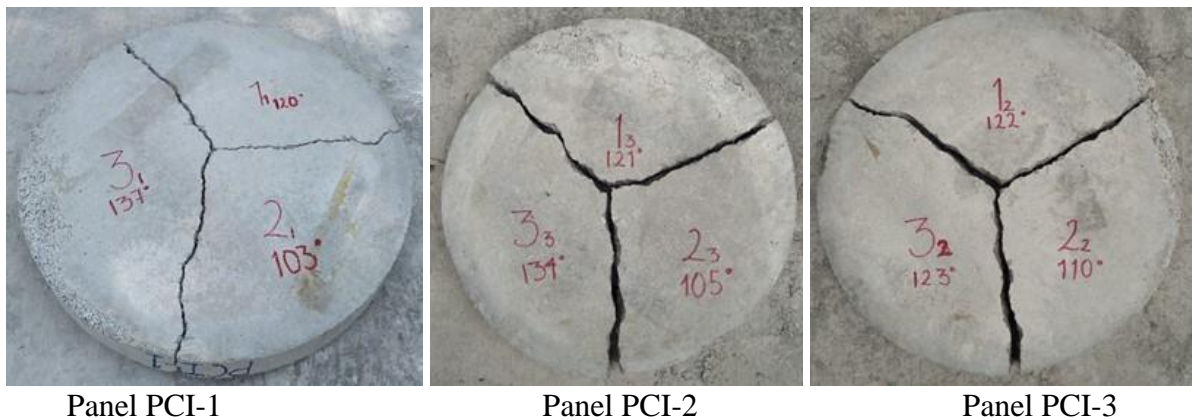


Figure 6. Round panels failure mode

Figure 7 shows the round panel test configuration and Figure 8 shows the load-displacement curves from obtained results. The initial ascendant line represents the load increase at small displacement increments, mostly taken by the concrete matrix. At that part of the test, the fibers contribution is minimal or null. In this stage, the curve reaches a maximum peak (maximum load) to proceed to the concrete cracking stage when the load is taken by the fibers, which work together with the

concrete. Loss of load is observed when the concrete cracks; however, a load recovery follows as a result of the fibers contribution and its perfect anchorage with the concrete. The displacement increases (deflection) while the load lowers progressively. This unload stage is mainly due to the gradual fibers anchorage loss, which produces the fibers slip followed by the final concrete rupture.



Figure 7. Round panel test setup, ASTM C1550

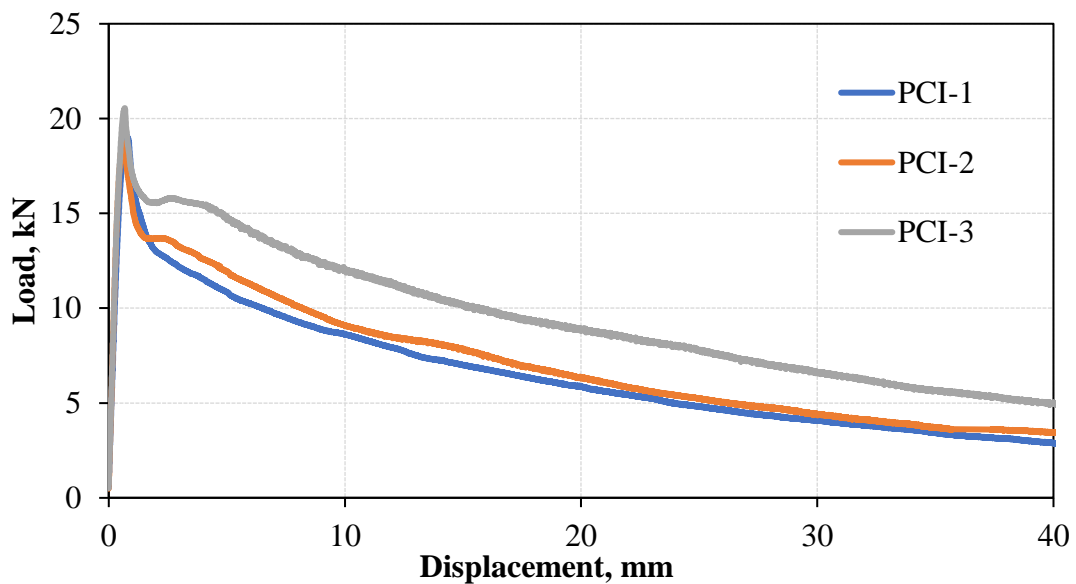


Figure 8. Round panels load vs displacement curve

Energy absorption (toughness) was determined as the area under the load-displacement curve between the origin and the central displacement specified in ASTM C1550. Results are shown in Table 2. Average energy absorption for tested panels is of 311 Joules for 40 mm displacement, with 19.7% variation coefficient.

Table 2. Toughness results,  $T_{\delta 5\text{mm}}$ ,  $T_{\delta 10\text{mm}}$ ,  $T_{\delta 20\text{mm}}$  y  $T_{\delta 40\text{mm}}$ 

ID	U	T $\delta 5\text{ mm}$	T $\delta 10\text{ mm}$	T $\delta 20\text{ mm}$	T $\delta 40\text{ mm}$
PCI-1	Joules	63.8	111.6	182.4	265.6
PCI-2	Joules	66.7	118.8	196.0	286.9
PCI-3	Joules	77.2	143.3	246.1	380.8
$T_{\text{average}}$	Joules	69.2	124.5	208.2	311.1
CV	%	10.2	13.3	16.1	19.7

Like square panels, round panels pose handling difficulties, because they weigh approximately 100 kg., each one, in addition to sampling, transport and testing. For round panel, an additional 0.15 m<sup>3</sup> volume of concrete is necessary to prepare the test specimens. In both cases, round and square panels pose difficulties in the curing process, especially because they require more space in the curing room. By the same token, as in the case of square panels, if the specification requires it, it will be necessary to carry out sampling and testing.

## 5. BARCELONA TEST– UNE 83515

Barcelona test was performed according to the Spanish Standard UNE 83515 on cylindrical specimens, 150 ×  $\phi$  150 mm. In Mexico, the standard test method equivalent to UNE 83515 is NMX C538 (NMX 538, 2017). This test method is used to determine the cracking strength, ductility and residual tensile strength of fiber reinforced concrete. It is based on a double punching test of a cylindrical test specimen. The essential elements to apply this test method are the circumferential extensometer, steel punches that will act as load elements and mounting disks. The test specimen is a cylinder with height approximately equal to its diameter. The standard diameter of the specimen is 150 mm. This cylinder can be obtained by direct moulding of a 150 mm diameter by 150 mm height specimen, or direct moulding of a 150 mm diameter by 300 mm height specimen, followed by cutting at the midpoint of the specimen height in a plane perpendicular to its axis of symmetry or 150 mm diameter by 150 mm height specimen extracted from a real structure, which represents an advantage of this method when casted in place concrete performance needs to be evaluated. Figure 9 shows a diagram of Barcelona test configuration.

The load is uniformly applied at a press-piston descending velocity of  $0.5 \pm 0.05$  mm/min throughout the entire test. The test is considered to be complete once the circumferential displacement has reached 6 mm.

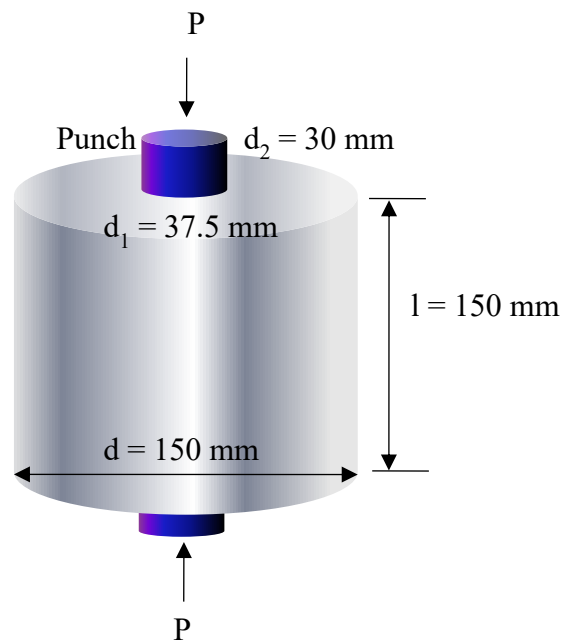


Figure 9 Barcelona test configuration – UNE 83515

To perform this test,  $650 B \times 350 b \times 150 h$  mm concrete blocks were sampled, from which 4 cylindrical cores were extracted. Figure 10 shows the equipment used to extract the samples. The specimens' vertical position was ensured leveling the support surface. The load was applied on the spraying direction. Figure 11 shows the test configuration.



Figure 10. Specimens removal for the Barcelona Test.



Figure 11. Double punching test, configuration, UNE 83515

A typical failure mechanism consists of three radial fracture planes, as shown in Figure 12.



Figure 12. Cylinders typical failure mode, Barcelona Test.

The load-circumferential displacement curves of the tested cylinders are shown in Figure 13. The curves have an almost null displacement from the beginning of the load application to the maximum load. At this stage, the cylinder does not develop cracks. When the maximum load is reached, the first cracks start to appear. At the post-crack stage, the load decreases up to a determined circumferential opening, when the structural fibers start their work. The load is then recovered, and a residual behavior is observed.

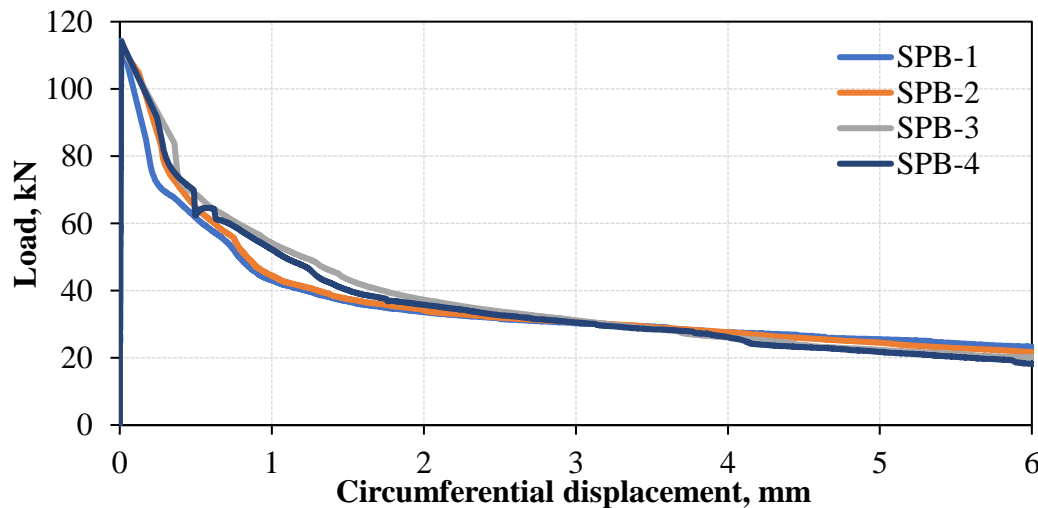


Figure 13. Circumferential load-opening curves from Barcelona test

Table 3 shows the toughness results of tested cylinders. The results variation coefficient varies between 2.5% and 6.8%.

Table 3. Toughness results,  $T_{\delta 2mm}$ ,  $T_{2.5mm}$ ,  $T_{\delta 4mm}$  y  $T_{\delta 6mm}$

ID	U	SPB-1	SPB -2	SPB -3	SPB -4	Average	CV %
$T_{ct 2 mm}$	Joules	102.9	108.9	120.2	115.5	111.9	6.8
$T_{ct 2.5mm}$	Joules	119.2	125.5	137.9	132.5	128.8	6.3
$T_{ct 4 mm}$	Joules	163.8	170.2	182.8	177.2	173.5	4.8
$T_{ct 6 mm}$	Joules	214.7	219.1	227.9	220.5	220.5	2.5

The UNE 83515 also has the advantage of low weight (5 kg) and volume specimens, casted in cylinders which can be easily handled, and is a more sustainable method. The lower press machine capacity required to carry out the test and the feasibility to core from squared panels for quality control and from an existing structure for post-placement verifications. Additionally, the concrete specimens require a small concrete volume and can be easily handled, which provides a more sustainable method.

## 6. CONCLUSIONS

From results obtained for the three proposed tests regarding energy absorption, the statistical analysis showed more variability in the round panels results and low variability in cylinders for the Barcelona Test. This situation results from the fact that the higher the width, the greater fiber concentration in the concrete core.

Samplings developed so far in the L12 extension work represent a pilot project to assess the methods application, which are not specified for the project, therefore, it cannot be confirmed that obtained values comply with the specified parameters regarding SFRS energy absorption, however, it is a turning point for the implementation of a Control Protocol that evaluates the SRFS performance and allows to know the different scenarios, advantages, difficulties and other things that happen in the work site during the sampling development, resulting from tests and analysis of all involved components.

Derived from the experimental campaign applied to the practical case of Mexico City Metro Line 12 Extension, sampling processes, specimens preparation and Barcelona Test (UNE 83515) are more practical from the viewpoint of the work site conditions, because we are dealing with lower weight and smaller test specimens, compared to panels, therefore, less time is needed to prepare them and when the staff is highly skilled, handling, preparation and tests can be done by only one person.

Increase in the use of FRC, experience obtained from field works and related research has encouraged private sector, construction companies and academic institutions such as Instituto de Ingeniería de la UNAM to bring up, propose and develop national test methods to evaluate FRC, based on international standards, using information in local applications. This will encourage a new quality control system for fiber reinforced concrete in Mexican underground works.

## 7. ACKNOWLEDGMENTS

The authors thank the General Direction of Work Construction for Transport from Mexico City for the facilities provided during the specimen sampling works in the tunnel, which allowed the development of this paper.

## 8. REFERENCES

- Aire, C., Rodríguez, M. (2011). *Estudio de las propiedades mecánicas básicas de concreto con fibras sintéticas*. Proyecto de investigación. Instituto de Ingeniería UNAM P1503. Informe elaborado para EUCLID. Junio. p. 78.
- Asociación Española de Normalización y Certificación. (2007). *UNE EN 14488-5: Ensayos de hormigón proyectado. Parte 5: Determinación de la capacidad de absorción de energía de probetas planas reforzadas con fibras*. Madrid, España.
- Asociación Española de Normalización y Certificación. (2007). *UNE EN 14651: Método de ensayo para hormigón con fibras metálicas. Determinación de la resistencia a la tracción por flexión (límite de proporcionalidad (LOP), resistencia residual)*. Madrid, España.
- Asociación Española de Normalización y Certificación (2008). *UNE 83515: Hormigones con fibras. Determinación de la resistencia a fisuración, tenacidad y resistencia residual a tracción. Método Barcelona*, Madrid, España.
- ASTM International. (2013). *ASTM C494/C494M-13 Standard Specification for Chemical Admixtures for Concrete*. [https://doi.org/10.1520/C0494\\_C0494M-13](https://doi.org/10.1520/C0494_C0494M-13)
- ASTM International. (2015). *ASTM C 1141/C1141M-15 Standard Specification for Admixtures for Shotcrete*. [https://doi.org/10.1520/C1141\\_C1141M-15](https://doi.org/10.1520/C1141_C1141M-15)
- ASTM International. (2012). *ASTM C1550-12 Standard Test Method for Flexural Toughness of Fiber Reinforced Concrete (Using Centrally Loaded Round Panel)*. <https://doi.org/10.1520/C1550-12>
- ASTM International. (2012). *ASTM C1609/C1609M-12 Standard Test Method for Flexural Performance of Fiber-Reinforced Concrete (Using Beam With Third-Point Loading)*. [https://doi.org/10.1520/C1609\\_C1609M-12](https://doi.org/10.1520/C1609_C1609M-12)
- Blom, C. B. M. (2002). “*Design philosophy of concrete linings in soft soil*”. Doctoral Thesis. Delft University of Technology, p. 6
- Burgers, R., Walraven, J., Plizzari, G., Tiberti, G. (2007). “*Structural Behaviour of SFRC tunnel segments during TBM operations*”. Proceedings of the World Tunnel Congress 2007 and 33<sup>rd</sup> ITA/AITES Annual General Assembly, London, England., pp. 1461-1467.
- Carmona, S., Aguado, A., Molins, C., Cabrera, M. (2009), *Control de la tenacidad de los hormigones reforzados con fibras usando el ensayo de doble punzonamiento (ensayo Barcelona)*. Revista Ingeniería de Construcción Vol. 24 N° 2, pp. 119-140. <http://dx.doi.org/10.4067/S0718-50732009000200001>
- Chen, W. F. (1970). “*Double punch test for tensile strength of concrete*”. ACI Journal, Proceedings Vol. 67, pp. 993-995.
- De La Fuente, A., Blanco, A., Pujadas, P., Aguado, A. (2013). *Advances on the use of fibres in precast concrete segmental*. Engineering a Concrete Future: Technology, Modeling & Construction. International Federation for Structural Concrete, pp. 691-694.
- De La Fuente, A., Pujadas, P., Blanco, A., Aguado, A. (2012). *Experiences in Barcelona with the use of fibres in segmental linings*. Tunneling and Underground Space Technology. Volumen 27, pp. 60-71. <https://doi.org/10.1016/j.tust.2011.07.001>
- De Waal, R. G., (2000). “*Steel fibre reinforced tunnel segments for the application in shield driven tunnel linings*”, Doctoral Thesis, Delft University of Technology.
- Gettu, R., Barragan, B., Garcia, T., Ramos, G., Fernandez, C., Oliver, R. (2004). *Steel fiber reinforced concrete for the Barcelona metro line 9 tunnel lining*, in: Di Prisco, M., Felicetti, R., Plizzari, G. A. (Eds.), 6<sup>th</sup> International RILEM Symposium on Fibre Reinforced Concretes RILEM PRO 039, Bagnaux, pp. 141-156.
- Gopalaratnam V., Gettu R. (1995). *On the Characterization of Flexural Toughness in Fiber Reinforced Concrete*. International Journal Cement and Concrete Composites. Vol. 17, pp 239-

254. [https://doi.org/10.1016/0958-9465\(95\)99506-O](https://doi.org/10.1016/0958-9465(95)99506-O)

Kasper, T., Edvardsen, C., Wittneben, G., Neumann, D. (2008). *Lining design for the district heating tunnel in Copenhagen with fibre reinforced concrete segments*. Tunnelling and Underground Space Technology. Volumen 23, pp 574-587.

<https://doi.org/10.1016/j.tust.2007.11.001>

Kooiman, A. G. (2000). “*Modelling steel fibre reinforced concrete for structural design*”, Doctoral Thesis, Delf University of Technology.

Norma Mexicana (2017). *NMX-C-414-ONNCCE-2017, Industria de la Construcción - Cementantes Hidráulicos – Especificaciones y Métodos de Ensayo*. México.

Norma Mexicana (2018). *NMX-C-111-ONNCCE-2018, Industria de la Construcción – Agregados para concreto Hidráulico – Especificaciones y Métodos de Ensayo*. México.

Norma Mexicana (2017). *NMX-C-538-ONNCCE-2017, Industria de la Construcción – Concreto Reforzado con Macrofibras – Determinación de la Resistencia al Agrietamiento, Tenacidad y Resistencia Residual a Tensión – Método de Ensayo*. México.

Norma Mexicana (2017). *NMX-C-539-ONNCCE-2017, Industria de la Construcción – Concreto Reforzado con Macrofibras – Determinación de la Tenacidad a la Flexión Utilizando el Panel Circular con carga central – Método de Ensayo*. México.

Zollo, R. F. (1997). *Fiber-reinforced concrete: an overview after 30 years of development*. Cement and Concrete Composites. Volumen 19, pp. 107-122. [https://doi.org/10.1016/S0958-9465\(96\)00046-7](https://doi.org/10.1016/S0958-9465(96)00046-7)

## Inspection of facades with Unmanned Aerial Vehicles (UAV): an exploratory study

R. D. B. Ruiz<sup>1\*</sup> , A. C. Lordsleem Júnior<sup>1</sup> , J. H. A. Rocha<sup>2</sup> 

\*Contact author: [Ramiro.DBR@hotmail.com](mailto:Ramiro.DBR@hotmail.com)

DOI: <https://doi.org/10.21041/ra.v11i1.517>

Reception: 07/10/2020 | Acceptance: 16/12/2020 | Publication: 01/01/2021

### ABSTRACT

The objective of this study was to evaluate the use of Unmanned Aerial Vehicles (UAVs) as a visual tool for the inspection of pathological manifestations in facades, through an exploratory study. Currently, the relevance of UAVs is growing as a new mechanism for obtaining data and visual inspection of buildings, optimizing time. The research strategy had three distinct steps: a literature review, an experimental procedure, and data processing, aiming to verify the viability of the inspection procedure. There is evidence of the convenience of UAV use, particularly where access is difficult, which reduces time and cost, generates greater security, and allows 3D reconstruction of the building under inspection, generating more accurate diagnoses.

**Keywords:** UAV; property inspection; visual inspection; monitoring; aerial photos.

**Cite as:** Silva, Ruiz, R. D. B., Lordsleem Júnior, A. C., Rocha, J. H. A. (2021), "Inspection of facades with Unmanned Aerial Vehicles (UAV): an exploratory study", Revista ALCONPAT, 11 (1), pp. 88 – 104, DOI: <https://doi.org/10.21041/ra.v11i1.517>

<sup>1</sup> Polytechnic School of Pernambuco, University of Pernambuco, Recife, Brazil.

<sup>2</sup> Departamento de Ingeniería Civil, Facultad de Tecnología, Universidad Privada del Valle, Cochabamba, Bolivia

#### Contribution of each author

In this work, author R.D.B. Ruiz contributed the original idea, experimentation, data collection, writing of the paper, and discussion of results, author A.C. Lordsleem Júnior contributed with the writing of the paper and discussion of results, and author J.H.A. Rocha contributed with the review of the paper and discussion of results.

#### Creative Commons License

Copyright 2021 by the authors. This work is an Open-Access article published under the terms and conditions of an International Creative Commons Attribution 4.0 International License ([CC BY 4.0](https://creativecommons.org/licenses/by/4.0/)).

#### Discussions and subsequent corrections to the publication

Any dispute, including the replies of the authors, will be published in the third issue of 2021 provided that the information is received before the closing of the second issue of 2021.

## **Inspeção de fachadas com Veículos Aéreos Não Tripulados (VANT): estudo exploratório**

### **RESUMO**

O objetivo desta pesquisa consistiu em avaliar o uso de VANT como ferramenta visual para a inspeção de manifestações patológicas em fachadas a través de um estudo exploratório. Na atualidade, os Veículos Aéreos Não Tripulados (VANT) assumem uma crescente relevância na construção civil como novo mecanismo de obtenção de dados e inspeção visual, otimizando o tempo. A estratégia de pesquisa considera três etapas distintas: revisão bibliográfica, o procedimento experimental e, finalmente o processamento de dados, objetivando verificar a viabilidade do procedimento de inspeção. Evidencia-se a conveniência de utilização do VANT particularmente onde o acesso é difícil, o que pode reduzir tempo, custos e gerar maior segurança, além da reconstrução 3D da edificação para ser inspecionada e gerar diagnósticos mais certos. **Palavras-chave:** VANT; inspeção predial; inspeção visual; monitoramento; fotos aéreas.

## **Inspección de fachadas con Vehículos Aéreos no Tripulados (VANT): estudio exploratorio**

### **RESUMEN**

El objetivo de esta investigación consistió en evaluar el uso de VANT como herramienta visual para la inspección de manifestaciones patológicas en fachadas a través de un estudio exploratorio. En la actualidad, los Vehículos Aéreos no Tripulados (VANT) asumen una creciente relevancia en la construcción civil como nuevo mecanismo de obtención de datos e inspección visual, optimizando el tiempo. La estrategia de investigación considera tres etapas distintas: revisión bibliográfica, el procedimiento experimental y, finalmente, el procesamiento de datos, con el objetivo de verificar la viabilidad del procedimiento de inspección. Se evidencia la conveniencia de utilizar el VANT particularmente donde el acceso es difícil, lo que puede reducir tiempo, costos y generar mayor seguridad, además de la reconstrucción 3D de la edificación para ser inspeccionada y generar diagnósticos más ciertos. **Palabras clave:** VANT; inspección predial; inspección visual; monitoreo; fotos aéreas.

### **Legal Information**

Revista ALCONPAT is a quarterly publication by the Asociación Latinoamericana de Control de Calidad, Patología y Recuperación de la Construcción, Internacional, A.C., Km. 6 antigua carretera a Progreso, Mérida, Yucatán, 97310, Tel.5219997385893, [alconpat.int@gmail.com](mailto:alconpat.int@gmail.com), Website: [www.alconpat.org](http://www.alconpat.org)

Reservation of journal title rights to exclusive use No.04-2013-011717330300-203, and ISSN 2007-6835, both granted by the Instituto Nacional de Derecho de Autor. Responsible editor: Pedro Castro Borges, Ph.D. Responsible for the last update of this issue, Informatics Unit ALCONPAT, Elizabeth Sabido Maldonado.

The views of the authors do not necessarily reflect the position of the editor.

The total or partial reproduction of the contents and images of the publication is carried out in accordance with the COPE code and the CC BY 4.0 license of the Revista ALCONPAT.

## 1. INTRODUCTION

Visual inspection of building facades seeks to assess the state of conservation of the vertical facade and the elements that comprise it, providing guidelines for effective maintenance with an adequate cost-benefit ratio. This practice makes it possible to guarantee the proper functioning of the vertical facade system, allowing it to fulfill the functions for which it was built and potentially extend its useful life (Pires et al., 2015; Flores-Colen et al., 2008).

To this end, an effective methodology that reduces both time and cost is visual inspection using Unmanned Aerial Vehicles (UAVs) (Melo and Costa, 2015). With the aid of this technology, it is possible to completely film and capture High Definition (HD) photographs of all of the principal points investigated. This detailed investigation can discover problems not visible to the naked eye from the ground, such as: infiltration, detachment, or holes in the covering and/or fissures and cracks in the facade (Tondelo and Barth, 2019).

Currently, in Brazil, visual inspection of buildings is mostly performed through the traditional method. Professional industrial climbers can perform visual verification and create a photographic record of the principal points to be analyzed, however, the cost and time are greater when compared to a survey using UAVs. According to data released by the Public Ministry, 40% of work accidents in Brazil are related to falls from height (EXAME, 2018).

The term UAV refers to a class of aircraft piloted remotely or automatically using predefined coordinates, an emerging technology known for its role in military applications (Irizarry and Costa, 2016).

More recently, both in Brazil and other countries, the use of these aerial vehicles in civilian environments has become increasingly common, in areas such as agriculture, forestry, archeology, architecture, and construction (Roca et al., 2013; Máthé and Buşoniu, 2015; Morgenthal and Hallermann, 2015; Nikolic et al., 2013; Hung et al., 2018; Yang et al., 2015; De Melo et al., 2017; Falorca and Lanzinha, 2020).

It was only in 2017 that the Brazilian law regulating general requirements for unmanned civilian aircraft was published by the National Civil Aviation Agency (ANAC), known as Brazilian Special Civil Aviation Regulation (RBAC-E) n° 94 (ANAC, 2017). This special regulation establishes the conditions for the operation of UAVs in Brazilian territory, taking into consideration their current stage of development, in order to promote their safe and sustainable use.

The use of UAVs in the construction industry is still limited (Melo and Costa, 2015), although this technology can be used in a variety of ways. Visual inspection of large construction projects to verify performance conditions and determine necessary preventive and corrective measures deserves special attention, due to the inherent complexity (height, size, difficulty of access, and exposure). UAVs can reduce the time required for these monitoring operations, as well as assist in other potentially hazardous inspection processes (Álvares et al., 2016).

The objective of this study is to evaluate the use of Unmanned Aerial Vehicles (UAVs) as a visual tool for inspecting pathological manifestations on facades through an exploratory study, in order to verify the feasibility of use and aiming to develop guidelines that integrate aerial image collection, data processing, and visual analysis.

## 2. UAVs IN VISUAL INSPECTION

Different types of UAVs are useful for the purpose of visually inspected buildings. Among them, those supported by rotating wings, when compared to fixed wing craft, allow for quicker displacement and greater versatility in flight, being effective in collecting horizontal images in areas of medium extension, as in the case of Vera (2016).

Similarly, the versatility of this aircraft allows it to move on all possible axes, being effective in capturing simple vertical and oblique vertical images as shown in the case studies of Mader et al. (2016), Morgenthal and Hallermann (2015), and Reagan et al. (2018) in the detection of specific surfaces or elements, making it a useful tool for the visual inspection of vertical facades or, as in the case of Irizarry and Costa (2016), a visual tool for construction site management. Figure 1 presents the summary of the main advantages and disadvantages of vehicles with fixed and rotating wings.

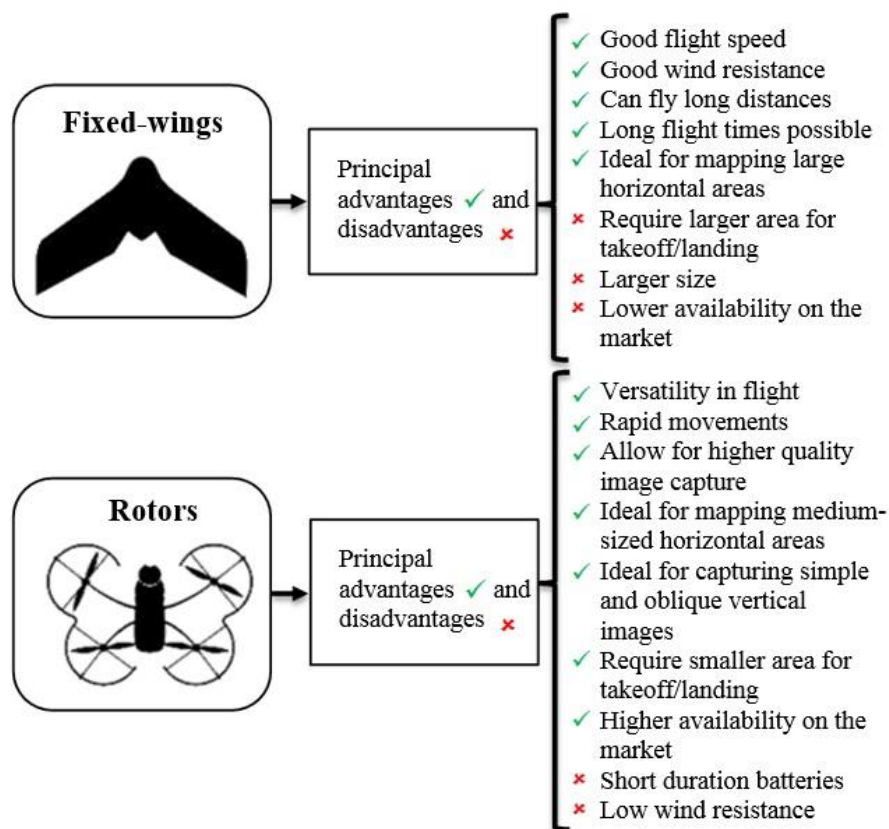


Figure 1. Advantages and disadvantages of UAVs depending on wing type.

According to the International Civil Aviation Organization (ICAO, 2017), any aircraft intended to fly without a pilot on board is referred to as an RPAS (Remotely Piloted Aircraft System). The rotary-wing UAVs used in these studies are classified by ANAC as RPAS Class 3, which have fewer flight requirements and restrictions, making it possible to use them in urban areas and at construction sites (Brazil, 2017).

These vehicles are also usually simple to fly, supported by a set of engines controlled by a sophisticated electronic system that generally guarantees the aircraft's stability, allowing for vertical takeoff and landing. They are therefore the preferred choice for carrying cameras and other objects for short distances from the takeoff point. Figure 2 shows the minimum suggested equipment characteristics for the purpose of visual inspection of facades.

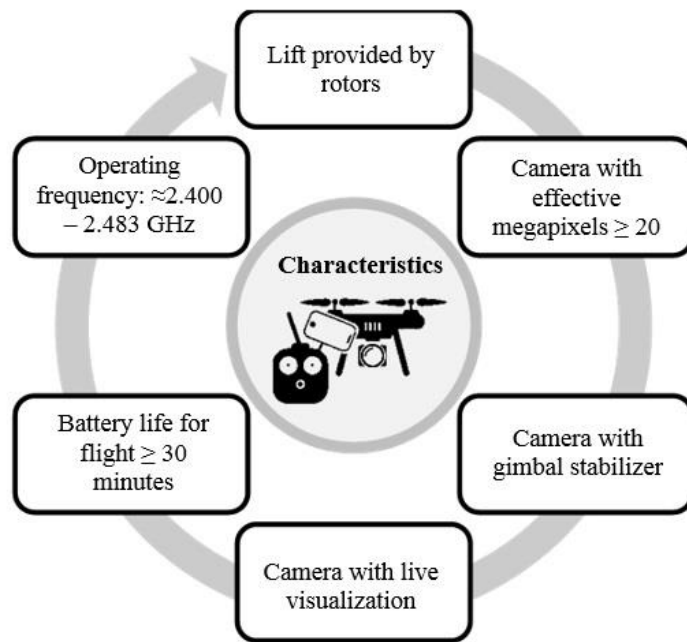


Figure 2. Minimum equipment characteristics for visual inspection of facades.

It is important to note that the current ease of acquiring a UAV does not mean that the user will be able to pilot the equipment. There are rules, standards, and procedures for becoming an Unmanned Aerial Vehicle pilot (Aguilar, 2018), which are specified in RBAC-E nº 94 Resolution n. 419 (Brazil, 2017).

In recent years, there has been an increase in the use of UAVs for inspection of structures, specifically buildings, due to their long range, area photogrammetry applications, efficient data recording, speed, security, and low cost, among others reasons (Izarry and Costa, 2016; Shariq and Hughes, 2020; Groso et al., 2020). In Figure 3, the advantages reported in the bibliographic review for the use of UAVs are compared to one of the most used traditional methods, industrial climbing.

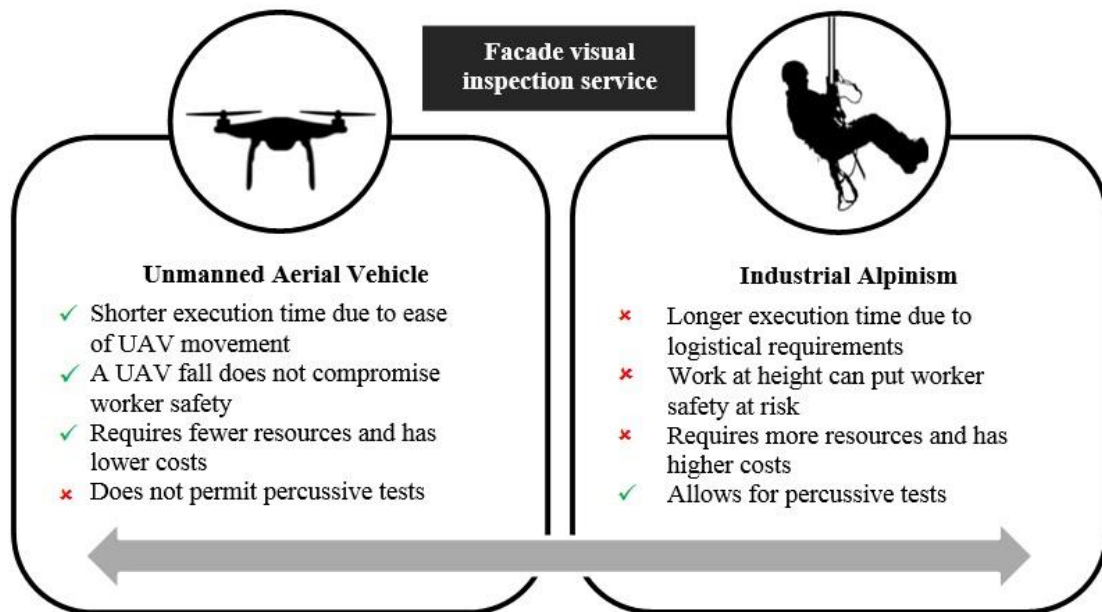


Figure 3. Comparison of visual façade inspection procedures.

### 3. EXPERIMENTAL PROCEDURE

Based on guidelines derived from the literature review and with an objective of verifying the feasibility of UAVs for inspection of pathological manifestations in facades, the Institute of Technological Innovation (IIT) at the University of Pernambuco was selected. This building (Figure 4) has four floors and is in Pernambuco's PARQTEL (Electro-electronic Technological Park), in the Curado district (Figure 4). This building was selected because of its geometric characteristics (multiple facades) and its isolated location regarding other nearby buildings, making it ideal for training and perfecting flights with the UAV and developing flight protocols.

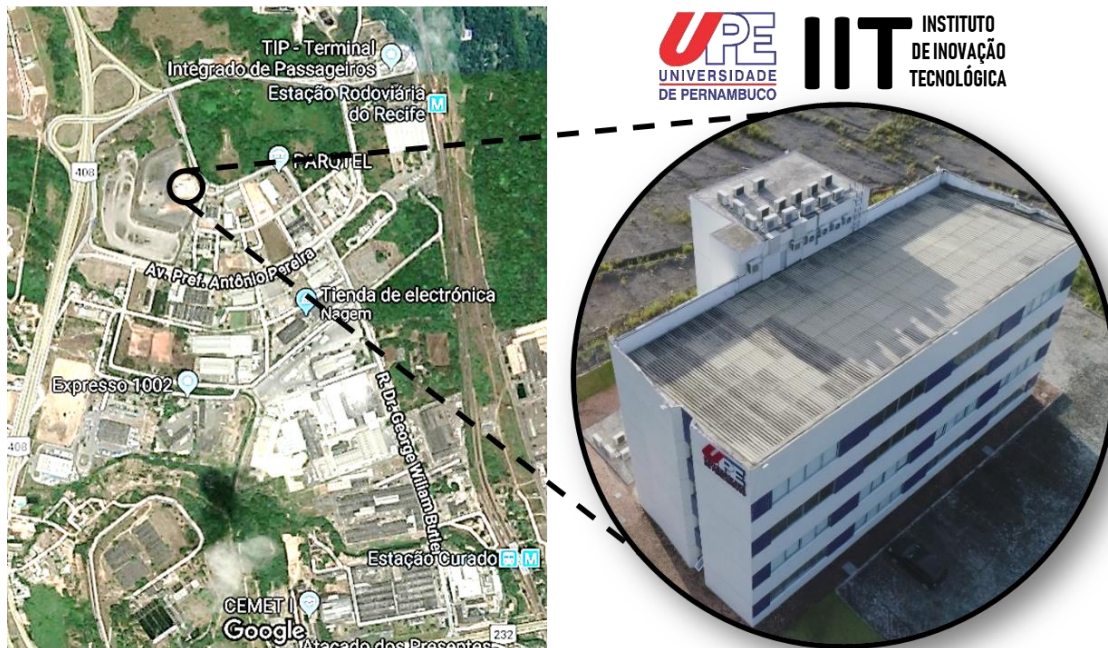


Figure 4. UPE Institute of Technological Innovation. Adapted from Google (2018).

Following this, training was carried out on the operation of the UAV. In this phase, test flights were performed around the building, in order to collect data and analyze what could be visualized through the imagery obtained, making it possible to refine the collection method and technical procedures necessary to perform such an operation following the required safety criteria. In summary, this step included training in the use of the technology, and the technical understanding of the equipment.

To perform the field surveys, the Phantom 4 Pro model V2.0 UAV, manufactured by DJI, was used, equipped with a 1" 20 MP camera, able to record videos in 4K 60 fps and shoot at 14 fps in continuous shooting mode. The UAV is controlled by a remote with built-in HD high illumination display and contains a lithium battery that offers 30 minutes of maximum flight time. Table 1 presents some additional features of the Phantom 4 Pro V2.0.

Table 1. Technical characteristics of the Phantom 4 Pro V2.0

Specifications	Phantom 4 Pro V2.0
Weight (including battery and propellers)	1388 g
Maximum flight time	30 min
Viewing system	Front, back, and below
Obstacle detection	Front and back
	Infrared left and right
Video transmission system	Lightbridge
Lens	FOV 84° 8.8 mm/24 mm (35 mm equivalent format) f/2.8 - f/11 autofocus at 1 m - ∞
Operating frequency	2.4 GHz/5.8 GHz
	5.8 GHz transmission is not available in some regions due to local regulations

Source: DJI (2017)

The data capture strategy followed the basic concepts of digital photogrammetry, seeking parallelism among photo positions and perpendicularity to the plane of the object of interest, as shown in Figure 5, and for each part of the object to be photographed from at least two different positions, guaranteeing image overlap (Groetelaars, 2015). These aspects are important for the correlations required to construct orthomosaics or three-dimensional reconstructions.

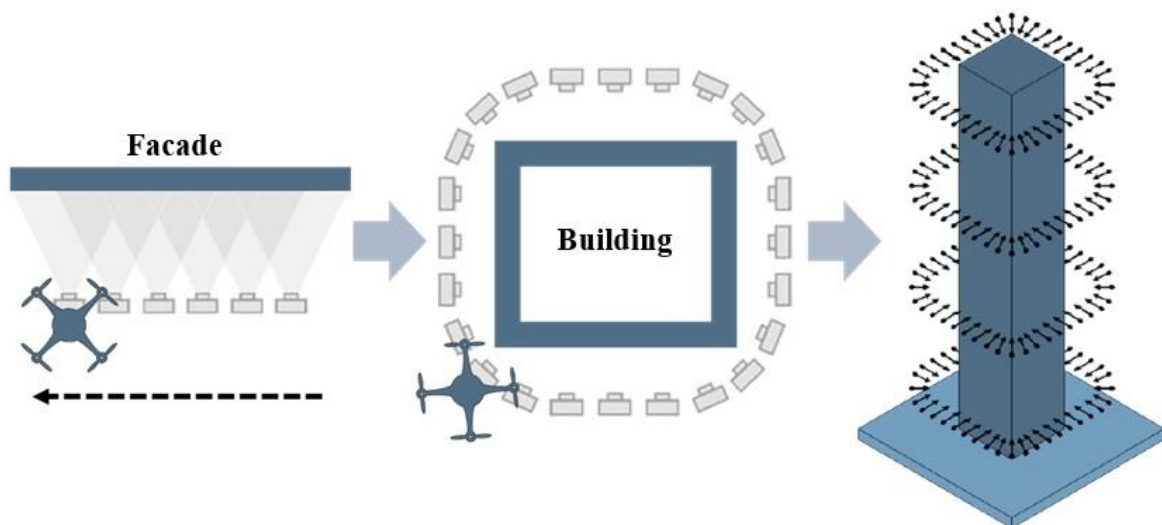


Figure 5. Image capture strategy. Adapted from Melo Jr (2016).

In total, eight experimental flights were carried out during four field tests, with a flight counted as each takeoff and landing, including when changing the SD memory or recharging the battery. The protocols for the activities to be carried out include filling out the form for the planning meeting (standardizes data collection to prepare the flight plan, define the takeoff and landing points, and indicate the areas covered for 3D modeling) and the mission checklist for the UAV (registration of flight technical data and a checklist of all procedures necessary for operation of the UAV in adequate safety conditions). The tests began in August 2018, resulting in approximately 2 hours and 30 minutes of flight training, as shown in Table 2 in the flight log spreadsheet (list of all physical flight data recorded in the application to be adopted and in the mission checklist). Among the information recorded during the flight using the DJI Go App, were the number of visual assets

collected (photos and videos), distance, maximum altitude, flight duration, photographic overlay, and flight speed.

Table 2. Experimental flight data (flight log spreadsheet)

Nº	Time	Number of photos	Distance (m)	Maximum height (m)	Flight duration (min)	Photographic overlap (%)	Flight velocity (km/h)
1	11:14	2	20	5	15	0	10
2	11:40	35	8	16	12	75	4
3	09:52	108	4	24	27	75	3
4	11:31	95	4	35	28	75	3
5	14:15	42	6	92	8	75	3
6	14:27	67	8	35	19	75	4
7	15:50	87	8	36	25	75	4
8	15:25	35	50	120	24	90	10

#### 4. DATA PROCESSING

After verifying the quality of the visual assets, it was determined that the photos collected during flights number 2, 6, and 7 presented excellent visual quality and distance ratio, 8 m away from the facade, and, consequently, a distance between stations of 1.8 m in the vertical direction and 3.2 m in the horizontal direction.

According to Ballesteros (2020) and Pierrot-Deseilligny et al. (2011), this ratio between the distance in position of the stations for taking photographs and distance from the stations to the photographed facade is ideal for 3D reconstruction. If this ratio is very small, the automatic correlation of the points is facilitated, but the geometric accuracy in the digital reconstruction of the facade becomes more difficult.

The 189 photographs collected 8 m from the facade were therefore selected for processing using the stereo matching technique, a process that finds corresponding points (Smartmatches) in two or more images.

Reconstruction in 3D is possible as long as there are at least two images of the same scene, obtained from different positions (different projection centers) such that, from the position, orientation, and focal distance, it becomes possible to determine the position of points in space from the two-dimensional coordinates of the images through the principles of epipolar geometry (Melo Jr., 2016).

In other words, photo-based scanning software compares small areas made up of a set of pixels present in two or more photos that, in turn, are formed by the textures or contrasting marks on the surface of the object or scene. The comparison process continues until the program finds the best matches between the images. When optimal or ideal matches are found, the position and orientation information already computed for the photographs is used to calculate the spatial location of the point.

The stereo matching software selected for this 3D reconstruction was Agisoft PhotoScan. This stage of the study aimed to defining the procedures and steps necessary for the proper development of 3D mapping and the generation of orthomosaics using UAVs. Therefore, the corresponding sequence of processing steps in the Agisoft PhotoScan software and the parameters used for the processing are described in Table 3.

Table 3. Workflow and parameters used for Agisoft PhotoScan.

Step	Parameters	
1.- Align Photos	Accuracy:	Highest
	Pair preselection:	Generic
	Sparse cloud:	31.578
2.- Build Dense Cloud	Quality:	High
	Depth filtering:	Aggressive
	Dense cloud:	22.767.991
3.- Build mesh	Surface type:	Arbitrary 3D
	Face count:	High
	Faces:	533.755
4.- Build texture	Mapping mode:	Adaptive orthophoto
	Blending mode:	Mosaic
5.- Build Orthomosaic	Type	Planar
	Blending mode:	Mosaic

## 5. RESULTS AND DISCUSSION

The first step consisted of the alignment of the images (align photos), in which Agisoft PhotoScan seeks similarities between the images. The result is the generation of a cloud of tie points, the basic product for the generation of the densified point cloud and 3D models, as well as the connection point between the orthophotos in the mosaic process and the generation of the orthophoto mosaic. In this step, support points were also collected in the field to improve positional accuracy of the point cloud, followed by the elimination of unwanted points or noise, such as: poorly captured surfaces, areas belonging to other objects, and distant points. The final result from this step was the model shown in Figure 6, a sparse or low-density point cloud, which also defines the building's geometry.

In the second step, the dense cloud of 3D points was built by filtering unwanted points or noise. From the estimated camera positions, the software calculates depth information for each camera to be combined at a single point in the dense cloud.

The highest level was chosen for the densification configuration, generating more than 22 million points. The main function of this step is to densify the point cloud generated in the previous process, increasing the number of points in the point cloud and reducing the empty spaces to better represent the mapped area. The model generated in this step is shown in Figure 7, with most of the geometric details of the building digitally reconstructed.

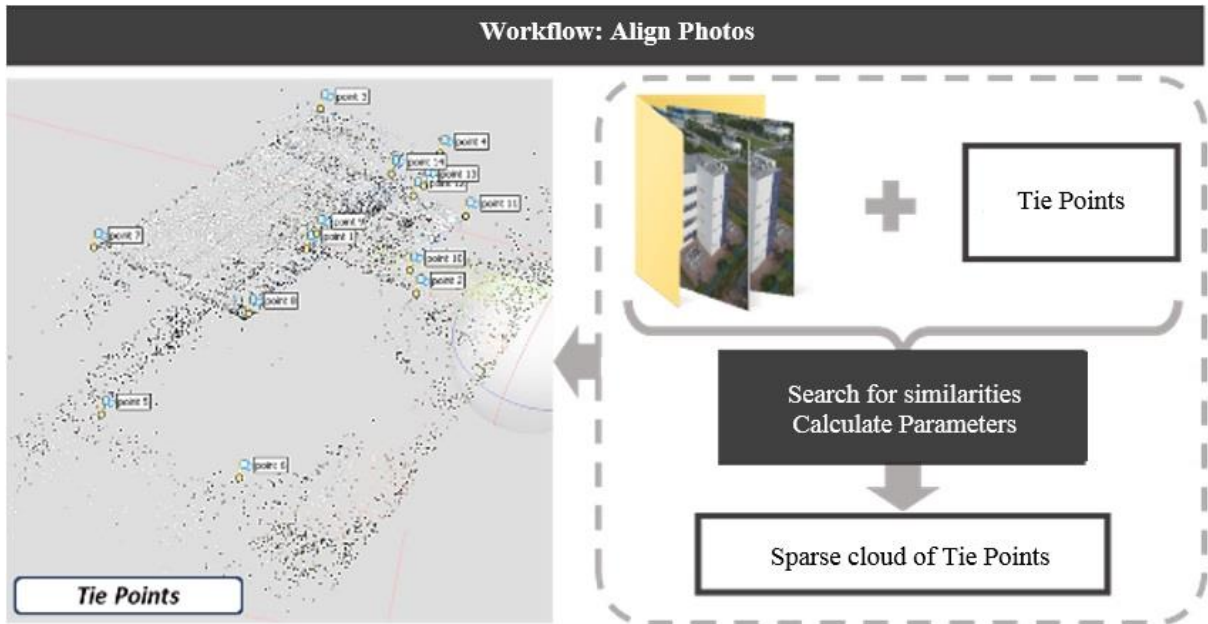


Figure 6. Cloud of tie points for IIT-UPE

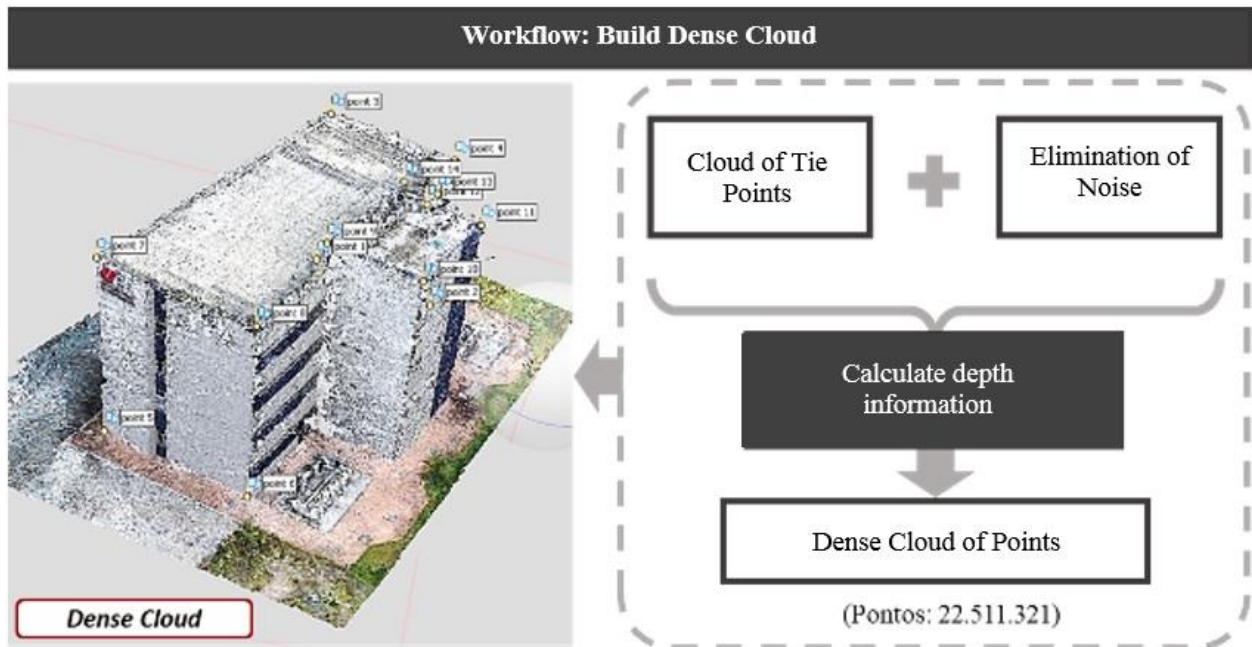


Figure 7. Densified point cloud for IIT-UPE

In the third step, the mesh was built, generated from the grouping of vertices from the dense point cloud. The 3D model generated in this step is shown in Figure 8, with more than 500,000 faces (or adjacent polygons) sharing edges of the object's boundary surface.

Note that the required number of faces for a model are related to the level of detail expected from it. The higher the level, the higher the computational cost (time needed for processing and hardware performance required). If the model is generated from the sparse point cloud, the number of faces and vertices will naturally be fewer.

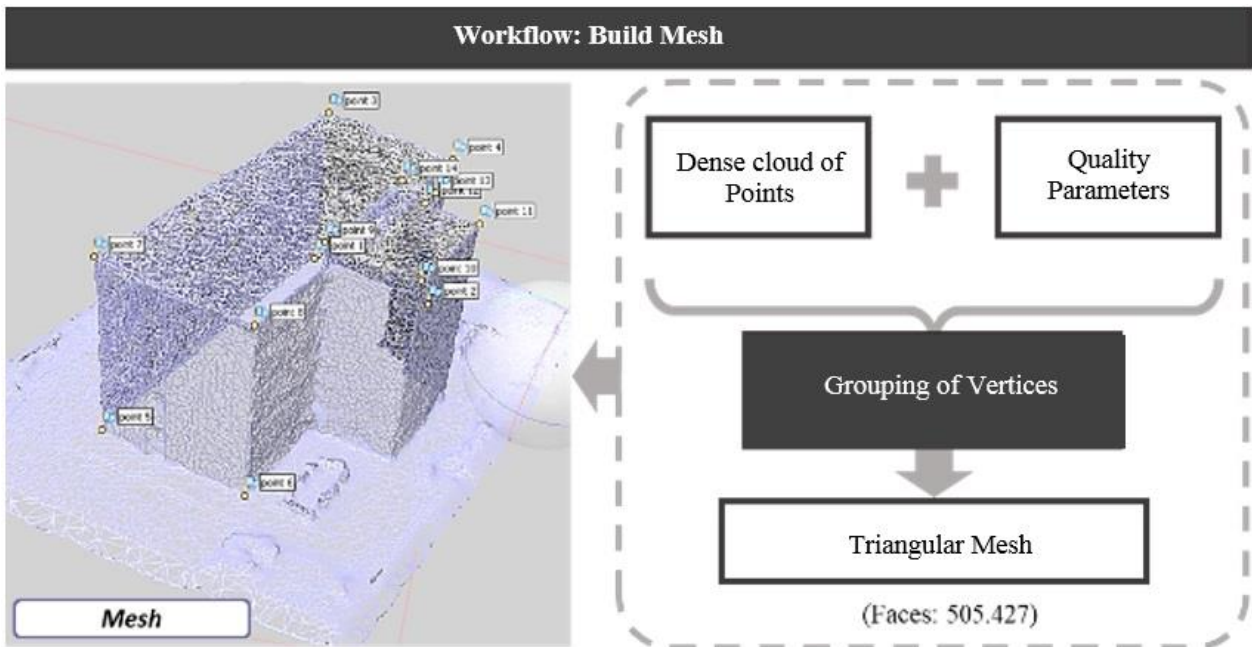


Figure 8. Triangular mesh model of IIT-UPE

In the fifth and final step, generation of the orthomosaic, the orthorectification of the images was carried out, with the image features projected orthogonally at constant scale, without displacements due to relief or the inclination of the camera. With the images properly corrected, the software mosaics the orthophoto to create a single product.

In the fourth step, the goal is to apply a texture to the three-dimensional model to improve its visual aspect, in order to allow visualization of the pathologies on the facade. The textured 3D model generated in this step is shown in Figure 9.

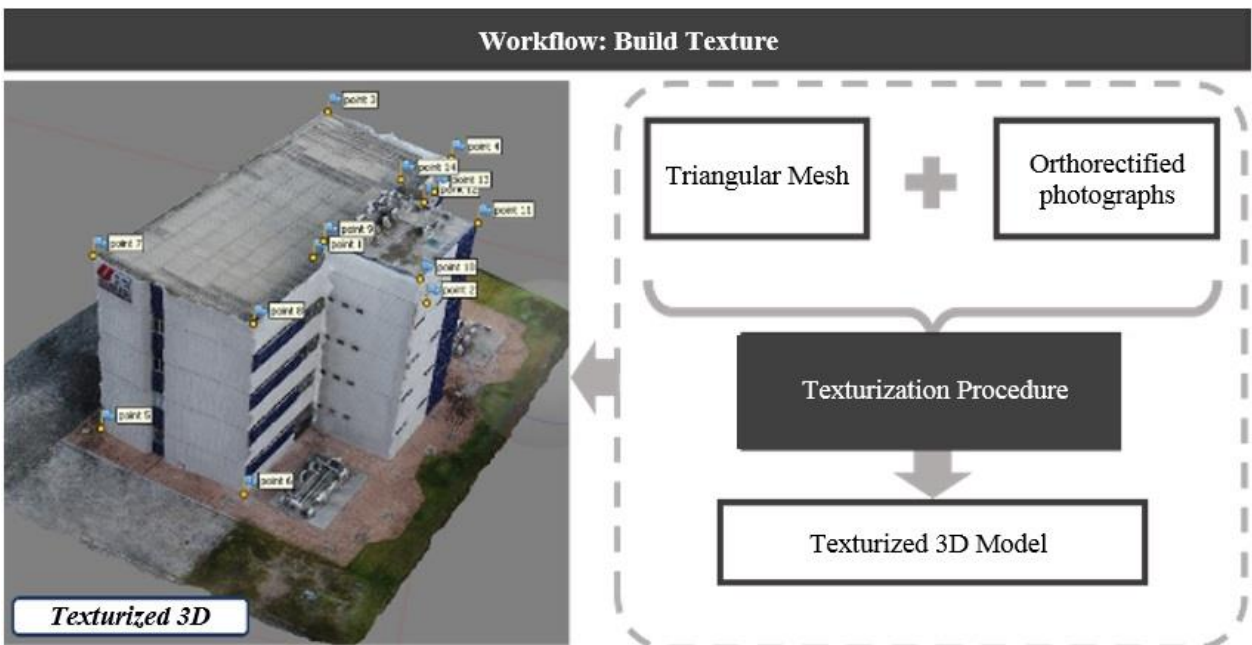


Figure 9. Texturized model of IIT-UPE

The Agisoft PhotoScan software allows orthomosaics to be exported from previously generated models. For example, Figure 10 shows the orthomosaic corresponding to the south facade of the IIT building.

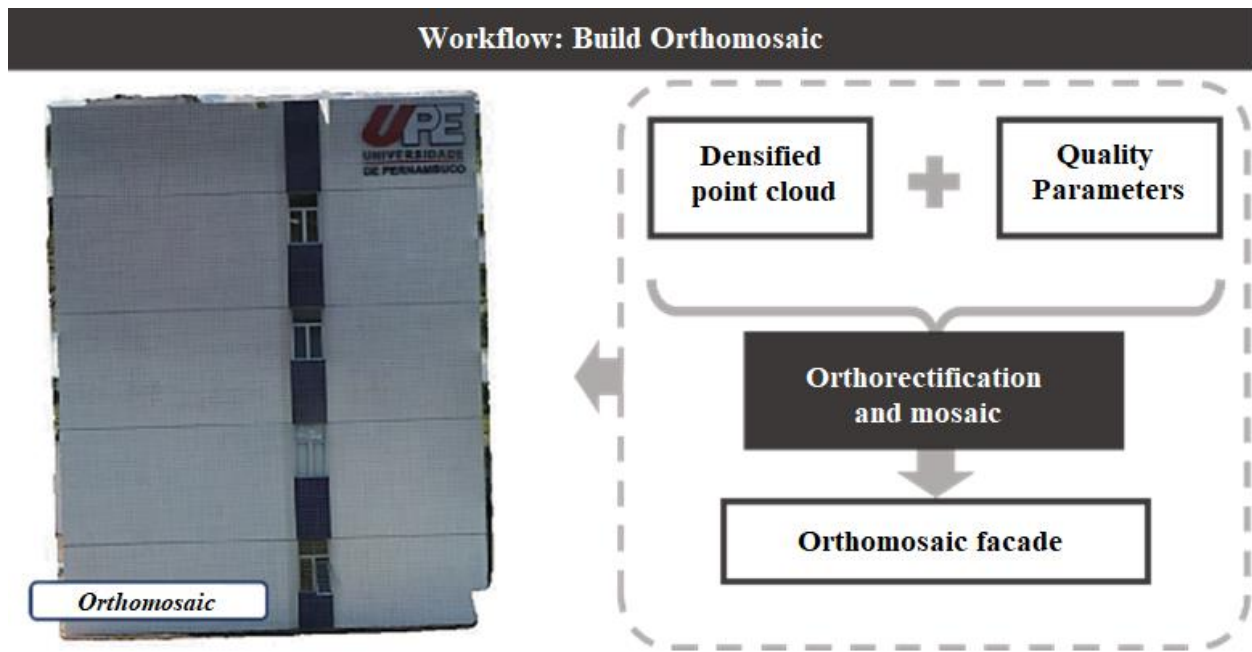


Figure 10. Orthomosaic model of IIT-UPE south Orthomosaic facade

The final product of these processing steps was the 3D digital model shown in Figure 11. A satisfactory result in terms of geometric reconstruction is exportable in various formats for various uses, according to the desired application.

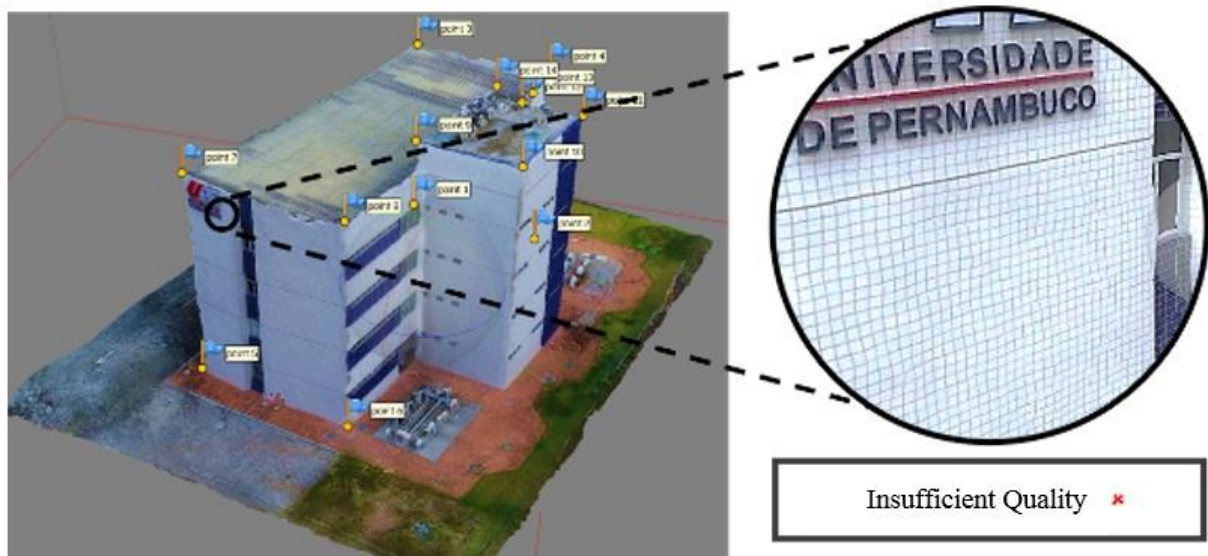


Figure 11. Final product – IIT-UPE 3D textured model

However, the quality of this model is insufficient for the purpose of detecting pathologies on the facade, due to distortions on the textured facades.

Authors such as Roca et al. (2018) and Rakha and Gorodetsky (2018) also generated 3D models in their respective studies and highlighted some limitations. Rodriguez-Gonzalvez et al. (2014) also pointed out that 3D reconstruction has limitations regarding the quality and integrity of the structure inspected.

Orthomosaics of each building facade were created to provide stronger and more useful results. These orthorectified images are of enough quality to allow for the detection of pathological manifestations through visual inspection.

This is shown in Figure 12, in which the orthomosaic of the south facade made possible to discover cracking in the ceramic coating, the beginning of efflorescence, and pathologies resulting from biological processes (mold and mildew).

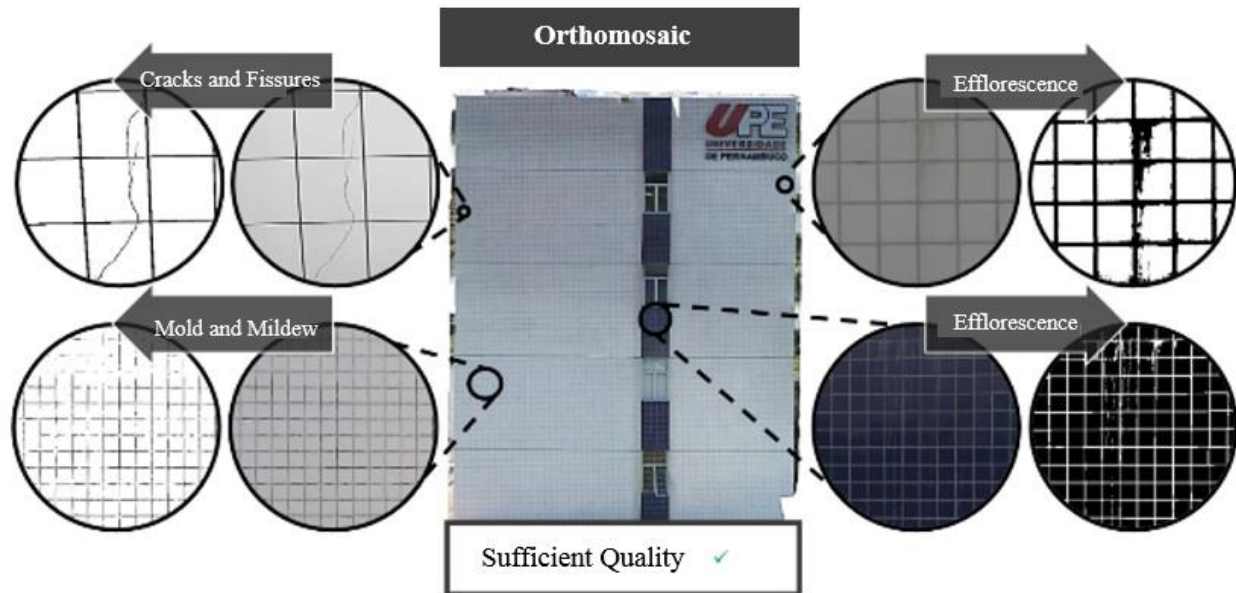


Figure 12. Detection of pathological manifestation on the south facade of IIT-UPE

Lastly, following the literature review and the development of the experimental study, the use of UAVs to detect pathological manifestations in facades was shown to be viable, as was also reported in the study by Tondelo and Barth (2019).

The use of UAVs for facade inspection is an alternative to the traditional method, providing the information necessary to diagnose the structure. The results can be obtained when a multi-rotor UAV with an HD camera is available, as used in the current study and pointed out by Falorca and Laninha (2020).

Although the current study was limited to the use of UAVs as a visual tool for inspecting pathological manifestations of facades, different techniques, such as deep learning, can be combined to assist and automate visual inspection, as proposed by Ruiz et al. (2021).

A need was identified to create a procedure that allows the visual inspection technique to be structured step by step using this technology. The procedure would include a suitable flight protocol for these purposes, and would also idealize the stages of data capture, storage, processing, and post-processing. Consequently, it is possible to guarantee the advantages of this procedure regarding the traditional inspection model, which includes industrial alpinism.

## 6. CONCLUSIONS

Following the elaboration of this study, the importance of the correct choice of UAV based on the different functions it can fulfill was highlighted. UAVs may have significant advantages and disadvantages according to their design characteristics, mainly depending on their lift type: rotors or fixed wings. For the specific case of visual inspection of facades, as already discussed, vehicles with rotors, a gimbal, and an aerial camera are ideal, providing agility and high quality in capturing high resolution images or video of the different points on the vertical walls or analysis elements. This refined procedure can expose problems not visible to the naked eye from ground level, such as: infiltration, detachment, mold, mildew, fissures, and cracks in the coating.

The convenient inclusion of this type of UAV in Brazilian legislation and its minor restrictions, allow for commercialization on a larger scale and generally at a lower price than its fixed-wing counterpart, making it more accessible to the public. It is recommended that the vehicle meet the minimum characteristics discussed above. Currently, commercial UAVs still have technical limitations, mainly regarding battery life and charging capacity. However, future perspectives point to the continuous development of this technology, mitigating these limitations and expanding the scenarios where this technology can be employed within the construction industry.

According to the experimental procedure and the preliminary results, it should be noted that the Agisoft PhotoScan software allows for a wide range of options regarding the quality of the result, from low resolution to highly elaborated, with an increasing computational cost.

With regard to the quality analysis of the 3D mappings developed, it is possible to state that the quality of the textured 3D models still does not reach sufficient quality to detect pathologies on the facades, although its use has not yet been ruled out, as this quality may be improvable with more powerful cameras and more trained image capture procedures. On the other hand, the orthomosaics generated from these models have quality enough to allow for visual inspection. The visual assets obtained indicate that both can be usable, presenting satisfactory general results.

There is sufficient evidence to emphasize the various advantages of using this vehicle as an efficient and flexible tool for inspection in the construction industry. Ultimately, these advantages allow a service to be performed with greater security, greater speed, and at lower cost, requiring fewer resources compared to the traditional method of industrial alpinism. The increasing development of this technology, combined with other types of cameras and sensors, will allow access to places previously inaccessible to humans and other technologies and make it feasible not only for visual inspection of facades, but also for other areas of construction.

## 7. ACKNOWLEDGEMENTS

This study was carried out with the support of the Coordination for the Improvement of Higher Education Personnel - Brazil - (CAPES) - Financing Code 001.

## 8. REFERENCES

- Agostinho, S. L. (2012), “*Inspeção e Monitorização de Estruturas em Engenharia Civil – Utilização de UAV na Inspeção e Monitorização*”, Master’s Thesis, Universidade da Madeira, p. 105.
- Álvares, J., Costa, D. B., Melo, R. R. S., Bello, A. (2016). “*Estudo exploratório de mapeamento 3D de canteiros de obras utilizando veículos aéreos não tripulados*” in: VI ENTAC, São Paulo: São Paulo (Brasil).

- Ballesteros, R. (2020), “*Inspeção de manifestações patológicas de fachadas utilizando Veículo Aéreo Não Tripulado (VANT): estudo exploratório*”, Master’s Thesis, Escola Politécnica de Pernambuco, Universidade de Pernambuco, p. 220.
- Brasil. Agência Nacional de Aviação Civil. Requisitos gerais para aeronaves não tripuladas de uso civil - RBAC-E nº 94. Resolução n. 419, 2 de maio de 2017. Brasília, 2017.
- De Melo, R., Costa, D., Álvares, J., Irizarry, J. (2017), *Applicability of unmanned aerial system (UAS) for safety inspection on construction sites*. Safety Science. 98:174-185. <https://doi.org/10.1016/j.ssci.2017.06.008>
- DJI (2017). Phantom 4 Pro Homepage. Recuperado em 26 de setembro de 2020 de [https://dl.djicdn.com/downloads/phantom\\_4\\_pro/20170719/Phantom\\_4\\_Pro\\_Pro\\_Plus\\_User\\_Manual\\_EN.pdf](https://dl.djicdn.com/downloads/phantom_4_pro/20170719/Phantom_4_Pro_Pro_Plus_User_Manual_EN.pdf)
- Emelianov, S., Bulgakow, A., Sayfeddine, D. (2014). “Aerial laser inspection of buildings facades using quadrotor” in: Creative Construction Conference, Prague (Czech Republic).
- EXAME. Revista Online Grupo Abril. (2016). Recuperado em 26 de setembro de 2020 de <https://www.exame.abril.com.br>
- Falorca, J. F., Lanzinha, J. C. G. (2020). *Facade inspections with drones—theoretical analysis and exploratory tests*. International Journal of Building Pathology and Adaptation, ahead-of-print. <https://doi.org/10.1108/IJBPA-07-2019-0063>
- Flores-Colen, I., De Brito, J., De Freitas, V. (2018). *Stains in facades’ rendering – Diagnosis and maintenance techniques’ classification*. Construction and Building Materials. 22(3):211-221. <https://doi.org/10.1016/j.conbuildmat.2006.08.023>
- Groetelaars, N. J. (2015), “*Criação de modelos BIM a partir de nuvens de pontos: estudo de métodos e técnicas para documentação arquitetônica*”, Doctoral Dissertation, Universidade Federal da Bahia, Faculdade de Arquitetura, Brasil.
- Grosso, R., Mecca, U., Moglia, G., Prizzon, F., Rebaudengo, M. (2020). *Collecting Built Environment Information Using UAVs: Time and Applicability in Building Inspection Activities*. Sustainability. 12:4731. <https://doi.org/10.3390/su12114731>
- Hung, M. N. W. B., Sampaio, T. V. M., Schultz, G. B., Siefert, C. A. C., Lange, D. R., Marangon, F. H. S., Santos, I. (2018). *Levantamento com veículo aéreo não tripulado para geração de modelo digital do terreno em bacia experimental com vegetação florestal esparsa*. Revista Ra'e Ga Espaço Geográfico em Análise. 43:215-231. <http://dx.doi.org/10.5380/raega.v43i0.56621>
- ICAO - International Civil Aviation Organization. (2017). Remotely Piloted Aircraft System (RPAS) concept of operations for international IFR operations. ICAO (USA), p. 30.
- Irizarry, J., Costa, D.B. (2016). *Exploratory Study of Potential Applications of Unmanned Aerial Systems for Construction Management Tasks*. Journal of Management in Engineering. 32(3):1-10. [https://doi.org/10.1061/\(ASCE\)ME.1943-5479.0000422](https://doi.org/10.1061/(ASCE)ME.1943-5479.0000422)
- Kim, S., Irizarry, J., Costa, D. B., Mendes, A. T. C. (2016). “*Lessons learned from unmanned aerial system-based 3D mapping experiments*” in: 52nd ASC Anual International Conference, Provo: Utah (USA).
- Liberati, A., Altman, D. G., Tetzlaff, J., Mulrow, C., Gotzsche, P. C., Ioannidis, J. P. A., Clarke, M., Devereaux, P., Kleijnen, J., Moher, D. (2009). *The PRISMA statement for reporting systematic reviews and meta-analyses of studies that evaluate healthcare interventions: explanation and elaboration*. BMJ, 339:b2700–b2700. <https://doi.org/10.1136/bmj.b2700>
- Mader, D., Blaskow, R., Westfeld, P., Weller, C. (2016). *Potential of UAV-Based laser scanner and multispectral camera data in building inspection*. International Archives of the Photogrammetry, Remote Sensing and Spatial Information Sciences. XLI-B1:1135-1142. <https://doi.org/10.5194/isprs-archives-XLI-B1-1135-2016>

- Máthé, K., Buşoniu, L. (2015). *Vision and Control for UAVs: A Survey of General Methods and of Inexpensive Platforms for Infrastructure Inspection*. *Sensors*. 15(7):14887-14916. <https://doi.org/10.3390/s150714887>
- Melo Jr., C. M. (2016), “*Methodology for generating façade damage maps from unmanned aerial vehicle photographs and digital image processing*”, Doctoral Dissertation, Universidad de Brasília, Brasil.
- Melo, R. R. S., Costa, D. B. (2015). “Uso de veículo aéreo não tripulado (VANT) para inspeção de logística em canteiros de obra” in: SIBRAGEC-ELAGEC, São Carlos: São Paulo (Brasil).
- Morgenthal, G., Hallermann, N. (2014). *Quality Assessment of Unmanned Aerial Vehicle (UAV) Based Visual Inspection of Structures*. *Advances in Structural Engineering*. 17(3):289-302. <https://doi.org/10.1260/1369-4332.17.3.289>
- Nascimento, M. L. M. (2017), “*Utilização de drone e termografia na detecção de manifestações patológicas em edificações*”, Monograph, Universidade Católica de Brasília, p. 21.
- Nikolic, J., Burri, M., Rehder, J., Leutenegger, S., Huerzeler, C., Siegwart, R. (2013). “*A UAV system for inspection of industrial facilities*” in: 2013 IEEE Aerospace Conference, Big Sky: Montana (USA). <https://doi.org/10.1109/AERO.2013.6496959>
- Pacheco, C., Vieira, G. (2017). “*Metodologias para Inspeções de Fachadas de Edifícios*” in: IV CIRMARE - Congresso Internacional na Recuperação, Manutenção e Restauração de Edifícios, São Paulo: São Paulo (Brasil).
- Pierrot-Deseilligny, M., De Luca, L., Remondino, F. (2011). *Automated image-based procedures for accurate artifacts 3D modeling and orthoimage generation*. *Geoinformatics CTU FCE*. 6:291-299. <https://doi.org/10.14311/gi.6.36>
- Piórkowski, D. T. (2008). “*Rectification and Intermediate View synthesis*”, Monograph, Universitat Politècnica de Catalunya, p. 47.
- Pires, R., De Brito, J., Amaro, B. (2015). *Inspection, Diagnosis, and Rehabilitation System of Painted Rendered Façades*. *Journal of Performance of Constructed Facilities*. 29(2):1-9. [https://doi.org/10.1061/\(ASCE\)CF.1943-5509.0000534](https://doi.org/10.1061/(ASCE)CF.1943-5509.0000534)
- Rakha, T., Gorodetsky, A. (2018). *Review of Unmanned Aerial System (UAS) applications in the built environment: Towards automated building inspection procedures using drones*. *Automation in Construction*. 93:252–264. <https://doi.org/10.1016/j.autcon.2018.05.002>
- Reagan, D., Sabato, A., Niezrecki, C. (2018). Feasibility of using digital image correlation for unmanned aerial vehicle structural health monitoring of bridges. *Structural Health Monitoring*. 17(5):1056-1072. <https://doi.org/10.1177/1475921717735326>
- Roca, R., Lagüela, S., Díaz-Vilariño, L., Armesto, J., Arias, P. (2013). *Low-cost aerial unit for outdoor inspection of building façades*. *Automation in Construction*. 36:128-135. <https://doi.org/10.1016/j.autcon.2013.08.020>
- Rodriguez-Gonzalvez, P., Gonzalez-Aguilera, D., Lopez-Jimenez, G., Picon-Cabrera, I. (2014). *Image-based modeling of built environment from an unmanned aerial system*. *Automation in Construction*. 48:44-52. <https://doi.org/10.1016/j.autcon.2014.08.010>
- Ruiz, R. D. B., Lordsleem Júnior, A. C., Fernandes, B. J. T., Oliveira, S. C. (2021). Unmanned Aerial Vehicles and Digital Image Processing with Deep Learning for the Detection of Pathological Manifestations on Facades. In: Toledo Santos E., Scheer S. (eds) *Proceedings of the 18th International Conference on Computing in Civil and Building Engineering. ICCCBE 2020. Lecture Notes in Civil Engineering*, vol 98. Springer, Cham. [https://doi.org/10.1007/978-3-030-51295-8\\_76](https://doi.org/10.1007/978-3-030-51295-8_76)
- Shariq, M. H., Hughes, B. R. (2020). *Revolutionising building inspection techniques to meet large-scale energy demands: A review of the state-of-the-art*. *Renewable and Sustainable Energy Reviews*. 130:109979. <https://doi.org/10.1016/j.rser.2020.109979>

- Tondelo, P. G., Barth, F. (2019). *Análise das manifestações patológicas em fachadas por meio de inspeção com VANT*. PARC Pesquisa Em Arquitetura E Construção, 10, e019009. <https://doi.org/10.20396/parc.v10i0.8652817>
- Vera-Rozo, E. (2016). *Medición de contaminación mediante UAV (Vehículo Aéreo no Tripulado)*. Mundo FESC. 6(11): 16-26.
- Yang, X., Qin, X., Wang, J., Wang, J., Ye, X., Qin, Q. (2015). *Building Façade Recognition Using Oblique Aerial Images*. Remote Sensing. 8(7): 10562-10588. <https://doi.org/10.3390/rs70810562>

## Advances in the implementation of optical fiber on structures. The present of an implementation with a future

V. Alegre<sup>1\*</sup>, S. Villalba<sup>2</sup> 

\*Contact author: [info@cotca.com](mailto:info@cotca.com)

DOI: <https://doi.org/10.21041/ra.v11i1.485>

Reception: 14/11/2019 | Acceptance: 30/10/2020 | Publication: 01/01/2021

### ABSTRACT

An example of a real case is discussed in which, on an existing tunnel, which is instrumented with optical fiber, a building is built. This makes possible to track the load history of a structure since the fiber is placed. To verify that the tunnel is not structurally affected during the construction period, sections of it are instrumented and the micro deformations that occur are measured, which are compared with those of the model. It has been possible to appreciate the ovalizations and tensions in the vault during the different phases of the construction process, all of them being below the limit values established in the contingency plan. This technique has made possible to validate the works carried out throughout the process.

**Keywords:** optical fiber, instrumentation, tunnels, microdeformations

**Cite as:** Alegre, V., Villalba, S. (2021), "*Advances in the implementation of optical fiber on structures. The present of an implementation with a future*", Revista ALCONPAT, 11 (1), pp. 105 – 122, DOI: <https://doi.org/10.21041/ra.v11i1.447>

<sup>1</sup> COTCA, S.A., Profesor Asociado Departamento de Ingeniería Civil y Ambiental, UPC, Barcelona, España.

<sup>2</sup> COTCA, S.A., Profesor Asociado Departamento de Ingeniería de Proyectos y de la Construcción, UPC, Barcelona, España.

#### Contribution of each author

In this work, the author V. Alegre, contributed to the management of convincing the administration of the advantages of this type of applications, and in the process of on-site implementation of fiber optics, definition of the ideal area according to the positions of the building and the tunnel, and commissioning.

The author S. Villalba developed the model used for the interpretation of results, carried out the planned reading plan according to the construction phases and analyzed and interpreted the results obtained and their conclusions throughout the construction process.

#### Creative Commons License

Copyright 2021 by the authors. This work is an Open-Access article published under the terms and conditions of an International Creative Commons Attribution 4.0 International License ([CC BY 4.0](https://creativecommons.org/licenses/by/4.0/)).

#### Discussions and subsequent corrections to the publication

Any dispute, including the replies of the authors, will be published in the third issue of 2021 provided that the information is received before the closing of the second issue of 2021.

## **Avances en la instrumentación de estructuras con fibra óptica. El presente de una instrumentación con futuro**

### **RESUMEN**

Se discute el ejemplo de un caso real en el que, sobre un túnel existente que se instrumenta con fibra óptica, se construye un edificio. Ello permite hacer el seguimiento de la historia de cargas de una estructura desde que se coloca la fibra óptica. Para constatar que no se ve afectado estructuralmente el túnel durante el período de construcción, se instrumentan secciones del mismo y se miden las microdeformaciones que se producen, que se comparan con las del modelo. Se han podido apreciar las ovalizaciones y tensiones en la bóveda durante las distintas fases del proceso constructivo, estando todas ellas por debajo de los valores límites establecidos en el plan de contingencias. Esta técnica ha permitido validar durante todo el proceso las obras realizadas.

**Palabras clave:** fibra óptica; instrumentación; túneles; microdeformaciones.

## **Avanços na instrumentação de estruturas com fibra ótica. O presente de uma instrumentação com futuro**

### **RESUMO**

É discutido o exemplo de um caso real em que, em um túnel existente, um edifício é construído com instrumentação de fibra ótica que permite monitorar o histórico de carregamento de uma estrutura desde sua instalação. Para verificar se o túnel não é estruturalmente afetado durante o período de construção, trechos do túnel são instrumentados e as microdeformações ocorridas são medidas, as quais são comparadas com as do modelo. Foi possível apreciar as ovalizações e tensões na abóbada durante as diferentes fases do processo de construção, estando todas abaixo dos valores limites estabelecidos no plano de contingência. Esta técnica permitiu validar os trabalhos realizados ao longo do processo.

**Palabras clave:** fibra ótica; instrumentação; túneis; microdeformações.

### **Legal Information**

Revista ALCONPAT is a quarterly publication by the Asociación Latinoamericana de Control de Calidad, Patología y Recuperación de la Construcción, Internacional, A.C., Km. 6 antigua carretera a Progreso, Mérida, Yucatán, 97310, Tel.5219997385893, [alconpat.int@gmail.com](mailto:alconpat.int@gmail.com), Website: [www.alconpat.org](http://www.alconpat.org)

Reservation of journal title rights to exclusive use No.04-2013-011717330300-203, and ISSN 2007-6835, both granted by the Instituto Nacional de Derecho de Autor. Responsible editor: Pedro Castro Borges, Ph.D. Responsible for the last update of this issue, Informatics Unit ALCONPAT, Elizabeth Sabido Maldonado.

The views of the authors do not necessarily reflect the position of the editor.

The total or partial reproduction of the contents and images of the publication is carried out in accordance with the COPE code and the CC BY 4.0 license of the Revista ALCONPAT.

## 1. INTRODUCTION

A common technical problem is the interaction between newly built works and existing infrastructures. The different parts of an infrastructure are managed for a lifespan, as is the case of the Barcelona Metro Network, whose current state was defined in an orderly manner between 2000 and 2003 leaving, among other documents, a 92 km - virtual tunnel, then with the geometry of the cross section and the catalogue of damage and dysfunctions for its management. The first kilometers of tunnel are from 1924 and, logically, the responsible administration (Generalitat de Catalunya) and the body that manages it (Transports de Barcelona, S.A.) require that in the new built buildings, within the area of influence of its infrastructure, it is verified that they do not affect the use and service of the network nor its structure. To this end, inter alia, it requires that the affected area be structurally assessed by providing the structural information available to it, and that the movements that occur in the infrastructure during the construction of the new work be recorded, acting accordingly.

To track this, measurements are sometimes made with monitored theodolites from various points in the cross section. If more precision is desired to assess risks, a very valid tool is optical fiber technology that, attached to the surface, allows to measure microdeformations in, for example, the cross sections centimeter by centimeter.

This technology consists of the use of an optical backscatter reflectometer called the OBR (Optical Backscatter Reflectometer) system as a monitoring tool, in this case, of a reinforced concrete structure of a tunnel with dovelas of Line 9 in Barcelona, which could present cracks or dysfunctions in service, as a result of the construction of a building that is partially carried out on that section of tunnel.

The main feature of the OBR system is its high sensitivity and high spatial resolution using optical fiber as a sensor. This produces deformation records in which the presence of cracks can be identified and located.

On this tunnel a building will be made, having modeled the whole process: emptying, foundation slab, execution of the structure and loading of all the subsystems that are part of the building (facades, pavements, partition, installations, ...).

For these loading stages, the expected values are set, and a contingency plan is created with warnings, alerts, and alarms in case they are exceeded. As the work progresses, the instrumentation carried out in the tunnel with the optical fiber registers the values obtained continuously or semi-continuously, which allows to know at all times the possible dysfunctions that occur in the section (ovalizations, microdeformations, new fissures, etc.) and act accordingly. The period provided for the execution of the work is 18 months, once the work is finished, the implementation could be maintained and readings could be made when, for example, incidents occurred and its impact on the structure of the tunnel from which its "history of loads" is obtained.

Optical fiber, which as a continuous monitoring system is resistant to water and corrosion, avoids problems of electromagnetic interference and currents that occur in other techniques, and allows simultaneous readings of up to 5000 points of the structure under study.

The objective of this work is to find that the tunnel is not structurally affected during the construction period of the building, through the implementation of sections of the former in which the microdeformations that occur are measured, and which are compared to those of the model. In this way, ovalizations and tensions can be observed in the vault during the different phases of the construction process.

## 2. MODELLING AND INSTRUMENTATION OF THE TUNNEL

The modelling of the different stages was carried out with the SAP2000 program and the two-dimensional PLAXIS, and gave, from the geometry defined in Figure, the following results indicated in Figure 1, Table 1 and Figure 2:

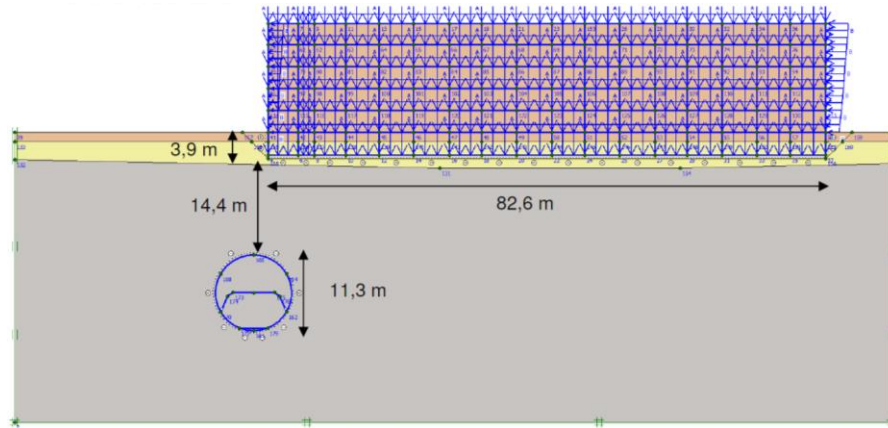


Figure 1. Geometry of the calculation section.

Table 1. Results obtained in the model

	In the current situation	Parking excavation phase	Building operation phase
<b>Tunnel cladding efforts</b>			
Nk (kN/m)	1.430	1.410	1.700
Vk (kN/m)	39,63	38,44	45,04
Mk (kN-m/m)	33,45	34,10	61,66
<b>Maximum displacements in the tunnel</b>			
Horizontal (mm)	0 (*)	1,49	-2,98
Vertical (mm)	0 (*)	1,63	-7,18

(\*) The current situation is adopted as a reference situation, that is, deformation state 0.

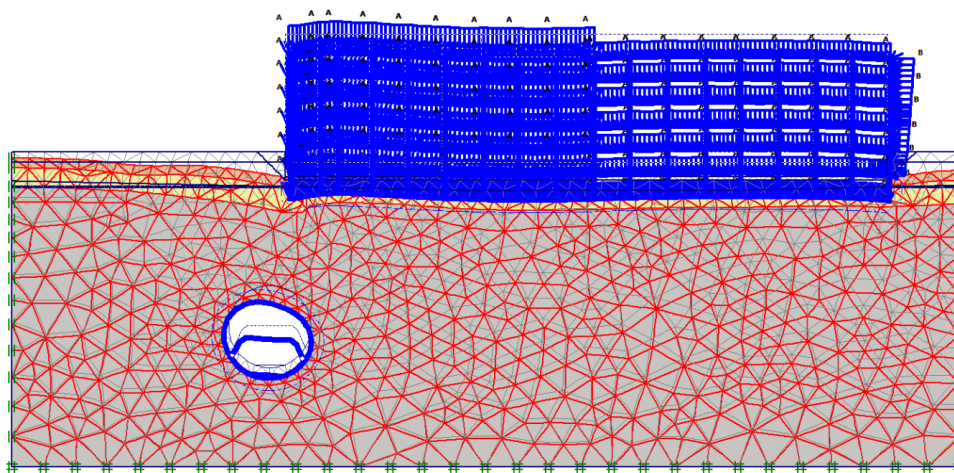


Figure 2. First breakage mechanism found, for a safety factor of 2.29.

As a result of the above, a contingency plan was established which is summarized in Table 2.

Table 2. Maximum tensions and deformations in voussoirs. Contingency plan.

	Compression zone values		Traction zone values
	Voussoirs		Voussoirs
	(MPa)	$\Delta\mu\epsilon$	Crack width (mm)
Notice	18.40	755	0.50
Alert	28.40	955	1.80
Alarm	33.40	1595	3.50

The L9 instrumented tunnel is a typical section with overlapping tracks and intermediate steel. The optical fiber has been placed on the perimeter of the cross section, always according to the Property.

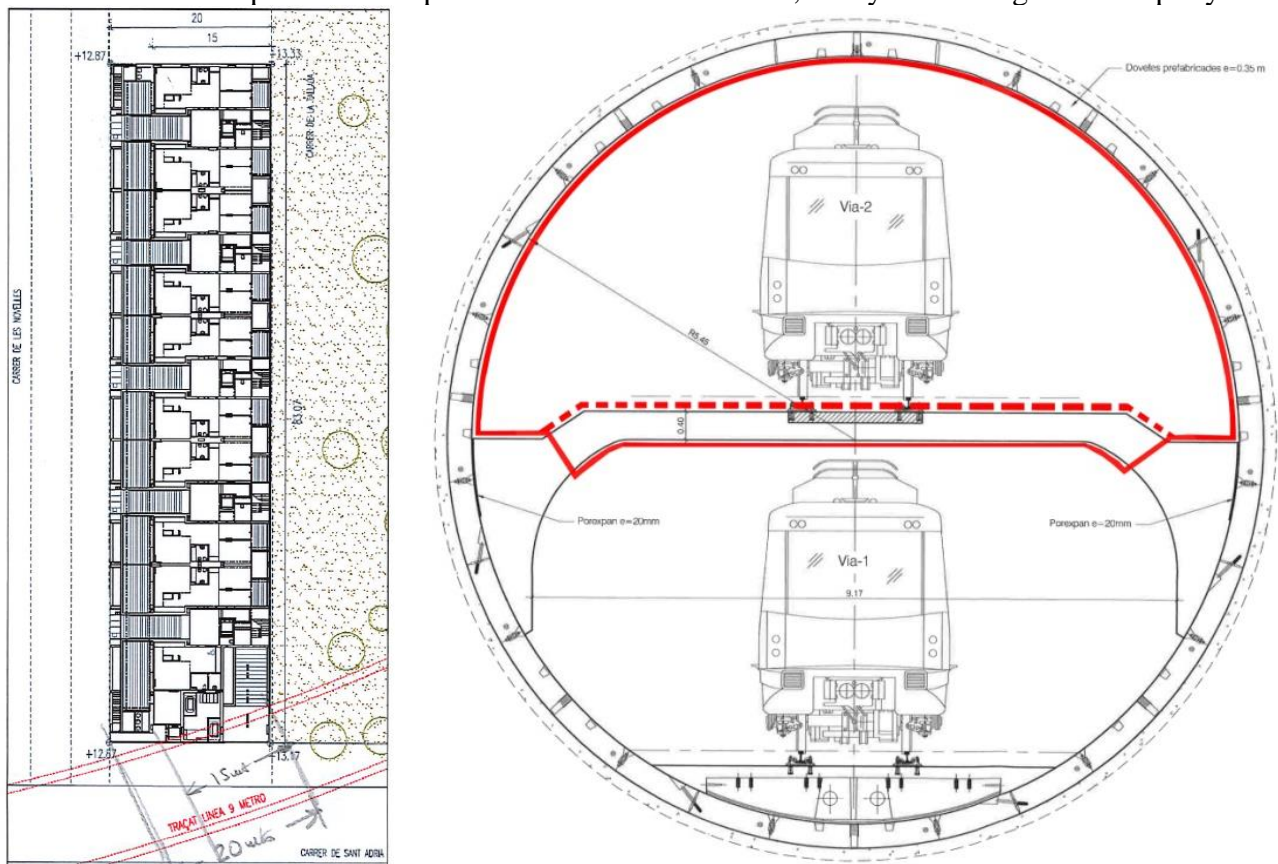


Figure 3 shows its placement. Fiber placement has been carried out following the perimeter of a cross section in the position indicated in the plant.

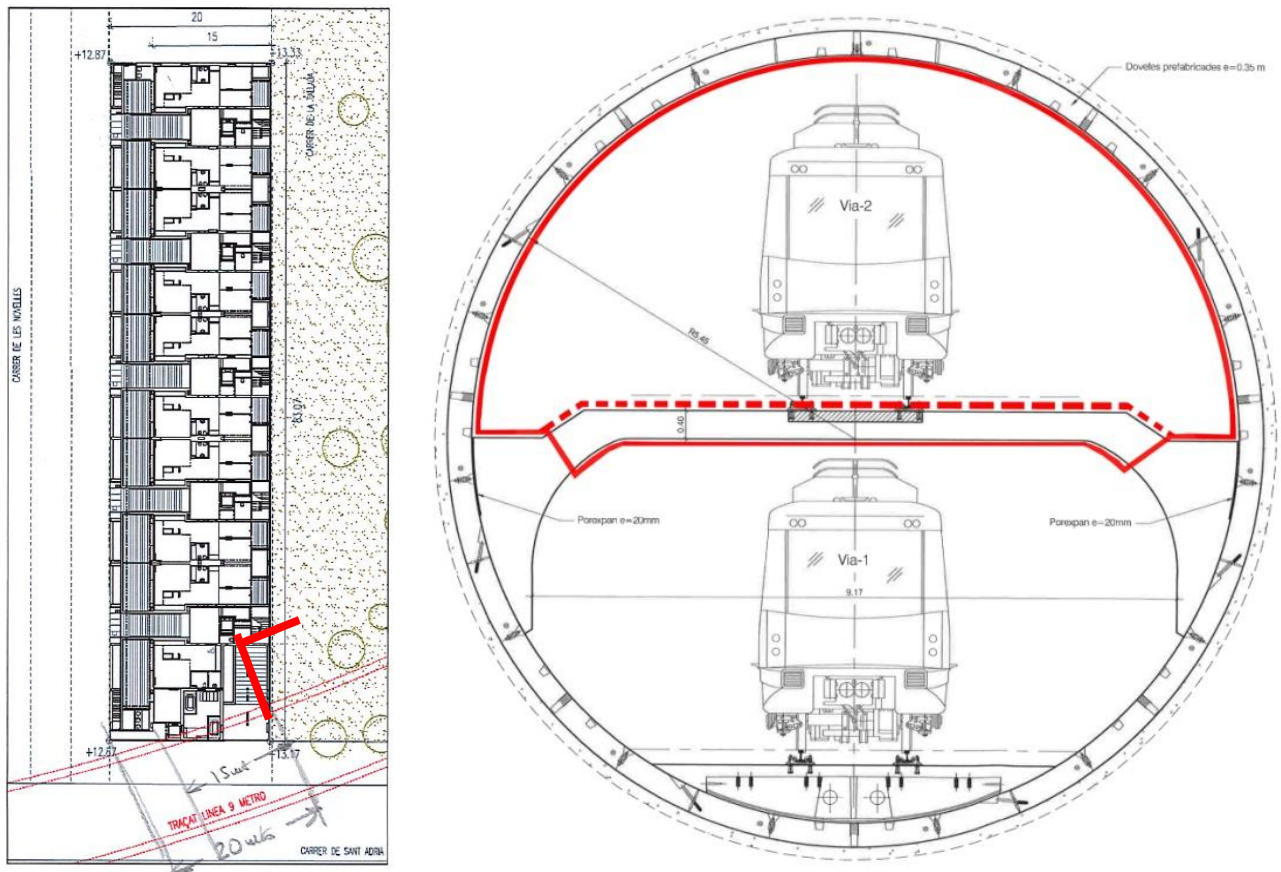


Figure 3. Detail floor of the building in relation to the subway tunnel and section of the optical fiber layout.

The proposed instrumentation measures microdeformations in the cross-section of the tunnel, i.e. possible movements, or dysfunctions of the cross section. In the initial reading of zeros with optical fiber a catalogue of current dysfunctions (cracks, humidity, coqueries, anomalous roughness, etc.) is made. Figure 4, Figure 5 and Figure 6 show some of the found dysfunctions in the initial inspection.

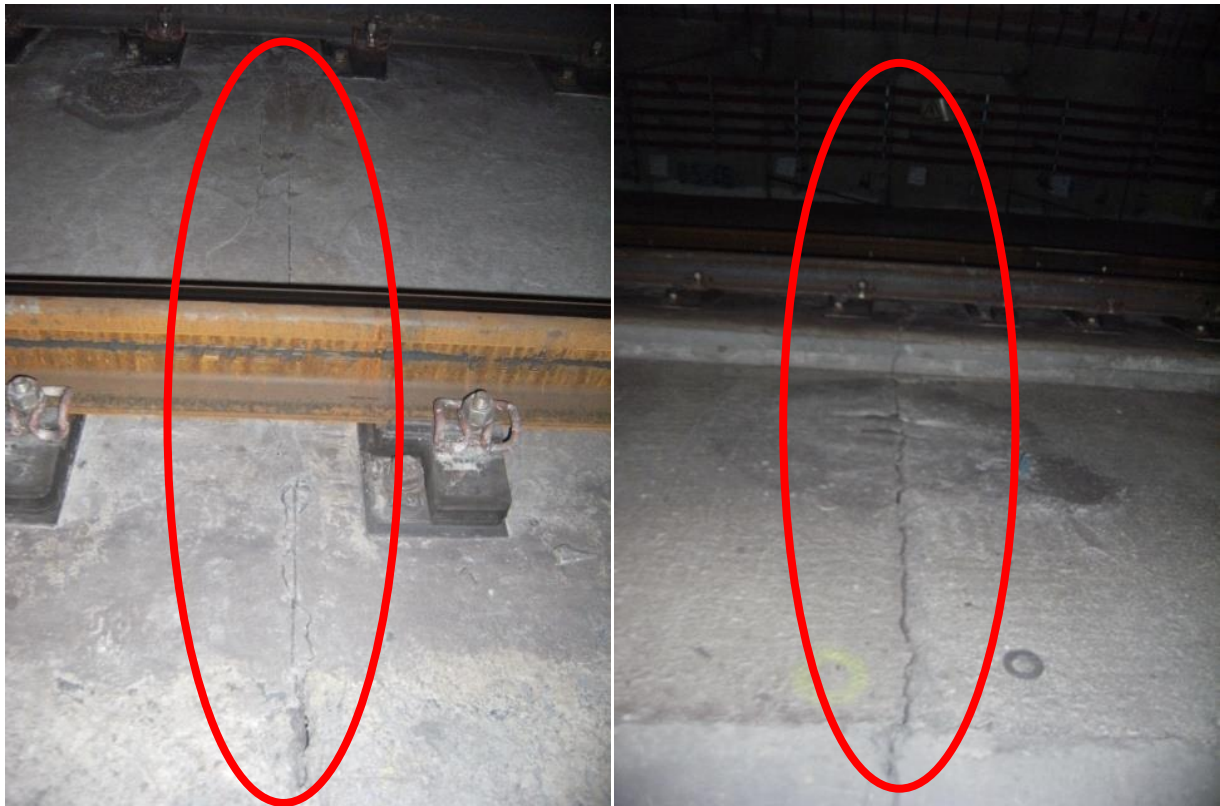


Figure 4. Joints on the track, which exist every 25m.



Figure 5. Filtrations (leachings of cement limes).



Figure 6 Roughness and clamping bolts that could affect the placement of the fiber.

At each subsequent reading raised in the different phases of the work (pre-start, emptying, completion of the foundation, structure and purpose of the work), microdeformations are measured in the perimeters of the cross sections, compared to the model made and reports are issued. Where the ovalization criteria prescribed in the regulations are exceeded or dysfunctions are detected, action shall be taken in accordance with the established contingency plan protocol. This allows to detect the main changes in the structural behavior of the tunnel and obtain information that will serve to evaluate its structural safety, during the construction of the building, at the end of the works and throughout its useful life.

## 2.1 Positioning schemes

The entire monitoring system has been located in the strategic area susceptible to the possible dynamics and evolution of the structural response (variations of microdeformations-stresses, movements, possible increments and / or development of cracking maps, etc.) of the tunnel throughout the construction work of the building. This instrumentation system has been selected considering the working conditions to which it will be subjected (thermal variation, conditions of use, etc.).

Below is the scope of monitoring used (see Figure 7).

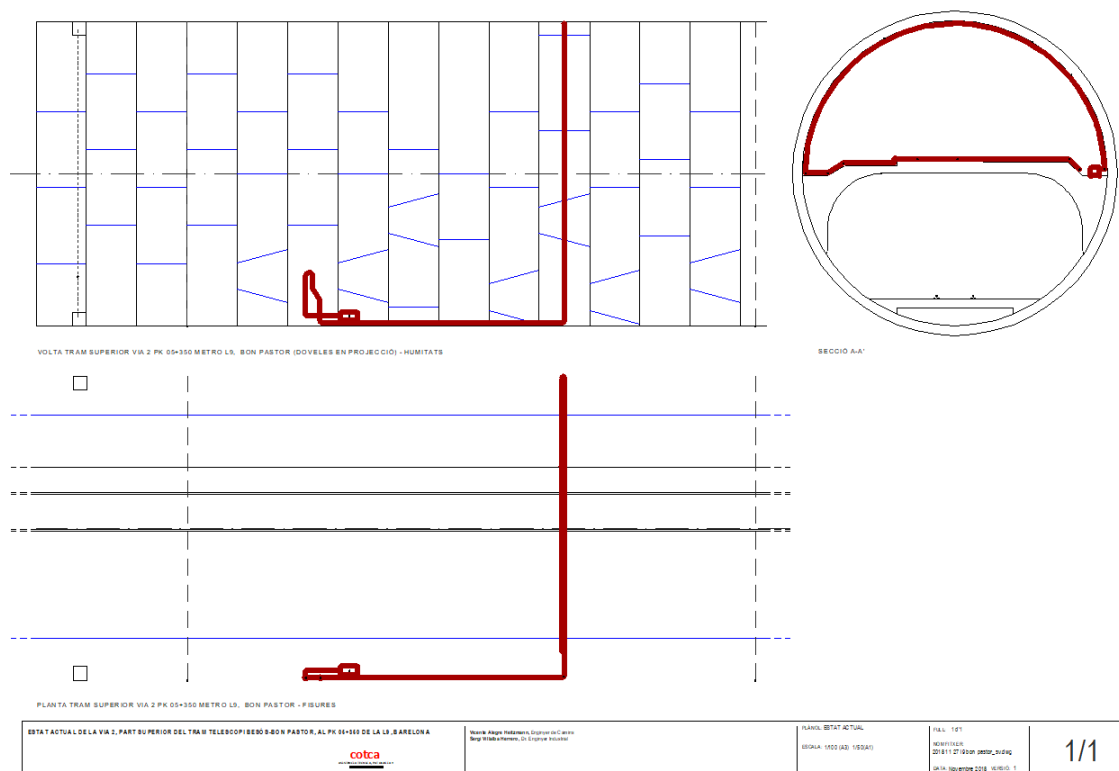


Figure 7 General tunnel scheme. Elevation and plant. The red line indicates the path of the optical fiber.

The actual tunnel monitoring length is adjusted to the actual length of a cross section and longitudinal section, this being 50.00m in length. That is, FOD1 optical fiber (Distributed Optical Fiber) is attached 40m and the last 10m were kept on the reel containing the optical fiber (without attaching), which was attached to the structure with American tape. This detail is shown in Figure 8, Figure 9 and Figure 10 along with the system installed within the tunnel cross section.



Figure 8. Remaining optical fiber reel subject to the structure and ODiSI (Optical Distributed Sensor Interrogator, by LUNA Technologies, Model A50) in operation.



Figure 9. Overview of the tunnel in the instrumented section.



Figure 10. Optical fiber protected under train tracks.

Figure 11 shows the adhesion procedure performed with the optical fiber on the traffic lane steed of track 2 and in the tunnel vault.



Figure 11. Optical fiber adhesion procedure on the steed of the track 2 circulation lane and in the tunnel vault.

### 3. RESULTS AND DISCUSSION.

#### 3.1 Model results

Tensions and displacements have been obtained in the tunnel before, during and after the construction of the building by means of a method of calculation by finite elements in scenarios of flat deformation. The software used is PLAXIS v8.

The following are the most significant results obtained from the monitoring raised, as seen in Figure 12 FOD processing.



**INITIAL STATE**

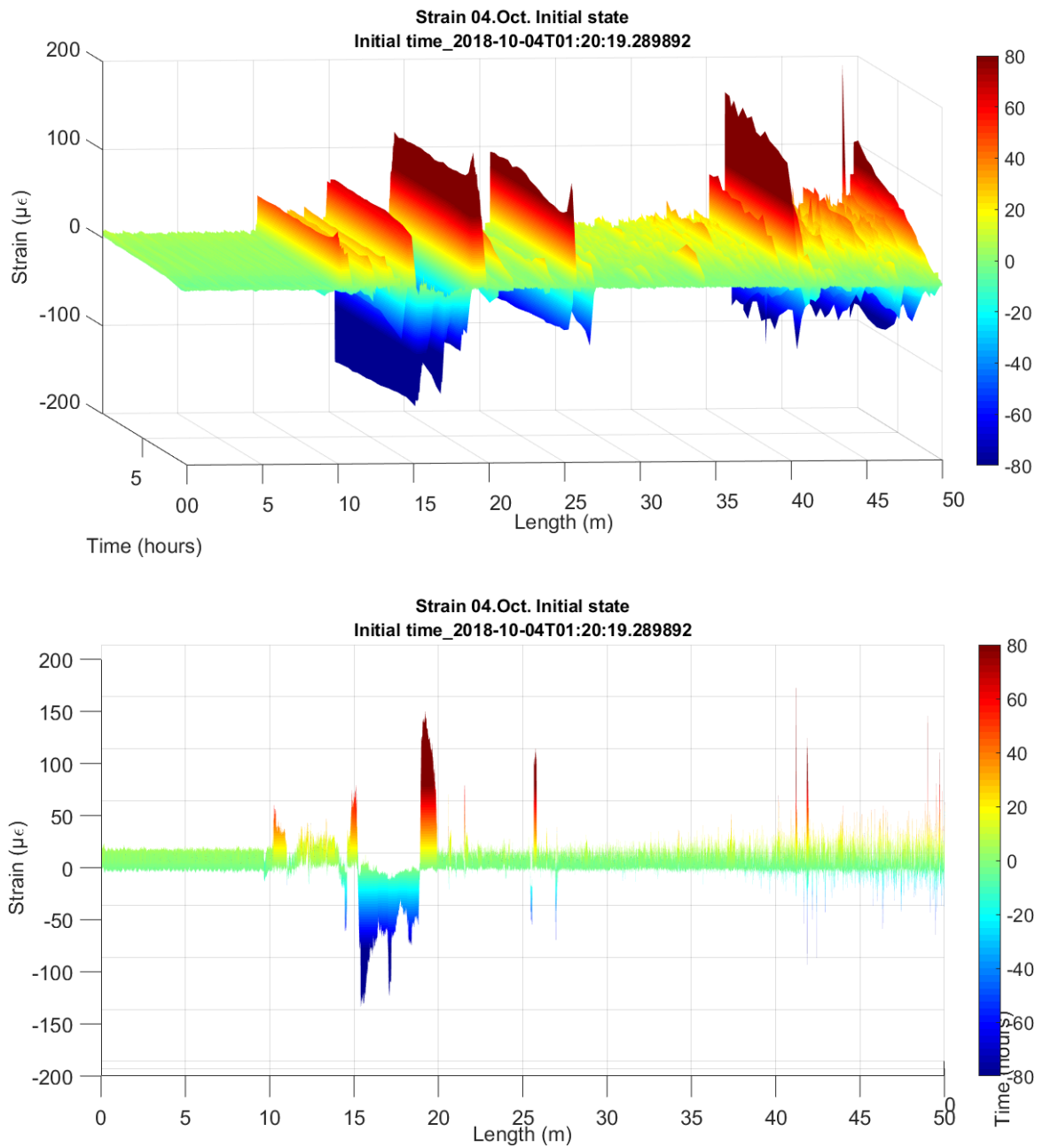


Figure 13. Initial and calibration status. Length 50m FOD. Axonometric and frontal view.

**PRE-EXCAVATION**

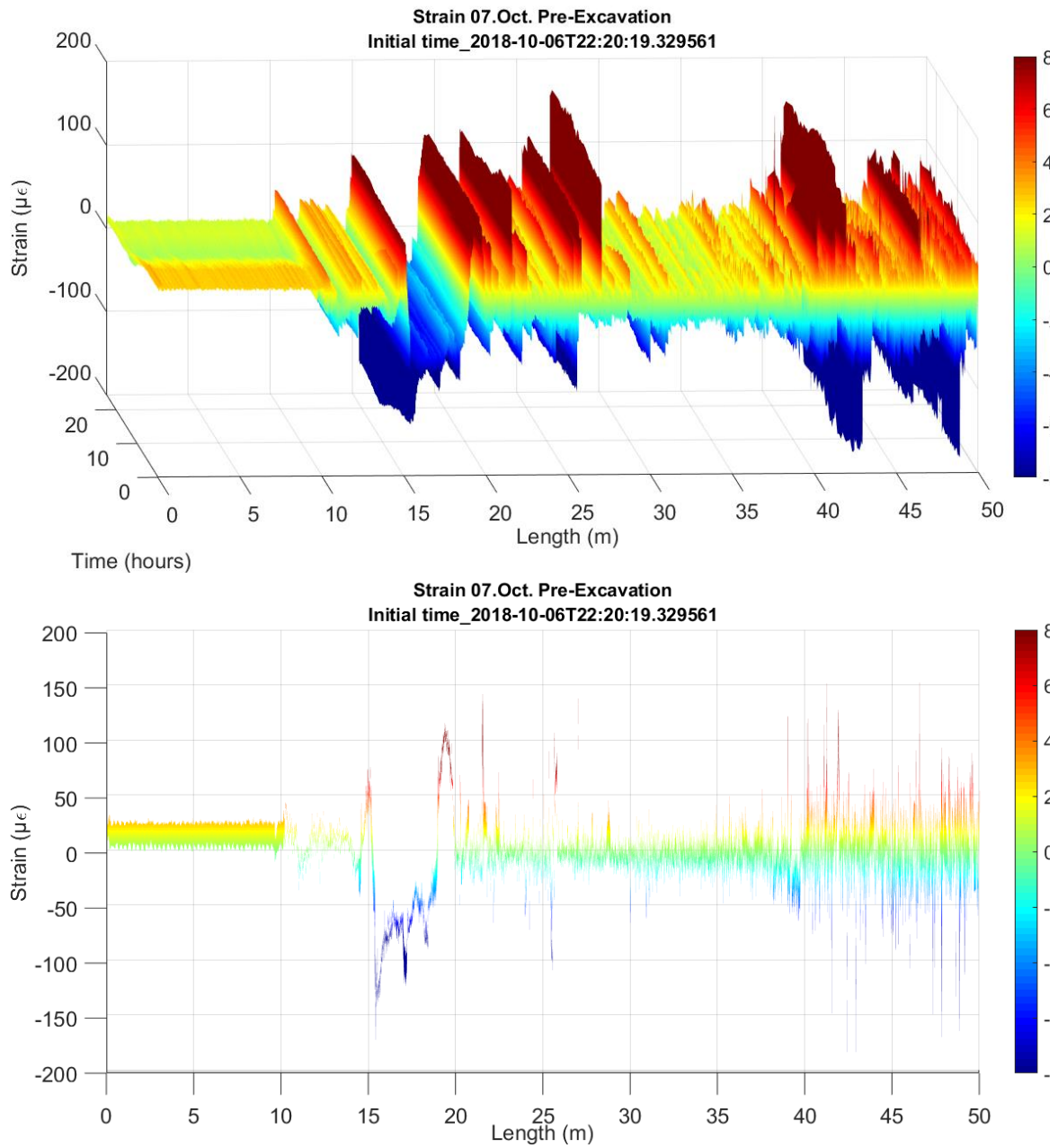


Figure 14. Pre-excitation. Length 50m FOD. Axonometric and frontal view.

**EXCAVATION**

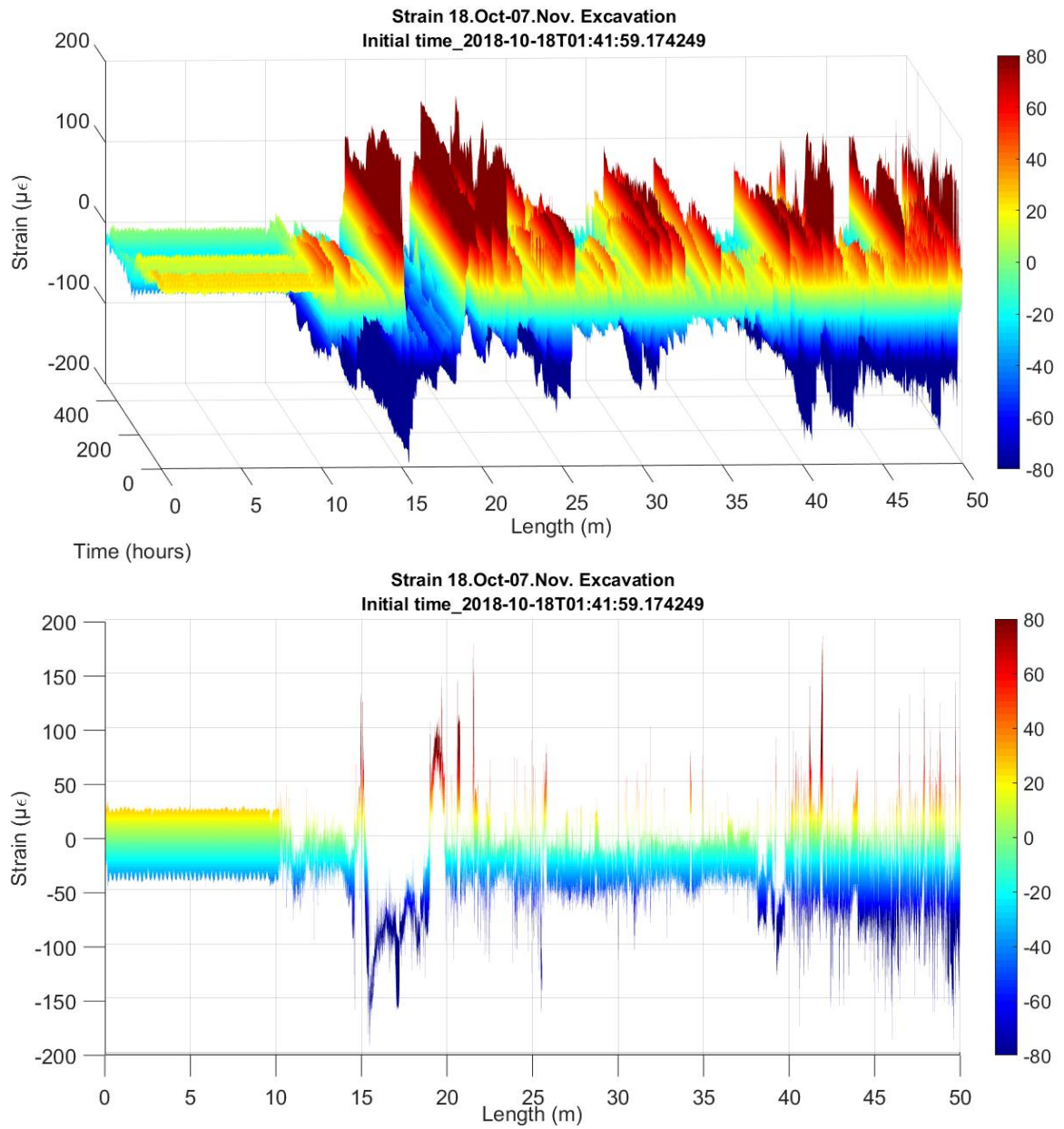


Figure 15. Complete excavation. Length 50m FOD. Axonometric and frontal view.

**EXECUTION 1ST FOUNDATION SECTION**

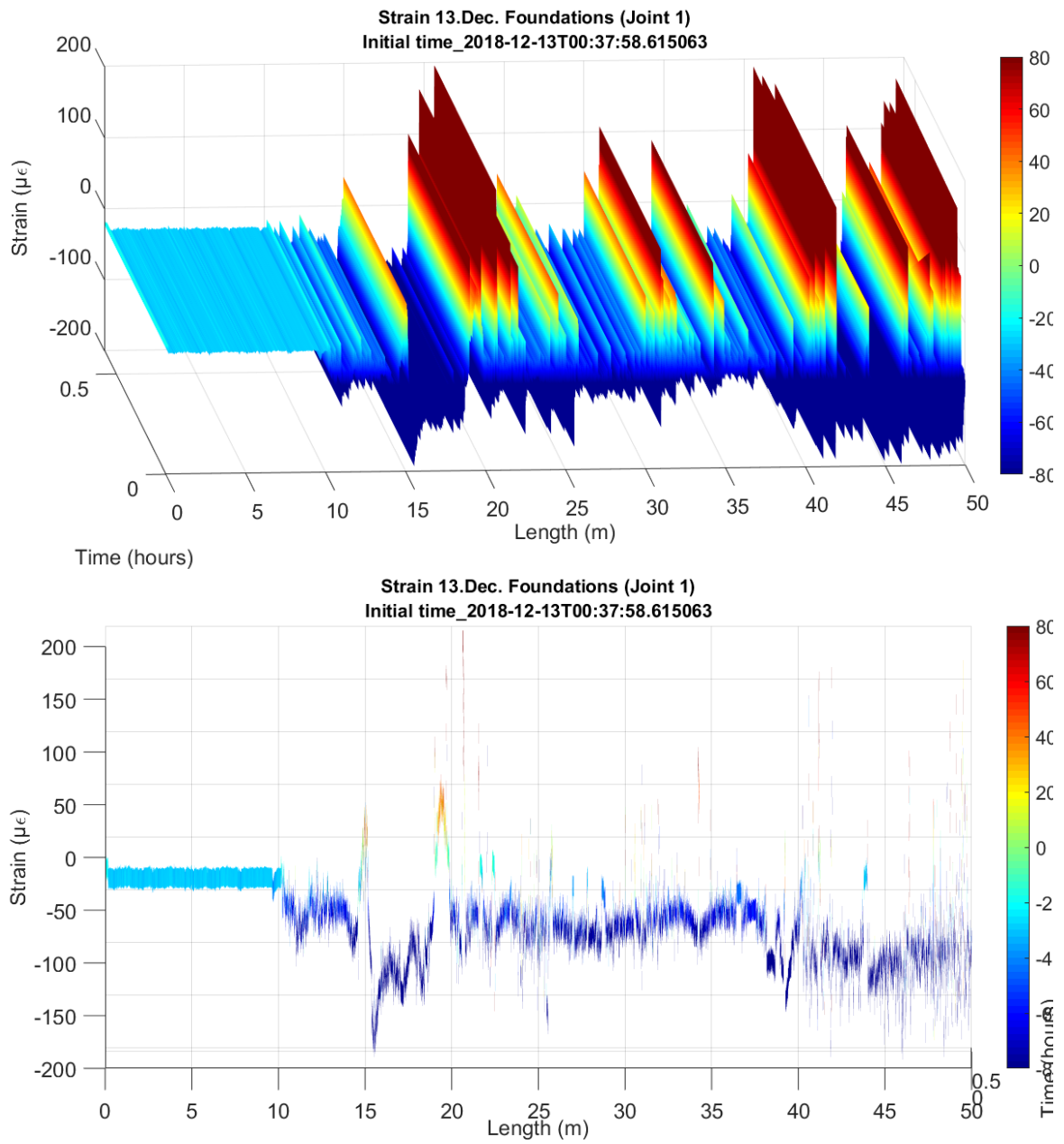


Figure 16. Execution of first section on foundation slab. Length 50m FOD. Axonometric and frontal view.

**TOTAL EVOLUTION**

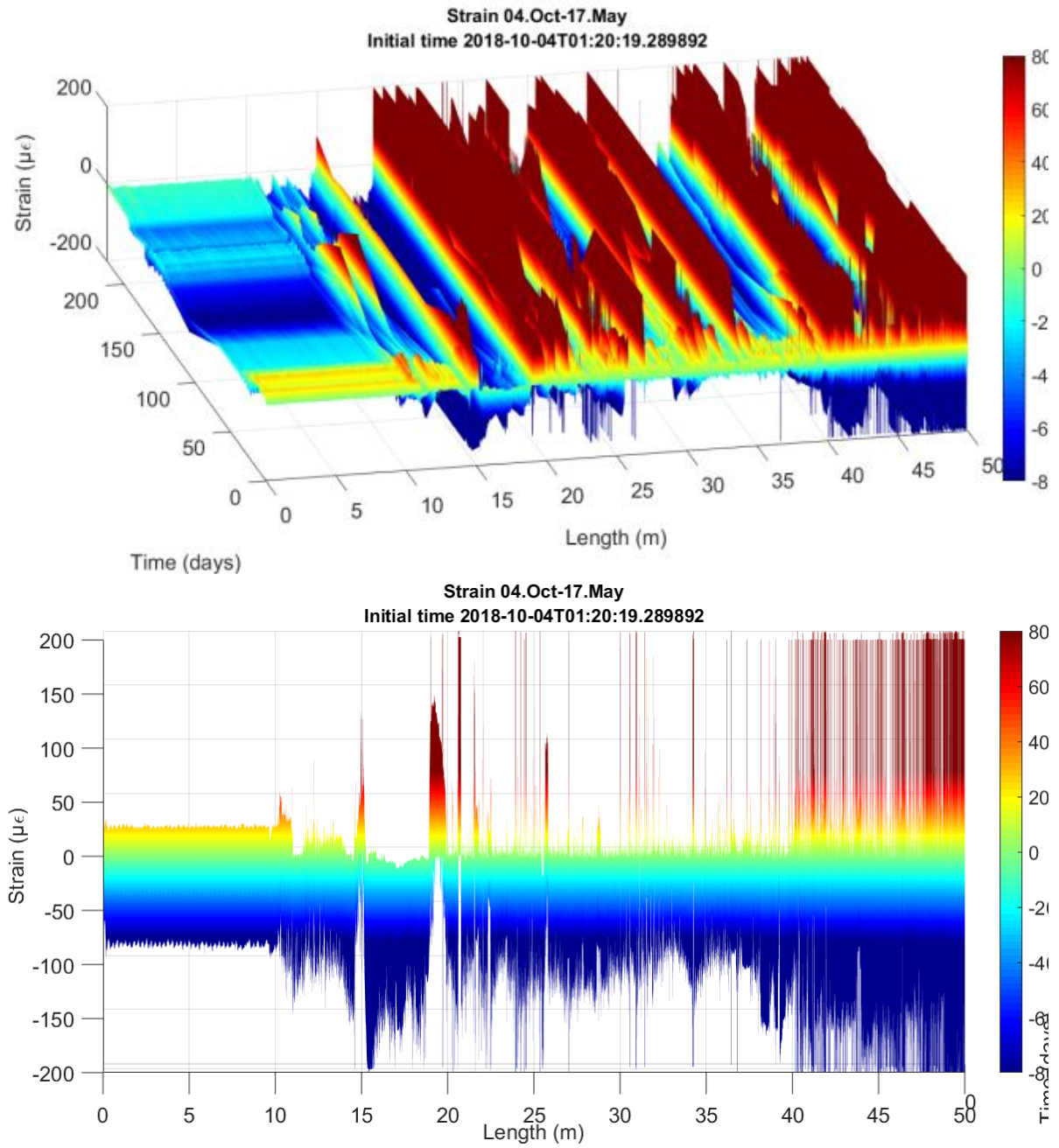


Figure 17 Temporary evolution of 4 October and 17 May. Length 50m FOD. Axonometric and frontal view.

Figure 18 and Figure 19 incorporate the reading log at 6 critical points along the tunnel vault section.

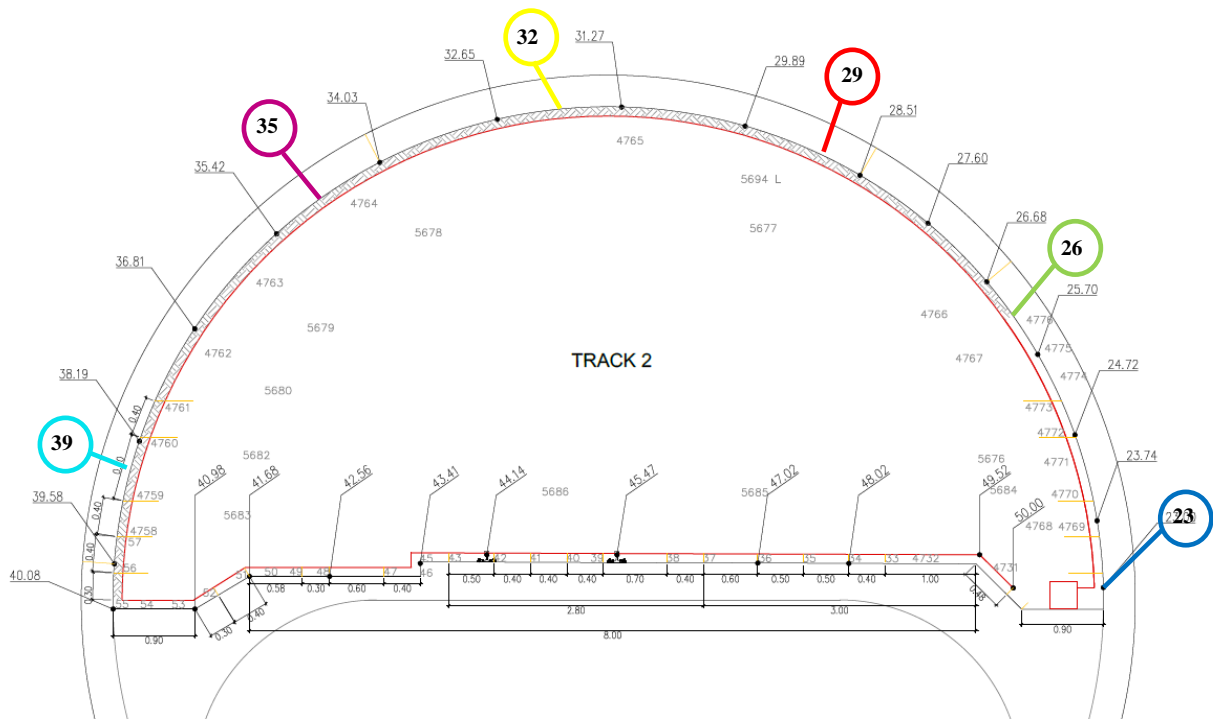


Figure 18. Identification of critical control points in the Tunnel vault.

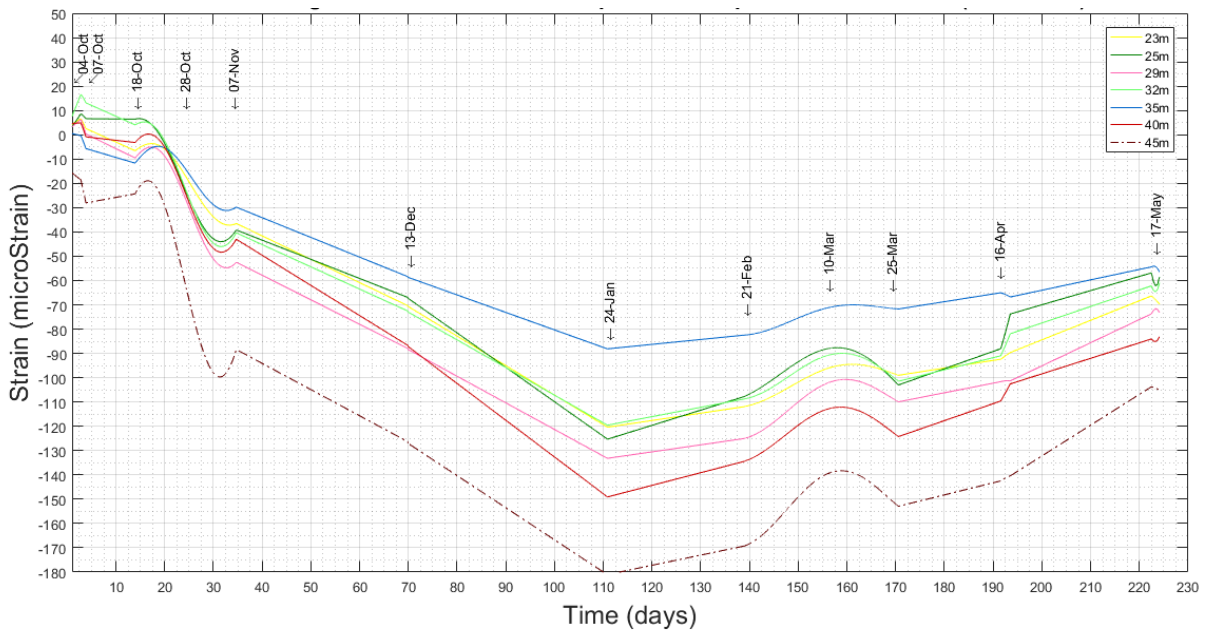


Figure 19. Temporary evolution from October 4, 2018 to May 17, 2019 at critical checkpoints.

It is generally noted that:

- 1) The fiber section between 40 and 50m→ corresponds to the track area. In this section is where there is more excitement of the fiber given the railway step. The vibration caused by the railway circulation results in more distortion of readings in this section. Even so, it is observed how these variations of recorded microdeformations have a tendency to increase to compression, which is consistent with the decompression and ovalization suffered by the curved section of the tunnel and which causes the slab to perform a strut function in response of this action. The ovalization of the tunnel is explained at the next point. Likewise, under no circumstances do the obtained values exceed the notice limit set out in the Auscultation and Contingency Plan.
- 2) The fiber section between 23 and 40m →corresponds to the area of the vault. This section shows how, in general, there has been an increase in compression microdeformations throughout the instrumentation. This is due to the decompression caused by the excavation and emptying of land from the work, so that this decompression produces a certain "ovalization" of the section, which results in an increase in compression in the inner fiber of the section (the inner fiber of the section is compressed and the outer fiber of the decompression section). It can be clearly seen as going from a green color (null and initial deformation) to a blue color indicating compression. Likewise, under no circumstances do the obtained values exceed the notice limit set out in the Auscultation and Contingency Plan.

With regard to stress analysis and from the definition of the concrete  $E_c$  drying longitudinal deformation module and for a state of stresses under service conditions, i.e. for an elastic state or stage where the stresses of the concrete fibers of the section are proportional to the deformations, it is apparent that, even if observing this increase of  $\mu\epsilon$ , they do not induce excessive stresses on it.

- 3) The fiber bouquet between 10 and 23m corresponds → to the longitudinal monitoring section. In this area we see values for compression and traction, but that throughout their evolution have been constant at all times, that is, without variation in the origin of the readings and calibration. This fact indicates that there have been no variations in this section in response to the structure, i.e. that the actions carried out have not led to appreciable changes in the structure.
- 4) The fiber section between 0 and 10m→ corresponds to the non-adhered fiber section. In this area there is a linear evolution without differential changes, where it is found that there are no substantial variations in temperature that induce significant tension variations, so that they do not influence the other zonas areas of FOD attached.

In addition, peaks and/or discontinuities obtained from monitoring can be seen, which correspond to the joint areas between sections of the dovelas where the optical fiber suffers a disadherence with the concrete, since its implementation at source. These peaks remain stable in terms of their location.

#### 4. CONCLUSIONS

The use of Optical Backscatter Reflectometer sensors is a promising technology for structural status monitoring, as it allows the possibility of continuous monitoring over time and voltage and temperature space along the fiber.

A tunnel section is being monitored, which has, to date, carried out a control of the structure in service during the eight months (October 2018 – May 2019) covering the construction of the structure of a building on the track, up to the 1st floor level, in the building area above the tunnel. Monitoring has been used to identify and technically characterize the increases in traction and compression stresses, as a result of the different phases of the work, from before we begin, with the previous calibration readings to the construction phase of the structure, in which we find ourselves. Monitoring will continue until the end of the work, scheduled for November 2020.

During this 8-month period, the microdeformation variations of FOD 1 fiber have been  $153\mu\epsilon$  which translated to stresses represent a maximum voltage variation of 5.75MPa.

These values are acceptable for such structures, as they are compression values in concrete. On the other hand, these values include thermal effects.

From the variations obtained in the monitoring of FOD 1 fiber throughout this medium thermal cycle, the impact of thermal action on the tunnel can be considered to have been negligible

Once it has been confirmed that the tunnel is in adequate safety conditions and once the work is finished, a permanent register will be available to access the section, and to be able to perform intermittent readings throughout its lifespan to know the deferred behavior. This has been raised within the mandatory tunnel maintenance plan.

## 5. ACKNOWLEDGEMENTS

The technicians of IMHAB (Institut Municipal del Habitatge i Rehabilitació de Barcelona) and TMB (Transports de Barcelona, S.A.) are thanked for the facilities given for the management of all operations.

## 6. REFERENCES

Li, H., Li, D., Song, G. (2004), “Recent applications of fiber optic sensors to health monitoring in civil engineering”. Engineering Structures, Volume 26, Issue 11, pp. 1647–1657.

<https://doi.org/10.1016/j.engstruct.2004.05.018>

Villalba, S., Casas, J. R. (2009), “Feasibility of Structural Health Monitoring of concrete structures by Optical Backscatter Reflectometer”. Proceedings of 7<sup>th</sup> International Workshop on Structural Health Monitoring. Stanford University (USA).

Alegre, V., Villalba, S. (2013), “Estructuras inteligentes. Instrumentación con fibra óptica”. XII Congreso Latinoamericano de Patología de la Construcción y XIV Congreso de Control de Calidad en la Construcción. CONPAT-2013. Colombia 2013. ISBN 978-958-58090-0-0.

Alegre, V., Villalba, S., Force, F., Ródenas, V. (2015), “Apeo y sustitución de un pilar de fábrica de ladrillo en un edificio modernista en uso”. XIII Congreso Latinoamericano de Patología de la Construcción y XV Congreso de Control de Calidad en la Construcción. CONPAT-2015. Lisboa 2015.

Alegre, V., Villalba, S. (2017), “Avances en la instrumentación con fibra óptica”. XIV Congreso Latinoamericano de Patología de la Construcción y XVI Congreso de Control de Calidad en la Construcción. CONPAT-2017. Vol. I. Control de Calidad. ISBN 978-99967-0-464-2.

## Inspection of pathological manifestations in buildings by using a thermal imaging camera integrated with an Unmanned Aerial Vehicle (UAV): a documental research

W. P. A. Silva<sup>1\*</sup> , A. C. Lordsleem Júnior<sup>1</sup> , R. D. B. Ruiz<sup>1</sup> , J. H. A. Rocha<sup>2</sup> 

\*Contact author: [wpas@poli.br](mailto:wpas@poli.br)

DOI: <https://doi.org/10.21041/ra.v11i1.447>

Reception: 14/11/2019 | Acceptance: 30/10/2020 | Publication: 01/01/2021

### ABSTRACT

This paper is intended to present the usage of an UAV integrated thermographic camera in building inspection processes. This study was based on a systematic review of related articles and technical documents, in order to investigate features and basic operations of thermographic cameras, UAVs usage and influencing factors on detection of pathological manifestations. The results enabled identification of advantages and limitations for camera and UAV integration, thus demonstrating their feasibility and effectiveness when employed together. As a contribution, this study developed a flight protocol including steps and procedures required to perform an inspection when using a thermal camera together with an UAV.

**Keywords:** UAV; thermal camera; building inspection.

**Cite as:** Silva, W. P. A., Lordsleem Júnior, A. C., Ruiz, R. D. B., Rocha, J. H. A. (2021), "*Inspection of pathological manifestations in buildings by using a thermal imaging camera integrated with an Unmanned Aerial Vehicle (UAV): a documental research*", Revista ALCONPAT, 11 (1), pp. 123 – 139, DOI: <https://doi.org/10.21041/ra.v11i1.447>

<sup>1</sup> Grupo de Tecnologia e Gestão da Construção de Edifícios (POLITECH), Universidade de Pernambuco, Recife.

<sup>2</sup> Universidad Privada del Valle, Cochabamba, Bolivia.

#### Contribution of each author

In this work, author W.P.A. Silva contributed the original idea, data collection, writing of the paper, and discussion of results, author A.C. Lordsleem Júnior contributed with the writing of the paper and discussion of results, author R.D.B Ruiz contributed with the writing of the paper and discussion of results, and author J.H.A. Rocha contributed with the data collection, review of the paper and discussion of results.

#### Creative Commons License

Copyright 2021 by the authors. This work is an Open-Access article published under the terms and conditions of an International Creative Commons Attribution 4.0 International License ([CC BY 4.0](https://creativecommons.org/licenses/by/4.0/)).

#### Discussions and subsequent corrections to the publication

Any dispute, including the replies of the authors, will be published in the third issue of 2021 provided that the information is received before the closing of the second issue of 2021.

## **Inspeção de manifestações patológicas em edifícios utilizando câmera termográfica integrada ao Veículo Aéreo Não Tripulado (VANT): uma pesquisa documental**

### **RESUMO**

Presente artigo tem como objetivo apresentar o emprego da câmera termográfica integrada ao VANT nos processos de inspeção de edifícios. O desenvolvimento do trabalho foi baseado em revisão sistemática de artigos e trabalhos da área de conhecimento, investigando as características e o funcionamento das câmeras termográficas, o emprego dos VANTs e os fatores que influenciam na detecção de manifestações patológicas. Os resultados permitiram identificar as vantagens e limitações da integração câmera e VANT, demonstrando a viabilidade e eficácia do uso conjunto. Como contribuição este trabalho proporcionou o desenvolvimento de um protocolo de voo ordenando as etapas e os procedimentos necessários para a realização de uma inspeção utilizando a câmera termográfica integrada ao VANT.

**Palavras-chave:** VANT; câmera térmica; inspeção predial.

## **Inspección de manifestaciones patológicas en edificios con cámara térmica integrada en Vehículo Aéreo No Tripulado (VANT): una investigación documental**

### **RESUMEN**

Este artículo tiene como objetivo presentar el uso de la cámara termográfica integrada en VANT en los procesos de inspección de edificios. El desarrollo de este trabajo se basó en una revisión sistemática de artículos y trabajos relacionados al tema, investigando las características y el funcionamiento de las cámaras termográficas, el uso de VANTs y los factores que influyen en la detección de manifestaciones patológicas. Los resultados permitieron identificar las ventajas y limitaciones de la integración de cámaras y VANT, demostrando la viabilidad y efectividad del uso conjunto. Como contribución, este trabajo proporcionó el desarrollo de un protocolo de vuelo que ordena los pasos y procedimientos necesarios para realizar una inspección utilizando la cámara térmica integrada en VANT.

**Palabras clave:** VANT; cámara térmica; inspección de edificios.

### **Legal Information**

Revista ALCONPAT is a quarterly publication by the Asociación Latinoamericana de Control de Calidad, Patología y Recuperación de la Construcción, Internacional, A.C., Km. 6 antigua carretera a Progreso, Mérida, Yucatán, 97310, Tel.5219997385893, [alconpat.int@gmail.com](mailto:alconpat.int@gmail.com), Website: [www.alconpat.org](http://www.alconpat.org)

Reservation of journal title rights to exclusive use No.04-2013-011717330300-203, and ISSN 2007-6835, both granted by the Instituto Nacional de Derecho de Autor. Responsible editor: Pedro Castro Borges, Ph.D. Responsible for the last update of this issue, Informatics Unit ALCONPAT, Elizabeth Sabido Maldonado.

The views of the authors do not necessarily reflect the position of the editor.

The total or partial reproduction of the contents and images of the publication is carried out in accordance with the COPE code and the CC BY 4.0 license of the Revista ALCONPAT.

## 1. INTRODUCTION

Pathological manifestations are present in most buildings to a greater or lesser extent, varying their appearance period and requiring diagnosis and repair, or sometimes in a more complex way, requiring a personalized analysis (Ferreira & Lobão, 2018). However, even when they directly interfere in a building useful life and performance, -generating discomfort and risk both for people who directly use the building and passers-by in surroundings-, analysis and treatment of pathological manifestations is not a priority (Bauer et al., 2011; Viégas, 2015). Many times this structure does not obtain required attention regarding design, execution and maintenance. This is a fact that increases susceptibility about development and aggravation of pathological manifestations (Silva, 2007).

Considering this, investigation and monitoring process for buildings is essential because such procedures enable monitoring their behavior throughout their use in an enterprise, thus gathering information that enable monitoring and detecting failures when sent to obtain analysis and decision models (Agostinho, 2012). In that sense, destructive tests applied to materials, components or building systems become undesirable when it comes to problem diagnosis in the context of in-use buildings. In fact, development of non-destructive techniques intended to diagnose building deterioration, has generally been study subject for many researches (Freitas et al., 2014). Since then, using infrared thermography and Unmanned Aerial Vehicles (UAVs) in building inspection processes has been explored and spread out in society (Nascimento, 2014; Ellenberg et al., 2016; Entrop & Vasenev, 2017).

Thus, infrared thermography is a non-destructive technique involving remote sensing images used to detect flaws in electrical equipment, as well as changes in different parts of a building such as roof, structural systems, masonry sealing systems and coatings. One of these changes refers to detection of excessive humidity and temperature, responsible for damaging materials, with consequences on human health (Cortizo, 2007; Lerma et al., 2011; Freitas et al., 2014). Despite infrared thermography technique has been widely spread in European countries, thanks to historical collection, in Brazil its use is relatively incipient, either due to analysis equipment cost or difficulty on practical application (Cortizo et al., 2008).

Simultaneously, UAV usage has been subject to studies regarding building inspection to verify performance conditions and determine preventive and corrective measures that might be required, due to inherent complexity (height, size, access difficulties and exposure conditions) (Witczuk et al., 2017). UAVs may reduce time in these monitoring operations, and also assist in other inspection processes involving human life risk (Álvarez et al., 2016). In this context, the current article presents application of an infrared camera integrated with Unmanned Aerial Vehicles (UAV) as a tool for building inspection and monitoring to define procedural factors (influencing factors to achieve accurate thermograms used to identify pathological manifestations), in addition to advantages and limitations of this technology.

## 2. BIBLIOGRAPHICAL REVIEW

### 2.1 Infrared Thermography

Infrared thermography is a predictive tool used in early diagnosis of failures and other problems (performance analysis study to predict and specify possible anomalies, assisting in preventive maintenance). Results are presented instantly, during inspection, in form of thermal images or thermograms, which represent surface temperature distribution for an observed object and, as such, recorded for subsequent action purposes by interested parties and archiving (ITC, 2014).

Infrared thermography systems capture thermal radiation, represented in an electromagnetic spectrum, -by the fact that all bodies are at a temperature above absolute zero and emit radiation that is converted into a thermogram which has a polychromatic (color) or monochromatic (gray) scale. Infrared radiation (IR) was first discovered by William Herschel in 1800, and thermoelectric effect was discovered by Thomas Johann Seebeck in 1821. This effect is a direct conversion between temperature difference and electrical voltage and vice versa, being this effect the basis for thermal camera operation (Mistry, 2009; Viégas, 2015). Thermal radiation emitted by an object and captured by a thermal camera is given by Stefan-Boltzmann's law (1).

$$E = \frac{q}{A} = \varepsilon \times \sigma \times T^4 \quad (1)$$

Where E is the radiation emitted by the object (W/m<sup>2</sup>), q is the degree of energy emission (W), A is the area of an emitting surface (m<sup>2</sup>), T is the absolute temperature (K),  $\sigma$  is the Stefan-Boltzmann constant of  $5.676 \times 10^{-8} \text{ Wm}^{-2}\text{K}^{-4}$ , and  $\varepsilon$  is the emissivity of an emitting surface, whose value is between 0 and 1, and indicates how close a surface is to the behavior of a black body, which would be an ideal surface where radiation rate would be maximum, so  $\varepsilon=1$ . (Çengel and Ghajar, 2012).

Additionally, this technique may be classified as active or passive according to thermal overload being used. In active thermography, an external stimulus is required to generate relevant temperature differences. Different techniques may be employed to cause a heat flow in the study subject, each with its own characteristics and limitations. The choice on the type of thermal stimulus depends on characteristics of the object to be tested and the type of information to be researched (Batista, 2019).

On the other hand, using passive thermography where no artificial stimulation is used, involves a natural temperature difference that must be present between the study subject and the medium where it is inserted, which is frequently at a higher temperature. A passive method analysis relies on natural conditions for a studied structure and its surroundings, sun heat being a determining factor (Cortizo, 2007). Therefore, as shown in Figure 1, thermographic cameras capture infrared energy emitted by objects to convert this energy into an electrical signal and, finally, into a visible image, in which each level of energy is represented in a color scale (Meola & Carlomagno, 2004).

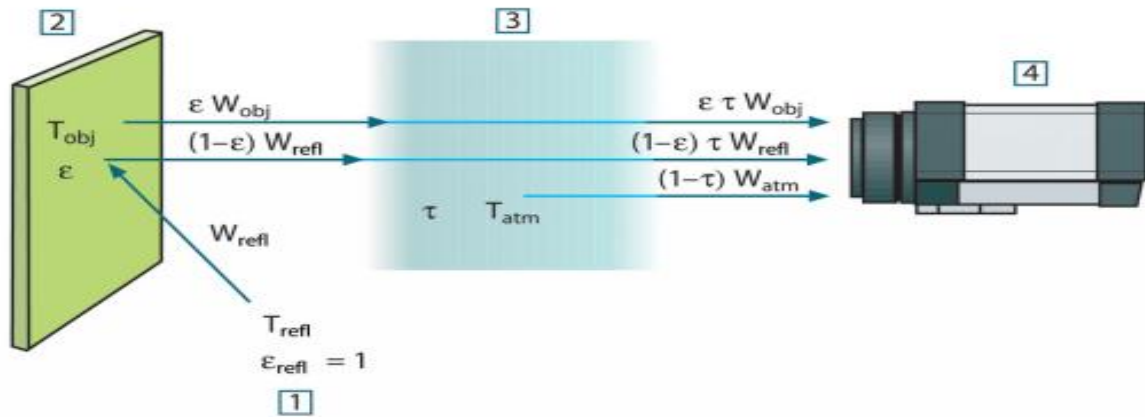


Figure 1. Schematic representation of general thermographic measurement location. 1) adjacent environment, 2) object, 3) atmosphere, 4) camera.  $T_{obj}$ : object temperature,  $T_{refl}$ : reflected temperature,  $T_{atm}$ : atmospheric temperature.  $W_{obj}$ : radiation power emitted by the object,  $W_{refl}$ : radiation power emitted by surrounding environment,  $W_{atm}$ : radiation power emitted by atmosphere (Caldeira & Padaratz, 2015).

Thus, this technique implemented in buildings may be used to evaluate comfort on floor covering (Barreira et al., 2013), detect insulation defects, air leaks (Ocaña et al., 2004) moisture problems (roof damage, moisture on walls), thermal bridges (Asdrubali et al., 2012), and inspect HVAC systems (Heating, Ventilating and Air Conditioning), construction details (Cerdeira et al., 2011; Barreira et al., 2013) and also in building inspection (Brique, 2016), as shown in Figure 2.

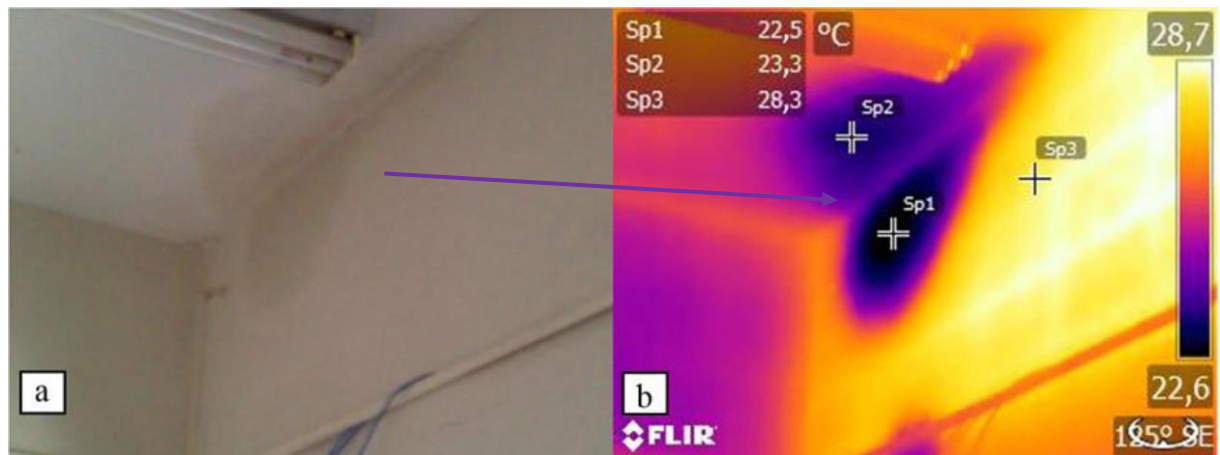


Figure 2. Pluvial water penetration: (a) digital image and (b) thermogram (Rocha et al., 2018).

According to variables highlighted in Table 1, the higher the thermal resolution (pixels) in a camera, the more likely to inspect larger areas with greater precision. Therefore, when using thermal cameras integrated with UAV, they must have the best resolution possible. Furthermore, the IFOV (Instantaneous Field of View) value and the lens opening angle are one of the main limitations in studies involving the analysis of buildings. The higher these parameters, the lower thermogram resolutions and study accuracy will be (Andrade et al., 2019). In addition, it should be noted that the inspection is limited only to a passive application of infrared thermography, which would mean that inspection to the structure would not be possible every day, or that it would be restricted to locally determined schedules.

Table 1. Key variables related to a thermographic camera (Andrade et al., 2019)

<b>PIXEL CAMERA RESOLUTION</b>	<b>IFOV (<i>Instantaneous Field of View</i>)</b>	<b>LENS OPENING ANGLE</b>
60 x 60, 120 x 120, 240 x 380, 320 x 240, 640 x 480.	The value varies between 0.6 and 3.7 mRad, using the equipment lens.	The most common lenses are 15 and 25 degrees but can vary between 7 and 80 degrees.

## 2.2 UAVs

According to ANAC (National Civil Aviation Agency, 2017), unmanned aerial vehicles (UAVs) are any unmanned aircraft that can be remotely or automatically driven. These aircrafts are remotely or automatically flown using predefined coordinates. It is a technology on the rise that is being used in several areas every day (Nascimento, 2014). UAVs were first developed in the 1950s and were exclusively intended for military purposes. Different projects started in several countries with the purpose of producing vehicles capable of performing missions without a pilot on board in order to avoid further losses (Agostinho, 2012). Over time, technology began to get disclosed, and its first use for a non-military purpose took place in 1986, when forest fires were monitored in Montana, United States (Agostinho, 2012). In this sense, increasing UAV usage is due to its low cost, agile processing collection, easy aircraft maneuvering, and efficient image capture system (Seibert & Teizer, 2014).

Besides, UAVs are effective tools to perform remote sensing procedures, including its capability for reaching places that are difficult to access as the main reason to be used, as well as a range of applicable sensors that can be incorporated such as an infrared camera, light detection and distance sensors (LIDAR, Light Detection And Ranging) (Freimuth & König, 2018).

Currently, two types of UAVs, whose basic difference is their aerodynamic system such as a rotation or fixed wing, are available in the market. The first aircrafts are similar to a helicopter or multicopter, a compact aircraft involving easy operation and low cost. On the other hand, fixed-winged aircrafts include different sizes according to functionality (Jorge & Inamasu, 2014; Melo & Costa, 2015).

Table 2. UAV Classification (Bento, 2008).

<b>CATEGORY</b>	<b>ACRONYM</b>	<b>RANGE [km]</b>	<b>FLIGHT ALTITUDE [m]</b>	<b>BATTERY AUTONOMY [h]</b>	<b>WEIGHT [kg]</b>
<i>Micro</i>	$\mu$ (micro)	< 10	250	1	<5
<i>Mini</i>	Mini	< 10	150 – 3000	< 2	150
<i>Close Range</i>	CR	10 – 30	3000	2 – 4	150
<i>Short Range</i>	SR	30 – 70	3000	3 – 6	200
<i>Medium Range</i>	MR	70 – 200	5000	6 – 10	1250
<i>Medium Range Endurance</i>	MRE	>500	8000	10 – 18	1250
<i>Low Altitude Deep Penetration</i>	LADP	>250	50 – 9000	0,5 – 1	350
<i>Low Altitude Long Endurance</i>	LALE	>500	3000	>24	<30
<i>Medium Altitude Long Endurance</i>	MALE	>500	14000	24 – 48	1500

Table 2 shows that UAVs used in building inspection process in general have a weight below 150 kg. The flight range, a dominant factor for flight protocol development and efficiency in building monitoring, is below two hours.

### 2.3 Thermography integrated with UAV

Although thermography and UAVs are subject to different recent investigations, an integrated study of both is still incipient. Analyzing benefits related to these two topics motivates a combination of their functionalities to obtain mutual benefits (Entrop & Vasenev, 2017). A thermal camera integrated with an UAV is an important tool to evaluate large areas in an automated way and in reduced runtime (Viana et al., 2018). Main challenges for this technology are low resolution of some thermographic cameras, regulations that limit operations involving UAV on a visual line and high dependence on climate (Witczuk et al., 2017).

In addition, heat sensors are a payload option for high resolution aerial thermal imaging. This technology enables quick and safe survey of thermal areas, often present in inaccessible or dangerous terrain (Harvey et al., 2016). These images collected by UAV are potentially critical tools in geothermal science, including geological, geochemical and geophysical surveys, study and environmental monitoring baselines, geotechnical and civil works, and as in the case of this research, an outstanding support for building inspection. Such technology may be used for mapping heat loss, and be able to gather thermal information such as heat leaks, by using an infrared camera and then processing any image obtained. Despite performing inspections, it is a less difficult process for small buildings, collecting thermal data with increasing height, especially on skyscrapers and roofs, and is a much more complex and dangerous process (Kayan et al., 2018). Aerial thermography is a technology that has been used in recent times to record thermal images without requiring access to buildings, and it is capable of reaching any difficult-access area such as a roof, while carrying an infrared camera and any other sensor (Chu et al., 2016).

Therefore, combining infrared thermography and UAVs enables optimization of maintenance tasks (Muñoz et al., 2017), and consequently, bringing significant economic advantages (Ramírez et al., 2018). Such aspects are due to the fact that UAVs may be equipped with high-resolution cameras allowing users to obtain data in real-time. Furthermore, aerial images previously captured from another light aircraft or helicopter and their fuel cost are disadvantages that make UAVs more viable, since power source for their flight can be easily recharged (Lavars, 2015). Therefore, being equipped with a high-resolution thermographic camera, an UAV becomes an excellent tool to collect thermal information from buildings (Zhang et al., 2015). In that sense, Figure 3 shows an UAV model that is already integrated with a digital camera as well as a thermographic camera, different from other models. Removing the first camera to install the second camera is required.



Figure 3. UAV with a thermographic camera attached to a digital camera (Topdrone, 2020).

### 3. BUILDING INSPECTION

Thermography implementation in inspection processes is based on existing anomalies or defects that impact thermal properties in the structure. Figure 4 shows defects interrupting heat transfer from concrete, since existing voids are filled with air or water, and due to different thermal conductivity in materials, temperature variation along the structure is verified (Rocha & Póvoas, 2017).

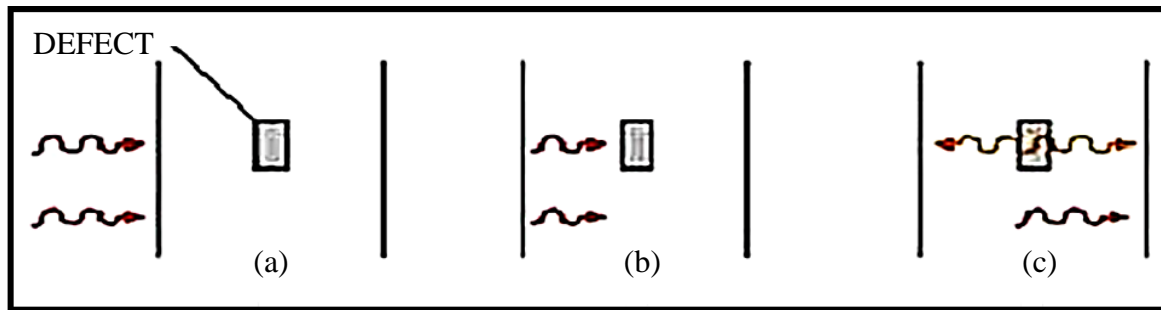


Figure 4. Modeled propagation of a single heat pulse in a material: (a) An energy pulse applied to the surface; (b) A heat pulse travels inside the material and finds a defect; (c) This defect partially reflects and partially transmits the pulse (Cortizo, 2007).

Additionally, infrared thermography produces a thermal image, where each color represents a surface temperature level in objects. By analyzing any image obtained by the equipment, it is possible to identify foci of humidity, anomalies, hidden elements, and other defects present (Grinzato et al., 2011). Consequently, infrared thermography enables detecting only anomalies associated with measurable modifications of thermal characteristics such as heat flow and resulting temperatures, and pathological manifestations with limited depths, i.e, near the surface (Bauer & Pavón, 2015). In civil construction, therefore, a temperature range from 1 °C to 2 °C is generally an indication of potential issues. From 4 °C on, existing body abnormality may be ascertained (Maldague & Marinetti, 1996; Cortizo et al., 2008).

Therefore, this technology enables identification of adhesion failure or absent mortar (Bauer et al., 2015), and confined moisture present in ceramic tiles (Edis et al., 2014; Bauer & Pavón, 2015), as well as existing cracks, detachment problems, and infiltrations, considering the thermal gradient verified in the thermogram (Freitas et al., 2014; Viégas, 2015; Rocha & Póvoas, 2017; Takeda & Mazer, 2018; Batista, 2019).



Figure 5. Inspection using an UAV integrated with a thermal camera (Nascimento, 2014)

In the case shown in Figure 5, according to Nascimento (2014), images were obtained in the early morning, making it possible to recognize areas including cracks and infiltrations, as the weather was mild and allowed a greater difference in temperature gradient, with lighter regions being those that have a higher temperature than those that are represented in darker tones.

### 3.1 Advantages and disadvantages

Table 3 shows the main advantages and limitations of using a thermographic camera integrated with an UAV according to literature (Yehia et al., 2007; Agostinho, 2012; Sham et al., 2012; Jorge & Inamasu, 2014; Mavromatidis et al., 2014; Seibert and Teizer, 2014; Domingues, 2015; Melo and Costa, 2015; Pajares, 2015; Watase et al., 2015; Zhang et al., 2015; Ariwoola, 2016; Ellenberg et al., 2016; Hiasa et al., 2016; Rehman et al., 2016; Entrop & Vasenev, 2017; Muñoz et al., 2017; Witczuk et al., 2017; Freimuth & König, 2018; Ramírez et al., 2018; Andrade et al., 2019).

Table 3 shows that main advantages of using this technology are linked to optimizing inspection procedures, obtaining data in real time and in a shorter interval of time. On the other hand, limitations are related to requirements to obtain an accurate thermogram, considering favorable climatic conditions and readings made from angles and distances unable to interfere with the results.

Table 3. Advantages and limitations of using a thermal camera integrated with an UAV.

VANTAGENS	LIMITAÇÕES
<ul style="list-style-type: none"> <li>• Capability of reaching difficult access areas;</li> <li>• Getting real-time data;</li> <li>• Reducing operational risks</li> <li>• Increasing operator and employee safety;</li> <li>• Reduced inspection time that generates savings and speeding up recovery planning for a structure;</li> <li>• Greater reliability compared to conventional methods;</li> <li>• Fast, non-invasive, non-destructive and contactless technology;</li> <li>• Applicable at a considerable distance to analyze and inspect large areas at short intervals of time.</li> </ul>	<ul style="list-style-type: none"> <li>• Flight autonomy from 30 min to 2 h, using &lt; 150 Kg models;</li> <li>• Favorable weather conditions, implying both flight and surface heat emissivity;</li> <li>• Subject to local regulations and restrictions for flight performances, unable to be performed in any location;</li> <li>• Interference in results due to reflections if used in a facility surrounded by buildings including mirrored facades;</li> <li>• Changes in scanning obtained at distances &gt; 10 meters between the camera and the target object;</li> <li>• Unable to measure thickness and depth of any pathological manifestation.</li> </ul>

Finally, one of the most critical factors when using aerial thermography is related to operation and equipment cost; however, when comparing benefits of this tool related to conventional methods, its potentialities considering its speed in data collection and safety for people performing an inspection are verified (Mavromatidis et al., 2014; Ariwoola, 2016).

### 3.2 Processing factors regarding thermal imaging

Thermographic analysis is a procedure where an inspector operates a thermal imager pointing at an object under inspection and detecting a defect by an analysis of thermogram obtained. Despite the technique is apparently simple, the result analysis might be complicated and would even lead to wrong conclusions if certain precautions are not taken before and during the test (Brique, 2016). Therefore, the operator himself must be aware of strong influence posed by solar radiation, wind and rain, and how these factors impact thermal distribution of any object analyzed in an open environment (Batista, 2019).

Considering this, in order to guarantee image quality, sensitivity and thermal contrast, awareness regarding some factors such as material emissivity (a function of surface temperature and observation angle) surface reflectivity, purpose of direct incident radiation and existing external sources (shadows, reflections), distance and measurement angle is required (Barreira, 2004; Cortizo, 2007; Bauer, 2015; Viégas, 2015; Batista, 2019). Besides, sun heat radiation may affect thermographic measurement, as it modifies normal heat flow from inside out. Distance from the equipment to the object may also modify surface temperature reading, as it reduces thermogram resolutions and influences atmospheric attenuation (Labat et al., 2011).

Regarding inspection time, it was found that differences between authors are present, but this parameter depends on environmental conditions found where a studied object is located (Rocha & Póvoas, 2017). In that sense, different behaviors were verified regarding measurement periods (dry and rainy), at 8 a.m., 3 and 9 p.m. (Freitas et al., 2014). In other cases, measurements were taken at different times during the morning and the afternoon (Nascimento, 2014), as emissivity by non-metal materials decreases with increasing temperature (Barreira, 2004). There were also cases where checking measurements throughout the day (6-18h), in order to evaluate the best measurement times, both in the morning and in the afternoon was decided (Viégas, 2015).

Finally, some authors (Uemoto, 2000; Watase et al., 2015; Hiasa et al., 2016) recommend an inspection at night in order to eliminate solar radiation effect, and have a better view between the defect and the intact regions, thus avoiding false detections (Rocha & Póvoas, 2017).

In addition, thermal gradients and turbulence modify air refractive index thus causing a reduction in image quality. Meanwhile, atmosphere present between the emission source and the receiver may cause disturbances in measurement. Therefore, a 10-meter distance between the emission source and the receiver must be maintained and measurements made at greater distances must be corrected (Barreira, 2004; Comitti, 2012; Viégas, 2015). Moreover, during days including winds above 7 m/s, measurements should not be made with infrared thermography, because data obtained will induce error in thermal analysis of the object (ITC, 2014).

According to Standard NBR 15572 (ABNT, 2013), an angle between the thermal imager and the inspected point must be as perpendicular as possible, so that no emissivity reduction due to inadequate observation angles (greater than 60°) is present. For this reason, Viégas (2015) states that nobody should remain directly facing the target so thermographer heat is not reflected. Therefore, positioning at an angulation of about 5°, in relation to object horizontal line to be thermally analyzed is recommended, as shown in Figure 6.

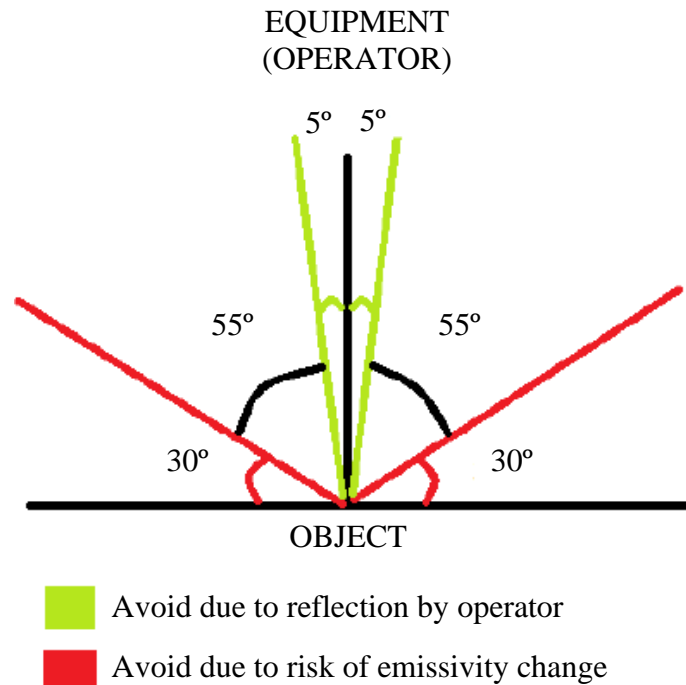


Figure 6. Measurement angles: precautions (Viégas, 2015)

### 3.3 Flight Protocol

Project planning and development may vary according to flight capacity, being influenced by their accuracy and course (Agostinho, 2012). However, it is perceived that commercially available flight preparation tools, in some cases are still insufficient to perform certain inspections, and it is up to an operator to create their own tools and protocols (Seibert & Teizer, 2014). As a result, the protocol shown below in Figure 7 and Table 4, was developed according to studies by several authors (Agostinho, 2012; Siebert & Teizer, 2014; Ariwoola, 2016; Ellenberg et al., 2016; Entrop & Vasenv, 2017; Freimuth & König, 2018).

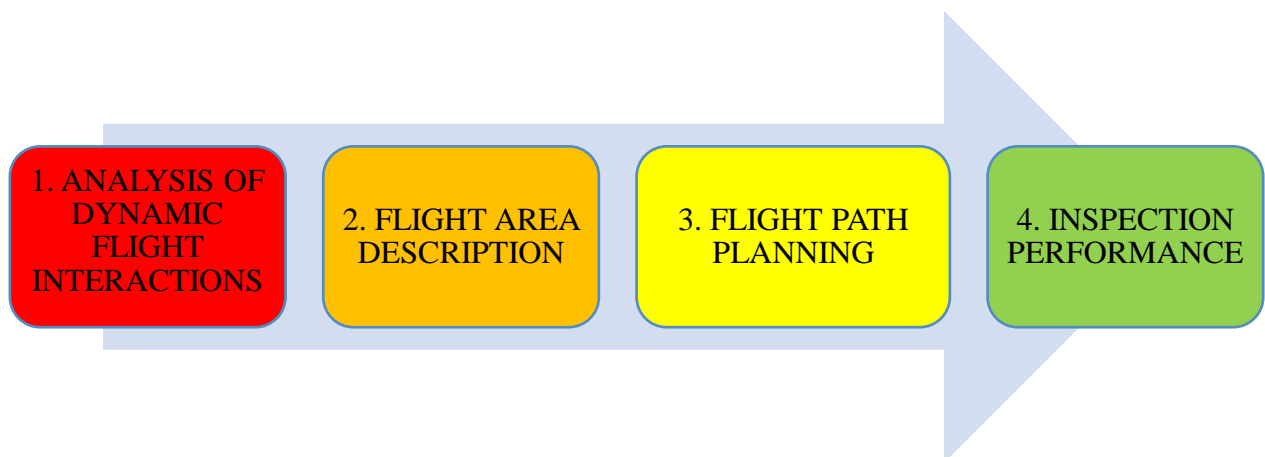


Figure 7. Flight protocol steps.

Table 4. Flight protocol.

STEPS	PROCEDURES
1. Analysis of dynamic flight interactions	At this stage, checking UAV use regulations where inspection will be performed is required. Additionally, a study on weather conditions for inspection day, and characteristics of object studied (area, number of floors, maximum level) must be obtained and then proceed with choosing an equipment.
2. Flight Area Description	On the second stage, performing a test flight to identify risk areas and establishing reading angles and distances is required.
3. Flight Path Planning	Once risk areas have been determined, a flight path must be developed so that 75% of UAV load for flight autonomy is guaranteed.
4. Inspection Performance	After completing previous steps, inspection may be performed in such a way that reading data safely and accurately is possible.

By analyzing Table 4, it is verifiable that an initial stage is related to previous requirements for the inspection using a thermographic camera integrated with an UAV, including verifying any regulation for such equipment where the procedure will be performed, weather conditions, being necessary winds of less than 7 m/s and not during cloudy days, having knowledge of the object to be studied, such as dimensions and location, and finally choosing an equipment that guarantees a flight autonomy for such procedure. Afterwards, inspection area where the UAV will be moving along the inspection must be determined, paying attention to risk areas such as places where people, animals and obstacles are present, and establishing angles and distances where readings will be taken, at distances < 10 meters and at angles according to Section 3.1, ensuring the accuracy of the data obtained. From there, a path to be traveled by the UAV must be planned in such a way that risk area displacement is avoided and the device has sufficient flying autonomy to finish a flight with 75% of charge in the battery, including energy consumed during landing and take-off procedures. Finally, once previous steps have been completed, the inspection may be performed.

### 3.4 Data Analysis provided by Literature

It was verified that despite simplicity in using a thermal imager to obtain thermograms during inspections, interferences and environmental conditions under which images were obtained should not be taken into account, thermogram analysis and interpretation might lead to erroneous conclusions (Takeda & Mazer, 2018). In addition, it was found that the larger and the more superficial a defect area is, the easier detection is (Rocha & Póvoas, 2017). In that sense, it was found that if R/d ratio (R: short defect dimension and d: defect depth from the surface) is greater than 1, defects are found; if this R/d ratio is equal to 0.45, they are detectable up to a depth of 10 centimeters (Farrag et al., 2016). Moreover, in thermal profiles presented in the thermograms for masonry a clear variation in surface temperature was present. This thermal difference denotes different materials present inside the masonry, due to quite distinct physical and chemical properties (Cortizo, 2007).

In addition, during inspection of a structure including ceramic coating it was verified that the best measurements were obtained after the facade was heated (passive technique), and that the thermogram in the afternoon had better clarity compared to morning thermogram (Viégas, 2015). Afterwards, when studying a building covered with mortar, it was found that the best times for measurement were from 11 a.m. to 12 p.m. and 5-6 p.m., and a "more vibrant" yellow coloration in the region including coating detachment was verified. In this region temperature increases unlike the rest of mortar-coated facade absent of pathological manifestations. Finally, when monitoring a structure covered with tile, the best times for measurement were between 9-10 a.m. and 2-3 p.m. (Viégas, 2015), thus confirming measurement times stated in 3.1.

A slight tendency in greater temperature differences (between areas with and without fissures) in the hottest areas, as well as greater dispersion of these variations measured in warmer areas were also observed (Freitas et al., 2014). Besides, at least a 5-meter distance between the UAV and the research objects to be safe was at first considered. While during the tests, this distance was increased to 10 meters, thus guaranteeing both reliable data obtained and aircraft safety (Entrop & Vasenev, 2017). Furthermore, simulation and flight model preparation comprises a more accurate inspection and better UAV performance, considering speed characteristics and battery recharge required (Freimuth & König, 2018).

#### 4. CONCLUSIONS

Based on previous discussion and presented data, confirming thermography integrated with UAV is a capable tool to identify thermal anomalies associated to pathological manifestations is possible. Additionally, this mechanism optimizes building inspection process, enabling characterization of difficult-access areas without risking human safety. Besides, it provides fast and precise data which helps during inspection procedures and structure recovery tests.

However, few limitations are described fourfold: charging capacity is rather vulnerable, weather variations during flight, data obtained in the thermogram and object reflections in the surroundings may interfere in the results. Main contributions of this study include a specific flight protocol to use a thermographic camera integrated with a UAV and a review on principles and techniques involved in this procedure. The latter being a basis for future studies and research on development and expansion of monitoring models that tend to overcome disadvantages and guarantee effectiveness of this tool.

#### 5. REFERENCES

- Agência nacional de aviação civil. (2017). *Requisitos gerais para aeronaves não tripuladas de uso civil - RBAC-E nº 94. Resolução n. 419*. Brasília.
- Agostinho, S. L. (2012), "*Inspeção e Monitorização de Estruturas em Engenharia Civil – Utilização de UAV na Inspeção e Monitorização*", Dissertação de Mestrado, Universidade da Madeira, p. 105.
- Álvares, J., Costa, D. B., Melo, R. R. S., Bello, A. (2016), "*Estudo exploratório de mapeamento 3D de canteiros de obras utilizando veículos aéreos não tripulados*", In: XVI Encontro Nacional de Tecnologia do Ambiente Construído, São Paulo, Brasil, pp. 5067-5080.
- Andrade, R. P., Resende, M. M., Maranhão, F. L., Portella, F., Bulzico, B. (2019), "*Estado da arte da utilização da técnica de termografia embarcada em drones para inspeção de revestimentos de fachadas*", In: 2º Workshop de Tecnologia de Processos e Sistemas Construtivos, São Paulo, Brasil, p.5, disponível em: <https://antaceventos.net.br/index.php/tecsic/tecsic2019/paper/view/304/139>

- Ariwoola, R. T. (2016), “*Use of Drone and Infrared Camera for a Campus Building Envelope Study*”, Master Thesis, East Tennessee State University, p. 83. <https://dc.etsu.edu/etd/3018>
- Asdrubali, F., Baldinelli, G., Bianchi, F. (2012), *A quantitative methodology to evaluate thermal bridges in buildings*. Applied Energy. 97(1):365–373. <https://doi.org/10.1016/j.apenergy.2011.12.054>
- Associação Brasileira de Normas Técnicas. (2013). *NBR 15572: Ensaios não destrutivos — Termografia — Guia para inspeção de equipamentos elétricos e mecânicos*. Rio de Janeiro.
- Barreira, E. (2004), “*Aplicação da Termografia ao Estudo do Comportamento Higrotérmico dos Edifícios*”, Dissertação de Mestrado, Universidade do Porto, p. 198.
- Barreira, E., de Freitas, S. S., de Freitas, V. P., Delgado, J. M. P. Q. (2013), *Infrared thermography application in buildings diagnosis: a proposal for test procedures, industrial and technological applications of transport in porous materials*. Advanced Structured Materials. 36. [https://doi.org/10.1007/978-3-642-37469-2\\_4](https://doi.org/10.1007/978-3-642-37469-2_4)
- Batista, T. S. (2019), “*Avaliação do desempenho da termografia infravermelha em diferentes espessuras e profundidades de trincas em edificações*”, Dissertação de Mestrado, Universidade de Pernambuco, p. 109.
- Bauer, E., Castro, E. K., Antunes, G. R., Leal, F. E. (2011), “*Identification and Quantification of Pathologies in Facades of New Buildings in Brasília*” in: XII DBMC International Conference on Durability of Building Materials and Components, Porto, Portugal.
- Bauer, E., Freitas, V. P., Mustelier, N., Barreira, E., Freitas, S. (2015), *Infrared Termography – Evaluation of the results reproducibility*. Structural Survey. 33(1): 82-86. <https://doi.org/10.1108/ss-05-2014-0021>
- Bauer, E., Pavón, E., (2015), *Termografia de infravermelho na identificação e avaliação de manifestações patológicas em edifícios*. Revista Concreto e Construções.79:93-98. ISSN:1809-7197.
- Bento, M. F. (2008), “*Unmanned aerial vehicles: an overview*”, Inside GNSS, pp. 54-61.
- Brique, S. K. (2016), “*Emprego da termografia infravermelha no diagnóstico de falhas de aderência de peças cerâmicas utilizadas em fachadas de edifícios*”, Dissertação de Mestrado, Universidade Federal de Santa Catarina, p. 180
- Caldeira, M. M., Padaratz, I. J. (2015), *Potentialities of infrared thermography to assess damage in bonding between concrete and GFRP*. Ibracon Structures and Materials Journal. 8:296-322. <http://dx.doi.org/10.1590/S1983-41952015000300004>
- Cengel, Y. A., Ghajar, A. J. (2012), “*Transferência de Calor e Massa - Uma Abordagem Prática*” (Porto Alegre, Brasil: Amgh Editora), p. 906.
- Cerdeira, F., Vázquez, M., Collazo, J., Granada, E. (2011), *Applicability of infrared thermography to the study of the behaviour of stone panels as building envelopes*. Energy Build. 43:1845–1851. <https://doi.org/10.1016/j.enbuild.2011.03.029>
- Chu, A-M., Westerhoff1, L., Sheppard1, S., Storey, S., Goodhew, J., Fox, M., Goodhew, S., Pahl, S., Higgins, C. (2016), “*Exploring the Use of Thermal Imagery for the Promotion of Residential Energy Efficiency. Report prepared for the City of Vancouver*”, available at: <http://calp2016.sites.olt.ubc.ca/files/2016/05/Thermal-Imaging-Report.pdf>
- Comitti, A. (2012), “*Engenharia de manutenção: Uso da Termografia*”, Revista Saber Eletrônica, 47(459):14-19.
- Cortizo, E. C. (2007), “*Avaliação da técnica de termografia infravermelha para identificação de estruturas ocultas e diagnóstico de anomalias em edificações: ênfase em edificações do patrimônio histórico*”, Tese de Doutorado, Universidade Federal de Minas Gerais, p. 178.
- Cortizo, E. C., Barbosa, M. P., Souza, L. A. C. (2008), *Estado da Arte da Termografia*. Ambiente Construído e Patrimônio Sustentável. 2(2):158-193.

- Domingues, A. D. (2015), “*Identificação de manifestações patológicas em fachadas prediais com revestimento cerâmico, utilizando a técnica de termografia de infravermelho*”, Monografia de Graduação, Universidade Católica de Brasília, p. 29.
- Edis, E., Flores-Colen, I., de Brito, J. (2014), *Passive thermographic detection of moisture problems in façades with adhered ceramic cladding*. Construction and Building Materials. 51(1):187-197. <http://dx.doi.org/10.1016/j.conbuildmat.2013.10.085>
- Ellenberg, A., Koutsos, A., Moon, F., Bartoli, I. (2016), *Bridge deck delamination identification from unmanned aerial vehicle infrared imagery*. Automation in Construction. 72(1):155-165. <https://doi.org/10.1016/j.autcon.2016.08.024>
- Entrop, A. G., Vasenev, A. (2017), *Infrared drones in the construction industry: designing a protocol for building thermography procedures*. Energy Procedia. 132(1):63-68. <https://doi.org/10.1016/j.egypro.2017.09.636>
- Farrag, S., Yehia, S., Qaddoumi, N. (2016), *Investigation of Mix-Variation Effect on Defect-Detection Ability Using Infrared Thermography as a Nondestructive Evaluation Technique*, J. Bridge Eng. 21(3):1-15. [http://dx.doi.org/10.1061/\(ASCE\)BE.1943-5592.0000779](http://dx.doi.org/10.1061/(ASCE)BE.1943-5592.0000779)
- Ferreira, J. B., Lobão, V. W. N. (2018). *Manifestações patológicas na construção civil*. Caderno De Graduação - Ciências Exatas E Tecnológicas. 5(1):71-80. Disponível em: <https://periodicos.set.edu.br/cadernoexatas/article/view/5853>
- Freimuth, H., König, M. (2018), *Planning and executing construction inspections with unmanned aerial vehicles*. Automation in Construction. 96(2):540–553. <https://doi.org/10.1016/j.autcon.2016.08.024>
- Freitas, J. G., Carasek, H., Cascudo, O. (2014), *Utilização de termografia infravermelha para avaliação de fissuras em fachadas com revestimento de argamassa e pintura*. Ambiente Construído. 14(1):57-73. <https://doi.org/10.1590/S1678-86212014000100006>
- Freitas, S. S., Freitas, V. P., Barreira, E. (2014), *Detection of façade plaster detachments using infrared thermography – A nondestructive technique*. Construction and Building Materials. 70(1):80-87. <https://doi.org/10.1016/j.conbuildmat.2014.07.094>
- Grinzato, E. (2011), “*State of the art and perspective of infrared thermography applied to building science*” in: Meola C, editor. Infrared thermography recent advances and future trends. Bentham Books. ISBN: 978-1-60805-521-0, <http://dx.doi.org/10.2174/97816080514341120101>
- Grinzato, E., Ludwig, N., Cadelano, G., Bertucci, M., Gargano, M., Bison, P. (2011), *Infrared Thermography For Moisture Detection: a laboratory study and in-situ test*. Materials Evaluation. 69(1):97-104.
- Harvey, M. C., Rowland, J. V., Luketina, K. M. (2016), *Drone with thermal infrared camera provides high resolution georeferenced imagery of the Waikite geothermal area, New Zealand*. Journal of Volcanology and Geothermal Research. 325(1):61-69. <https://doi.org/10.1016/j.jvolgeores.2016.06.014>
- Hiasa, S., Catbas, F., Matsumoto, M., Mitani, K. (2016), *Monitoring concrete bridge decks using infrared thermography with high speed vehicles*. Structural Monitoring and Maintenance, 3(3): 277-296. <https://doi.org/10.12989/smm.2016.3.3.277>
- Infrared Training Center – ITC. (2014). *Manual do usuário – Certificação Nível I*. Sorocaba.
- Jorge, L. A. C., Inamasu, R. Y., “*Uso de veículos aéreos não tripulados (VANT) em agricultura de precisão*” in: A. Bernadi, J. Naime, A. Resende, L. Bassoi, Y. Inamasu (Ed.) (2014), *Agricultura de precisão: resultados de um novo olhar*. Brasília, DF: Embrapa, pp. 109-134.
- Kayan, H., Eslampanah, R., Yeganli, F., Askar, M. (2018), “*Heat leakage detection and surveillance using aerial thermography drone*” in: 26th Signal Processing and Communications Applications Conference (SIU), Izmir, Turkey, pp. 1-4. <https://doi.org/10.1109/SIU.2018.8404366>

- Labat, M., Garnier, G., Woloszyn, M., Roux, J. J. (2011), “*Infrared measurements on ventilated cladding for assessing its surface temperature and insulated part of the envelope using a simulation tool*” in: NBS 2011 – 9th Nordic Symposium on Building Physics, Tampere, Finland, pp. 315-322.
- Lavars, N. (2015), “*How drones are poised to help build the cities of tomorrow*”, acesso em 1 de julho de 2019, disponível em: <http://www.gizmag.com/drones-building-constructionindustry/36306/>
- Lerma, J. L., Cabrelles, M., Portalés, C. (2011), *Multitemporal thermal analysis to detect moisture on a building façade*. Construction and Building Materials. 25(1):2190-2197. <https://doi.org/10.1016/j.conbuildmat.2010.10.007>
- Maldague, X., Marinetti, S. (1996), *Pulse phase infrared thermography*. Journal Applied Physics. 79(1):2694-2698. <https://doi.org/10.1063/1.362662>
- Mavromatidis, L. E., Dauvergne, J. L., Saleri, R., Batsale, J. C. (2014), *First experiments for the diagnosis and thermophysical sampling using impulse IR thermography from Unmanned Aerial Vehicle (UAV)*. Quantitative InfraRed Thermography. <http://dx.doi.org/10.21611/qirt.2014.213>
- Melo, R. R. S., Costa, D. B. (2015), “*Uso de veículo aéreo não tripulado (VANT) para inspeção de logística em canteiros de obra*”. in: SIBRAGEC-ELAGEC, São Carlos, pp. 674-681.
- Meola, C., Carlomagno, G. (2004), *Recent advances in the use of infrared thermography*. Measurement Science and Technology. 15(9):27-58. <http://dx.doi.org/10.1088/0957-0233/15/9/R01>
- Mistry, B. D. (2009), “*A Handbook of Spectroscopic Data*” (Oxford, England: Oxford Book Company), p. 247.
- Muñoz, C. Q. G., Marquez, F. P. G., Lev, B., Arcos, A. (2017), *New pipe notch detection and location method for short distances employing ultrasonic guided waves*. Acta Acustica united with Acustica. 103(5):772-781. <https://doi.org/10.3813/AAA.919106>
- Nascimento, M. L. M. (2014), “*Utilização de drone e termografia na detecção de manifestações patológicas em edificações*”, Monografia de Graduação, Universidade Católica de Brasília, p. 21.
- O. T. Takeda, W. Mazer (2018), *Potencial da análise termográfica para avaliar manifestações patológicas em sistemas de revestimentos de fachadas*. Revista ALCONPAT. 8(1):38-50 <http://dx.doi.org/10.21041/ra.v8i1.181>
- Ocaña, S., Guerrero, I., Requena, I. (2004), *Thermographic survey of two rural buildings in Spain*. Energy Build, 36(6):515-523. <https://doi.org/10.1016/j.enbuild.2003.12.012>
- Pajares, G. (2015), *Overview and current status of remote sensing applications based on unmanned aerial vehicles (UAVs)*. Photogrammetric Engineering & Remote Sensing. 81(1):281-329. <https://doi.org/10.14358/PERS.81.4.281>
- Ramírez, I. S., Marugán, A. P., Márquez, F. P. G. (2018), “*Remotely Piloted Aircraft System and Engineering Management: A Real Case Study*” in: Xu J., Cooke F., Gen M., Ahmed S. (eds) Proceedings of the Twelfth International Conference on Management Science and Engineering Management. Springer, Cham. pp. 1173-1185. [https://doi.org/10.1007/978-3-319-93351-1\\_92](https://doi.org/10.1007/978-3-319-93351-1_92)
- Rehman, S., Ibrahim, Z., Memon, S., Jameel, M. (2016), *Nondestructive test methods for concrete bridges: A review*. Construction and Building Materials. 107(15):58-86. <http://dx.doi.org/10.1016/j.conbuildmat.2015.12.011>
- Rocha, J. H. A., Póvoas Y. V. (2017), *Infrared thermography as a non-destructive test for the inspection of reinforced concrete bridges: A review of the state of the art*. Revista ALCONPAT. 7(3):200-214. <http://dx.doi.org/10.21041/ra.v7i3.223>
- Rocha, J. H. A., Santos, C. F., Oliveira, J. B., Albuquerque, L. K. S., Póvoas, Y. V. (2018), *Detecção de infiltração em áreas internas de edificações com termografia infravermelha: estudo de caso*. Ambiente Construído, 18(4): 329-340. <https://doi.org/10.1590/s1678-86212018000400308>

- Sham, J., Lo, T., Memon, S. (2012), *Verification and application of continuous surface temperature monitoring technique for investigation of nocturnal sensible heat release characteristics by building fabrics*. Energy Build. 53:108–116. <https://doi.org/10.1016/j.enbuild.2012.06.018>
- Siebert, S., Teizer, J. (2014), *Mobile 3D mapping for surveying earthwork projects using an Unmanned Aerial Vehicle (UAV) system*. Automation in Construction. 41:1-14. <https://doi.org/10.1016/j.autcon.2014.01.004>
- Silva, A. F. (2007), “*Manifestações patológicas em fachadas com revestimento argamassado: Estudo de caso em edifícios em Florianópolis*”, Dissertação de Mestrado, Universidade Federal de Santa Catarina, p. 190.
- Topdrone. (2020), “*DJI Mavic 2 Enterprise Dual*”, acesso em 25 de setembro de 2020, disponível em: <https://www.topdrone.com.br/dji-mavic-2-enterprise-dual/p>
- Uemoto, T. (2000), “*Maintenance of concrete structure and application of nondestructive inspection in Japan*”, in: T. Uemoto (Ed.), Proc. Non-Destructive Testing in Civil Eng., ELSEVIER, 2000, Kidlington: OX (UK), pp. 1–11.
- Viana, L. A., Zambolim, L., Sousa, T. V., Tomaz, D. C. (2018), *Potencial uso de câmera termal acoplada a VANT para monitoramento de culturas*. Brazilian Journal of Biosystems Engineering. 12(3):286-298. <http://dx.doi.org/10.18011/bioeng2018v12n3p286-298>
- Viégas, D. J. A. (2015), “*Utilização da termografia infravermelha em fachadas para verificação de descolamento de revestimento*”, Dissertação de Mestrado, Universidade de Pernambuco, p. 165.
- Watase, A., Birgul, R., Hiasa, S., Matsumoto, M., Mitani, K., Catbas, F. (2015), *Practical identification of favorable time windows for infrared thermography for concrete bridge evaluation*. Construction and Building Materials. 101(1):1016-1030. <https://doi.org/10.1016/j.conbuildmat.2015.10.156>
- Witczuk, J., Pagacz, S., Zmarz, A., Cypel, M. (2017), *Exploring the feasibility of unmanned aerial vehicles and thermal imaging for ungulate surveys in forests - preliminary results*. International Journal of Remote Sensing. 39:5504-5521. <https://doi.org/10.1080/01431161.2017.1390621>
- Yehia, S., Adudayyeh, O., Nabulsi, S., Abdelqader, I. (2007), *Detection of common defects in concrete bridge decks using nondestructive evaluation techniques*. Journal of Bridge Engineering, 12, (2):215-225. [https://doi.org/10.1061/\(ASCE\)1084-0702\(2007\)12:2\(215\)](https://doi.org/10.1061/(ASCE)1084-0702(2007)12:2(215))
- Zhang, J., Jung, J., Sohn, G., Cohen, M. (2015), “*Thermal Infrared Inspection of Roof Insulation Using Unmanned Aerial Vehicles*” in: The International Archives of the Photogrammetry, Remote Sensing and Spatial Information Sciences, International Conference on Unmanned Aerial Vehicles in Geomatics, Toronto, Canada, pp. 1-6. <https://doi.org/10.5194/isprsarchives-XL-1-W4-381-2015>